Comprehensive analytical approaches to determine the sources, fate and effects of marine oil spills

Jagoš Radović

Comprehensive analytical approaches to determine the sources, fate and effects of marine oil spills

Jagoš Radović

Barcelona, 2014

Facultat de Química

Departament de Química Analítica

Programa de Doctorat: "Química Analítica del Medi Ambient i la Pol·lució"

Comprehensive analytical approaches to determine the sources, fate and effects of marine oil spills

Memòria presentada per optar al grau de Doctor per la Universitat de Barcelona per

Jagoš Radović

Directors: Tutor:

Dr. Josep Maria Bayona i Termens
Professor d' Investigació
Dep. Química Ambiental
IDAEA-CSIC

Dr. Sergi Díez i Salvador
Cientific Titular
Dep. Química Ambiental
IDAEA-CSIC

Dr. Fco. Javier Santos
Professor Titular
Facultat de Química
Universitat de Barcelona

Barcelona, 2014

Josep Maria Bayona i Termens, Professor d' Investigació del CSIC i Sergi Díez i Salvador, Científic Titular del CSIC, ambdós membres del Departament de Química Ambiental de l'Institut de Diagnosi Ambiental i Estudis de l'Aigua (IDAEA-CSIC),

CERTIFIQUEM

que els estudis descrits a la present memòria que porta per títol "Comprehensive analytical approaches to determine the sources, fate and effects of marine oil spills", que presenta Jagoš Radović, llicenciat en Química, han estat realizats sota la nostra direcció per optar al Títol de Doctor per la Universitat de Barcelona.

Directors: Tutor:

Dr. Josep Maria   **Dr. Sergi Díez i**   **Dr. Fco. Javier Santos**
Bayona i Termens   **Salvador**
Professor d' Investigació   Cientific Titular   Professor Titular
Dep. Química Ambiental   Dep. Química Ambiental   Facultat de Química
IDAEA-CSIC   IDAEA-CSIC   Universitat de Barcelona

Barcelona, 2014

"Let us learn to dream, gentlemen, and then perhaps we shall learn the truth."

August Kekulé
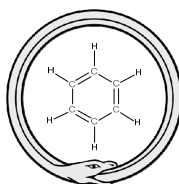
To my family

Mojoj porodici

Acknowledgments

"In every career, your job is to make and tell stories, of course. You will build a body of work, but you will also build a body of affection, with the people you've helped who've helped you back. This is the era of Friends in Low Places. The ones you meet now, who will notice you, challenge you, work with you, and watch your back. Maybe they will be your strength." ~ Robert Krulwich

Although pursuing a PhD seems, at times, as a quite solitary business, now, when the moment has come to reflect the past four years, I realized that to arrive at this point could not have been possible without numerous people that were directly or indirectly supporting me. This will be an attempt to express my gratitude to all of them.

First to be acknowledged are the directors of my thesis, Josep Maria Bayona and Sergi Díez, for giving me an opportunity to come to Barcelona and work in their group. Some people say that joint supervision can be complicated; in my case it was more than complementary and constructive. I could always count on their support and disponibility during this time, both professionally and personally. Their effort and support were particularly important for the timely finalization of this manuscript. Moltes gràcies als dos!

Constructive comments and revisions from the tutor of this thesis, Prof. Francisco Javier Santos and my PhD commission, helped to improve the final manuscript, and are kindly appreciated.

I had a privilege to be introduced to the world of petroleum geochemistry and oil spill forensics by one of the pioneers in these fields, Prof. Joan Albaigés. His contribution to the studies presented in this thesis is profound, and his scientific enthusiasm after such a long career is admirable. Gràcies Joan, ha sigut un plaer!

An important part of this thesis is based on the studies performed during my research stay at Woods Hole Oceanographic Institution, where I had a pleasure to work in Chris Reddy's group, and a unique opportunity to investigate one of the largest oil spill incidents in history, the Deepwater Horizon blowout. Chris, Bob, Christoph, Catherine, Karin, thank you for the friendly reception, enjoyable stay and a fruitful collaboration!

Another research stay I realized at the Department of Marine Environmental Technology, SINTEF. My kind hosts and supervisors during this time were Andy Booth and Alf Melbye. To them, as well as to Marianne, Oddveig, Siv-Hege, and others - tysen takk!

The study presented in the final part of this thesis, could not have been possible without the productive and collegial collaboration with Prof. Romà Tauler, Dr. Kevin V. Thomas, and Dr. Hadi Parastar.

And now for the hard part, to mention, and acknowledge in few words, all those persons who during these four years made my days in the laboratory more easy and productive, and/or with whom I had such good times during *out-of-work* adventures.

Carmen, it's not an exaggeration to say that without you our laboratory would not be able to function normally. Thank you for being always available to resolve any doubt, and helping me to learn the techniques and procedures I needed to realize all the day-to-day tasks in the laboratory. Y sobre todo, gracias por ser tan buena gente!

Victor, thank you for introducing me to the always problematic "Bidi" (GC×GC), and for your company during the long afternoons in the lab 320, especially while writing this thesis.

To the support from "gases-masas", Roser, Dori, María, Inma, many thanks for your help with the instruments!

Núria, I appreciate your collaboration in the studies I present in this thesis. I tried to keep alive the lab's "oil business" after you left! Y per cert, gràcies per introduir-me a Manel, i per ajudar-me amb el català!

Working in a small group of people for a certain amount of time has a curious "side-effect" of converting them from colleagues to good friends. This was the case with Carla, Carolina, Cristal, Diana, Luis, María, and Susana, in whose company some of the best memories of my Barcelona years were made. Guys, thank you for your friendship, for the nights-out, dinners, movies, coffees, hiking, road-trips, parties, birthdays, presents, laughs, tears, discussions, for sharing all the ups and downs in the past years. João and David, thank you for being an integral part of this group (David, special thanks for your help with GIS!). Although the joker called Life already started to separate our paths, I hope it will be good enough to cross them again in the future.

Dani and Carles - xicots, it was so much fun to spend this time with you, too bad we didn't meet few years ago! I will miss the morning coffees with you two (ahora se oye Sr. Chang diciendo HA!...). Carlico, wish you all the best with your thesis, no worries, ets un crack! The Boss from the Badlands, ya lo sabes – born to run, like a rolling stone, so we'll see each other again I am sure. If not in some other part of the world, we'll always have Apolo!

My thanks also go to all the other people that I had pleasure to meet during my time in this group: Tami, Cristina, Yolanda, Riccardo, Wilkinson, Soledad, Gina, Isabel. My sincere apologies to the ones I unwillingly missed.

A special mention goes to the "basicos": my EX-YU girls (CG, SR, HR), Aleksandra, Milica, and Maja with whom I shared all the troubles of "*excomunitarios*", but also so many great times; to Giordano (druže moj!), Maria Luisa, Fabio, Johann, and Stephane. Chic@s, mil gracias!

To all my friends and colleagues in Serbia and around the world, I'm sorry for not contacting more often; it was not because I forgot about you!

Finally, but most importantly, my infinite gratitude goes to my parents and my sister in Serbia, for their unconditional love, encouragement, and patience during this time. Although not physically with me, they were and will be my greatest support. The least thing I can do is dedicate this thesis to them. Hvala vam!

There are cities to be born in, and there are cities to live in. And then, there are cities to fell in love with. The latter was the case with Barcelona and me. To Barcelona and to all the people I shared its streets with:

Adéu, fins sempre, sort!

Contents

Index of tables

Index of figures

Abstract

Despite the positive trends in the past decades, spills from the exploration, extraction and transport of oil remain an important threat to marine and coastal ecosystems.

This thesis deals with all the important aspects of marine oil spills – the sources, environmental fate and possible effects. To allow their comprehensive understanding, different complementary methodologies were used.

Firstly, a physicochemical database of frequently transported crude and refined oils was created using elemental analysis, thin-layer liquid chromatography (TLC) with flame ionization detector (FID) analysis of principal oil compound groups, gas chromatography-mass spectrometry (GC-MS) fingerprinting of polycyclic aromatic hydrocarbons (PAHs) and biomarkers, and available oil assays. This database was then applied to assess their possible fate in the case of a spill, and to model three spill scenarios in different European regional seas using ADIOS2 software from NOAA (National Oceanic and Atmospheric Administration). Fingerprints of selected oils were assessed and statistically compared to discover the most relevant compositional differences that could facilitate the identification of oil spill sources.

Secondly, the GC-MS methodology used to create the fingerprint database of selected oils was evaluated in an international interlaboratory ring test. The objective was to test the capability of this fingerprinting methodology to identify the type and source of weathered (biodegraded) oil samples.

Thirdly, the weathering of oil samples from *Prestige* and *Deepwater Horizon* spills, in particular the photooxidation, was studied. Samples weathered in field and in laboratory experiments were analyzed using TLC-FID, GC-MS, comprehensive two dimensional gas chromatography (GC×GC) with FID, and Fourier transform infrared spectrometry (FT-IR) to discover compositional changes on the bulk level as well as on the molecular level. PAHs and triaromatic steranes (TAS) were of particular interest, as well as the effects of the photooxidation on the robustness of the oil fingerprinting methodology.

Finally, the effects of selected fresh and weathered (evaporated, photooxidized) crude and refined oils were studied, using the effect-directed analysis (EDA). The samples were sequentially fractionated using open-column liquid chromatography and

normal-phase semipreparative HPLC, and the obtained fractions were subjected to bioassays to test their AhR agonist and AR antagonist activity. The most active fractions were then analyzed using GC×GC coupled to time-of-flight mass spectrometry (TOFMS), and this data was related to bioassay results using N-way partial least square (N-PLS) chemometric model, in order to identify the compounds responsible for the observed effects.

Resumen

A pesar de las tendencias positivas en las últimas décadas, los vertidos ocasionados por la exploración, extracción y transporte de petróleo siguen siendo una importante amenaza para los ecosistemas marinos y especialmente costeros.

Esta Tesis se ocupa de todos los aspectos importantes sobre los vertidos marinos de petróleo: el origen, el destino ambiental y sus posibles efectos. Para permitir su comprensión global, se utilizaron diferentes metodologías complementarias.

En primer lugar, se ha creado una base de datos físico-químicos de diferentes petróleos (crudos y refinados) que se transportan frecuentemente usando el análisis elemental, la cromatografia en capa fina (TLC) acoplada a un detector de ionización de llama (FID) de los principales grupos de compuestos de petróleo, la toma de huellas químicas de los hidrocarburos aromáticos policíclicos (HAP) y los biomarcadores mediante cromatografía de gases acoplada a espectrometría de masas (GC-MS), y ensayos de petróleo disponibles. A continuación, se aplicó esta base de datos para evaluar su posible destino en el caso de un vertido, y para modelar tres escenarios de vertidos en diferentes mares regionales europeos usando el software ADIOS2 de la Administración Nacional Oceánica y Atmosférica (NOAA). Las huellas químicas de los petróleos seleccionados fueron evaluadas y comparadas estadísticamente para investigar las diferencias de composición más relevantes que podrían facilitar la identificación del origen de vertido.

En segundo lugar, la metodología de GC-MS utilizada para crear la base de datos de las huellas químicas de los petróleos seleccionados se ha evaluado en una prueba interlaboratorio internacional. El objetivo fue investigar la capacidad que tiene esta metodología de toma de huellas químicas para identificar el tipo y el origen de las muestras envejecidas (biodegradadas) de petróleo.

En tercer lugar, se ha estudiado el envejecimiento de las muestras de petróleo de los vertidos de *Prestige* (2002) y de la plataforma *Deepwater Horizon* (2010), en particular, debido a la fotooxidación. Se analizaron muestras envejecidas en el campo y en experimentos de laboratorio mediante TLC-FID, GC-MS, cromatografía de gases bidimensional integrada (GC×GC) acoplada a un FID, y espectroscopia infrarroja por transformada de Fourier (FT-IR) para investigar los cambios de composición tanto a nivel global como a nivel molecular. Los HAP y esteranos triaromáticos fueron de

especial interés, así como los efectos de la foto-oxidación en la robustez de la metodología de toma de huellas químicas de petróleo.

Finalmente, se estudiaron los efectos de las muestras no tratadas y envejecidas (evaporadas, fotooxidadas) de los petróleos crudos y refinados seleccionados, utilizando el análisis dirigido por los efectos tóxicos (EDA). Las muestras se fraccionaron secuencialmente usando la cromatografía líquida en columna abierta y la cromatografía líquida de alta eficacia (HPLC) semipreparativa en fase normal. Las fracciones obtenidas se sometieron a bioensayos para investigar su actividad agonista de los receptores AhR y la actividad antagonista de los receptores AR. En el siguiente paso, las fracciones más activas fueron analizadas mediante GC×GC acoplada a espectrometría de masas en tiempo de vuelo (TOFMS), y estos datos se relacionaron con los resultados de los bioensayos utilizando un modelo quimiométrico de regresión por mínimos cuadrados parciales en N direcciones (N-PLS), con el fin de identificar los compuestos responsables de los efectos observados.

Resum

Malgrat les tendències positives en les últimes dècades, els abocaments ocasionats per l'exploració, extracció i transport de petroli segueixen sent una important amenaça per als ecosistemes marins i especialment els costaners.

Aquesta Tesi s'ocupa de tots els aspectes importants sobre els abocaments marins de petroli: l'origen, el destí ambiental i els seus possibles efectes. Per permetre la seva comprensió global, s'han utilitzat diferents metodologies complementàries.

En primer lloc, s'ha creat una base de dades fisicoquímiques de diferents petrolis (crus i refinats) que es transporten freqüentment, mitjançant l'anàlisi elemental, la cromatografia de capa fina (TLC) amb detecció per ionització de flama (FID) dels principals grups de compostos de petroli, la presa d'empremtes químiques d'hidrocarburs aromàtics policíclics (HAP) i biomarcadors mitjançant la cromatografia de gasos acoblada a un espectròmetre de masses (GC-MS), així com assaigs de petroli disponibles. A continuació, s'ha aplicat aquesta base de dades per avaluar el seu possible destí en el cas d'un vessament, i per modelar tres escenaris d'abocaments en diferents mars regionals europeus fent servir el programari ADIOS2 de Administració Nacional Oceànica i Atmosfèrica (NOAA). Les empremtes químiques dels petrolis seleccionats s'han avaluat i comparat estadísticament per investigar les diferències de composició més rellevants que podrien facilitar la identificació del abocament.

En segon lloc, s'ha avaluat la metodologia de GC-MS utilitzada per crear la base de dades de les empremtes químiques dels petrolis seleccionats s'ha avaluat en una prova interlaboratori internacional. L'objectiu va ser investigar la capacitat d'aquesta metodologia de presa d'empremtes químiques per identificar el tipus i l'origen de les mostres envellides (biodegradades) de petroli.

En tercer lloc, s'ha estudiat l'envelliment de les mostres de petroli dels abocaments de *Prestige* (2002) i de la plataforma *Deepwater Horizon* (2010), en particular, a causa de la fotooxidació. S'han analitzat mostres envellides al camp i en experiments de laboratori mitjançant TLC-FID, GC-MS, la cromatografia de gasos bidimensional integrada (GC×GC) amb FID, i la espectroscòpia infraroja per transformada de Fourier (FT-IR) per investigar els canvis de composició a nivell global com nivell molecular. Els HAP i esterans triaromàtics van ser d'especial interès, així

com els efectes de la fotooxidació en la robustesa de la metodologia de presa d'empremtes químiques de petroli.

Finalment, s'han estudiat els efectes de les mostres no tratades i envellides (evaporades, fotooxidades) dels petrolis crus i refinats seleccionats, utilitzant l'anàlisi dirigida pels efectes tòxics (EDA). Les mostres es van fraccionar seqüencialment per cromatografia líquida en columna oberta i la cromatografia líquida d'alta eficacia (HPLC) semipreparativa en fase normal. Les fraccions obtingudes s'han sotmès a bioassajos per investigar l' activitat antagonista dels receptors AhR i l'activitat antagonista dels receptors AR. En el següent pas, les fraccions més actives s'han analitzat mitjançant GC×GC acoblada a un espectròmetre de masses de temps de vol (TOFMS), i aquestes dades s'han relacionat amb els resultats dels bioassajos utilitzant un model quimiomètric de regressió per mínims quadrats parcials en N direccions (N-PLS), per tal d'identificar els compostos responsables dels efectes observats.

List of acronyms

AhR	Aryl hydrogen receptor
API	American Petroleum Institute
AR	Androgen receptor
BTEX	Benzene, toluene, ethylbenzene and xylenes
CEN	European Committee for Standardization
cSt	Centistokes
DCM	Dichloromethane
DWH	Deepwater Horizon
EDA	Effect-directed analysis
EIC	Extracted ion chromatogram
EMSA	European Maritime Safety Agency
EPA	Environmental Protection Agency
FID	Flame ionization detector
FT-ICR	Fourier transform ion cyclotron resonance
FT-IR	Fourier transform infrared
GC	Gas chromatography
GC×GC	Comprehensive two-dimensional gas chromatography
HFO	Heavy fuel oil
HPLC	High-performance liquid chromatography
IGT	Isobaric gas-tight
IR	Infrared
MBOE	Million Barrels of Oil Equivalent
MS	Mass-spectrometry
MW	Macondo well
MWV	Microwave
NOAA	National Oceanic and Atmospheric Administration
N-PLS	N-way partial least square
NSC	North Sea crude
NSO	Nitrogen, sulfur and oxygen
PAH-CALUX	PAH Responsive Chemically Activated LUciferase eXpression
PAHs	Polycyclic aromatic hydrocarbons
PCA	Principal component analysis
QSAR	Quantitative structure–activity relationship
ROVs	Remote operated vehicles
SAR	Synthetic Aperture Radar
SARA	Saturates–aromatics–resins–asphaltenes
TAS	Triaromatic steranes
TIC	Total ion chromatogram
TLC	Thin-layer chromatography
TOFMS	Time-of-flight mass spectrometry
UCM	Unresolved complex mixture
UV	Ultraviolet
VOCs	Volatile organic compounds
YAS	Yeast Androgen Screen

Objectives and structure of the thesis

The main goal of this thesis was to develop and apply a comprehensive set of methods that can be used to determine and/or assess all the important aspects of marine oil spills: their sources, environmental fate, and the possible effects.

General objectives

1. To chemically characterize frequently transported crude and refined oils and obtain information that can be used in the case of a spill to identify the selected oils and to assess their environmental fate.
2. To apply the oil fingerprinting methodology to identify the type, possible source(s) and weathering transformations of marine oil spill.
3. To assess the effects of photooxidation on selected oils and its implications for oil fingerprinting.
4. To analyze the toxic effects of the selected fresh and weathered oils and to identify the responsible compounds.

Specific objectives

In order to fulfill the abovementioned general objectives, the following specific objectives had to be accomplished:

- To compile the physicochemical data on the selected 21 oils, from available oil assays, or by chemical analysis by means of elemental analysis, thin-layer chromatography coupled to flame ionization detector (TLC-FID), and fingerprinting using gas chromatography coupled to mass spectrometry (GC-MS).
- To utilize the created oil database to assess the fate and effects in a case of a spill.
- To use the database as an input to model the short-term fate of the selected oils under the environmental conditions of three distinct regional European seas.
- To statistically analyze the created database of fingerprinting ratios and determine their significance in oil identification.

- To apply the GC-MS fingerprinting methodology in a case study (interlaboratory ring test) and evaluate its capability to determine the type and the source(s) of a weathered (biodegraded) oil spill.

- To obtain weathered samples of selected oils by means of evaporation and irradiation (natural and simulated Sunlight).

- To assess the effects of the photooxidation on the bulk and molecular composition of selected oils and evaluate its implications for the marine oil spill fingerprinting.

- To apply the effect-directed analysis (EDA) for the identification of the responsible toxic compounds in fresh, evaporated and irradiated oils. This included chemical fractionation, bioassays (AhR and AR), chemical characterization of the obtained fractions by means of comprehensive two-dimensional gas chromatography (GC×GC), the development of an N-way partial least square (N-PLS) model to relate chemical and bioassay data, and the confirmation using quantitative structure–activity relationship (QSAR) tools.

Structure of the thesis

This thesis is structured in five Chapters. **Chapter I** of the thesis is introductory, providing theoretical and environmental contextualization of the main marine oil pollution topics, and a general review of methodologies used for oil analysis. **Chapter II** contains a detailed description of the materials and methods used in the presented studies.

In the **Chapter III**, the results and discussion of the performed studies are presented as follows:

In the *Section III.1.*, a general physicochemical characterization of various frequently transported oils was performed, with the aim to assess their potential environmental fate and effects, and facilitate the identification of the potential polluters (sources) in the case of a spill. In this way, a more proactive approach for the oil spill risk assessment strategies is introduced;

Section III.2. presents the results of the annual interlaboratory ring test with the aim to evaluate and improve the existing GC-MS oil fingerprinting methodology, particularly its fidelity in spill source identification. In this respect, the methodology that

was previously used to fingerprint various fresh oils was now evaluated in terms of its ability to identify the sources of weathered (biodegraded) oil spills. Potential of the described methodology to detect various weathering processes was demonstrated;

Section III.3. continues further with in-depth elucidation of weathering transformations of oil, in particular the effects of photooxidative weathering, and the possible implications that this process can have on the reliability of oil fingerprinting methodologies. Compositional changes on bulk level and detail molecular level were demonstrated, and the possible mechanisms of the observed transformations are discussed;

Section III.4. deals with the last important aspect of oil spills - their effects, and the compounds that are the main contributors to the overall oil toxicity. It presents an innovative approach, based on the effect-directed analysis (EDA) strategy, which was extended by introducing additional chemometric modeling to relate the chemical composition of oil with the measured effects.

Chapter IV contains the main conclusions of the thesis. In the **Chapter V**, a summary of the thesis in Spanish language is provided.

Finally, **Annexes** contain supplementary information, graphs and tables related to the presented results. The content of this thesis is related to peer-reviewed articles, the list of which is provided in the Annex **D**.

Chapter I.

Introduction

I.1. Past, present and future of oil

Crude oil is also called petroleum which literally translates as "rock oil" [from the Greek petros (rock) and elaion (oil)], and it was known to human civilization since its beginnings. Different forms of oil, such as asphalt and bitumen were used as early as 6,000 years ago, in Mesopotamia, Persia, ancient China and Egypt, for different purposes, e.g. caulking for ships, mortar, waterproofing and adhesive agent, or medicine (Abraham, 1960; Clay, 1922; Zhang, 1997). However, the modern oil industry had not been born until the late 19th century, when the oil extraction and refining started in Pennsylvania, to produce kerosene used as lighting fuel in lamps (Bell, 1946). Since then, the production and use of oil has grown exponentially, with unprecedented economical, technological, geopolitical, and environmental consequences, to create modern petroleum-based society (Yergin, 2011). Despite the continuous predictions that the oil era is coming to its end (Kerr, 2011; Maggio and Cacciola, 2012), advances in extraction technology (e.g. fracking, deep-sea drilling), use of non-conventional oil sources (e.g. tar sands, oil shales), and the exploration of the regions that are becoming accessible due to the global warming (e.g. Arctic), indicate that petroleum will remain the primary energy source in the foreseeable future (**Figure I-1**) (OPEC, 2012; Yergin, 2013).
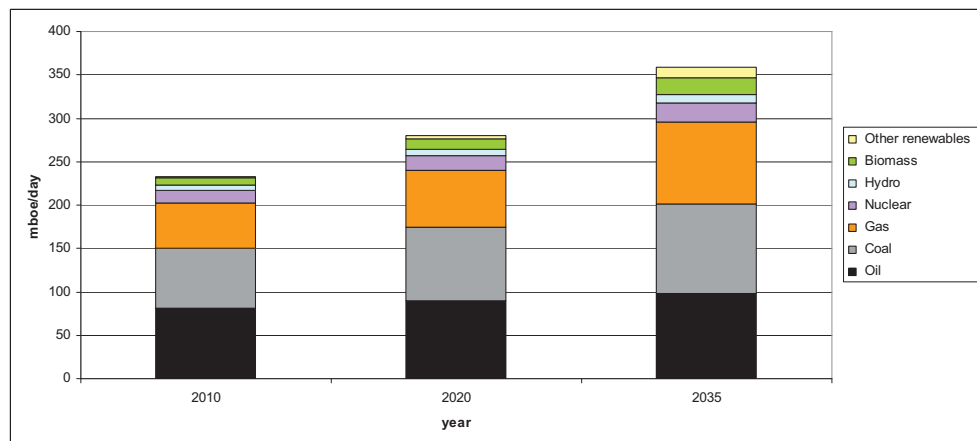
Figure I-1 Energy use by source type [adapted from OPEC (2012)].

I.2. Oil composition and properties

Crude oil, or petroleum, is a naturally occurring mixture of hydrocarbons, generally in a liquid state, which may also include compounds of sulfur, nitrogen, oxygen, metals, and other elements (Speight, 2002). Thus, the petroleum elemental composition usually varies in the following ranges (Speight, 2006):

- Carbon, 83% to 87%;
- Hydrogen, 10% to 14%;
- Nitrogen, 0.1% to 2.0%;
- Oxygen, 0.05% to 1.5%;
- Sulfur, 0.05% to 6.0%;
- Metals (Ni and V), <1000 ppm.

The **hydrocarbon** components of petroleum can be divided into the following three classes (Speight, 2006; Tissot and Welte, 1984):

1. Paraffins, which are saturated hydrocarbons with straight or branched chains, but without any ring structure (also known as aliphatic hydrocarbons);

2. Naphthenes, which are saturated hydrocarbons containing one or more rings, each of which may have one or more paraffinic side chains (also known as alicyclic hydrocarbons);

3. Aromatics, which are hydrocarbons containing one or more aromatic nuclei, i.e. monoaromatic and polycyclic aromatic hydrocarbons (PAHs), which may be substituted with naphthene rings or paraffinic side chains. In fact, PAHs in oil are dominated by the C_1 to C_4 alkylated homologues of the parent compounds, in particular naphthalene, phenanthrene, dibenzothiophene, fluorene and chrysene (Wang et al., 1999).

The relationship between these different hydrocarbon classes is dynamic and changing during formation, maturation, and in situ alteration of petroleum, occurring through complex evolutional sequence of reactions affecting the initial organic matter (i.e. kerogen) (**Figure I-2**) (Speight, 2006; Tissot and Welte, 1984).

Paraffins

$CH_3(CH_2)_4CH_3$

$+H_2$ $-H_2$

Naphthenes   Aromatics

$-H_2$

$+H_2$

Polynuclear
Aromatics

Polynaphthenes

$-H_2$

$+H_2$
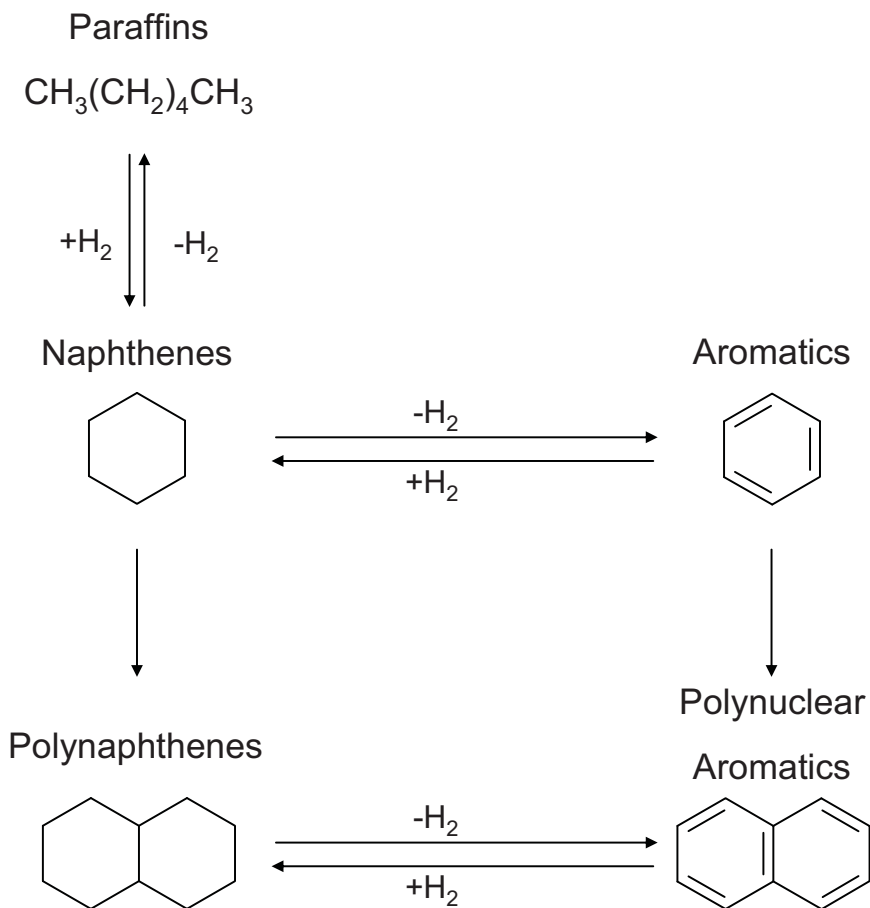
Figure I-2 Simplified scheme of the hydrocarbon types interrelationships during petroleum formation (Speight, 2006).

The **sulfur** is present predominantly in the form of thiophene and its derivatives, e.g. benzothiophene, dibenzothiophene, benzonaphthothiophene (**Figure I-3**). Oils containing less than 0.5% of sulfur are usually known as "sweet", while the ones containing more sulfur are called "sour" oils (API, 2011).

Oxygen is present in different forms, e.g. alcohols (R–OH), phenols (Ar–OH), ethers (R–O–R'), acids (e.g. naphthenic) (R–CO_2H, Ar–CO_2H), esters (R–CO_2R, Ar–CO_2R), ketones (R_2C=O). In the environment, the content of oxygenated compounds in oil can increase due to weathering processes (e.g. biodegradation, photooxidation) (Aeppli et al., 2012; McKenna et al., 2013).
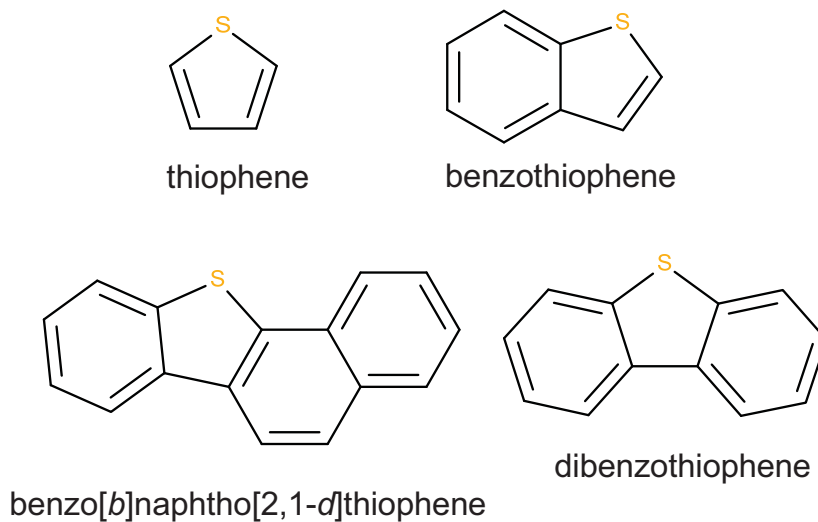
Figure I-3 Sulfur compounds found in oil.

The ***nitrogen*** is also present in the form of heterocyclic ring systems, such as carbazoles, or quinolines, and their derivatives (**Figure I-4**).
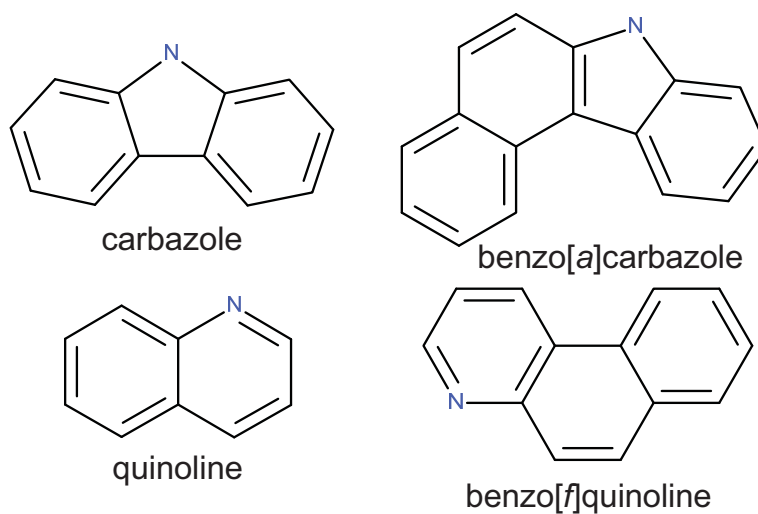
Figure I-4 Nitrogen compounds found in oil.

High molecular weight polycyclic compounds (>400-500 amu, approx.) containing nitrogen, sulfur and oxygen (NSO) are often referred to as resins and asphaltenes. They are more polar and insoluble in n-hexane, which is often used to separate them from saturate (paraffinic and naphthenic) and aromatic fractions, using the so called **SARA** (**s**aturates–**a**romatics–**r**esins–**a**sphaltenes) fractionation procedure (Speight, 2006; Tissot and Welte, 1984). These four major oil fractions are interdependent and their relative proportions can change due to natural or refining processes but always sum up to a total of 100%. For example, the **Figure I-5** shows the relative content of major hydrocarbon groups in 636 crude oils.
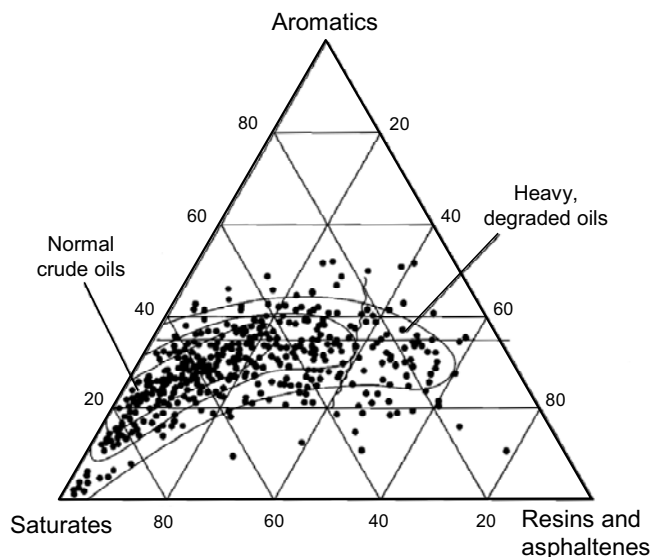
Figure I-5 Ternary diagram showing the gross composition of 636 crude oils: saturated hydrocarbons, aromatic hydrocarbons, resins and asphaltenes (wt% in the fraction boiling above 210 °C) [adapted from (Tissot and Welte, 1984)].

Metals are also present in petroleum either as salts of carboxylic acids or as porphyrin chelates (**Figure I-6**). They are derived from the parent compound called porphine formed of four pyrrole molecules joined by methine (–CH=) bridges. Often, hydrogens on the ring carbons are substituted to create different porphyrin compounds (e.g. benzoporphyrins and tetrahydrobenzoporphyrins) (Speight, 2006). Nickel (Ni) and vanadium (V) are most frequent and abundant metals found in oil, but others such as

lead, manganese, barium, boron, cobalt and molybdenum could also be found occasionally (Bailey et al., 2002).
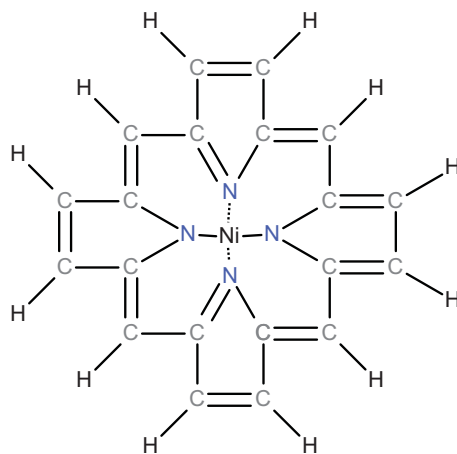
Figure I-6 Nickel chelate of porphyrine.

In order to be used commercially, crude oil compounds must be separated into different fractions based on their boiling points, via distillation process in refineries. **Figure I-7** shows distillation curves of main hydrocarbon groups, and oil fractions cutoffs. Obtained petroleum products can be used directly as energy sources ("straight-run gasoline", fuel oil, etc.), or are modified chemically (e.g. cracking) to obtain more efficient fuels, such as high-octane gasoline (Bailey et al., 2002). Finally, oil derived hydrocarbons can be converted to petrochemical compounds, such as monomers, polymers, solvents, and others, to be used in myriad of applications and products (Bailey et al., 2002; Speight, 2002).

Density (or specific gravity) is the mass of oil per unit volume at 15 °C, typically expressed as $kg \cdot m^{-3}$ or $kg \, L^{-1}$. It is measured using a hydrometer, pycnometer, or more modern digital density meter. Often, it is expressed as API (American Petroleum Institute) gravity, a measure which can be used to roughly estimate the quality of oil, i.e. approximate hydrocarbon composition (paraffinic, naphthenic, or intermediate) (Speight, 2006). It is calculated from the specific gravity, using the following expression:

API gravity (°) = (141.5/sp.gr.)-131.5; where sp.gr. is specific gravity (in $kg \cdot m^{-3}$). The lower specific gravity, the higher is the API gravity.
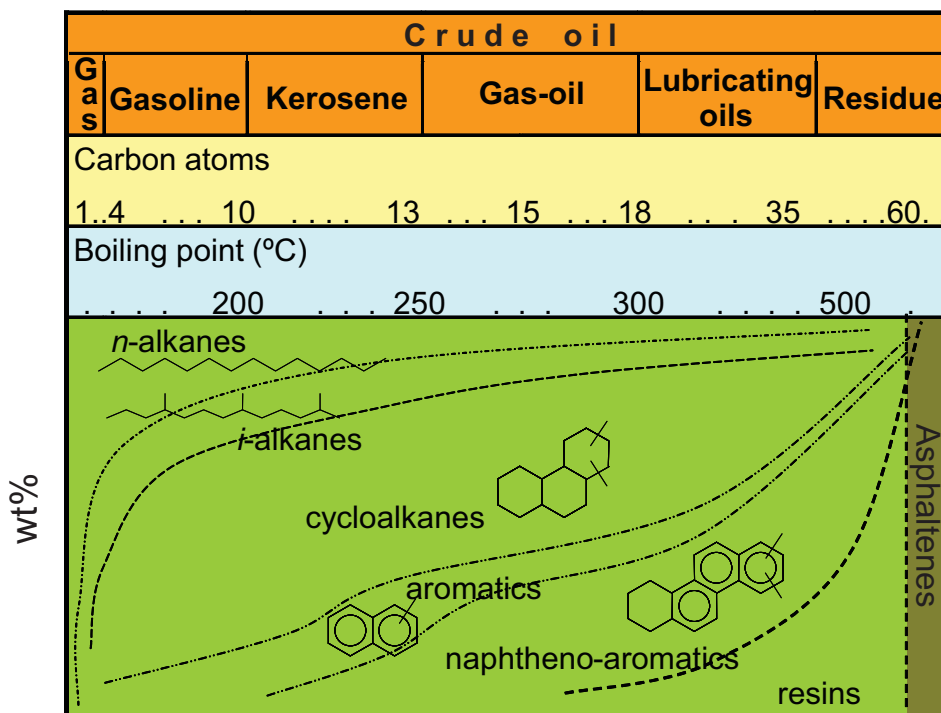
Figure I-7 Distribution of various petroleum compounds based on their boiling points [modified from (Speight, 2006)].

Viscosity and pour point are the measure of flow characteristics of petroleum at low temperatures. Viscosity is usually determined at different temperatures (e.g. 25 °C) by measuring the time for a volume of liquid to flow under gravity through a calibrated glass capillary viscometer, and is expressed in centistokes (cSt) or Saybolt Universal seconds (SUS) (Speight, 2002). The pour point of petroleum is an index of the lowest temperature at which the crude oil will flow under specified conditions.

Crude oils with lower densities and viscosities, and thus higher API gravities, usually contain higher levels of naphtha (gasoline-range hydrocarbons) with predominately volatile paraffinic hydrocarbons, which can be processed readily to produce gasoline and are considered as "light" crudes (NOAA, 1996). "Heavy" crude oils are more viscous, have higher boiling ranges and higher densities, and thus lower API gravities. They are usually rich in aromatics and tend to contain more heteroatom-containing (NSO and metal containing) constituents (Speight, 2002).

I.3. Oil inputs to the sea

An estimated 1.2 million metric tonnes of oil enters oceans every year from variety of sources, both natural and anthropogenic (**Table I-1**) (GESAMP, 2007).

Table I-1 Annual oil inputs to the sea.

Source	tonnes/year
Unknown	200
Offshore	19,750
Small craft activity	53,000
Coastal facilities	115,000
Ships	457,000
Natural seeps	600,000
Total	1,244,950

As shown in **Figure I-8**, almost half of that oil (48%) comes from natural oil seeps, and the other half is released from human sea-based activities (shipping, coastal facilities, offshore oil production, etc.) (GESAMP, 2007). The volume of maritime (seaborne) trade has risen in the past decades as it affords cost effective global transport. During recent years, it amounted to about 8 billion metric tonnes of goods annually, of which more than 30% were crude oils and petroleum products (UNCTAD, 2010). Therefore, the shipping is the main anthropogenic source of oil released to the oceans (37%) (**Figure I-8**).
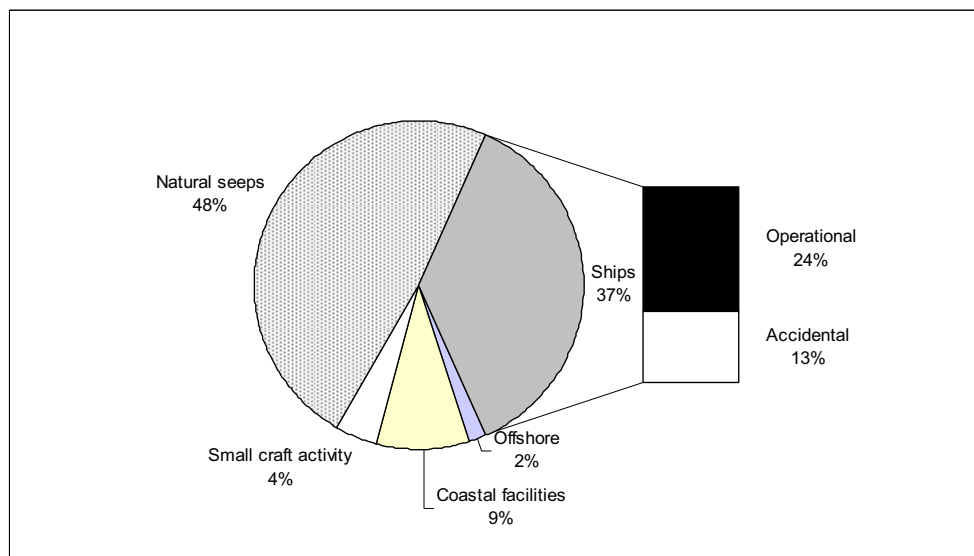
Figure I-8 Breakdown of marine oil inputs by source.

One part of this oil is released during ship accidents (collisions, grounding, etc.), which often occur in busy maritime routes (**Figure I-9**), particularly in locations with heavy traffic and/or challenging natural conditions such as the Straits of Gibraltar, Bosphorus, and Hormuz, Suez Channel, Atlantic coast of the Iberian Peninsula, the English Channel and parts of Baltic and North Sea, and others (EMSA, 2010; Rodrigue, 2013). This is corroborated in **Figure I-10**, which shows the locations of largest marine oil spills in recent history, majority of which occurred along those routes. The volume of the oil spilled in these incidents is given **Table I-2**, showing that some of the largest spills in history are very recent, such as the *Deepwater Horizon* (*DWH*) spill in 2010, and demonstrating that the risk of major oil incidents is constantly present.
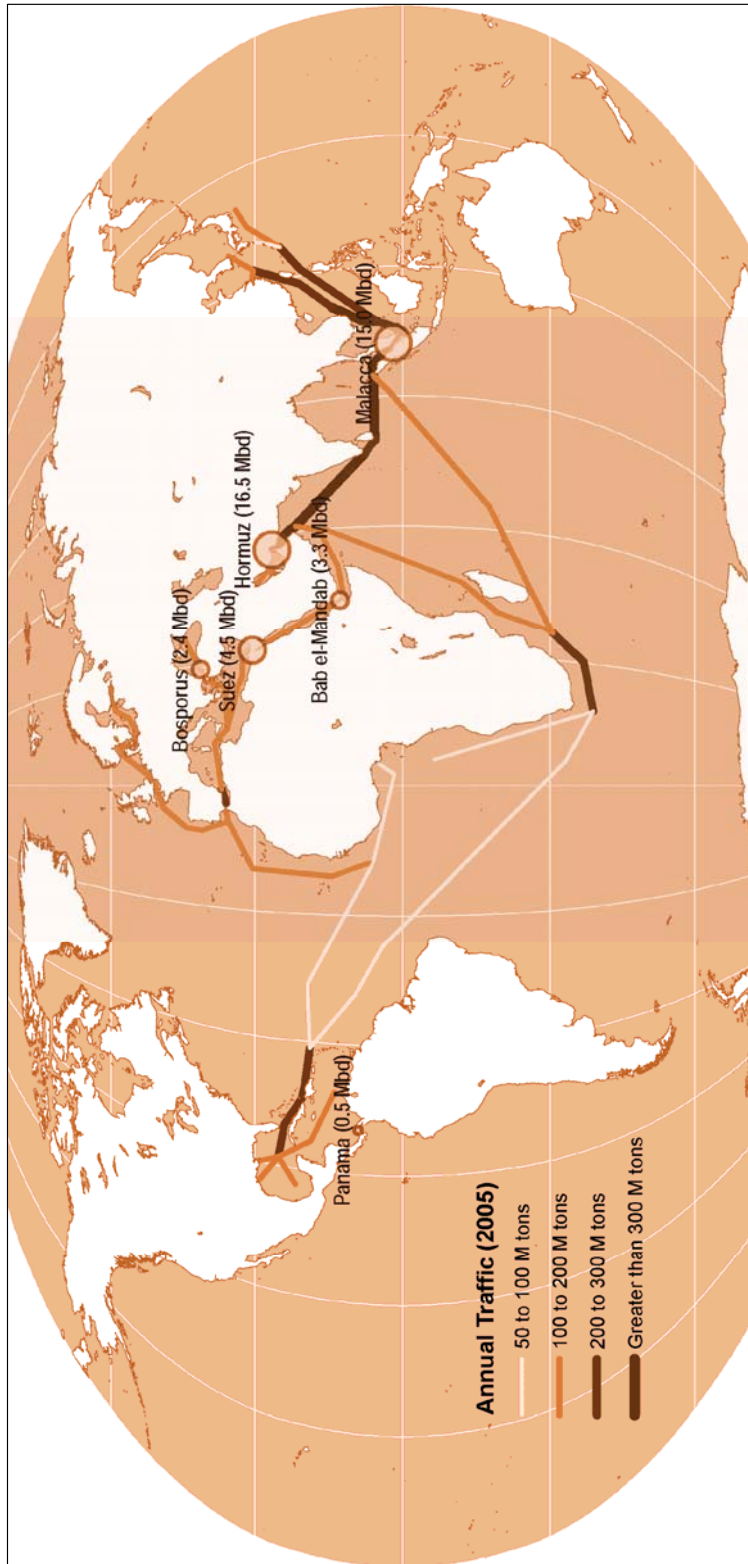
Figure I-9 Major oil flows and chokepoints (EIA, 2012; ITOPF, 2013; Rodrigue, 2013).
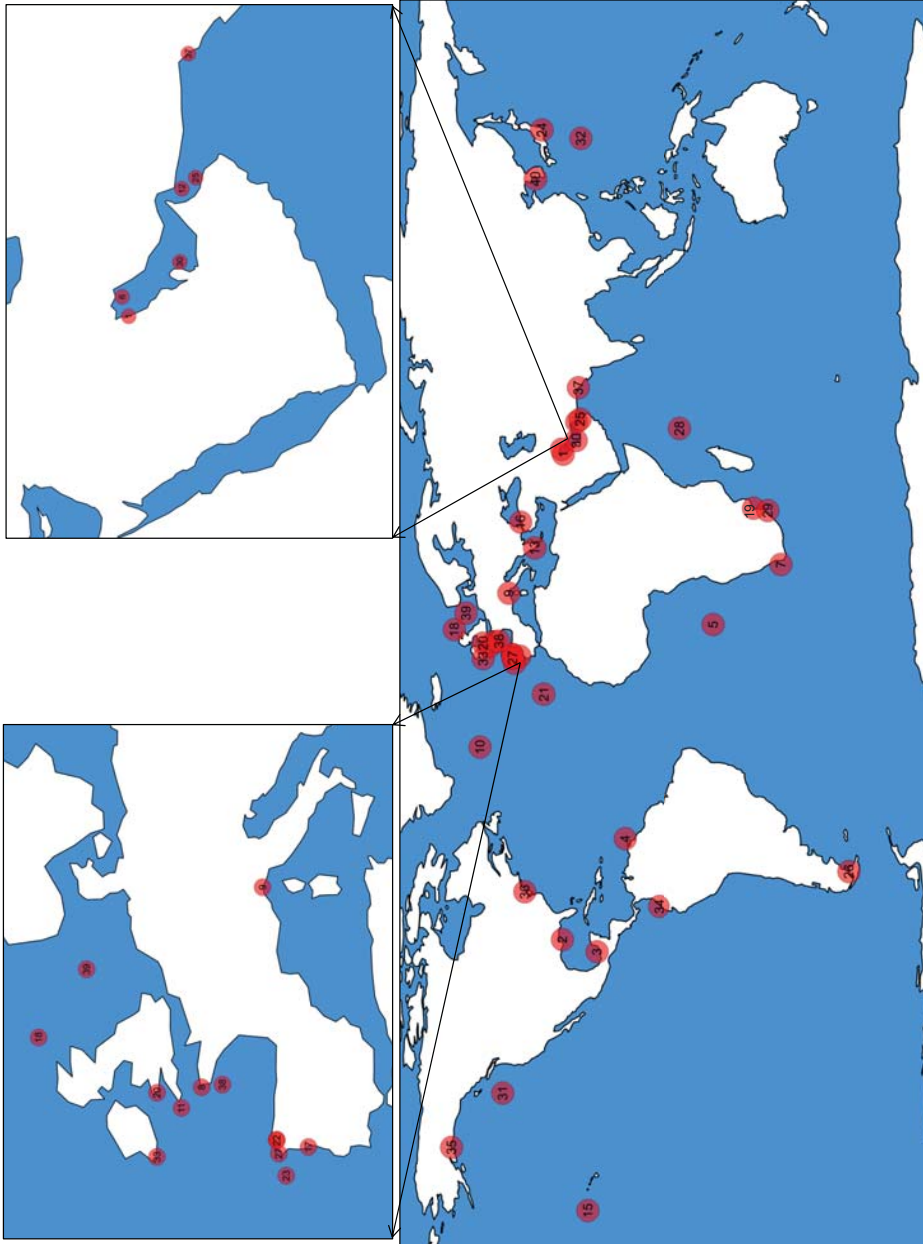
Figure I-10 Locations of major marine oil spills in history (see Table I-2 for more details).

Table I-2 Major marine oil spills in history (Cedre, 2013; CTX, 2013; Environment Canada, 2013; ITOPF, 2013; NOAA, 2013; Oil Rig Disasters, 2013).

	Spill	Date	Location	Type	Cause	Volume spilled (low-high est.) tonnes	barrels
1	Gulf War oil spill	21 Jan 1991 - May 1991	Persian Gulf	Oil wells	War	546,000 - 1,500,000	4,002,180 - 10,995,000
2	BP Deepwater Horizon	20 Apr 2010 - 15 Jul 2010	Gulf of Mexico	Oil well	Blowout	400,000 - 700,000	2,932,000 - 5,131,000
3	Ixtoc I	3 Jun 1979 - 23 Mar 1980	Gulf of Mexico	Exploratory oil well	Drilling error, blowout	454,000 - 480,000	3,327,820 - 3,518,400
4	Atlantic Empress/Aegean Captain	19 Jul 1979 - 2 Aug 1979	Trinidad and Tobago	Oil tanker	Ship collision	276,000 - 287,000	2,023,080 - 2,103,710
5	ABT Summer	28 May 1991	700 nautical miles off Angola	Oil tanker	Explosion, fire, sank	260,000	1,905,800
6	Nowruz oil field	4 Feb 1983 - May 1985	Persian Gulf	Oil well	War, tanker-platform collision	250,000 - 260,000	1,832,500 - 1,905,800
7	Castillo de Bellver	5 Aug 1983	Saldanha Bay, South Africa	Oil tanker	Caught fire, broke in two	254,000	1,861,820
8	Amoco Cadiz	16 Mar 1978	Portsall Rocks, Brittany, France	Oil tanker	Ran aground in bad weather	223,000 - 229,000	1,634,590 - 1,678,570
9	Haven	11 Apr 1991	Mediterranean Sea near Genoa, Italy	Oil tanker	Caught fire while anchored, exploded	141,000 - 144,000	1,033,530 - 1,055,520
10	Odyssey	10 Nov 1988	700 nautical miles off Nova Scotia, Canada	Oil tanker	Broke in two in bad weather	132,000	967,560
11	Torrey Canyon	18 Mar 1967	Scilly Isles, England	Oil tanker	Navigation error, ran aground	119,000 - 122,000	872,270 - 894,260
12	Sea Star	19 Dec 1972	Gulf of Oman	Oil tanker	Ship collision	115,000 - 121,000	842,950 - 886,930
13	Irenes Serenade	23 Feb 1980	Navarino Bay, Greece	Oil tanker	Explosion while anchoring	100,000 - 103,000	733,000 - 754,990
14	Urquiola	12 May 1976	A Coruña, Spain	Oil tanker	Ran aground	96,000 - 101,000	703,680 - 740,330
15	Hawaiian Patriot	23 Feb 1977	300 nautical miles off Honolulu, Hawaii	Oil tanker	Explosion, fire, broke in two	95,000 - 101,000	696,350 - 740,330
16	Independenta	15 Nov 1979 - 14 Dec 1979	Bosphorus, Turkey	Oil tanker	Ship collision, caught fire and ran aground	95,000	696,350
17	Jakob Maersk	29 Jan 1975	Leixoes, Portugal	Oil tanker	Ran aground while entering port	85,000 - 88,000	623,050 - 645,040
18	Braer	5 Jan 1993	Shetland Islands, UK	Oil tanker	Engine failure, ran aground in bad weather	84,700 - 86,200	620,851 - 631,846
19	Katina P	16 Apr 1992	Maputo, Mozambique	Oil tanker	Storm damage	72,600	532,158
20	Sea Empress	15 Feb 1996	Milford Haven Bay, Wales	Oil tanker	Ran aground	72,400	530,692

Table I-2 contd.

	Spill	Date	Location	Type	Cause	Volume spilled (low-high est.) tonnes	barrels
21	Khark 5	19 Dec 1989	400 miles north of the Canary Islands	Oil tanker	Fire, explosion	62,000 - 80,000	454,460 - 586,400
22	Aegean Sea	3 Dec 1992	A Coruña, Spain	Oil tanker	Ran aground in bad weather, caught fire	67,000 - 74,600	491,110 - 546,818
23	Prestige	13 Nov 2002 - 19 Nov 2002	Bay of Biscay, Galicia, Spain (170 miles west of Vigo)	Oil tanker	Heavy seas	63,000 - 77,000	461,790 - 564,410
24	Yuyo Maru 10	9 Nov 1974	Tokyo Bay	Oil tanker	Ship collision	68,000	498,440
25	Assimi	7 Jan 1983	Gulf of Oman	Oil tanker	Fire, explosion	51,600	378,228
26	Metula	9 Aug 1974	Eastern Strait of Magellan, Chile	Oil tanker	Ran aground	50,000 - 53,000	366,500 - 388,490
27	Andros Patria	31 Dec 1978	Bay of Biscay, France	Oil tanker	Fire, explosion	50,000	366,500
28	Ennerdale	1 Jun 1970	Seychelles	Oil tanker	Grounding	44,800 - 47,000	328,384 - 344,510
29	World Glory	13 Jun 1968	South Africa	Oil tanker	Broke up in bad weather	45,500	333,515
30	Pericles GC	9 Dec 1983	Persian/Arabian Gulf	Oil tanker	Fire, explosions, sank	39,000 - 47,000	285,870 - 344,510
31	Mandoil II	28 Feb 1968	550km west of Oregon	Oil tanker	Ship collision	40,000 - 43,300	293,200 - 317,389
32	British Ambassador	10 Jan 1975	North Pacific	Oil tanker	Engine room leak	40,000	293,200
33	Betelgeuse	8 Jan 1979	Bantry Bay, Ireland	Oil tanker	Explosion while unloading	40,000	293,200
34	St. Peter	4 Feb 1976	30 miles west of Cabo Mangalares, Colombia	Oil tanker	Fire, sank	38,000	278,540
35	Exxon Valdez	24 Mar 1989	Bligh Reef in Prince William Sound, Alaska	Oil tanker	Ran aground	37,000 - 38,800	271,210 - 284,404
36	Corinthos	31 Jan 1975	Delaware River, Marcus Hook, Pennsylvania	Oil tanker	Ship collision	35,700 - 36,200	261,681 - 265,346
37	Tasman Spirit	28 Jul 2003	Karachi Port, Pakistan	Oil tanker	Ran aground at port entrance	27,000 - 30,000	197,910 - 219,900
38	Erika	12 Dec 1999	Bay of Biscay, France	Oil tanker	Broke in two in bad weather	19,000 - 28,000	139,270 - 205,240
39	Ekofisk Bravo	22 Apr 1977	North Sea	Oil well	Blowout	15,000 - 27,600	109,950 - 202,308
40	Hebei Spirit	8 Dec 2007	10 km off the coast of South Korea, west of Taean county	Oil tanker	Ship collision	9,000 - 10,800	65,970 - 79,164

However, due to the increased safety of navigation and ships' technical standards (e.g. double hulled tankers) the number of such accidents was constantly decreasing in the past few decades, from an average of about 24 incidents per year in the 1970s to just over three per year in the last ten years (**Figure I-11**) (ITOPF, 2013).
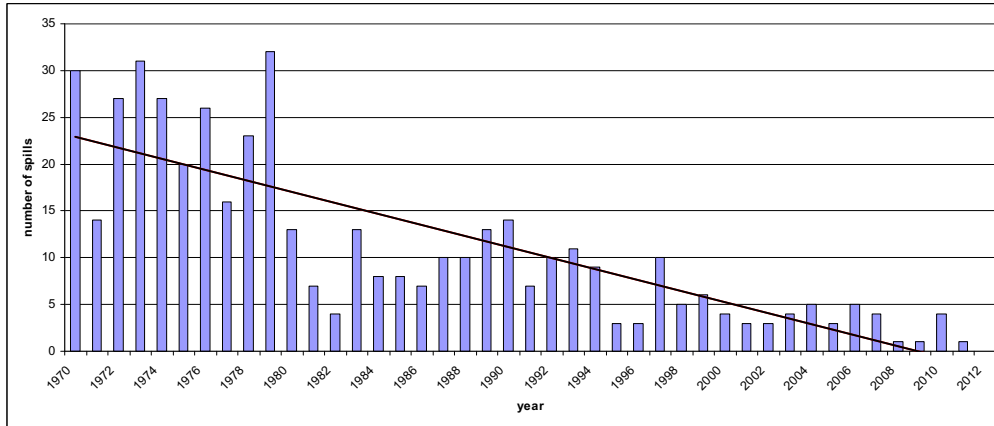
Figure I-11 The number of tanker spills per year [adapted from [(ITOPF, 2013)].

On the other hand, the majority of oil pollution from ships (24%) comes from daily routine operations such as bunkering, legal and illicit discharging of bilge oils, oiled sludges and ballast waters, etc., (**Figure I-12**). This also includes a portion of volatile organic compounds (VOCs) emissions from ships that deposits to the ocean.

On average, annual inputs from offshore oil exploration and extraction (platforms, pipelines) are not a major contributor to marine oil pollution (2%), and originate predominantly from the operational releases (e.g. produced water). Accidental spills from offshore platforms are less frequent than the spills from shipping, however, if they occur, they are very difficult to contain and can last for months, releasing immense volumes of oil to the marine environment. Therefore, offshore exploration and production are activities of considerable environmental risk (Eckle et al., 2012), as confirmed by the fact that some of the worst marine oil spills in history are deepwater spills from offshore oil wells, e.g. Ixtoc I and *Deepwater Horizon* (**Table I-2**).
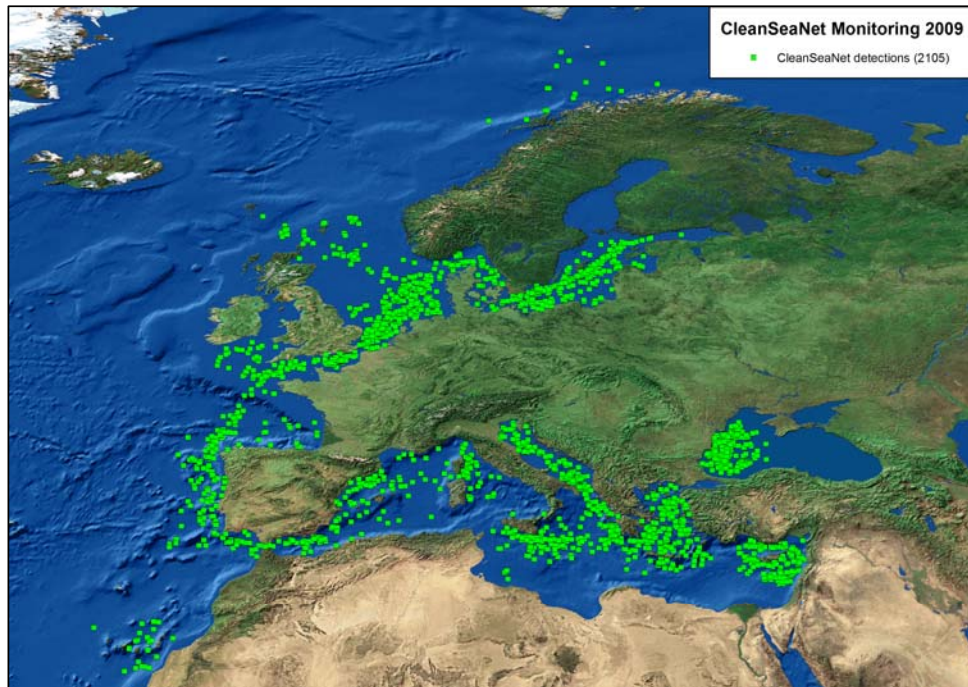
Figure I-12 Operational oil spills in European seas detected during 2009 using CleanSeaNet satellite monitoring (EMSA, 2013).

Despite the positive trends (**Figure I-11**), it is expected that oil spills will remain an important threat to marine environment in foreseeable future. Climate change and increasing temperature are driving the oil production and transportation to previously inaccessible regions, such as Arctic, where sea and weather conditions are unfavorable and the oil spill response resources are lacking (Cruz and Krausmann, 2013). Extreme weather such as tropical cyclones and sea storms, aggravated by climate change, will pose additional risk to existing offshore production in some regions such as Gulf of Mexico, as well as to oil shipping (Cruz and Krausmann, 2013).

In this thesis, among others, the oil samples from two major oil spills were of special interest: the *Prestige* tanker incident in 2002, near the Atlantic coast of Spain; and the *Deepwater Horizon* spill in the Gulf of Mexico, offshore Louisiana (United States of America) in 2010.

I.3.1. Prestige tanker spill

On 13th November 2002, *Prestige* oil tanker transporting 77,000 tonnes of heavy fuel oil (M-100 type) encountered severe weather, suffered a hull failure and started leaking oil approximately 50 km off the Galician coast (NW Spain) (Albaigés et al., 2006). After denied safe haven in Spain and Portugal, the *Prestige* was towed towards the open sea in an attempt to minimize the consequences of the leaking oil. Finally, on 19th November 2002 the tanker broke in two, and sunk at about 240 km west off the Galician coast with 20,000 tonnes of fuel oil already spilt. **Figure I-13** shows the satellite image of the spill and the trajectory of the tanker from the beginning of the incident until its sinking (Albaigés et al., 2006).
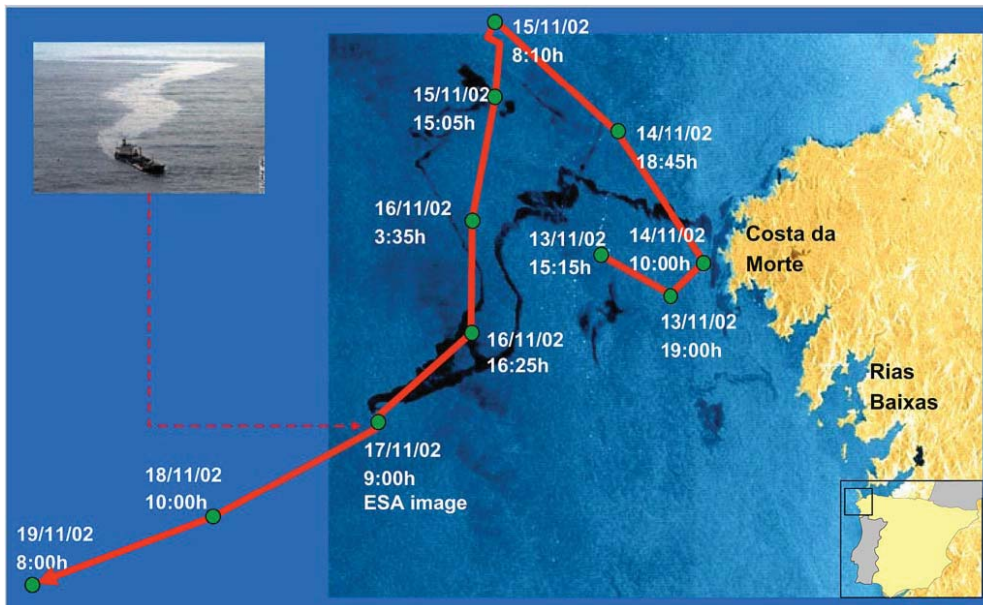
Figure I-13 Satellite image and the timeline of the *Prestige* spill (Albaigés et al., 2006).

The wreck continued leaking oil underwater from the damaged tanks releasing additional 40,000 tonnes of oil (Albaigés et al., 2006). Recovery efforts were diminished due to the strong emulsification and patching of highly viscous oil, unfavorable weather conditions, as well lacking organizational capacities. As a consequence, the spill was able to affect large costal areas, including sensitive ecological, fishing and touristic localities, and cause extensive ecological (De La Huz

et al., 2005) and socio-economical damages (García Negro et al., 2009; Garza-Gil et al., 2006), making it one of the worst marine incidents in the region's history.

I.3.2. Deepwater horizon platform spill

On April 20th, 2010, high pressure methane blowout led to an explosion on the British Petroleum operated *Deepwater Horizon* exploratory oil platform in the northern Gulf of Mexico, approximately 60 km off the coast of Louisiana (**Figure I-14**), which sank two days later. The explosion killed 11 people, and set off an uncontrolled release of oil from the Macondo well (*MW*) at approximately 1,500 m depth, which lasted until July 15th, 2010 when the well was finally capped.
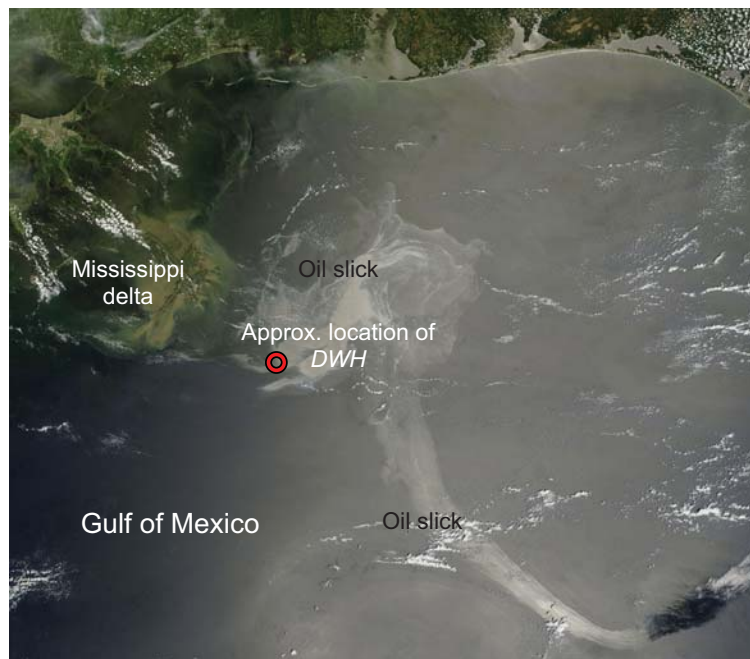
Figure I-14 Satellite image of the oil slick from the *Deepwater Horizon* on May 17, 2010 [adapted from (NASA, 2013)].

By the time the oil leak was stopped, an estimated 4.9 million barrels were released into the Gulf (Camilli et al., 2012; Reddy et al., 2012), making it the largest marine oil spill in the history of the United States of America. Only 20% of that oil was

recovered, and another 5% was burned, leaving the vast majority of oil (75%) in the environment, i.e. dissolved in the water, evaporated to the air, stuck to the coastline, or settled on the seafloor (McNutt et al., 2012). This caused serious environmental (White et al., 2012) and economical (McCrea-Strub et al., 2011) consequences; however, in order to fully understand and estimate the fate and effects of this unprecedented spill a comprehensive monitoring and research in the upcoming years will be necessary.

I.4. Fate of oil in the marine environment

After oil is spilt into the environment, a complex interplay of physical, chemical, and biological processes begins to transform the discharged oil, and distribute it between different environmental compartments. Collectively, these processes are referred to as **weathering** and act to change the composition, behavior, routes of exposure, and toxicity of the discharged oil. They include spreading, evaporation, dissolution, dispersion, emulsification, photooxidation and biodegradation, among others (**Figure I-15**), which take place simultaneously or consecutively over a time scale ranging from a few hours (e.g. evaporation) up to a couple of months or even years (e.g. biodegradation), and whose contribution to weathering transformations is different and changing over time (ITOPF, 2013; NOAA, 1996). Finally, speed and scale of these processes depends on the oil type and site-specific environmental conditions present in the moment of the spill (**Figure I-16**) (NOAA, 1996). Therefore, the fate of every oil spill is different, and its elucidation is a challenging task.

When discussing the fate of the spilt oil, distinction is made between non-persistent oils, which rapidly disappear from the sea surface, usually via evaporation, and persistent oils, which in contrast remain in the environment for a longer period of time. This classification is based on distillation characteristics and specific gravity (expressed as °API), and it divides oils into 4 groups (EPA, 2013; ITOPF, 2013). According to these criteria, Group 1 oils are non-persistent, which lose at least 50% of their volume at a temperature of 340 °C and at least 95% at a temperature of 370 °C, and have °API specific gravity >45. Other oils that do not have such distillation characteristics are considered as persistent and are further divided according to their specific gravity: Group 2 (°API 35-45), Group 3 (°API 17.5-35), and Group 4 (°API<17.5).
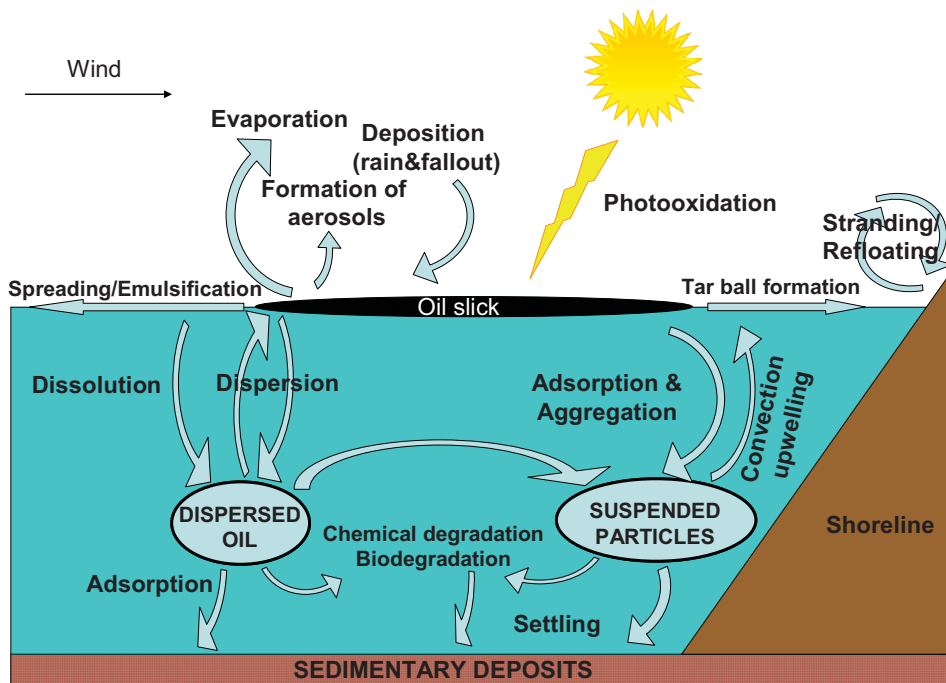
Figure I-15 Major processes affecting oil spill in the marine environment [adapted from (ITOPF, 2013; NOAA, 1996)].
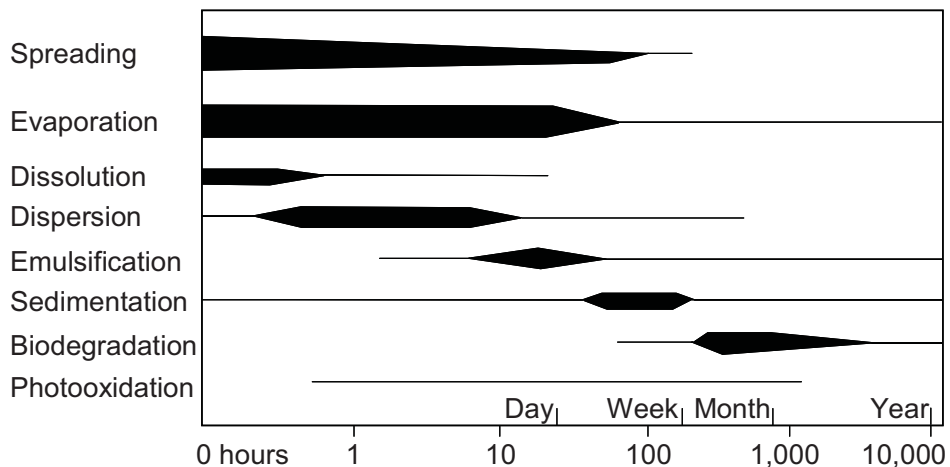
Figure I-16 Timeline and relative importance of different weathering processes [adapted from (NOAA, 1996)].

I.4.1. Spreading

After the spill, oil starts to spread over the water surface, and the speed at which this happens depends on the viscosity and pour point of oil (ITOPF, 2013). Very fluid oils will spread rapidly, creating very thin silver sheens. On the contrary, medium and low viscous oils would form thicker patches, which float and are carried by currents and waves. Since the viscosity and pour point decrease on lower temperatures, depending on the environmental conditions and the location of the spill, more viscous oils can solidify and change their spreading behavior. Spreading assessment is important for the planning of spill response strategies, because very fluid oils spread fast and are difficult to contain, while the spreading of patchy spills of viscous oils can be limited relatively easy using booms.

I.4.2. Evaporation

In general, evaporation is the predominant process immediately following an oil spill, resulting in significant mass transfer from the water phase of lighter volatile hydrocarbons, such as saturated hydrocarbons, or benzene, toluene, ethylbenzene and xylenes (BTEX), and lower molecular mass PAHs (Neff et al., 1996; Timmis and Smith, 2010). The most intense evaporation occurs in first hours and days posterior to the spill, when oil can lose as much as 75% of its volume in the case of lighter crudes, or about 40% and 10% in the case of medium and heavy oils, respectively (NRC, 2003). Fingas (Fingas, 2004) showed that evaporation is not boundary-layer regulated and that the time and the temperature are the most important factors that determine evaporation. Furthermore, the rate (speed) of the evaporation depends on the amount of oil, and on the type of oil, i.e. lighter oils, containing more low-molecular weight hydrocarbons will evaporate faster (Fingas, 1997).

I.4.3. Dissolution

Dissolution, like evaporation, occurs immediately after the spill and, similarly, affects the lower weight aromatic in addition to some polar oxygenated compounds

present in oil, such as naphthenic acids. In contrast, it is 10 to 1,000 times slower than evaporation (ITOPF, 2013), thus it is not very important post-spill process. Notwithstanding, during the later stages of weathering many insoluble compounds could be transformed to oxygenated, more polar species (Aeppli et al., 2012) which are potentially more soluble, bioavailable and/or toxic (Bellas et al., 2013; Rial et al., 2013).

I.4.4. Dispersion

Natural dispersion, besides evaporation, is one of the most important weathering processes during the first days after the spill. It involves the formation of small droplets, which are subsequently incorporated into the water column. Lower viscosity facilitates oil dispersion as well as the turbulence of water surface (e.g. breaking waves). Smaller oil droplets (<70 μm) will remain in the water column, while larger ones tend to coalesce and return to the surface (ITOPF, 2013). Therefore, dispersion reduces the volume of the surface slick and evaporative loss, but it does not lead to changes in the physicochemical properties of the spilled material. However, dispersed droplets have higher surface area which facilitates biodegradation (NOAA, 1996). Natural dispersion can be promoted by use of chemical dispersing agents, but their effectiveness can be limited depending on the type of dispersant, oil characteristics (e.g. viscosity) and environmental conditions (e.g. cold seas) (Wang et al., 2013).

I.4.5. Emulsification

This process starts after certain degree of weathering and involves the dispersion of water droplets into the oil medium to form water-in-oil emulsions or "mousse". Only oils with certain asphaltene content (>0.5 %) and nickel and vanadium concentration (>15 ppm in total) tend to form emulsions (ITOPF, 2013). Furthermore, turbulent sea conditions are needed to promote the mousse formation. As a consequence of emulsification the apparent volume of the oil may increase up to four or five times, while other weathering processes will slow down, especially evaporation (CONCAWE, 1983; NOAA, 1996). In addition, viscosity of some lighter oils can

increase and make them behave more like heavy fuel oils, increasing their persistence in the environment (Prince et al., 2004).

I.4.6. Photooxidation

This process occurs under the influence of the Sun's irradiation, predominantly in the ultraviolet (UV) band. It involves the loss of one or more electrons from a chemical species as a result of photoexcitation of that species; or the reaction of a substance with oxygen under the influence of light (IUPAC, 1997). In the sea surface microlayer, the process is thought to be driven by a series of radical reactions due to the presence of photosensitizers (e.g. dissolved organic matter), which can be excited by light to form various reactive species ($RO^{\bullet}$, $HO_2^{\bullet}$, $HO^{\bullet}$, etc.) (Miller, 1983; Schwarzenbach et al., 2005), i.e. indirect photooxidation. Deeper in the euphotic zone, dissolved or particulate-associated oil molecules, such as PAHs, can be photooxidized directly by absorbing UV radiation (Lee, 2003), with photooxidation rate being faster for alkyl substituted PAHs compared to parent compounds (Garrett et al., 1998). Furthermore, the rate of the photooxidation depends primarily on the intensity of the irradiation, suspended particulates and not on the temperature (Prince et al., 2003; Sydnes et al., 1985). The irradiation intensity, in turn, depends on the season, time of day, latitude, thickness of the atmosphere and the ozone layer, altitude, and cloud cover (Larson, 1988), thus if a spill is located in highly insolated regions, photooxidation can be an important weathering process.

As a result of photooxidation, more polar, oxygen containing species, akin in basic characteristics to resins and asphaltenes found in crude oils, are created (Aeppli et al., 2012; McKenna et al., 2013; Prince et al., 2004) through transformation of aromatic and saturate fractions (Han et al., 2006; Prince et al., 2003). These products include aliphatic and aromatic carboxylic acids, carbonyl and phenolic compounds, aryl and alkyl ethers, peroxides, sulfoxides, sulfones, sulfonates, etc. (Akhmedbekova, 2012; Garrett et al., 1998; Larson et al., 1977; McKenna et al., 2013; Payne and Phillips, 1985). Their solubility can be modified in respect to parent compounds due to the increased polarity thus changing their bioavailability and/or toxicity (Bellas et al., 2013; Fathalla and Andersson, 2011; Larson, 1988; Larson et al., 1977; Rial et al., 2013). Furthermore, some of them, such as fatty acids, can act as surfactants and

mobilize the insoluble parent compounds (Fathalla and Andersson, 2011). Finally, photooxidative compositional changes can decrease the stability of oil-in-water emulsions (Genuino et al., 2012).

I.4.7. Biodegradation

The marine environment is rich with microorganisms, like bacteria, fungi, and yeasts that can use oil hydrocarbons as carbon and energy source. These microorganisms are especially abundant near natural petroleum seeps, and are capable of biodegrading petroleum by oxidizing hydrocarbons, which then can be further degraded or dissolved. Biodegradation usually starts between the 2nd and 4th week after the spill, but it can occur much faster if the microbial community is already adapted to metabolizing compounds present in oils (e.g. locations near natural oil seeps or urban runoff discharges) (Atlas, 1995). It is facilitated by preceding weathering processes such as dispersion that increase the surface area of the oil phase, making it more available to biodegradation. The rate of biodegradation primarily depends on the oil composition. In general, saturated hydrocarbons are most readily biodegraded, especially those with 12 to 20 carbons (Fingas, 2001). Aromatic compounds degrade at a much slower rate, which decreases with increased molecular size and alkyl substitution, contrary to photooxidation (Prince et al., 2004). Temperature is the second key factor influencing biodegradation. In general, higher temperatures promote biodegradation, but the optimal temperature conditions can vary greatly depending on the microorganism type. Oxygen availability also controls biodegradation. In oxygen scarce environments, biodegradation takes the anaerobic pathway, where the final electron acceptor can be sulfate, nitrate, chlorate, metal ions or carbon dioxide (Prince et al., 2004). Although oil is an abundant source of carbon, other nutrients, namely phosphorous and nitrogen are essential for microbial growth. If the carbon/nitrogen/phosphorous ratio is not optimal, biodegradation can be substantially limited (Jimenez et al., 2007). Among the weathering processes described, only the biodegradation chemically transforms the hydrocarbon compounds and ultimately removes them from the environment.

I.4.8. Assessment of oil spill fate

In order to have a comprehensive assessment of oil spill fate it is necessary to integrate as much as possible all the important factors discussed previously: source of the spill (i.e. the type of oil and the quantity spilled), environmental conditions in the spill location, and weathering processes affecting the spill. This can be done by using the conceptual model that takes into account the transfer and partitioning of oil constituents between different environmental compartments (modules), i.e. water-column, bottom-sediment, and/or biota module (NRC, 2003). In the past decades, various **computer models** have been developed, which are able to provide quantifiable outputs to this theoretical conceptual model. They are used by different stakeholders interested in assessing the environmental fate and effects of oil spills (government agencies, industry). The potential applications of these models include (NRC, 2003):

- Tactical (emergency) spill response, composite models are used to predict the trajectories and weathering of accidental spills in order to determine the protection priorities;
- Strategic (contingency) planning, uses stochastic (multiple-runs) models which provide probability maps of the spill impacts in a studied region;
- Post-spill assessment, the models are used after a spill to fill observation gaps and estimate damage or to determine the source of unknown spill.

Some of the frequently used models are GNOME and ADIOS2 from the National Oceanic and Atmospheric Administration (NOAA) used to estimate advection, spreading, first-order evaporation, dispersion and emulsification; OSRA model used by the Minerals Management Service to estimate spill impact probability associated with offshore oil development; OSIS, a commercial oil fate model similar to NOAA models; etc., (NRC, 2003).

Furthermore, modern instrumental techniques such as comprehensive two-dimensional gas chromatography (GC×GC), able to separate oil hydrocarbons based on their different partitioning properties (volatility, solubility), can be used to estimate the contribution of different weathering processes (i.e. dissolution, evaporation and biodegradation) to the environmental transformations of oil (Arey et al., 2007; Farwell et al., 2009).

I.5. Legal framework and enforcement

The first framework to regulate the oil pollution in the marine environment was the International Convention for the Prevention of Pollution of the Sea by Oil (OILPOL), adopted in 1954. It recognized routine shipboard operations as the main source of marine oil pollution and prohibited the dumping of oily wastes within a certain distance from land and in areas of special environmental interest (Bernem et al., 2008).

However, not until the Torrey Canyon disaster in 1967, a fully comprehensive regulation of the marine pollution, to include not only accidental and operational oil spills, but also chemical, sewage, garbage and air pollution did not exist. The incident led to the adoption of international agreements on marine pollution such as the International Convention for the Prevention of Pollution from Ships, (MARPOL 73/78), and the United Nations Convention on the Law of the Sea, (UNCLOS) (Bernem et al., 2008). Another accident, the grounding and subsequent spill from the Exxon Valdez tanker in 1989 near coast of Alaska, led to the adoption of the Oil Pollution Act of 1990 (OPA 90), the primary US law regulating the liability for oil pollution damages, thus maintaining its national regime in marine pollution regulation (Schoenbaum, 2012). The oil content limit for discharges to sea is set at 15 ppm by these regulations (Ferraro and Pavliha, 2010).

Marine pollution regulation is usually enforced by the national coast guards, such as US Coast Guard (USCG). However, in Europe, the coast guard regime and spill response lacked supranational coordination, which was made evident during two accidents that occurred in European waters, one near the French coast (Erika, in 1999) and another at the Spanish coast (*Prestige*, in 2002). This led to the creation of the European Maritime Safety Agency (EMSA), which evolved from regional and sub-regional agreements such as the Bonn Agreement and the Helsinki and Lisbon conventions (Peperzak et al., 2010). The task of this agency is to facilitate the prevention and the response to pollution by ships as well as to provide Member States and the European Commission with technical and scientific assistance. Furthermore, the European Union policy on the safety of seaborne oil trade was improved and tightened by adopting so called Erika I and II packages of measures (EC, 2000; EU, 2000). They include port state control, stricter ship inspections, replacement of single-

hull for double-hull tankers, setting-up of a compensation fund for oil spills in European waters, etc.

In general, the cornerstone of marine pollution legislation is "polluter pays" principle; therefore the efficient and unambiguous techniques for detection, sampling and analysis of spills leading to the identification of polluting vessels are of paramount importance.

I.5.1. Remote sensing techniques for oil spill detection

Remote sensing devices for oil spill detection can be divided into passive and active remote sensing systems. Whereas the passive remote sensing uses the natural radiation to detect oil spills, the active system uses external source of radiation (e.g. laser). In addition, they can be subdivided into airborne (aircraft) and space-borne (satellite) operated systems, depending on where the signal is received and processed. Sensors can provide the following information for oil spill contingency planning and the polluter identification (Fingas and Brown, 1997; Jha et al., 2008):

- The location and spread of an oil spill over a large area;
- The thickness distribution of an oil spill to estimate the spilled oil quantity;
- A rough classification of the oil type;
- The main oil slicks trajectories.

Airborne remote sensing uses *optical* and *microwave* (MWV) sensors operated from an aircraft (airplane, helicopter or drone). Optical sensors detect different light phenomena in visible, UV and infrared (IR) spectra which indicate a potential oil spills (**Figure I-17**). On the other hand, the MWV sensors use the differences in the interactions of electromagnetic waves with sea water and oil slick to discover a spill. However, in both cases, interferences and false positives from natural marine products or phenomena (weeds, chlorophyll, shorelines, currents, oceanic fronts, etc.) are possible, depending on the sensor characteristics.

Satellite sensors provide a synoptic view of the affected area. The main problem associated with satellite surveillance is the timing and frequency of the overpass. Also, satellite remote sensing has a lower spatial resolution than airborne remote sensing. In Europe, the CleanSeaNet satellite operated by EMSA is fully

operational and equipped with *Synthetic Aperture Radar* (SAR). It applies the radar principle to form an image by utilizing the time delay of the backscattered signals. SAR sensors send out short pulses of MWV energy and then record the strength and origin of the returning reflections. The overall rate of confirmation is better than 50% if the spill is checked by aircraft no later than 3 h after satellite acquisition (**Figure I-18**).

Figure I-17 Oil slick trail from a polluting vessel detected using airborne visible optical sensor (EMSA, 2010).
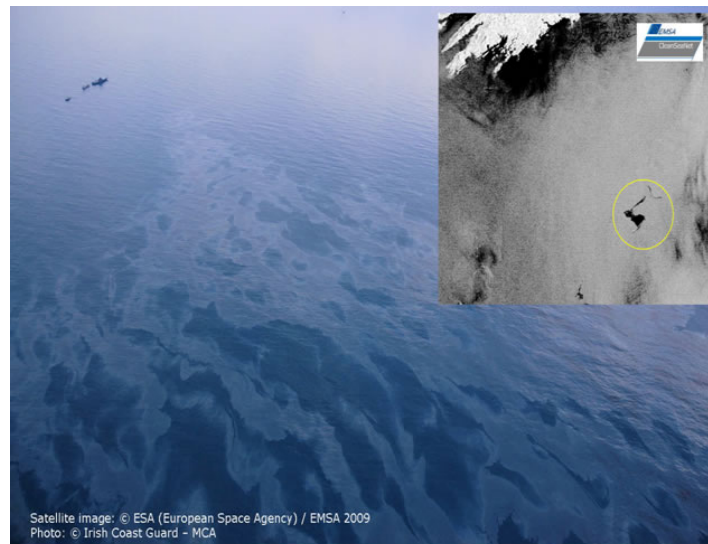
Figure I-18 A satellite image of an oil slick taken by CleanSeaNet, and confirmation of the spill and polluting vessel by aerial detection (EMSA, 2013).

I.5.2. Sampling and sample handling for oil spill assessments

Each spill event has individual characteristics, which have to be taken into account when planning the sampling strategy. Sampling and subsequent analysis should answer questions regarding the spills' origin as well as its properties and effects, which determine what type of samples and from what locations should be taken. Finally, should litigation ensue, sampling strategies need to comply with legal requirements. These include, in sampling terms, the recording of fundamental data on pro-forma sheets for each station (such as GPS position, data, time, coding, observations etc.), sampling should avoid cross contamination from other sources (e.g. containers must be pre-cleaned with surfactants, acid and solvent rinsing), and in the case of oil, should account for contributions from multiple inputs such as urban and storm water runoff. In addition, a chain of custody needs to be established to ensure validation of sample identification. Replicates should also afford a measure of variability. Sample labeling should be secure and unique. Clearly, personnel involved will need to adhere to all health and safety requirements and selection of protective clothing needs, also, to prevent sample contamination. For example, nitrile gloves should be worn.

Source oil sampling is essential for comparative and fingerprinting purposes. A detailed strategy has been compiled by the Helsinki Commission (HELCOM) (HELCOM, 2001) and further guidelines are provided by the International Maritime Organization (IMO) and the United Nations Environment Program (UNEP) (IMO/UNEP, 2009). Initially, all relevant paperwork on recent oil cargoes of the stricken vessel should be compiled. Samples (1–10 mL) of oil should be placed in pre-cleaned vials from strategic locations. These should include reference samples, cargo tanks, slop tanks, ballast, pump-room bilges, cross over and de-ballasting lines and cargo manifolds. Source oil from deepwater spills can be sampled using remotely operated vehicles (ROVs) or autonomous underwater vehicles (AUVs), as in the case of recent spill from *MW* in the Gulf of Mexico (Reddy et al., 2012). Samples should be stored refrigerated (4 °C).

Water samples include both surface slick (or microlayer) and sub-surface waters. In close proximity to a stricken oil tanker, frequently surface samples comprise almost the pure cargo leaking from the vessel. With weathering, the oil thickens

through loss of volatiles and emulsifies to form a mousse consistency. These can be readily removed using a solvent rinsed stainless steel spoon. With dissipation, the surface layer can thin to form so called sheens, and a variety of devices have been designed to afford efficient sampling of the microlayer, including simple glass plates, bottles, cornets, rotating drums, and special polytetrafluoroethylene (Teflon™) pads (Guitart et al., 2008; Peperzak et al., 2010; Swedish Coast Guard, 2002). Teflon™ is preferably used for slick or sheen sampling because other materials interfere with the subsequent analytical processes in the chemical laboratory (Peperzak et al., 2010). If surface oil is not visible, but the location would potentially be susceptible to contamination, sub-surface water samples (1–5 L) are frequently taken, often at 1 m depth, using variety of pre-cleaned sampling vessels, e.g. Winchester solvent bottles (Guitart, 2012; Guitart et al., 2008; Kelly et al., 2000). For subsequent hydrocarbon analyses, samples should be acidified and stored at 4 °C in darkness. If water samples are for toxicological testing, storage should be at 4 °C, in darkness, with return to the appropriate laboratory as quickly as possible.

Beached or stranded oil is sampled by scraping and/or gathering into a pre-cleaned sample jars taking care to minimize the sand and debris content (ITOPF, 2013).

Three types of *sediment* sampling devices are commonly used, namely grabs, corers and dredges. In the case of deep-water marine sampling campaigns, they are usually large-scale instruments that are mounted on ship decks or floating platforms and are manipulated using powerful cranes and winches (Radović et al., 2012).

Biota samples, in the form of fish, shellfish and plants can provide detailed information on which oil components the organisms have been exposed to (Law and Hellou, 1999). The techniques used for analyzing oil components in biota are generally very similar, involving extraction of petroleum hydrocarbons from the biota sample, a clean-up step to remove interfering endogenous material, followed by chemical analysis.

I.6. Chemical characterization of oil spills

Oil is a complex mixture of thousands of compounds, some with very different physicochemical properties; therefore, for a comprehensive analysis of various oil components, not one, but a set of complementary analytical methods must be applied. Typically, various chromatographic methods are used for separation and analysis of oil compounds or compound groups. More recently, some non-chromatographic methods are being applied for oil analysis, however complemented by chromatographic techniques.

I.6.1. TLC-FID

Thin-layer chromatography (TLC) is a type of liquid-planar chromatography performed on a stationary phase in the form of a thin layer usually on a glass support. A solution of sample is applied as a small spot or narrow band to the thin layer of adsorbent, typically silica gel, which has been spread uniformly over the support, e.g. a quartz rod. The mobile phase are solvents of different (increasing) polarity, which are passed through the adsorbent by capillary action, and the sample is resolved into discrete components based on the distance it migrated on the stationary phase. The separated components are then detected and quantified by either physical methods or chemical staining reagents after the solvent has evaporated. Coupling to flame ionization detector (FID) is a particularly useful option for petrochemical studies involving quantitative hydrocarbon-type determination. In this way, it is possible to measure the relative proportions of four major oil fractions, i.e. saturates, aromatics, resins and asphaltenes (SARA fractionation) (**Figure I-19**).

Using the relative quantification has the advantage of being independent of physical oil losses in the environment, thus making it more robust to spatial heterogeneity associated with oil spills. This method has been successfully used for group-type analysis of fresh and weathered oils (Aeppli et al., 2012; Bi, 2000; Kamiński et al., 2003; Radović et al., 2012).
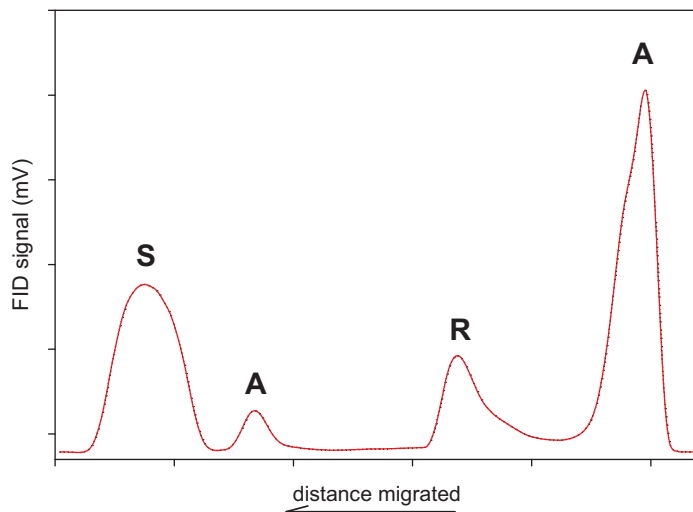
Figure I-19 TLC-FID chromatogram of a weathered *Macondo well* oil collected in the Gulf of Mexico oil showing the peaks corresponding to four major oil fractions (SARA – saturates (S), aromatics (A), resins (R), asphaltenes (A)).

I.6.2. Liquid chromatography

Open-column liquid chromatography is simple and extensively used method for hydrocarbon class separation of oils. It uses adsorbents such as silica gel or alumina as the stationary phase, and different solvents or solvent mixtures as eluents (**Figure I-20**). Therefore, the retention mechanism is governed by interactions (arising from polarity differences) between adsorbent and sample, solvent and sample, and solvent and adsorbent (Barman et al., 2000). Although some carry-over between SARA fractions is possible (Islas-Flores et al., 2005), this method is still preferred for rapid coarse fractionation of large quantities of oil due to its simplicity.

High-performance liquid chromatography (HPLC) has been applied for hydrocarbon-type separation and determination, as well as separation, identification, and, in some cases, quantitative determination of target compounds in many petrochemical samples. Both (semi)preparative and analytical applications of HPLC are possible using different normal-or reversed phase columns (silica and amino-, cyano-, or diol-bonded silica), isocratic or gradient elution of solvents, and various

detection systems, such as UV-visible, fluorescence, diode array (DAD) and IR (Barman et al., 2000).
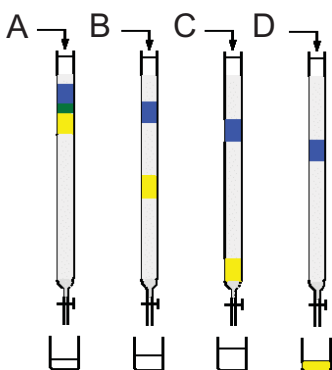
Figure I-20 Oil components in open-column liquid chromatography are separated by sequential solvent elution (A, B, C and D) [adapted from (Chemguide, 2013)].

I.6.3. Gas chromatography

Discerning the nature of the spilled oil, determining its source and tracking its environmental fate are a cumbersome task. Various pre-spill and post-spill factors (e.g. crude oil genesis, refining, weathering and/or mixing in the environment) collectively contribute to the chemical character of petroleum to create so called "oil fingerprint" (Wang and Stout, 2010). A conventional, well established methodology used for ***chemical fingerprinting*** of oils is based on gas chromatography (GC), which is able to resolve many of the characteristic oil compounds. In order to detect them, GC can be coupled to different types of detectors. For example, non-specific detectors such as ***FID***, can be used for the determination of limited number of oil compounds (e.g. n-alkanes and isoprenoids), in order to determine the type of oil, and to indicate the onset of some weathering processes (e.g. evaporation, biodegradation). However, for more detailed chemical fingerprint that includes other oil-specific compounds, such as various PAH isomers and biomarker molecules, different, more selective detection is needed. This was obtained by coupling of GC to ***mass spectrometry (MS)*** which greatly increased the number of detected compounds and their ratios used in oil fingerprinting and enabled more robust determination of the type of spilled oil, its

sources and weathering transformations. Since it was introduced (Albaiges and Albrecht, 1979), GC-MS fingerprinting methodology has been continually improved (Daling et al., 2002; Wang and Fingas, 2003) and, as a result, the European Committee for Standardization (CEN) recently accepted it as a new standard for oil spill identification (CEN, 2012), based on the existing Nordtest method (Nordtest, 1991).

However, the resolution power of conventional GC methods is limited to sufficiently volatile hydrocarbons eluting below ~300-400 °C, thus not fully reflecting the real complexity of oil. This is particularly evident in weathered oil spill samples, which contain a complex mixture of more polar, less volatile and high molecular weight compounds, eluting as unresolved "hump" in the gas chromatograms, denoted as "unresolved complex mixture" (UCM) (**Figure I-21**). Finally, lack of resolution of standard GC methods can be a problem when analyzing ship discharges which are mixtures of different oil types (e.g. from bilges, sewage, slops), as well as the spill samples from locations where concurrent sources are present (e.g. close to natural seeps, in ports, along busy maritime routes).
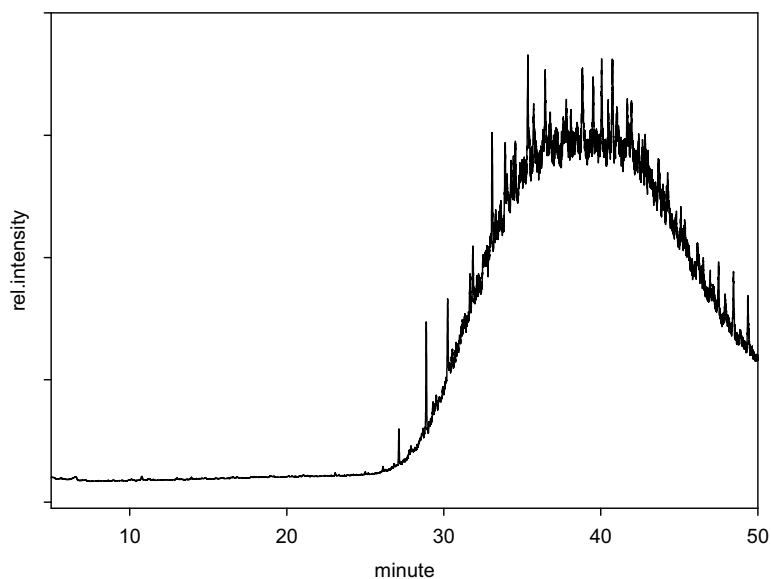
Figure I-21 GC-FID chromatogram of a weathered *MW* oil collected in the Gulf of Mexico showing the UCM hump.

The GC fingerprinting method can be combined with other analytical techniques, such as inductively coupled plasma-atomic emission spectroscopy (ICP-AES) for determination of nickel and vanadium content and X-ray fluorescence spectroscopy (XFS) for sulfur content analysis (Taki et al., 2009). Similarly, it can be integrated with Fourier transform infrared (FT-IR) spectroscopy (Shang and Kirkwood, 2010) or liquid chromatography tandem mass spectrometry (LC/MS–MS) (Shang and McPherson, 2009) in combination with pattern recognition techniques to provide rapid oil spill identification. In order to overcome problems associated with the loss of biomarkers through weathering, GC can be coupled with isotope ratio mass spectrometry (GC–IRMS) to provide stable carbon isotopic compositions of individual hydrocarbons (Li et al., 2009). This can facilitate identification of weathered spill samples. However, in all the cases, the limited resolution of conventional GC is an intrinsic problem which restricts the power of the fingerprinting methods.

I.6.4. Comprehensive two-dimensional gas chromatography (GC×GC)

In the past decade, GC×GC emerged as a technique that revolutionized the separation of complex mixtures such as petroleum because of its enhanced resolution and sensitivity (Nizio et al., 2012; Seeley and Seeley, 2013).

High resolution is accomplished by serial coupling of two columns with an orthogonal chromatographic separation principle (e.g., first volatility, then polarity), and includes transfer from the first to the second column using a modulator (e.g. thermal). The first column is typically of similar dimensions to that used in a conventional one-dimensional separation (10–30 m×0.18–0.25 mm) while the second dimension column is typically shorter and narrower (0.5–2 m×0.1–0.18 mm) (Nizio et al., 2012). The modulator periodically samples first column peaks, focuses them, and then injects them into the second column as narrow peaks (typically 100–200 ms), thus increasing sensitivity. **Figure I-22** shows the scheme of a dual-jet N_2 modulator and the principle of peak cryofocusing.
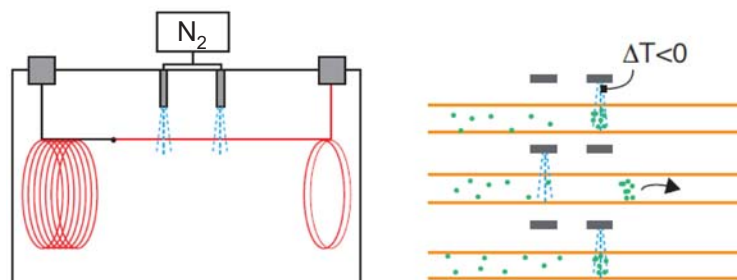
Figure I-22 Dual-jet N$_2$ thermal modulator mode of operation [adapted from (Vendeuvre et al., 2007)].

In order to detect such narrow peaks, detectors with high acquisition rates are necessary. Most widely used are FID and time-of-flight mass detectors (TOFMS) (Seeley and Seeley, 2013). The latter adds an additional dimension (*m/z* ratio) and facilitates compound identification. GC×GC increases separation capacity by an order of magnitude when compared to conventional GC, fundamentally transforming oil fingerprinting. **Figure I-23** shows how the peaks eluting from the first column are periodically "sliced" in the modulator and transferred to the second column to obtain additional separation. GC×GC has already been proven as an efficient method for separation and identification of group-type oil compounds (Van Deursen et al., 2000), analysis of weathered oil samples (Wardlaw et al., 2008), compound class oil fingerprinting (Ventura et al., 2010), and characterization of UCM (Booth et al., 2007).

However, in order to release its full potential, innovative chemometric techniques that can handle the vast amount of data provided by GC×GC become indispensable (Pierce et al., 2008). Their performance and reliability can be impaired due to challenges such as baseline/background contribution, retention time shifts, and peak overlap that occur in GC×GC practice (Pierce et al., 2008). Multivariate resolution methods such as generalized rank annihilation, parallel factor analysis (PARAFAC), PARAFAC2, and multivariate curve resolution (MCR) alternating least squares (ALS) have been developed to overcome these challenges (Parastar et al., 2011; Zeng et al., 2011).
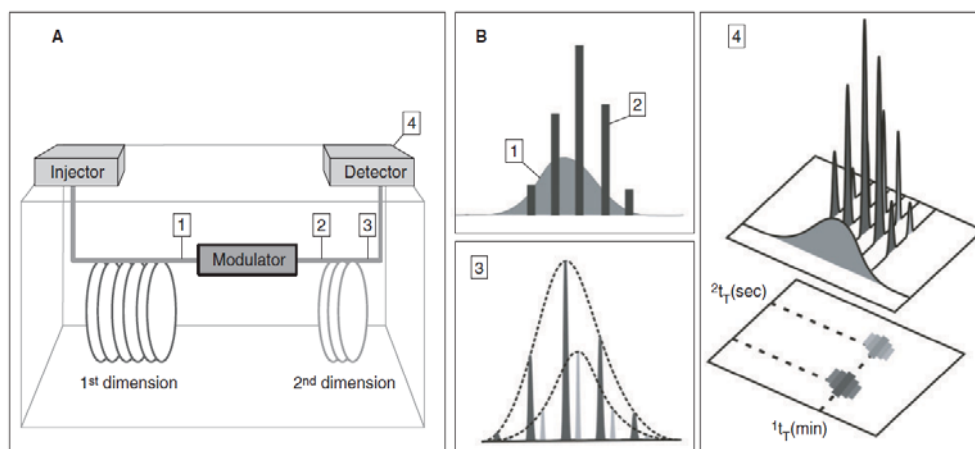
Figure I-23 GC×GC configuration (A) and principle of modulation (B). Peak eluting from the first column (1) is focused by the modulator (2) and re-injected into the second column for further separation (3). The signal recorded by the detector (4) is sliced according to the modulation period; the combination of secondary chromatograms and their projection in a retention plane allows the reconstruction of two-dimensional contour plots [reprinted from (Vendeuvre et al., 2007)].

I.6.5. Non-chromatographic methods

Comprehensive GC×GC extends the analytical window compared to conventional GC, however, polar, non-volatile, and heavy molecular weight oil compounds are not amenable by either of the techniques. For such compounds, a possible alternative is the high-resolution Fourier transform ion cyclotron resonance (**FT-ICR**) mass spectrometry which enables the characterization of petrocompounds (i.e. petroleomics) up to ~C_{100}, although limited to elemental composition (McKenna et al., 2013). Furthermore, the instrumentation for this technique is resource demanding and not widely available. Another technique available for this type of compounds is matrix-assisted laser desorption/ionization time-of-flight (**MALDI-TOF**) mass spectrometry, which was successfully applied to study asphaltene fraction of oil (Pantoja et al., 2013).

Other non-chromatographic methods for oil spill forensics exist, such as **FT-IR** method based on the absorption on different characteristic bands (e.g. 811, 742 and 723 cm^{-1}) (Taki et al., 2011). Also, concentrations of **metals** (vanadium [V], nickel [Ni],

magnesium [Mg], iron [Fe], cobalt [Co], and copper [Cu]) can used to identify sources of oil contamination (Hegazi, 2009).

However, the applicability of non-chromatographic methods is, in general, limited, therefore for the comprehensive oil characterization they should be complemented by chromatographic methods.

I.7. Effects of oil spills

The effects of oil spills on **marine life** can be caused by *physical contamination* leading to clogging, interference with mobility or feeding, or smothering, leading to suffocation, and heat stress. This is particularly affecting the seabirds and shoreline mammals (e.g. seals, otters) (ITOPF, 2013).

On the other hand *biological effects* are dominated by the chemical components of the oil, leading to acute toxicity, i.e. immediate short-term effect of a single exposure to a toxicant, or chronic toxicity, which is defined as either the effect of long-term and continuous exposure to a toxicant or the long-term sublethal effect of acute exposure (Bernem et al., 2008; NRC, 2003).

Acute and chronic toxicity of petroleum hydrocarbons to marine organisms is dependent upon (NRC, 2003):

- the concentration of petroleum hydrocarbons and length of exposure;
- the persistence and bioavailability of specific hydrocarbons;
- the ability of organisms to accumulate and metabolize various hydrocarbons;
- the fate of metabolized products;
- the interference of specific hydrocarbons (or metabolites) with normal metabolic processes that may alter an organism's chances for survival and reproduction in the environment; and
- the specific narcotic effects of hydrocarbons on nerve transmission.

Most of the risk assessment studies up to date focused predominantly on the acute toxicity of petroleum hydrocarbons, particularly via narcosis (McGrath et al., 2005; Verbruggen et al., 2008). Although this might be the most important mode of action immediately after spill, as the oil is affected by weathering processes, such as evaporation, lighter volatile saturate and monoaromatic (BTEX) hydrocarbons, which

are mainly responsible for narcotic effect, are lost. Concomitantly, the proportion of PAHs is increased, as well as the contribution of their chronic effects in the overall oil toxicity (NRC, 2003). Furthermore, other weathering processes, such as photooxidation, can transform oil compounds into more polar species. These oxygen containing weathering products (Aeppli et al., 2012; McKenna et al., 2013) and other components present in the UCM (Booth et al., 2007) are potentially more soluble, bioavailable, and toxic (Melbye et al., 2009; Smith et al., 2001; Thomas et al., 1995). In particular, the potential for the chronic toxicity of such compounds is of growing importance (Scarlett et al., 2008).

In comparison, the studies on the effects of oil spills on **human health** are relatively scarce. However, the available data provide the evidence on the relationship between exposure to spilled oils and the appearance of acute physical, genotoxic and endocrine effects in the exposed individuals especially during the early oil spill stages (Aguilera et al., 2010).

I.7.1. Effect-directed analysis (EDA)

Effective and complete assessment of the risks posed to the environment post-incident requires knowledge on which specific compounds are present. In the majority of incidents, it is envisaged that targeted analysis of spill specific toxicants would be sufficient in establishing the extent of any contamination. This would be based on prior knowledge of which oil substances may have been released. Should there be no a priori knowledge on the chemicals released or that complex mixtures of many chemicals may be present then there may be a need to identify which of the released chemicals represent the greatest risk to the environment. One approach that can inform this process by identifying which compounds are present in the incident area, post-spill, is effect-directed analysis (EDA). EDA is essentially an approach where the broad-spectrum analysis is directed by an effect response, typically from a bioassay (Brack, 2003). The EDA approach reduces the complexity of a sample through separating the individual components of a complex mixture based upon different physicochemical properties. The fractionation process is directed by a suitable bioassay, i.e. after each separation step the fractions are biotested for selection of active fractions for further investigation (**Figure I-24**).
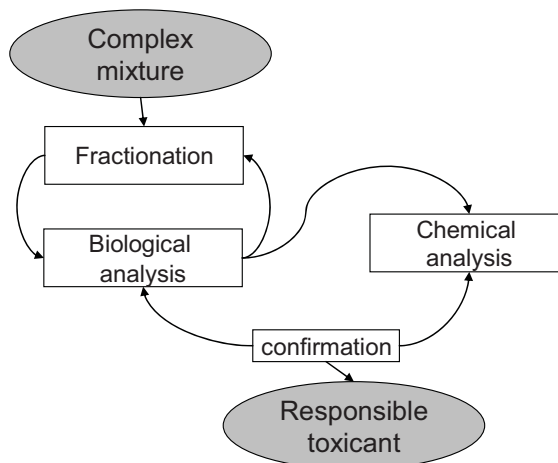
Figure I-24 Flowchart of the effect-directed analysis.

The most suitable bioassays are those that require a low volume, are sensitive, relatively cheap to run and suitable for high throughput. The greatest success using EDA has been achieved using bioassays that have very specific endpoints, such as receptor binding (i.e. aryl hydrogen, AhR; androgen, AR; and estrogen, ER receptors) (Thomas et al., 2004; Thomas et al., 2002; Thomas et al., 2009). Bioavailability can be incorporated into the EDA procedure through using extraction techniques that extract the "bioavailable" fraction, such as TENAX (Cornelissen et al., 1998; Schwab et al., 2009; Schwab and Brack, 2007).

Fractionation is often performed using HPLC or other chromatographic approaches, such as gel permeation chromatography (Fernandez and Bayona, 1992). The sheer complexity of samples often requires that multi-step fractionation procedures are required that employ a number of different chromatography mechanisms (Brack et al., 2003; Brack and Schirmer, 2003; Brack et al., 2005). These can be particularly effective for the separation of complex mixtures of hydrocarbons. Preparative gas chromatography has also proved to be a successful approach for separating volatile non-polar mixtures (Meinert et al., 2007). Finally, existent fractionation methods for polar compounds (Lübcke-von Varel et al., 2008; Meinert et al., 2007) should be further developed, since polar fraction is abundant in weathered oil samples and potentially toxic.

Isolated fractions that exert the type of effect under investigation can be analyzed by a number of different of non-target, broad-spectrum methods. Typically, a

first screen may involve analysis by GC–MS operated in full-scan utilized in combination with deconvolution software such as AMDIS (Automated Mass Spectral Deconvolution and Identification System) (Thomas et al., 2002). Should this technique not identify the cause(s) of effect then techniques that use either higher resolution separations (GC×GC) or GC coupled to high resolution TOFMS may be alternative options (Thomas et al., 2009). For polar compounds where GC is not an option then liquid chromatography coupled to accurate mass MS has previously been successfully used to identify the previously unknown causes of effect (Weiss et al., 2010). Other techniques that may assist the identification process include the use of molecular descriptors from bioassay data (Kazius et al., 2005; Von Der Ohe et al., 2005) or computational tools, such as molecular structure generation (MOLGEN) (Schymanski et al., 2009; Schymanski et al., 2008). The final, and often neglected, stage of the EDA process is to confirm that the compound(s) identified are actually responsible for the observed effect. This can be performed at a number of levels and includes confirmation of a compound(s) identity, effect and hazard (Brack et al., 2009; Grote et al., 2005). Potentially useful, but still not sufficiently investigated alternative for EDA confirmation are the *in-silico* tools for quantitative structure–activity relationship (QSAR) modeling (Lilienblum et al., 2008; Veith et al., 1984).

The outcome of a successful EDA study is the identity of those compounds that are contributing to the hazard posed by the released compounds, which is often an essential step in post-incident risk assessments.

I.8. References

Abraham, H., 1960. Asphalts and Allied Substances: Their Occurrence, Modes of Production, Uses in the Arts, and Methods of Testing, Vol 1. Historical Review and Natural Raw Materials. Van Nostrand, Princeton, NJ.

Aeppli, C., Carmichael, C.A., Nelson, R.K., Lemkau, K.L., Graham, W.M., Redmond, M.C., Valentine, D.L., Reddy, C.M., 2012. Oil Weathering after the *Deepwater Horizon* Disaster Led to the Formation of Oxygenated Residues. Environmental Science & Technology 46, 8799-8807.

Aguilera, F., Méndez, J., Pásaroa, E., Laffona, B., 2010. Review on the effects of exposure to spilled oils on human health. Journal of Applied Toxicology 30, 291-301.

Akhmedbekova, S.F., 2012. Inhibiting properties of photooxidized secondary oil refining

products. Chemistry and Technology of Fuels and Oils 48, 149-155.

Albaiges, J., Albrecht, P., 1979. Fingerprinting marine pollutant hydrocarbons by computerized gas chromatography-mas spectrometry. International Journal of Environmental Analytical Chemistry 6, 171-190.

Albaigés, J., Morales-Nin, B., Vilas, F., 2006. The *Prestige* oil spill: A scientific response. Marine Pollution Bulletin 53, 205-207.

API, 2011. High Production Volume (HPV) Chemical Challenge Program - Crude oil category - Category assessment document.

Arey, J.S., Nelson, R.K., Reddy, C.M., 2007. Disentangling oil weathering using GC x GC. 1. Chromatogram analysis. Environmental Science and Technology 41, 5738-5746.

Atlas, R.M., 1995. Petroleum biodegradation and oil spill bioremediation. Marine Pollution Bulletin 31, 178-182.

Bailey, R.A., Clark, H.M., Ferris, J.P., Krause, S., Strong, R.L., 2002. Petroleum, hydrocarbons and coal. Chemistry of the Environment, 835.

Barman, B.N., Cebolla, V.L., Membrado, L., 2000. Chromatographic techniques for petroleum and related products. Critical Reviews in Analytical Chemistry 30, 75-120.

Bell, H.S., 1946. American Petroleum Refining. Van Nostrand Company, Inc., New York.

Bellas, J., Saco-álvarez, L., Nieto, T., Bayona, J.M., Albaigés, J., Beiras, R., 2013. Evaluation of artificially-weathered standard fuel oil toxicity by marine invertebrate embryogenesis bioassays. Chemosphere 90, 1103-1108.

Bernem, C., Wesnigk, J., Wunderlich, M., Adam, S., Callies, U., 2008. Oil Pollution in Marine Ecosystems — Policy, Fate, Effects and Response. Environmental Crises, 101-139.

Bi, Y.G., 2000. Application of TLC-FID technique for analysis of characteristic groups in heavy oils. Journal of Fuel Chemistry and Technology 28, 388-391.

Booth, A.M., Sutton, P.A., Lewis, C.A., Lewis, A.C., Scarlett, A., Chau, W., Widdows, J., Rowland, S.J., 2007. Unresolved complex mixtures of aromatic hydrocarbons: Thousands of overlooked persistent, bioaccumulative, and toxic contaminants in mussels. Environmental Science and Technology 41, 457-464.

Brack, W., 2003. Effect-directed analysis: A promising tool for the identification of organic toxicants in complex mixtures? Anal Bioanal Chem 377, 397-407.

Brack, W., Bandow, N., Schwab, K., Schulze, T., Streck, G., 2009. Bioavailability in effect-directed analysis of organic toxicants in sediments. TrAC - Trends in Analytical Chemistry 28, 543-549.

Brack, W., Kind, T., Hollert, H., Schrader, S., Moder, M., 2003. Sequential fractionation procedure for the identification of potentially cytochrome P4501A-inducing compounds. Journal of Chromatography A 986, 55-66.

Brack, W., Schirmer, K., 2003. Effect-directed identification of oxygen and sulfur heterocycles

as major polycyclic aromatic cytochrome P4501A-inducers in a contaminated sediment. Environmental Science and Technology 37, 3062-3070.

Brack, W., Schirmer, K., Erdinger, L., Hollert, H., 2005. Effect-directed analysis of mutagens and ethoxyresorufin-O-deethylase inducers in aquatic sediments. Environmental Toxicology and Chemistry 24, 2445-2458.

Camilli, R., Di Iorio, D., Bowen, A., Reddy, C.M., Techet, A.H., Yoerger, D.R., Whitcomb, L.L., Seewald, J.S., Sylva, S.P., Fenwick, J., 2012. Acoustic measurement of the *Deepwater Horizon* Macondo well flow rate. Proceedings of the National Academy of Sciences 109, 20235-20239.

Cedre, 2013. Classement alphabétique des accidents. http://www.cedre.fr/fr/accident/classement-alphabetique.php.

CEN, 2012. CEN/TR 15522-2:2012, Oil spill identification - Waterborne petroleum and petroleum products - Part 2: Analytical methodology and interpretation of results.

Chemguide, 2013. Column chromatography. http://www.chemguide.co.uk/analysis/chromatography/column.html.

Clay, A.T., 1922. A Hebrew Deluge Story in Cuneiform and Other Epic Fragments in the Pierpont Morgan Library. Ams PressInc.

CONCAWE, 1983. Characteristics of petroleum and its behaviour at sea. CONCAWE, Oil Spill Clean-up Technology Special Task Force No. 8.

Cornelissen, G., Rigterink, H., Ferdinandy, M.M.A., Van Noort, P.C.M., 1998. Rapidly desorbing fractions of PAHs in contaminated sediments as a predictor of the extent of bioremediation. Environmental Science and Technology 32, 966-970.

Cruz, A.M., Krausmann, E., 2013. Vulnerability of the oil and gas sector to climate change and extreme weather events. Climatic Change, 1-13.

CTX, 2013. The CTX Tanker Casualty Database. http://www.c4tx.org/ctx/job/cdb/summary.html.

Daling, P.S., Faksness, L.G., Hansen, A.B., Stout, S.A., 2002. Improved and standardized methodology for oil spill fingerprinting. Environmental Forensics 3, 263-278.

De La Huz, R., Lastra, M., Junoy, J., Castellanos, C., Viéitez, J.M., 2005. Biological impacts of oil pollution and cleaning in the intertidal zone of exposed sandy beaches: Preliminary study of the "*prestige*" oil spill. Estuarine, Coastal and Shelf Science 65, 19-29.

EC, 2000. Communication from the Commission to the European Parliament and the Council on a second set of community measures on maritime safety following the sinking of the oil tanker ERIKA /* COM/2000/0802 final */.

Eckle, P., Burgherr, P., Michaux, E., 2012. Risk of large oil spills: A statistical analysis in the aftermath of *deepwater horizon*. Environmental Science and Technology 46, 13002-13008.

EIA, 2012. World Oil Transit Chokepoints. US Energy Information Administration.

EMSA, 2010. Maritime Accident Review 2009. European Maritime Safety Agency.

EMSA, 2013. Oil spill detection examples: Admiral Kuznetsov, February 2009.

Environment Canada, 2013. Tanker Spills.

http://www.etc-cte.ec.gc.ca/databases/TankerSpills/Default.aspx.

EPA, 2013. 40 CFR Appendix E to Part 112 - Determination and Evaluation of Required Response Resources for Facility Response Plans. Environmental Protection Agency.

EU, 2000. Proposal for a Regulation of the European Parliament and of the Council on the accelerated phasing-in of double hull or equivalent design requirements for single hull oil tankers /* COM/2000/0142 final */. Official Journal C 212 E, 0121 - 0126.

Farwell, C., Reddy, C.M., Peacock, E., Nelson, R.K., Washburn, L., Valentine, D.L., 2009. Weathering and the fallout plume of heavy oil from strong petroleum seeps near Coal Oil Point, CA. Environmental Science and Technology 43, 3542-3548.

Fathalla, E.M., Andersson, J.T., 2011. Products of polycyclic aromatic sulfur heterocycles in oil spill photodegradation. Environmental Toxicology and Chemistry 30, 2004-2012.

Fernandez, P., Bayona, J.M., 1992. Use of off-line gel permeation chromatography - Normal-phase liquid chromatography for the determination of polycyclic aromatic compounds in environmental samples and standard reference materials (air particulate matter and marine sediment). Journal of Chromatography 625, 141-149.

Ferraro, G., Pavliha, M., 2010. The European and International legal framework on monitoring and response to oil pollution from ships. Journal of Environmental Monitoring 12, 574-580.

Fingas, M., 2001. The Basics of Oil Spill Cleanup, Second Edition ed. Lewis Publishers CRC Press LLC.

Fingas, M.F., 1997. Studies on the evaporation of crude oil and petroleum products: I. The relationship between evaporation rate and time. Journal of Hazardous Materials 56, 227-236.

Fingas, M.F., 2004. Modeling evaporation using models that are not boundary-layer regulated. Journal of Hazardous Materials 107, 27-36.

Fingas, M.F., Brown, C.E., 1997. Review of oil spill remote sensing. Spill Science and Technology Bulletin 4, 199-208.

García Negro, M.C., Villasante, S., Carballo Penela, A., Rodríguez Rodríguez, G., 2009. Estimating the economic impact of the *Prestige* oil spill on the Death Coast (NW Spain) fisheries. Marine Policy 33, 8-23.

Garrett, R.M., Pickering, I.J., Haith, C.E., Prince, R.C., 1998. Photooxidation of crude oils. Environmental Science and Technology 32, 3719-3723.

Garza-Gil, M.D., Prada-Blanco, A., Vázquez-Rodríguez, M.X., 2006. Estimating the short-term economic damages from the *Prestige* oil spill in the Galician fisheries and tourism.

Ecological Economics 58, 842-849.

Genuino, H.C., Horvath, D.T., King'Ondu, C.K., Hoag, G.E., Collins, J.B., Suib, S.L., 2012. Effects of visible and UV light on the characteristics and properties of crude oil-in-water (O/W) emulsions. Photochemical and Photobiological Sciences 11, 692-702.

GESAMP, 2007. Estimates of Oil Entering the Marine Environment from Sea-based Activities. GESAMP Reports and Studies 75.

Grote, M., Brack, W., Walter, H.A., Altenburger, R., 2005. Confirmation of cause-effect relationships using effect-directed analysis for complex environmental samples. Environmental Toxicology and Chemistry 24, 1420-1427.

Guitart, C., Readman, J.W. and Bayona, J.M., 2012. Seawater. Organic Contaminants. . Comprehensive Sampling and Sample Preparation.

Guitart, C., Frickers, P., Horrillo-Caraballo, J., Law, R.J., Readman, J.W., 2008. Characterization of sea surface chemical contamination after shipping accidents. Environmental Science and Technology 42, 2275-2282.

Han, S., Qiu, C., Cheng, X., Ma, S., Ren, T., 2006. Compositional changes in hydrotreated naphthenic oil under ultraviolet radiation. Petroleum Science and Technology 24, 859-870.

Hegazi, A.H., 2009. Utilization of trace metals in source diagnosing of tar balls from the Mediterranean City of Alexandria, Egypt. Petroleum Science and Technology 27, 386-395.

HELCOM, 2001. Oil sampling. HELCOM Combating Manual.

IMO/UNEP, 2009. The Guidance Manual on the Assessment and Restoration of Environmental Damage Following Marine Oil Spills, London, UK.

Islas-Flores, C.A., Buenrostro-Gonzalez, E., Lira-Galeana, C., 2005. Comparisons between open column chromatography and HPLC SARA fractionations in petroleum. Energy and Fuels 19, 2080-2088.

ITOPF, 2013. Case Histories.

http://www.itopf.com/information-services/data-and-statistics/case-histories/.

ITOPF, 2013. Fate of marine oil spills, Technical information paper no. 2. International Tanker Owners Pollution Federation Ltd.

ITOPF, 2013. ITOPF Handbook 2013/2014. International Tanker Owners Pollution Federation Ltd.

ITOPF, 2013. ITOPF WebGIS application.

http://www.itopf.com/information-services/data-and-statistics/gis-map/.

ITOPF, 2013. Sampling and monitoring of marine oils spills, Technical information paper no. 14. International Tanker Owners Pollution Federation Ltd.

IUPAC, 1997. Compendium of Chemical Terminology (the "Gold Book"), 2nd ed. Blackwell Scientific Publications, Oxford.

Jha, M.N., Levy, J., Gao, Y., 2008. Advances in remote sensing for oil spill disaster

management: State-of-the-art sensors technology for oil spill surveillance. Sensors 8, 236-255.

Jimenez, N., Viñas, M., Bayona, J.M., Albaiges, J., Solanas, A.M., 2007. The *Prestige* oil spill: Bacterial community dynamics during a field biostimulation assay. Applied Microbiology and Biotechnology 77, 935-945.

Kamiński, M., Gudebska, J., Górecki, T., Kartanowicz, R.X., 2003. Optimized conditions for hydrocarbon group type analysis of base oils by thin-layer chromatography-flame ionisation detection. Journal of Chromatography A 991, 255-266.

Kazius, J., McGuire, R., Bursi, R., 2005. Derivation and validation of toxicophores for mutagenicity prediction. Journal of Medicinal Chemistry 48, 312-320.

Kelly, C.A., Law, R.J., Emerson, H.S., 2000. Methods of analysing hydrocarbons and polycyclic aromatic hydrocarbons (PAH) in marine samples. Science Series, Aquatic Environment Protection: Analytical Methods (12), 18.

Kerr, R.A., 2011. Peak Oil Production May Already Be Here. Science 331, 1510-1511.

Larson, R.A., 1988. Environmental phototoxicity. Environmental Science and Technology 22, 354-360.

Larson, R.A., Hunt, L.L., Blankenship, D.W., 1977. Formation of toxic products from a #2 fuel oil by photooxidation. Environmental Science & Technology 11, 492-496.

Law, R.J., Hellou, J., 1999. Contamination of fish and shellfish following oil spill incidents. Environmental Geosciences 6, 90-98.

Lee, R.F., 2003. Photo-oxidation and Photo-toxicity of Crude and Refined Oils. Spill Science and Technology Bulletin 8, 157-162.

Li, Y., Xiong, Y., Yang, W., Xie, Y., Li, S., Sun, Y., 2009. Compound-specific stable carbon isotopic composition of petroleum hydrocarbons as a tool for tracing the source of oil spills. Marine Pollution Bulletin 58, 114-117.

Lilienblum, W., Dekant, W., Foth, H., Gebel, T., Hengstler, J.G., Kahl, R., Kramer, P.J., Schweinfurth, H., Wollin, K.M., 2008. Alternative methods to safety studies in experimental animals: Role in the risk assessment of chemicals under the new European Chemicals Legislation (REACH). Archives of Toxicology 82, 211-236.

Lübcke-von Varel, U., Streck, G., Brack, W., 2008. Automated fractionation procedure for polycyclic aromatic compounds in sediment extracts on three coupled normal-phase high-performance liquid chromatography columns. Journal of Chromatography A 1185, 31-42.

Maggio, G., Cacciola, G., 2012. When will oil, natural gas, and coal peak? Fuel 98, 111-123.

McCrea-Strub, A., Kleisner, K., Sumaila, U.R., Swartz, W., Watson, R., Zeller, D., Pauly, D., 2011. Potential Impact of the *Deepwater Horizon* Oil Spill on Commercial Fisheries in the Gulf of Mexico. Fisheries 36, 332-336.

McGrath, J.A., Parkerton, T.F., Hellweger, F.L., Di Toro, D.M., 2005. Validation of the

narcosis target lipid model for petroleum products: Gasoline as a case study. Environmental Toxicology and Chemistry 24, 2382-2394.

McKenna, A.M., Nelson, R.K., Reddy, C.M., Savory, J.J., Kaiser, N.K., Fitzsimmons, J.E., Marshall, A.G., Rodgers, R.P., 2013. Expansion of the Analytical Window for Oil Spill Characterization by Ultrahigh Resolution Mass Spectrometry: Beyond Gas Chromatography. Environmental Science & Technology 47, 7530-7539.

McNutt, M.K., Chu, S., Lubchenco, J., Hunter, T., Dreyfus, G., Murawski, S.A., Kennedy, D.M., 2012. Applications of science and engineering to quantify and control the *Deepwater Horizon* oil spill. Proceedings of the National Academy of Sciences 109, 20222-20228.

Meinert, C., Moeder, M., Brack, W., 2007. Fractionation of technical p-nonylphenol with preparative capillary gas chromatography. Chemosphere 70, 215-223.

Melbye, A.G., Brakstad, O.G., Hokstad, J.N., Gregersen, I.K., Hansen, B.H., Booth, A.M., Rowland, S.J., Tollefsen, K.E., 2009. Chemical and toxicological characterization of an unresolved complex mixture-rich biodegraded crude oil. Environmental Toxicology and Chemistry 28, 1815-1824.

Miller, S., 1983. Photochemistry of natural water systems. Environmental Science & Technology 17, 568A-570A.

NASA, 2013. http://earthobservatory.nasa.gov. NASA - The Earth Observatory.

Neff, J.M., Ostazeski, S.A., Stejskal, I., 1996. The weathering properties of four unique crude oils from Australia. Spill Science and Technology Bulletin 3, 203-205.

Nizio, K.D., McGinitie, T.M., Harynuk, J.J., 2012. Comprehensive multidimensional separations for the analysis of petroleum. Journal of Chromatography A 1255, 12-23.

NOAA, 1996. Injury Assessment: Guidance Document for Natural Resource Damage Assessment Under the Oil Pollution Act of 1990, Appendix C. Oil Behavior, Pathways, and Exposure. NOAA, the Damage Assessment Remediation and Restoration Program.

NOAA, 2013. IncidentNews. http://incidentnews.noaa.gov/.

Nordtest, 1991. Oil spill identification NT Chem 001 - Ed 2. 1-24.

NRC, 2003. Oil in the Sea III : Inputs, Fates, and Effects. The National Academies Press, Washington DC.

Oil Rig Disasters, 2013. Rig Incident List. http://www.oilrigdisasters.co.uk/.

OPEC, 2012. World Oil Outlook 2012. Organization of the Petroleum Exporting Countries, Vienna, Austria.

Pantoja, P.A., Mendes, M.A., Nascimento, C.A.O., 2013. Contribution of mass spectrometry in assessing quality of petroleum fractions: The use of mass spectrometry for assessing asphaltenes. Journal of Petroleum Science and Engineering 109, 198-205.

Parastar, H., Radović, J.R., Jalali-Heravi, M., Diez, S., Bayona, J.M., Tauler, R., 2011. Resolution and quantification of complex mixtures of polycyclic aromatic hydrocarbons in heavy fuel oil sample by means of GC × GC-TOFMS combined to multivariate curve resolution. Analytical Chemistry 83, 9289-9297.

Payne, J.R., Phillips, C.R., 1985. Photochemistry of petroleum in water. Environmental Science and Technology 19, 569-579.

Peperzak, L., Kienhuis, P., Brussaard, C.P.D., Huisman, J., 2010. Accidental and Deliberate Oil Spills in Europe: Detection, Sampling and Subsequent Analyses. Handbook of Hydrocarbon and Lipid Microbiology, 3471-3489.

Pierce, K.M., Hoggard, J.C., Mohler, R.E., Synovec, R.E., 2008. Recent advancements in comprehensive two-dimensional separations with chemometrics. Journal of Chromatography A 1184, 341-352.

Prince, R.C., Garrett, R.M., Bare, R.E., Grossman, M.J., Townsend, T., Suflita, J.M., Lee, K., Owens, E.H., Sergy, G.A., Braddock, J.F., Lindstrom, J.E., Lessard, R.R., 2003. The roles of photooxidation and biodegradation in long-term weathering of crude and heavy fuel oils. Spill Science and Technology Bulletin 8, 145-156.

Prince, R.C., Lessard, R.R., Cutler, J.C., 2004. Crude Oil Releases to the Environment: Natural Fate and Remediation Options. Encyclopedia of Energy, 727-736.

Radović, J.R., Domínguez, C., Laffont, K., Díez, S., Readman, J.W., Albaigés, J., Bayona, J.M., 2012. Compositional properties characterizing commonly transported oils and controlling their fate in the marine environment. Journal of Environmental Monitoring 14, 3220-3229.

Radović, J.R., Rial, D., Lyons, B.P., Harman, C., Viñas, L., Beiras, R., Readman, J.W., Thomas, K.V., Bayona, J.M., 2012. Post-incident monitoring to evaluate environmental damage from shipping incidents: Chemical and biological assessments. Journal of Environmental Management 109, 136-153.

Reddy, C.M., Arey, J.S., Seewald, J.S., Sylva, S.P., Lemkau, K.L., Nelson, R.K., Carmichael, C.A., McIntyre, C.P., Fenwick, J., Ventura, G.T., Van Mooy, B.A.S., Camilli, R., 2012. Composition and fate of gas and oil released to the water column during the *Deepwater Horizon* oil spill. Proceedings of the National Academy of Sciences 109, 20229-20234.

Rial, D., Radović, J.R., Bayona, J.M., Macrae, K., Thomas, K.V., Beiras, R., 2013. Effects of simulated weathering on the toxicity of selected crude oils and their components to sea urchin embryos. Journal of Hazardous Materials 260, 67-73.

Rodrigue, J.P., 2013. The Geography of Transport Systems. 3, 416.

Scarlett, A., Rowland, S.J., Galloway, T.S., Lewis, A.C., Booth, A.M., 2008. Chronic sublethal effects associated with branched alkylbenzenes bioaccumulated by mussels. Environmental Toxicology and Chemistry 27, 561-567.

Schoenbaum, T.J., 2012. Liability for Damages in Oil Spill Accidents: Evaluating the USA and International Law Regimes in the Light of *Deepwater Horizon*. Journal of Environmental Law 24, 395-416.

Schwab, K., Altenburger, R., Lubcke-Von Varel, U., Streck, G., Brack, W., 2009. Effect-directed analysis of sediment-associated algal toxicants at selected hot spots in the River Elbe basin with a special focus on bioaccessibility. Environmental Toxicology and Chemistry 28, 1506-1517.

Schwab, K., Brack, W., 2007. Large volume TENAX® extraction of the bioaccessible fraction of sediment-associated organic compounds for a subsequent effect-directed analysis. Journal of Soils and Sediments 7, 178-186.

Schwarzenbach, R.P., Gschwend, P.M., Imboden, D.M., 2005. Environmental Organic Chemistry, 2nd ed. Wiley.

Schymanski, E.L., Bataineh, M., Goss, K.U., Brack, W., 2009. Integrated analytical and computer tools for structure elucidation in effect-directed analysis. TrAC - Trends in Analytical Chemistry 28, 550-561.

Schymanski, E.L., Meinert, C., Meringer, M., Brack, W., 2008. The use of MS classifiers and structure generation to assist in the identification of unknowns in effect-directed analysis. Analytica Chimica Acta 615, 136-147.

Seeley, J.V., Seeley, S.K., 2013. Multidimensional Gas Chromatography: Fundamental Advances and New Applications. Analytical Chemistry 85, 557-578.

Shang, D., Kirkwood, J., 2010. Integrated fourier transform infrared spectroscopy and gas Chromatography tandem Mass Spectrometry for forensic engine lubricating oil and biodiesel analysis, Proceedings of the 33rd AMOP Technical Seminar on Environmental Contamination and Response, pp. 79-100.

Shang, D., McPherson, B., 2009. Integrated gas and liquid chromatography tandem mass spectrometry for forensic engine lubricating oil identification, Proceedings of the 32nd AMOP Technical Seminar on Environmental Contamination and Response, pp. 51-66.

Smith, E., Wraige, E., Donkin, P., Rowland, S., 2001. Hydrocarbon humps in the marine environment: Synthesis, toxicity, and aqueous solubility of monoaromatic compounds. Environmental Toxicology and Chemistry 20, 2428-2432.

Speight, J.G., 2002. Handbook of petroleum product analysis. Wiley-Interscience.

Speight, J.G., 2006. The Chemistry and Technology of Petroleum, Fourth Edition. Taylor & Francis.

Swedish Coast Guard, 2002. Oil sampling at sea. Swedish Coast Guard Headquarters, Karlskrona, Sweden.

Sydnes, L.K., Hemmingsen, T.H., Skare, S., Hansen, S.H., Falk-Petersen, I.B., Lonning, S., Ostgaard, K., 1985. Seasonal variations in weathering and toxicity of crude oil on

seawater under arctic conditions. Environmental Science & Technology 19, 1076-1081.

Taki, M., Asahara, T., Mandai, Y., Uno, T., Nagai, M., 2009. Discriminatory analysis of crude oils using biomarkers. Energy and Fuels 23, 5003-5011.

Taki, M., Otomo, N., Otani, H., Tomiya, S., Uno, T., Nagai, M., 2011. Rapid analysis method for type of oil discharged into sea areas. Journal of the Japan Petroleum Institute 54, 103-107.

Thomas, K.V., Balaam, J., Hurst, M., Nedyalkova, Z., Mekenyan, O., 2004. Potency and characterization of estrogen-receptor agonists in united kingdom estuarine sediments. Environmental Toxicology and Chemistry 23, 471-479.

Thomas, K.V., Donkin, P., Rowland, S.J., 1995. Toxicity enhancement of an aliphatic petrogenic unresolved complex mixture (UCM) by chemical oxidation. Water Research 29, 379-382.

Thomas, K.V., Hurst, M.R., Matthiessen, P., McHugh, M., Smith, A., Waldock, M.J., 2002. An assessment of *in vitro* androgenic activity and the identification of environmental androgens in United Kingdom estuaries. Environmental Toxicology and Chemistry 21, 1456-1461.

Thomas, K.V., Langford, K., Petersen, K., Smith, A.J., Tollefsen, K.E., 2009. Effect-directed identification of naphthenic acids as important *in vitro* xeno-estrogens and anti-androgens in North Sea offshore produced water discharges. Environmental Science and Technology 43, 8066-8071.

Timmis, K.N., Smith, K.E.C., 2010. The Evaporative Weathering of Oil. Handbook of Hydrocarbon and Lipid Microbiology, 3751-3757.

Tissot, B.P., Welte, D.H., 1984. Petroleum Formation and Occurrence. Springer-Verlag.

UNCTAD, 2010. Review of Maritime Transport 2010. United Nations Conference on Trade and Development, New York, Geneva.

Van Deursen, M., Beens, J., Reijenga, J., Lipman, P., Cramers, C., Blomberg, J., 2000. Group-type identification of oil samples using comprehensive two-dimensional gas chromatography coupled to a time-of-flight mass spectrometer (GC x GC-TOF). HRC Journal of High Resolution Chromatography 23, 507-510.

Veith, G.D., De Foe, D., Knuth, M., 1984. Structure-activity relationships for screening organic chemicals for potential ecotoxicity effects. Drug Metabolism Reviews 15, 1295-1303.

Vendeuvre, C., Ruiz-Guerrero, R., Bertoncini, F., Duval, L., Thiébaut, D., 2007. Comprehensive two-dimensional gas chromatography for detailed characterisation of petroleum products. Oil and Gas Science and Technology 62, 43-55.

Ventura, G.T., Raghuraman, B., Nelson, R.K., Mullins, O.C., Reddy, C.M., 2010. Compound class oil fingerprinting techniques using comprehensive two-dimensional gas

chromatography (GC×GC). Organic Geochemistry 41, 1026-1035.

Verbruggen, E.M.J., Beek, M., Pijnenburg, J., Traas, T.P., 2008. Ecotoxicological environmental risk limits for total petroleum hydrocarbons on the basis of internal lipid concentrations. Environmental Toxicology and Chemistry 27, 2436-2448.

Von Der Ohe, P.C., Kuhne, R., Ebert, R.U., Altenburger, R., Liess, M., Schuurmann, G., 2005. Structural alerts - A new classification model to discriminate excess toxicity from narcotic effect levels of organic compounds in the acute daphnid assay. Chemical Research in Toxicology 18, 536-555.

Wang, W., Zheng, Y., Lee, K., 2013. Chemical dispersion of oil with mineral fines in a low temperature environment. Marine Pollution Bulletin 72, 205-212.

Wang, Z., Fingas, M., Page, D.S., 1999. Oil spill identification. Journal of Chromatography A 843, 369-411.

Wang, Z., Fingas, M.F., 2003. Development of oil hydrocarbon fingerprinting and identification techniques. Marine Pollution Bulletin 47, 423-452.

Wang, Z., Stout, S., 2010. Oil Spill Environmental Forensics: Fingerprinting and Source Identification. Elsevier Science.

Wardlaw, G.D., Arey, J.S., Reddy, C.M., Nelson, R.K., Ventura, G.T., Valentine, D.L., 2008. Disentangling oil weathering at a marine seep using GCxGC: Broad metabolic specificity accompanies subsurface petroleum biodegradation. Environmental Science and Technology 42, 7166-7173.

Weiss, J.M., Simon, E., Stroomberg, G.J., De Boer, R., De Boer, J., Van Der Linden, S.C., Leonards, P.E.G., Lamoree, M.H., 2010. Identification strategy for unknown pollutants using high-resolution mass spectrometry: Androgen-disrupting compounds identified through effect-directed analysis. Anal Bioanal Chem 400, 3141-3149.

White, H.K., Hsing, P.Y., Cho, W., Shank, T.M., Cordes, E.E., Quattrini, A.M., Nelson, R.K., Camilli, R., Demopoulos, A.W.J., German, C.R., Brooks, J.M., Roberts, H.H., Shedd, W., Reddy, C.M., Fisher, C.R., 2012. Impact of the *Deepwater Horizon* oil spill on a deep-water coral community in the Gulf of Mexico. Proceedings of the National Academy of Sciences of the United States of America 109, 20303-20308.

Yergin, D., 2011. The Prize: The Epic Quest for Oil, Money & Power. Free Press.

Yergin, D., 2013. Testimony submitted for Hearings on "America's Energy Security and Innovation". Subcommittee on Energy and Power of the House Energy and Commerce Committee.

Zeng, Z.-D., Hugel, H., Marriott, P., 2011. Chemometrics in comprehensive multidimensional separations. Anal Bioanal Chem 401, 2373-2386.

Zhang, C., 1997. Drilling and Gas Recovery Technology in Ancient China. Wictle Offset Printing, Shell Oil, Beijing.

Chapter II.

Materials and Methods

II.1.   Samples

II.1.1. Oil samples

Twenty-one (21) oil samples were obtained from local sources. They included a broad range of crude oils from Africa, America, Europe, and the Middle East, as well as different types of distilled products, creating a representative sample set of different oil classes, typically transported for the current oil market.

Fuel oil from the *Prestige* tanker spill was obtained from the ships' cargo tanks. The oil released during the *Deepwater Horizon* accident was collected from the gushing Macondo well (*MW)* using isobaric gas-tight (IGT) sampler deployed from a ROV in June 2010 (Reddy et al., 2012) (**Figure II-1**).

II.1.2. Field samples

Field sampling of *Prestige* oil was focused not on the major oil paths or the recently oiled shorelines, but on the slumps appearing at sea or arriving at the coast from time to time during 2003 and 2004. Samples were collected with a metal spoon, placed in pre-cleaned amber glass jars and stored in a portable refrigerator for transport to the laboratory.

The *MW* oil was recovered from oil splashes on jetty rocks ("rock scrapings") collected at two time points, first in April 2011 (350 days after the spill) at Buckaneer State Park (30° 15' 65", -89° 24' 22") and Waveland (32° 16' 55", -91° 22' 07"), MS and second in August 2012 (750 days after the spill) at Fort Gaines, AL (30° 14' 47", -88° 4' 32"), USA. They were found above the sea level, and were exposed to sunlight (**Figure II-2**). Samples were scraped off the rocks using pre-cleaned spatulas, transferred to clean jars and kept in dark and refrigerated until analyzed.
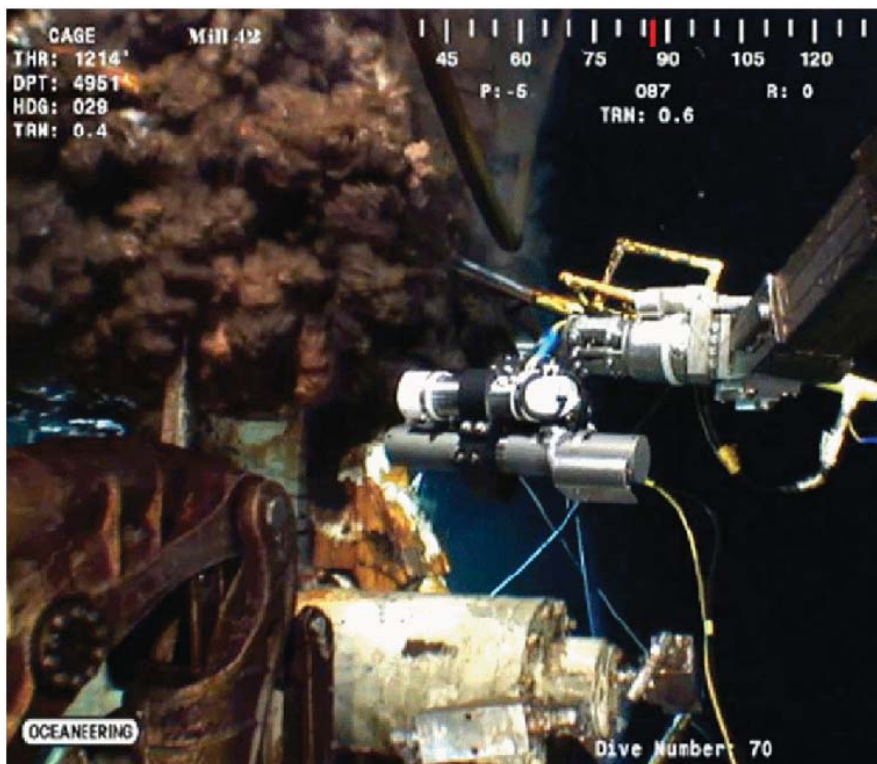
Figure II-1 Photograph of fluids exiting the Macondo well being collected on June 21, 2010, with an IGT sampler deployed by the Millennium 42 ROV from the vessel Ocean Intervention III. The IGT sampler, located in the center of the picture, is held by a robotic arm seen on the right side of the image (Reddy et al., 2012).

II.2.   *Physicochemical properties*

The oil properties that determine the environmental fate (e.g. evaporation, dispersion, emulsification, etc.) and effects in the case of a marine spill were selected. They include API gravity, density, pour point, viscosity, distillation properties (boiling points), sulfur and nitrogen content and metals content (Ni, V).

Data were obtained from online databases and reports (crude assays) of relevant authorities (e.g. Environment Canada), oil companies (Total, Statoil, etc.), and other web-based sources. Where missing, elemental compositions (S and N) were determined experimentally using elemental analyzer Model 1108 (Carlo-Erba, Milan, Italy) with flash combustion reactor and thermal conductivity detector.

Figure II-2 An example of a "rock scraping" sample containing *MW* oil collected on the Gulf of Mexico beaches.

II.3.   Fourier transform infrared spectroscopy (FT-IR)

Samples were characterized by FT-IR with a Nicolet Avatar 360 Thermo Scientific Spectrometer (Waltham, MA, USA) working at 32 scans per sample and a resolution of 4 cm^{-1}. Samples were applied on a KBr pellet and exposed to infrared light to eliminate the dissolvent, before being introduced to the instrument. IR spectra were acquired via computerized data processing system.

II.4.   MALDI-TOF

Asphaltene fraction of selected oils was analyzed using Bruker Autoflex III MALDI-TOF mass spectrometer (Bruker Daltonics, MA, USA). About 100 mg of fuel

was firstly diluted with pentane (pentane/fuel ratio is 60:1 (w/w)) in a 20 mL vial which was then sonicated 15 minutes to maximize the content of the pentane soluble fraction. The obtained mixture was filtered in the filtration equipment using HVLP 4700 Milipore® membrane filter. After that, the equipment was carefully cleaned with pentane to remove the amount of maltenic fraction sticking on the wall.

Secondly, the filter containing precipitated asphaltenes was extracted overnight in a Soxhlet apparatus with pentane to extract the remaining resin fraction. This solution was then mixed with the formerly obtained maltenes, rotary evaporated and dried under nitrogen to remove all pentane and finally kept in a refrigerator for further separation stages.

In the following day, the asphaltene fraction was dissolved in dichloromethane (DCM) and extracted by using the Soxhlet equipment overnight. 1-2 μl of the resulting solution was spotted on the polished steel MALDI target plate. The 2,5-dihydroxybenzoic acid (DHB) dissolved in acetonitrile:trifluoroacetic acid (1:2) was used as the matrix. The plate was dried at room temperature and then loaded to Bruker Autoflex III. Laser power of 60% was used for desorption/ionization.

II.5.   TLC-FID

The fresh and weathered oil samples were analysed using TLC-FID to obtain quantitative data on the composition of oils, i.e. the relative contents of saturates, aromatics, resins and asphaltenes (SARA analysis) (Aeppli et al., 2012; Radović et al., 2012).

Depending on the concentration, 0.8 to 5 µL of sample extracts (in DCM or DCM/methanol) were spotted on the base of a silica-gel sintered glass rods (ChromaRod®-SIII, Iatron Labs, Tokyo, Japan) using a microsyringe or SES 3202/IS-02 (Ses GmbH, Nieder-Olm, Germany) sample spotter. Next, the rods were sequentially eluted in the development tank using three solvents (or solvent mixtures) of increasing polarity (hexane, toluene, methanol) (**Figure II-3**).
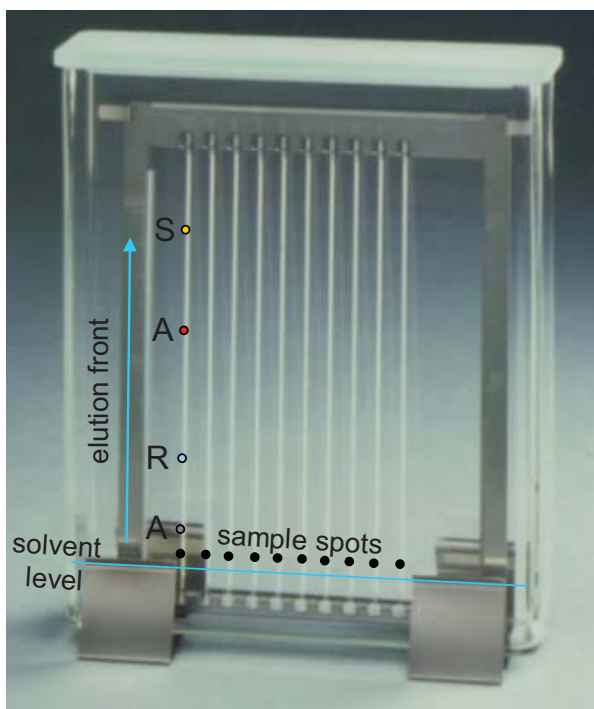
Figure II-3 TLC development chamber and a frame with ChromaRods®. Solvent level must be below the sample spots. Elution front is moved upwards by capillary forces carrying the sample and separating the main four oil fractions (saturates (S), aromatics (A), resins (R) and asphaltenes (A), SARA).

Eluents are successively changed either after determined development time has elapsed, or when the elution front has migrated up the ChromaRod® to a predetermined distance (**Table II-1**).

Between each development, the rods were dried for 1 to 5 minutes at 40 to 70 °C, and then transferred into a MK-5 TLC–FID Iatroscan® apparatus (Iatron Labs, Tokyo, Japan) where each Chromarod® was scanned with the FID to detect the oil compound classes separated on the silica.

The hydrogen flow rate of the detector was 160-180 mL·min^{-1}, the airflow rate was 2000 mL·min^{-1} and the scanning speed was 30 s per Chromarod® burned.

Table II-1 TLC eluents and development conditions.

Compound class	Eluent	Development time (min)	Elution front (cm)
Saturates	hexane	26	10
Aromatics	toluene (toluene/hexane 80/20)	12	5
Resins	MeOH/DCM (95%-97%/5%-3%)	5	2
Asphaltenes	/	0	0

Repeatability of the methodology was controlled by periodically analyzing a "standard" solution of crude oil of known composition and concentration. Relative standard deviation (RSD) was in the limits of ±5 %.

II.6. GC-FID

GC–FID analysis of oil extracts was performed on a Hewlett-Packard 5890 Series II GC (Paolo Alto, CA; USA) controlled by ChemStation software. Samples (10 to 50 mg·mL^{-1} DCM/methanol solution) were injected (1 µL injection volume) in splitless mode, and separated on a Restek Rtx-1 capillary column (30 m, 0.25 mm I.D., 0.25 µm film) with 5 mL·min^{-1} H$_2$ as the carrier gas. The temperature program was 7 min at 35 °C, ramped to 315 at 6 °C·min^{-1} and to 320 at 20 °C·min^{-1} (held 15 min).

II.7. GC-MS oil fingerprinting

Oil fingerprinting was based on the standard methodology accepted by the European Committee for Standardization (CEN) which involves GC-MS analysis of a suite of oil specific compounds including PAHs and molecular biomarkers and subsequent calculation of their characteristic "diagnostic ratios" (CEN, 2012). These ratios can then be evaluated, taking into account post-spill changes (e.g. weathering, mixing) and analytical variability, to determine the type of spilled oil (e.g. crude or

refined oil, lubricating oil, bilge oil, etc.) as well as the matching with candidate source samples. The standard procedure involves different steps:

- visual characterization of the samples;

- sample preparation;

- GC-MS analysis of spill and candidate source(s) and subsequent visual evaluation of chromatograms, and calculation and evaluation of diagnostic ratios;

- comparison of diagnostic ratios between spill samples and candidate source(s) taking into account the analytical variability;

- conclusion.

II.7.1. Sample characterization and preparation

After arriving to laboratory, samples should be examined respect to type (spill or source oil), matrix (e.g. water or Teflon® mesh), amount, container, etc. Based on this, samples should be prepared in such a way to minimize any possible compositional changes. Preparation normally includes solvent extraction and/or two-step cleanup in an open glass column, over anhydrous sodium sulfate (Na_2SO_4), and neutral alumina (activated at 400°C, 5% water deactivated), respectively (**Figure II-4**).

II.7.2. GC-MS instrumental conditions

GC-MS analysis was carried out with a TRACE-MS Thermo-Finnigan gas chromatograph (Manchester, UK) in the electron impact (EI) mode at 70 eV. A 20-m$\times$0.18-mm capillary column coated with 0.18 μm TRB-5MS stationary phase was obtained from Teknokroma (Sant Cugat del Vallès, Spain). The carrier gas was helium, with a constant flow rate of 0.6 mL·min^{-1}. The sample (1 μL) was injected in the splitless mode, injector temperature was held at 280 °C and the purge valve was activated 50 s after the injection. Column temperature was held at 60°C for 1 min, then the temperature was increased to 200 °C at 14 °C·min^{-1} and finally to 320 °C at 7.5 °C·min^{-1}, holding that temperature for 4 min. Transfer line and ion source temperatures were held at 250 and 200 °C, respectively. Data were acquired in the

full-scan mode from 50 to 350 amu (10 scan·s^{-1}) with 6 min of solvent delay and processed by the Xcalibur Thermo Finnigan software v. 2.0.7 (San Jose, CA, USA).
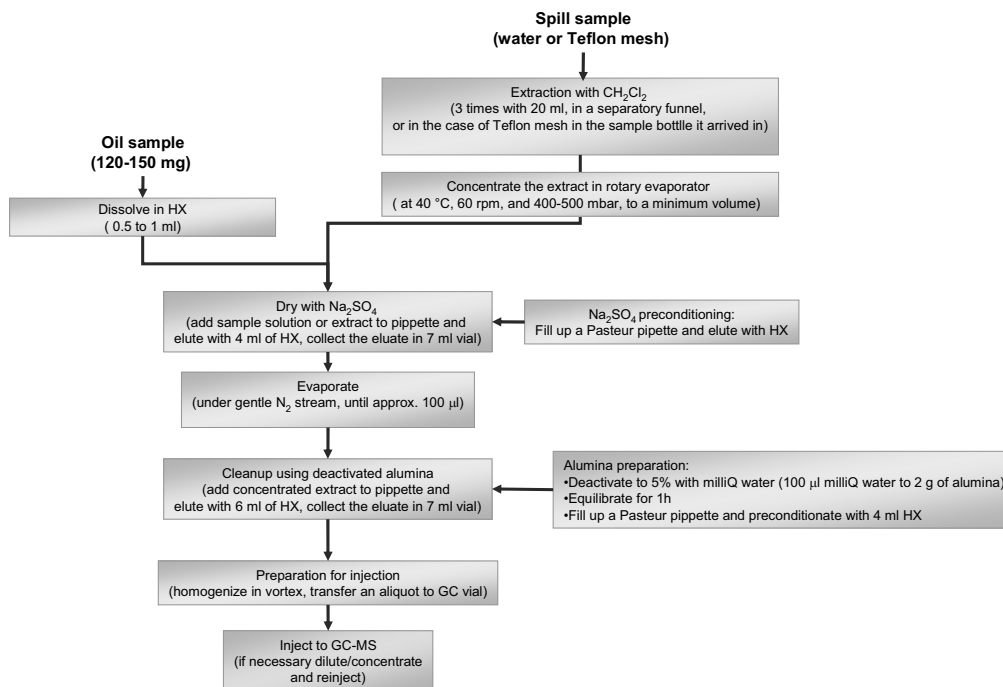
Figure II-4 Sample preparation flowchart.

II.7.3. Fingerprinting compounds and diagnostic ratios

Various fingerprinting compounds are selected to represent the diversity in chemical composition of petroleum and petroleum products and because of their recalcitrance or known behavior in weathering processes, including alkanes, PAHs and biomarker compounds. The list of the fingerprinting compounds recommended by the CEN norm (CEN, 2012), their abbreviations, structures and characteristic *m/z* are given in the **Table A-1**, Annex **A**.

This fingerprinting methodology is semiquantitative, i.e. the peak heights or areas of fingerprinting compounds are used as the measure to calculate the diagnostic ratios. There are 25 **normative ratios** according to the CEN standard methodology (CEN, 2012), which are considered the minimum useful set of ratios needed for

reliable identification of oil (**Table II-2**). Various other, **"informative" ratios** can be calculated to facilitate the oil identification or to elucidate the weathering changes.

Table II-2 Normative diagnostic ratios (CEN, 2012).

	Ratio			Ratio	
	Alkane ratios			*Biomarker ratios*	
1	C17/Pris	n-heptadecane/pristane	13	27Ts/30ab	18α(H)-22,29,30-trisnorhopane/17α(H),21β(H)-hopane
2	C18/Phy	n-octadecane/phytane	14	27Tm/30ab	17α(H)-22,29,30-trisnorhopane/17α(H),21β(H)-hopane
3	Pris/Phy	pristane/phytane	15	28ab/30ab	17α(H),21β(H)-28,30-bisnorhopane/17α(H),21β(H)-hopane
	PAH ratios		16	29ab/30ab	17α(H),21β(H)-30-norhopane/17α(H),21β(H)-hopane
4	4-MD/1-MD	4-methyldibenzothiophene/1-methyldibenzothiophene	17	30O/30ab	18α(H)-oleanane/17α(H),21β(H)-hopane
5	2-MP/1-MP	2-methylphenanthrene/1-methylphenanthrene	18	31abS/30ab	17α(H),21β(H),22S-homohopane/17α(H),21β(H)-hopane
6	2-MFl/4-MPy	2-methylfluoranthene/4-methylpyrene	19	30G/30ab	gammacerane/17α(H),21β(H)-hopane
7	B(a)F/4-MPy	benzo[*a*]fluorene/4-methylpyrene	20	27dbR/27dbS	13β(H),17α(H),20R-cholestane/13β(H),17α(H),20S-cholestane
8	B(b+c)F/4-MPy	benzo[*b+c*]fluorene/4-methylpyrene	21	27bb/29bb	5α(H),14β(H),17β(H),20(R+S)-cholestane/24-ethyl-5α(H),14β(H),17β,20(R+S)-cholestane
9	2-MPy/4-MPy	2-methylpyrene/4-methylpyrene	22	SC26/RC26+SC27	C26,20S-triaromatic sterane/C26,20R+C27,20S-triaromatic steranes
10	1-MPy/4-MPy	1-methylpyrene/4-methylpyrene	23	SC28/RC26 + SC27	C28,20S-triaromatic sterane/C26,20R+C27,20S-triaromatic steranes
11	Retene/TMP	retene/tetramethyl-phenanthrene	24	RC27/RC26+ SC27	C27,20R-triaromatic sterane/C26,20R+C27,20S-triaromatic steranes
12	BNT/TMP	benzo[*b*]naphto[1,2-d]thiophene/tetramethyl-phenanthrene	25	RC28/RC26+SC27	C28,20R-triaromatic sterane/C26,20R+C27,20S-triaromatic steranes

In order to minimize the analytical error, the ratios are normally calculated between compound peaks in the same *m/z* profile and within the same reasonable retention time range. The ratios of different samples are then compared taking into account the critical difference of 14%. This value is calculated as the repeatability limit of the analytical methodology using the following equation:

$$r95\% = z \times \sqrt{2} \times RSD = 2.8 \times RSD = 14\% \qquad (Eq.1)$$

where z is percentile value for a normal distribution (1.96) and RSD is relative standard deviation of 5%.

The relative difference of two ratios greater than 14% is considered to be statistically significant, i.e. the compared oil samples do not originate from the same source (**Table II-3**).

Table II-3 Example of a ratio comparison based on the repeatability limit (CEN, 2012).

Ratios to be compared in %		Mean	Absolute difference	Relative difference	Conclusion
Ratio sample 1	Ratio sample 2				
48	52	50	52 – 48 = 4	4/50*100 = **8%**	< 14% => No difference
35	45	40	45 – 35 = 10	10/40*100 = **25%**	> 14 % => Different

Finally, in order to be able to compare different samples and compensate for the concentration differences, the peak heights (or areas) of fingerprinting compounds are normalized to 17α(H),21β(H)-hopane (C_{30}-hopane) which behaves as a conservative internal marker, i.e. it is recalcitrant to weathering transformations (Prince et al., 1994). Tetramethylphenantrene (TMP) can be used as an alternative compound for normalization in case of a low concentration or absence of hopane (CEN, 2012). The differences between normalized peak heights (or areas) in original and weathered samples can be calculated according to the Equation 2:

$$\%remaining = 100 - \%depleted = 100 - \left(1 - \frac{X_{weathered}/H_{weathered}}{X_{original}/H_{original}}\right) \times 100 \quad \text{(Eq.2)}$$

where $X_{weathered}$ and $X_{original}$ represent the measure (peak area or height) of a compound or compound class in the weathered and original samples, respectively, and $H_{weathered}$ and $H_{original}$ the peak area or height of the C_{30}-hopane (or TMP) peak in the weathered and original samples, respectively.

These differences can then be visually represented using so called percentage weathering plots (PW-plots), by plotting them against the retention times corresponding to each fingerprinting compound.

As their name suggests, PW-plots are useful tool to visually detect loss of fingerprinting compounds due to weathering. For example, **Figure II-5** shows a PW-plot of a spill sample compared to the fresh oil, showing the evaporative loss of lighter volatile PAH and biomarker fingerprinting compounds (red oval).
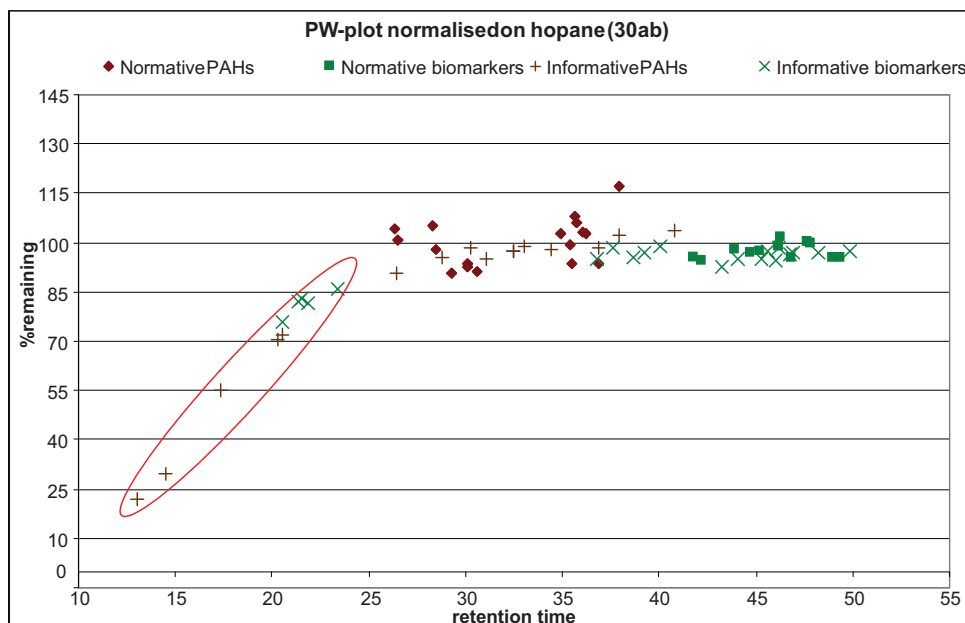
Figure II-5 PW plot comparison of a weathered spill sample relative to the source, showing the loss of lower boiling point fingerprinting compounds (red oval) due to evaporation (CEN, 2012).

Based on the comparison of diagnostic ratios and PW-plots according to described criteria following **conclusions** about the oil identity can be arrived at (CEN, 2012):

Positive match

When differences in chromatographic patterns and diagnostic ratios of the samples submitted for comparison are lower than the variability of the method or can be explained unequivocally, for example by weathering. The samples are concluded to be identical beyond any reasonable doubt.

Non-match

When differences in chromatographic patterns and diagnostic ratios of the samples submitted for comparison are distinct and larger than the variability of the method and they cannot be explained by external factors like weathering, contamination and heterogeneity. The samples are concluded to be distinctly different.

Probable match

When differences in chromatographic patterns and diagnostic ratios do not unequivocally permit a positive match, but they may be reasonably explained by

external factors, for example weathering in combination with mixing or the non-representative or heterogeneous character of the available samples.

Inconclusive

When differences in chromatographic patterns and diagnostic ratios do not permit a probable or non-match conclusion; for example in case the concentration of the contaminant in a sample is too small.

II.7.4. Quality assurance

For reliable oil identification results using the described GC-MS fingerprinting methodology proper quality assurance (QA) procedure is necessary.

In order to validate the method, first the linearity was checked using calibration curve with five concentration levels (0.5 to 50 mg·mL^{-1}) of n-alkane standard. Then the variability is tested using the laboratory reference oil (crude oil of known characteristics), which is analyzed eight times using the GC-MS methodology, and subsequently the diagnostic ratios are calculated. All diagnostic ratios should have less than 5% RSD.

To ensure the quality during daily analysis, several criteria are evaluated:

- *Retention time*

Variation of retention times is tested by injecting the reference oil at the beginning and the end of a sequence, and then two chromatograms are superimposed. The retention time variation should be inferior to 6 seconds.

- *Sensitivity*

In order to test the mass detector sensitivity, the reference oil is injected at the beginning and at the end of a sequence, and the 3-MP to C_{30}-hopane ratio is then calculated for two injections. The relative difference between the ratios of two injections should be inferior to 14%.

- *Resolution of the chromatographic column*

It is evaluated by injecting the reference oil, and calculating the resolution between the peaks of 3-MP and 2-MP, or 31abS and 31 abR. The resolution between 3-MP and 2-MP should be higher than 0.7 and the resolution between 31abS and 31abR higher than 0.9.

- *Method blanks*

For every analysis, a hexane method blank is prepared following the same procedure as for the sample, and it is injected during the sample sequence. The signal to noise ratio (S/N) must be higher than 3-5 for the determined analytes.

- *Reference oil*

At the beginning and at the end of each analytical sequence reference oil is injected, and then two chromatograms are superimposed to check that there are no significant variations of fingerprinting compound peaks.

II.8.   *GC×GC-TOFMS and GC×GC-FID*

The **GC×GC-TOFMS system** was a Pegasus 4D (LECO, St. Joseph, MI, USA), which is an Agilent Technologies 6890 GC (PaloAlto, CA, USA) equipped with a split/splitless injector, a secondary oven to fit the secondary column, and a ZX1 two stage thermal modulator (Zoex, Houston, TX, USA). Liquid nitrogen was used to cool down the nitrogen gas for cold pulses and automatically filled from a Dewar using a liquid leveler which accessed to a 60 L liquid nitrogen storage tank. The GC column set consisted of a TRB-5MS coated with 5% diphenyl 95% dimethylpolysiloxane from Teknokroma (Sant Cugat del Vallès, Spain) (20 m, 0.18 mm i.d., 0.18 µm d_f) as the 1st dimension and a TRB50-HT coated with 50% diphenyl 50% dimethylpolysiloxane from Teknokroma (2.0 m, 0.10 mm i.d., 0.10 µm film thickness) as the 2nd dimension. The second column was connected to the TOFMS via transfer line.

The **GC×GC-TOFMS method** was optimized for the analysis of aromatic hydrocarbons in the oil fractions. The primary oven temperature program was at 65 °C for 1 min, ramped at 10 °C·min^{-1} to 315 °C, and then held for 3 min. The secondary oven temperature program had a temperature 10 °C higher than that of the primary one and with similar ramp. Carrier gas flow rate was 0.60 mL·min^{-1} using helium. The modulation period (P$_M$) was 6 s with 0.5 s hot pulse duration and a 15 °C modulator temperature offset versus the primary oven temperature. The MS transfer line was held at 250 °C, and the TOFMS was operated in the electron ionization (EI) mode with a collected mass range of 50-300 *m/z*. The ion source temperature was 250 °C, the detector was operated at 1650 V, the applied electron energy was 70 eV, and the

acquisition rate was 80 spectra·s^{-1}. Temperature ramp and the modulation period were optimized by injecting standard mixtures of PAHs to avoid wrap-around of late-eluting high molecular weight compounds. The parameters of the TOF analyzer were adjusted to obtain satisfactory sensitivity for the detection of higher molecular weight PAHs.

The **GC×GC–FID system** employed a dual stage cryogenic modulator (Leco Corp., St. Joseph, MI, USA) installed in an Agilent 7890A gas chromatograph configured with a 7683 series split/splitless auto-injector.

The **GC×GC–FID method** was optimized for the analysis of oil biomarker compounds. Each sample was injected in splitless mode and the purge vent was opened at 0.5 min. The inlet temperature was 300 °C. The 1st dimension column was a nonpolar Restek DB-1 (60 m×0.25 mm i.d., 0.25 μm d_f) held at 60 °C for 10 min and then ramped to 325 °C at 1.25 °C·min^{-1}. The thermal modulator cold jet gas was dry N_2, chilled with liquid N_2. The thermal modulator hot jet air was heated to 15 °C above the temperature of the secondary GC oven. The hot jet was pulsed for 1 s every 12 s (P_M) with a 5 s cooling period between stages. The 2nd dimension separations were performed with a 50% phenyl polysilphenylene–siloxane column (SGE BPX50, 1.25 m×0.10 mm i.d., 0.1 μm d_f) held at 65 °C for 10 min and then ramped to 330 °C at 1.25 °C·min^{-1}. The carrier gas was H_2 at a constant flow rate of 1 ml·min^{-1}. The FID detector signal was sampled at a rate of 100 Hz. Biomarker compounds were identified based on established elution order (Eiserbeck et al., 2012; Gaines et al., 2007) and using the authentic standards obtained from Sigma-Aldrich, Chiron, and NIST. Using the authentic standards, the FID response factors of the individual biomarker compounds were determined; they were equal (±9%) for all compounds, and the peak heights proved to be proportional to the peak volume. In addition, GC×GC coupled to time-of-flight mass spectrometry (GC×GC-TOFMS; according to reference (Ventura et al., 2010)) was used to confirm the identity of compounds based on their mass spectra. Peaks were manually integrated using the ChromaTOF® software v. 4.43.3.0 (LECO Corp., St. Joseph, MI, USA).

II.9.   Interlaboratory ring test for oil spill identification

Round Robin 2010 (RR2010) was the fifth worldwide ring test of the Bonn-OSINet expert group on oil spill identification of the Bonn-Agreement, in which 24 laboratories from 18 countries participated.

The laboratories received five samples, three spill samples and two candidate sources, prepared by North China Sea Environmental Monitoring Center of State Oceanic Administration (Peoples Republic of China). Participants were requested to report the type of oil, and to compare the spill samples (RR2010-1, -2 and -3) with the candidate source samples (RR2010-4 and -5).

First spill sample (RR2010-1) comes from unidentified oil spill from May 2010 collected in the Bohai Sea. The spill samples 2 (RR2010-2) and 3 (RR2010-3) were prepared from source sample 4 (RR2010-4) using experimental reactor to simulate biodegradation in marine conditions. Biodegradation was carried out at 25 °C using hydrocarbon degrading bacteria (*Ochrobactrum* N1, *Brevibacillus parabrevis* N2, N3, and N4) and biosurfactant producing bacterium (*Brevibacillus parabrevis* B-1) which were screened from petroleum contaminated seawater. Float oil samples were collected for analysis: RR2010-2 was a light weathered sample, fetched at 10th day; RR2010-3 was a heavily weathered sample, fetched at the end of the experiment (144th day). Source sample 5 (RR2010-5) is from a crude oil that is found in the same area as sample 4.

II.10.   Oil evaporation

Evaporation was performed to simulate the short-term weathering of oil (ca. 2 h) following a spill. Oil samples (1L) were placed in a pre-weighed crystallizing dish (2L) in a fume hood (air flow 0.5 m·s^{-1}) at room temperature for 24 h. Evaporative loss was calculated for each oil based on weight.

II.11.   *Oil photooxidation*

Both natural and simulated solar irradiation was used to investigate the photooxidation of the *Prestige* and *MW* oil. Simulated irradiation was used to prepare photooxidized samples of North Sea Crude (NSC) oil and heavy fuel oil (HFO) used in the EDA study.

In the first experiment, approximately 80 mg of the *Prestige* oil was placed in an uniform thin layer in Petri plates and irradiated using a SUNTEST® CPS flatbed Xe-exposure system (Atlas, Chicago, IL, USA), equipped with a 1500B NrB4 Xe-lamp that was operated at the potential of 507.5 W·m^{-2} to simulate natural irradiation. **Figure II-6** shows that the irradiation spectrum of this lamp closely matches the spectral distribution recommended for irradiation testing (CIE, 1989). The system is equipped with a ventilator to maintain a constant temperature (40 °C approx.) and prevent sample overheating.

Dark control plates covered with Al foil were irradiated simultaneously (**Figure II-7**). Samples were collected after 12 h, and the oil was washed off the plates with 3-5 mL of DCM and collected for further analysis. NSC and HFO for the EDA studies were prepared in a similar way, the same irradiation potential was used (507.5 W·m^{-2}), while the irradiation time was 6h. Similar irradiation conditions have previously been used to simulate the short-term moderate weathering in the temperate environments and have been demonstrated to change the composition and toxic effects of the treated oils (Radović et al., 2013; Rial et al., 2013).

For the *MW* oil experiments, approximately 50 mg of oil was added to each quartz glass tube to form relatively uniform thin layer. Control tubes were wrapped in Al foil. The tubes were mounted horizontally on an Al foil wrapped surface and exposed to sunlight on the top of a three-meter high cargo container in the Woods Hole Oceanographic Institution Quisset Campus (Woods Hole, MA, USA) (**Figure II-8**).
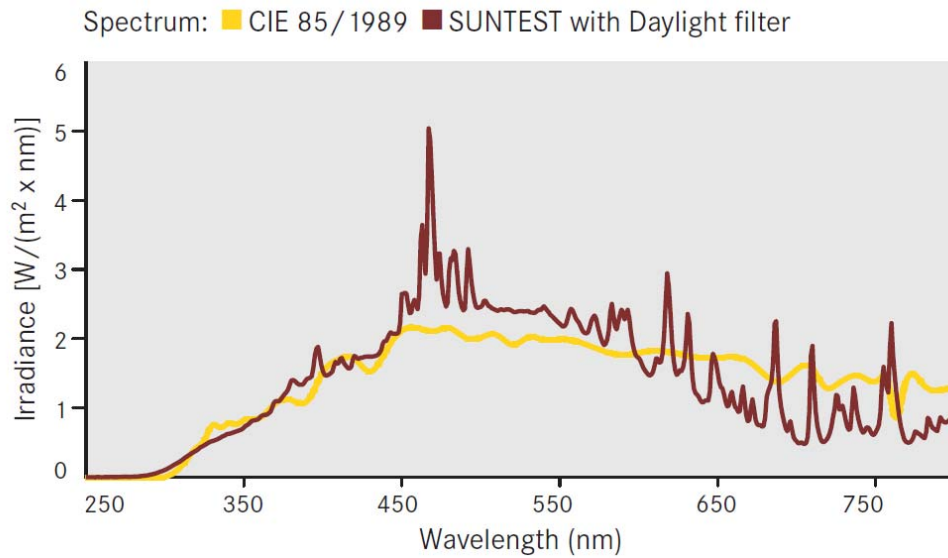
Figure II-6 Spectrum of irradiation obtained using SUNTEST® Xe-lamp compared to recommended spectral distribution of simulated solar radiation for standardized testing purposes (CIE, 1989).

Figure II-7 Atlas SUNTEST® instrument used to simulate solar irradiation and the Petri plates with *Prestige* oil (dark control is wrapped in Al foil).

Figure II-8 Quartz tubes containing *MW* oil were exposed to natural sunlight.

The duplicate tubes were collected every day during the first week, then after 20 and 70 days when the experiment finished (18 samples in total). Oil was extracted with DCM/methanol (80/20) and dried over anhydrous Na_2SO_4 for further analysis. Experiment was performed from May to August 2012, and the average irradiation potential during this period was 750 W·m^{-2} as recorded by the nearby solar station (41° 42' 38", -70° 4' 31").

II.12.   *Short-term oil fate modeling*

Automated Data Inquiry for Oil Spills (ADIOS2, version 2.0.1) software from the NOAA was used to perform short-term oil fate modeling for selected oils. The model was populated using the database constructed for a total of 20 oils (Diesel C was not included since distillation data were not available). Three spill scenarios for a continuous release of 120 tons (i.e. 109 metric tonnes, representing a medium scale spill) of oil during a 24 hour period were modeled for three contrasting geographical areas: the Northwestern Mediterranean Sea (Tarragona buoy, 40° 40' 48", 1° 28' 12"), the Northeastern Atlantic Ocean (Coast of Galicia, buoy of Villano-Sisargas, 43° 30' 0", 9° 12' 36"), and the Norwegian coast of the North Sea (Troll A oil platform, 60° 38' 24", 3° 43' 12"). Averaged annual data were used for wind/current speed and direction, and summer water temperature (Haugan, 1991; Jonassen, 2012; Meteorologisk institutt, 2011; Puertos del Estado, 2011). Wave height was computed by the model based on

wind speed. Finally, typical salinity and concentrations of suspended particulate matter (SPM) at the three locations were inputted to the model (García-Flor et al., 2005; MUMM, 2002-2012; Nolting and Eisma, 1988; Oliveira et al., 1999; Sundermann et al., 1993).

II.13.   Effect-directed analysis

Effect-directed analysis (EDA) was performed on fresh and weathered (evaporated and photooxidized) samples of crude and heavy residual oil. This work was realized in collaboration with Dr. Kevin V. Thomas from the Norwegian Institute for Water Research (NIVA), where bioassays were performed; and Prof. Romà Tauler from the Institute of Environmental Assessment and Water Research (IDAEA-CSIC), Spain, and Dr. Hadi Parastar from the University of Isfahan, Iran, who developed the applied chemometric model.

Flowchart of the applied EDA strategy is shown in **Figure II-9**. Sample complexity was sequentially reduced by coarse (open-column chromatography, first level) and fine (HPLC, second level) fractionation. This was followed by biotesting (AhR and AR bioassays) and chemical characterization of the most active fractions using GC×GC–TOFMS. Moreover, an additional computational step was added to the typical EDA strategy, whereby an N-PLS model was developed to estimate the contribution of detected compounds to the observed effects, enabling further "chemometrical reduction" of the samples' complexity. The effects of the identified compounds were confirmed using quantitative structure-activity relationship (QSAR) estimates.
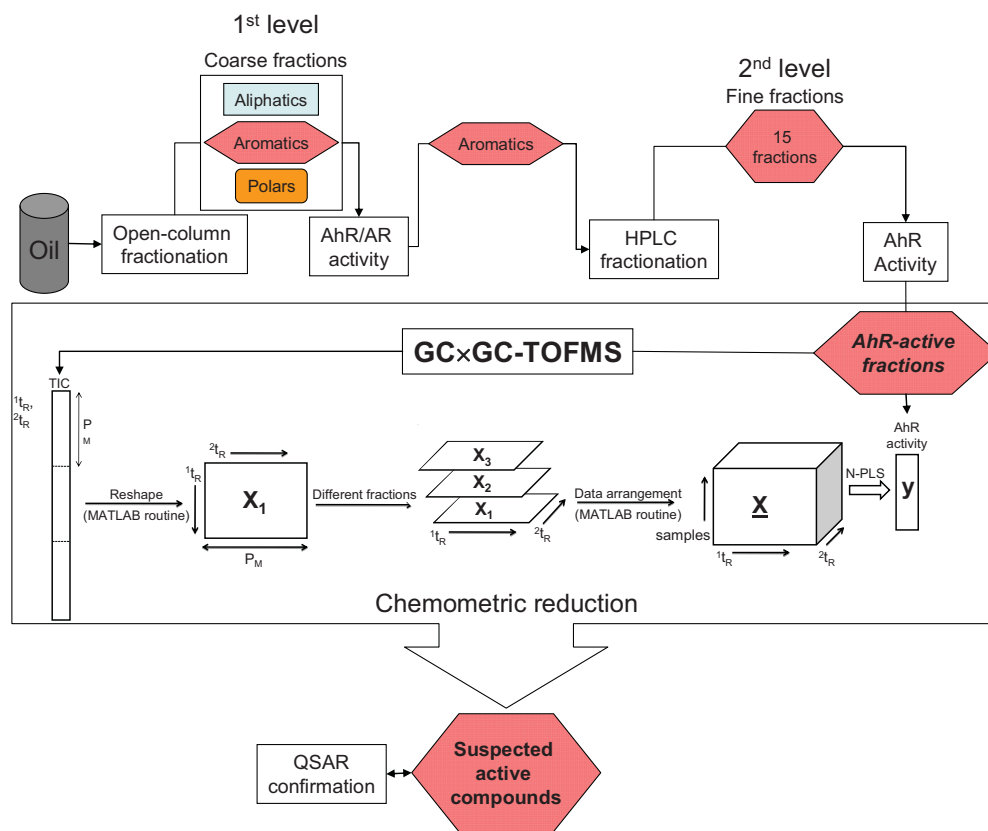
Figure II-9 Flowchart of the applied EDA strategy.

II.13.1. Coarse fractionation

Fresh and weathered oil samples were fractionated into saturate, aromatic and polar fractions by open-column liquid chromatography A glass column packed with silica gel (60-100 mesh; 5% H_2O; 40 g) under alumina (grade 1 neutral; 1.5% H_2O; 20 g) was loaded with oil (1 g approx.) and eluted with hexane (2 column void volumes), dichloromethane (2 column void volumes) and methanol (2 column void volumes) to provide saturate, aromatic and polar (i.e. resin) fractions, respectively. Solvent was then removed by rotary evaporation and the fractions transferred to a vial, evaporated under the stream of N_2 and weighed.

II.13.2.   Fine fractionation

The coarse aromatic fraction extracts were sub-fractionated by normal-phase HPLC (Shimadzu VP Series HPLC system with an SPD-10A UV/Vis detector and FRC-10A fraction collector) using an aminopropyl-modified Hypersil APS-2 semi-preparative column (250×7 mm i.d., Shandon, Cheshire, UK) which is a configuration typically used for group-type separation of the aromatic compounds by their increasing aromaticity (double bond equivalent) (Rønningsen and Skjevrak, 1990; Sutton and Nesterenko, 2007).

The method was optimized by injecting individual (or combined) PAH standards of different aromaticity as model calibration compounds (naphthalene, phenanthrene, pyrene, benz[a]anthracene, and perylene), as well as the standard EPA mix of 16 PAHs, while monitoring their elution times at characteristic wavelengths (Karcher et al., 1985). Subsequently, about 10 mg of aromatic fraction dissolved in hexane was injected on the column at a flow rate of 2 mL·min^{-1} using gradient elution for 35 min. LiChrosolv® grade n-hexane was pumped isocratically for a period of 10 min, ramped up to 20% dichloromethane (DCM, LiChrosolv® grade) over a period of 20 min, held for 5 min, and then returned to the initial conditions. Fifteen 4-mL fractions were collected using fraction collector at 2-min intervals from 0−30 min. In order to check whether the retention times remained constant, the standard PAH mixtures were injected periodically between the sample injections. Complete recovery of the injected aromatic fraction was controlled by GC-MS screening of the column blanks.

II.13.3.   AhR agonism assay

The oils' AhR agonist content was determined using rat-hepatoma (h4IIE) cell lines stably transfected with the firefly luciferase gene as a reporter (pGudLuc) provided as a service by BioDetection Systems (BDS, Amsterdam, Netherlands). In order to include the total AhR binding affinity of all receptor agonists in the oils, a high-throughput PAH-CALUX® (PAH Responsive Chemically Activated LUciferase eXpression) assay was used with a 4-h exposure and performed as described by Pieterse et al (Pieterse et al., 2013). The PAH-CALUX assay is optimized for the AhR-mediated hazard identification of total PAHs and provides a response relative to benzo[a]pyrene.

II.13.4. AR antagonism assay

Samples were analyzed for AR antagonists using the Yeast Androgen Screen (YAS), a yeast-based (*Saccharomyces cerevisiae*) screen developed by Glaxo-Wellcome, plc (Stevenage, Herts, UK) (Sohoni and Sumpter, 1998). The YAS assay contains stably transfected human ARs and androgen-responsive elements. The assay was run as described by Thomas et al. (Thomas et al., 2009). In brief, to detect AR agonist and antagonist activity, dihydrotestosterone (DHT) was added to each well at a concentration calculated to produce a sub-maximal androgenic response (1.56×10^{-9} M). Flutamide was used at a concentration of 25 mg·L^{-1} (1.1×10^{-4} M) as an anti-androgenic positive control. The plates were shaken at 20-25 Hz and incubated at 32($\pm$1) °C for the first 24 h and at 28($\pm$1) °C thereafter. They were colorimetrically read after 48 h using a PowerWaveX plate reader (Biotek Instruments, Winooski, VT, USA) at an absorbance of 540 nm for color and 620 nm for the turbidity.

II.13.5. N-PLS model

The applied N-PLS methodology is schematically represented in **Figure II-9** while detailed description can be found in the Annex **C**.

II.13.6. QSAR confirmation

The binding affinity of the suspected active compounds to the AhR was assessed using the VirtualToxLab™ (Biographics Laboratory 3R, Switzerland), an *in-silico* technology used to estimate the toxic potential of chemicals by simulating and quantifying the binding of molecules to a series of proteins (Vedani et al., 2012).

II.13.7. Software

GC×GC–TOFMS data acquisition and processing was carried out using ChromaTOF® software, version 4.43.3.0 (LECO Corp., St. Joseph, MI, USA), with the NIST 05 mass spectral library (National Institute of Standards and Technology,

Gaithersburg, MD, USA). The data were exported in comma-separated values (CSV) format and imported into MATLAB, version 7.11 (MathWorks Inc., Natick, MA, USA). All data preparation and arrangement were performed using a customized MATLAB routine in MATLAB 7.11. In addition, PLS Toolbox v. 5.8 (Eigenvector Inc., WA, USA) was used for N-PLS and U-PLS modeling. VirtualToxLab™ (Biographics Laboratory 3R, Switzerland) was used for QSAR confirmation. Potential toxicity of chemicals to marine organisms was estimated using ECOSAR (Ecological Structure Activity Relationships) v 1.11 model from Environmental Protection Agency (EPA).

II.14.   Statistical analysis

Principal component analysis (PCA) was performed on the fingerprinting data set using the PASW Statistics 18 package from SPSS Inc. (Chicago, IL, USA), in order to examine contribution of applied diagnostic ratios to differentiation between the selected oil types. Data were arranged in a matrix in which different oil types (20) were represented in columns, whereas diagnostic ratios (25) were in rows.

II.15.   References

Aeppli, C., Carmichael, C.A., Nelson, R.K., Lemkau, K.L., Graham, W.M., Redmond, M.C., Valentine, D.L., Reddy, C.M., 2012. Oil Weathering after the Deepwater Horizon Disaster Led to the Formation of Oxygenated Residues. Environmental Science & Technology 46, 8799-8807.

CEN, 2012. CEN/TR 15522-2:2012, Oil spill identification - Waterborne petroleum and petroleum products - Part 2: Analytical methodology and interpretation of results.

CIE, 1989. CIE 85/1989 - Solar Spectral Irradiance. International Commission on Illumination.

Eiserbeck, C., Nelson, R.K., Grice, K., Curiale, J., Reddy, C.M., 2012. Comparison of GC-MS, GC-MRM-MS, and GC×GC to characterise higher plant biomarkers in Tertiary oils and rock extracts. Geochimica et Cosmochimica Acta 87, 299-322.

Gaines, R.B., Frysinger, G.S., Reddy, C.M., Nelson, R.K., 2007. Oil Spill Source Identification by Comprehensive Two-Dimensional Gas Chromatography (GCxGC). Oil Spill Environmental Forensics - Fingerprinting And Source Identification, 169-206.

García-Flor, N., Guitart, C., Ábalos, M., Dachs, J., Bayona, J.M., Albaigés, J., 2005. Enrichment of organochlorine contaminants in the sea surface microlayer: An organic

carbon-driven process. Marine Chemistry 96, 331-345.

Haugan, P.M., G. Evensen, J.A. Johannessen, O.M. Johannessen, L.H. Pettersson, 1991. Modeled and observed mesoscale circulation and wave current refraction during the 1988 Norwegian continental shelf experiment. Journal of Geophysical Research, 10487-10506.

Jonassen, M.O., 2012. Multi-scale variability of winds in the complex topography of southwestern Norway. Tellus. Series A, Dynamic meteorology and oceanography 64, 11962.

Karcher, W., Fordham, R.J., Dubois, J.J., Glaude, P.G.J.M., Ligthart, J.A.M., 1985. Spectral Atlas of Polycyclic Aromatic Compounds: including Data on Occurrence and Biological Activity. Springer.

Meteorologisk institutt, 2011. Sea and coast. http://www.met.no/.

MUMM, 2002-2012. North Sea facts. Management Unit of the North Sea Mathematical Models, Royal Belgian Institute of Natural Sciences.

Nolting, R.F., Eisma, D., 1988. Elementary composition of suspended particulate matter in the North Sea. Netherlands Journal of Sea Research 22, 219-236.

Oliveira, A., Rodrigues, A., Jouanneau, J.M., Weber, O., Alveirinho-Dias, J.M., Vitorino, J., 1999. Suspended particulate matter distribution and composition on the northern Portuguese margin. Boletin - Instituto Espanol de Oceanografia 15, 101-109.

Pieterse, B., Felzel, E., Winter, R., Van Der Burg, B., Brouwer, A., 2013. PAH-CALUX, an optimized bioassay for AhR-mediated hazard identification of polycyclic aromatic hydrocarbons (PAHs) as individual compounds and in complex mixtures. Environmental Science and Technology 47, 11651-11659.

Prince, R.C., Elmendorf, D.L., Lute, J.R., Hsu, C.S., Haith, C.E., Senius, J.D., Dechert, G.J., Douglas, G.S., Butler, E.L., 1994. 17.alpha.(H)-21.beta.(H)-hopane as a conserved internal marker for estimating the biodegradation of crude oil. Environmental Science & Technology 28, 142-145.

Puertos del Estado, 2011. Datos en tiempo real, predicciones y banco de datos. Ministerio de Fomento, Gobierno de España.

Radović, J.R., Aeppli, C., Nelson, R.K., Jimenez, N., Reddy, C.M., Bayona, J.M., Albaigés, J., 2013. Assessment of photochemical processes in marine oil spill fingerprinting. Marine Pollution Bulletin http://dx.doi.org/10.1016/j.marpolbul.2013.11.029.

Radović, J.R., Domínguez, C., Laffont, K., Díez, S., Readman, J.W., Albaigés, J., Bayona, J.M., 2012. Compositional properties characterizing commonly transported oils and controlling their fate in the marine environment. Journal of Environmental Monitoring 14, 3220-3229.

Reddy, C.M., Arey, J.S., Seewald, J.S., Sylva, S.P., Lemkau, K.L., Nelson, R.K., Carmichael, C.A., McIntyre, C.P., Fenwick, J., Ventura, G.T., Van Mooy, B.A.S., Camilli, R., 2012.

Composition and fate of gas and oil released to the water column during the Deepwater Horizon oil spill. Proceedings of the National Academy of Sciences 109, 20229-20234.

Rial, D., Radović, J.R., Bayona, J.M., Macrae, K., Thomas, K.V., Beiras, R., 2013. Effects of simulated weathering on the toxicity of selected crude oils and their components to sea urchin embryos. Journal of Hazardous Materials 260, 67-73.

Rønningsen, H.P., Skjevrak, I., 1990. Characterization of north sea petroleum fractions: Aromatic ring class distribution. Energy & Fuels 4, 608-626.

Sohoni, P., Sumpter, J.P., 1998. Several environmental oestrogens are also anti-androgens. Journal of Endocrinology 158, 327-339.

Sundermann, J., Prandle, D., Lankester, R., McCave, I.N., 1993. Suspended Particulate Matter in the North Sea: Field Observations and Model Simulations [and Discussion]. Philosophical Transactions: Physical Sciences and Engineering 343, 423-430.

Sutton, P.A., Nesterenko, P.N., 2007. Retention characteristics of aromatic hydrocarbons on silica and aminopropyl-modified monolithic columns in normal-phase HPLC. Journal of Separation Science 30, 2900-2909.

Thomas, K.V., Langford, K., Petersen, K., Smith, A.J., Tollefsen, K.E., 2009. Effect-directed identification of naphthenic acids as important *in vitro* xeno-estrogens and anti-androgens in North Sea offshore produced water discharges. Environmental Science and Technology 43, 8066-8071.

Vedani, A., Dobler, M., Smiesko, M., 2012. VirtualToxLab - A platform for estimating the toxic potential of drugs, chemicals and natural products. Toxicology and Applied Pharmacology 261, 142-153.

Ventura, G.T., Raghuraman, B., Nelson, R.K., Mullins, O.C., Reddy, C.M., 2010. Compound class oil fingerprinting techniques using comprehensive two-dimensional gas chromatography (GC×GC). Organic Geochemistry 41, 1026-1035.

Chapter III.

Results and discussion

III.1. Compositional properties of commonly transported oils and the assessment of their fate and effects in the marine environment

III.1.1. Introduction

Despite the positive trends, environmental and socio-economic impacts of oil spills on marine ecosystems and coastal regions remain an issue of great concern demanding constant efforts in terms of oil spill preparedness and response. In this respect, chemical characterization is a key tool that is indispensable for assessing risks associated with oil spills. It involves characterization of crude oils and petroleum products, as well as elucidation of weathering processes that affect and change the oil composition once it is released into the marine environment.

Since physicochemical properties for different crude oils and oil products vary greatly, detailed information on them is valuable to reliably estimate the sources, environmental behavior, impact, and ultimate fate in a particular oil spill scenario. Also, this type of information is a necessary input when using oil spill models. Although such databases are available for a number of oils, they are often incomplete, variable and insufficiently comprehensive. Furthermore, oil spill studies are usually performed post-incident, focusing on the specific oil involved in the incident (i.e. a reactive approach). Databases afford a more pro-active strategy that provides characterization and weathering assessments for a selection of representative oils and oil products in advance.

In this section, physicochemical properties that control the environmental fate and impact of 21 frequently transported oils were compiled from, where possible, publicly available sources (e.g. environmental databases, crude assays, etc.) and, where necessary, experimentally using elemental analysis and TLC-FID.

Created oil properties database was then used to assess short-term weathering of the oils using the publicly available Automated Data Inquiry for Oil Spills (ADIOS2) model. Finally, GC-MS fingerprinting was used to determine specific PAH and biomarker molecules in the selected oils, and to calculate their characteristic diagnostic ratios which were statistically analyzed using PCA.

III.1.2.   Physicochemical properties

Selected physicochemical properties for the investigated oil samples are given in the **Table III-1**. According to the EPA criteria (EPA, 2013), distinction is made between persistent and non-persistent oils (see section **I.4**). According to their API densities (**Table III-1**), out of the selected oils, only Diesel A and Diesel B (probably also Diesel C, but distillation data are lacking) could be considered as non-persistent. The remainder are persistent (EPA, 2013; ITOPF, 2013) belonging predominantly to Group 2 (°API=35-45; eight oils: Kirkuk, Azeri, Oseberg, Siberian Light, North Sea oil, Murban, Nemba, Sirtica) and Group 3 (°API=17.5-35; nine oils: Sorosh, Maya, Dalia, Hungo, Forcados, Kuwait, Norne, Arabian Light, Flotta). Only one oil, namely Heavy fuel oil (HFO) falls into Group 4 (°API<17.5).

Oil **density** determines floating/sinking characteristics of an oil spill. Normally, oils float on the water, but due to changes in the water temperature and/or weathering (evaporation, dispersion, interaction with sediment particles) oil density can increase up to a point where it sinks, either to the bottom, or to a point in the water column that has higher density (Castle et al., 2005). In some cases, e.g. high particulate load with a large proportion of the oil in the dispersed phase, this is even possible for light oils such as diesels (NOAA/EPA, 1978; NRC, 2003). Densities of the selected oils range from 815 kg·m^{-3} (43.3 °API) in the case of light Sirtica crude up to 988.8 kg·m^{-3} (11.47 °API) for residual HFO. Therefore, out of the investigated oils, HFO, Maya, and Sorosh would classify as "heavy" oils (°API less than 20, approx.) with sinking tendency (Speight, 2006).

Table III-1 Physicochemical properties of the selected oils (Belgo Egyptian, 2009; BP, 1996-2013; Buist, 2003; CEPSA, 2010, 2010; CONCAWE, 1998; Jokuty, 1999; McNamara, 1998; Smith, 1968; STATOIL, 2011; TOTSA, 2003; Tramier, 1987).

Name	Origin	API[b], °	Viscosity[b], cSt	Density@15°C[b], kg·m⁻³	Pour point[b], °C	TBP[b], wt%(vol%)	Sulfur, %wt	Nitrogen, %wt (total,ppm)	Nickel[b], ppm	Vanadium[b], ppm
ARABIAN LIGHT	Saudi Arabia	33.4	16.15@15°C	865.8	-53	49@350°C 57@400°C	1.77[b]	0[b]	2.5	16
AZERI	Azerbaijan	36.6	8.21@20°C	841.5	-3	53.97(57.64)@342°C 59.36(62.85)@369°C	0.12[a]	0.16[a]	3.7	0.3
DALIA	Angola	23.14	198@10°C	914.5	-39	40.66(43.56)@375°C	0.5[a]	0.27[a]	17	7
DIESEL A	product	38.32	3.25@40°C	832.5	-6	(85)@350°C (95)@360°C	<0.1[a]	<0.05[a]	<0.05	<0.05
DIESEL B	product	34.8	3.25@40°C	850	-4	(85)@350°C (95)@370°C	<0.1[a]	<0.05[a]	<0.05	<0.05
DIESEL C	product	30	7@40°C	900	<0	(95)@405°C	<0.1[a]	<0.05[a]	<0.05	<0.05
FLOTTA	North Sea	34.7	12@20°C	848.7	-21	(74)@370°C	1.01[b]	1400[b]	2.78	10.09
FORCADOS	Nigeria	29.7	17.4@10°C	873.3	-27	58.69(61.59)@340°C 66.89(69.58)@370°C	0.18[b]	1400[b]	3.9	1
HEAVY FUEL OIL	product	11.47	23037.28@15°C	988.8	-1	23.3@350°C 33.5@400°C	2.63[a]	0.36[a]	<100	<600[b]
HUNGO	Angola	28.7	26.30@20°C	882.9	-48	43.25(48.24)@342°C 47.55(52.47)@369°C	0.55[a]	0.3[a]	19.7	16.6
KIRKUK	Iraq	35.1	13@10°C	844.7	-22	(53)@300°C (54)@FBP	1.97[b]	900[b]	12.5	28.5

[a]values obtained by elemental análisis, [b]values from publicly available sources, NA-not available, TBP-true boiling point, FBP-final boiling point

Table III-1 contd.

Name	Origin	API[b], °	Viscosity[b], cSt	Density@15°C[b], kg·m^{-3}	Pour point[b], °C	TBP[b], wt%(vol%)	Sulfur, %wt	Nitrogen, %wt (total,ppm)	Nickel[b], ppm	Vanadium[b], ppm
KUWAIT	Kuwait	31.4	25.2@15°C	872.2	-15	(58.5)@400°C	2.52[b]	1400[b]	8	30
MAYA	Mexico	21.5	302.68@15°C	924.3	-30	32@350°C	3.4[b]	3500[b]	53	278
MURBAN	United Arab Emirates	39.73	5.9@10°C	826	-6	59.58(63.58)@340°C 64.78(68.53)@370°C	0.79[b]	(425)[b]	4.3	2.6
NEMBA	Angola	39.79	8.4@10°C	825.7	-24	62.29(66.72)@340°C 67.22(71.41)@370°C	1.54[a]	0.28[a]	11.8	4.9
NORNE	North Sea	32.7	14.1@20°C	861.5	9	61.18@375°C	0.25[a]	0.12[a]	0.9	0.3
NORTH SEA OIL	North Sea	38.41	9.8@10°C	832.4	-18	61.38(65.37)@375°C 84.48(86.67)@550°C	0.22[b]	(1108)[b]	3	2
OSEBERG	North Sea	37.8	6.8@10°C	835.4	-5.6	60.11(64.27)@343°C 87.96(89.87)@538°C	0.25[b]	0.098[b]	2	2
SIBERIAN LIGHT	Russia	37.8	7@20°C	835.8	-17	(46)@370°C	0.42[b]	900[b]	8	15
SIRTICA	Libya	43.3	3.43@40°C	815@20°C	-3	(73)@370°C	0.43[b]	1400[b]	15	10
SOROSH	Iran	18.1	1381@20°C	945	-12	(30)@370°C	3.3[b]	3000[b]	35	101

Viscosity and **pour point** influence the spreading of an oil slick on the sea surface. Very fluid, low viscosity oils spread rapidly making their containment difficult. If the water temperature drops below the pour point, oil will solidify and instead of spreading, it will travel large distances in the form of solid patches under the influence of currents and waves. Viscosities available for the investigated oils are somewhat difficult to compare since the temperatures at which they are measured vary widely. Notwithstanding, extreme values are observed for heavy oils such as residual HFO (23037.23 cSt) and Sorosh crude (1381 cSt). Such oils would have severe detrimental fouling effects on marine wildlife and coastlines, but would be relatively easy to mechanically contain using booms (Pezeshki et al., 2000). At the other extreme are highly fluid light diesel distillates (3.25 cSt) and Sirtica crude (3.43 cSt) which would spread very fast making their containment very difficult. There is only one high pour point oil, namely Norne (9 ºC). The other oils have their pour points below 0 ºC, although low water and air temperatures in cold seas can significantly limit the fluidity of such oils. In general, higher temperature will facilitate oil spreading (EPA, 1999). Viscosity also influences oil evaporation and emulsification (see section **III.1.4**).

Sulfur and **nitrogen** concentrations can indicate the presence of heterocyclic aromatic compounds, e.g. carbazoles (Zhang et al., 1998) and dibenzothiophenes (Chakhmakhchev et al., 1997). These compounds show mutagenic (Pelroy et al., 1983; Rasmussen et al., 1991) and carcinogenic (Croisy et al., 1984) activities and are found in high concentrations near oil spill sites (Kropp and Fedorak, 1998). Furthermore, N and S contents also control the nitrogen and sulfur oxides release potential during any spill burning operations posing a hazard for the clean-up personnel (NIEHS, 2010; Park and Holliday, 1999) and contributing to atmospheric pollution (e.g. acid rain) (Smith et al., 2001). Usually, oils contain trace amounts of these elements, but some of the selected oils are characterized by increased sulfur (e.g. HFO, Maya) or nitrogen content (e.g. Maya, Sorosh), and can therefore present increased environmental risk. Light distillates (diesels) do not contain sulfur or nitrogen. Some crude oil samples also have very low S and N content (e.g. Azeri).

III.1.3.   SARA composition

TLC-FID analyses of the fresh, non-weathered oils reveal their compositions in terms of the main compound classes (saturates, aromatics, resins and asphaltenes, SARA). Observed differences are the consequence of their geochemical origins or the refining processes they have undergone (**Table III-2**).

Table III-2 SARA composition of the selected oils.

	Saturates (%)	**Aromatics (%)**	**Resins (%)**	**Asphaltenes (%)**
ARABIAN LIGHT	35.3	39.6	16.8	8.3
AZERI	84.0	3.7	10.9	1.4
DALIA	46.3	26.1	22.7	4.9
DIESEL A	83.0	2.9	12.5	1.6
DIESEL B	87.6	6.9	5.5	ND
DIESEL C	88.4	7.3	4.2	ND
FLOTTA	14.1	10.2	74.3	1.3
FORCADOS	49.2	25.0	22.2	3.6
HEAVY FUEL OIL	22.1	38.2	28.8	10.9
HUNGO	39.2	9.9	41.8	9.1
KIRKUK	43.2	43.4	6.6	6.7
KUWAIT	35.6	35.7	16.3	12.5
MAYA	29.4	18.6	43.5	8.4
MURBAN	82.4	6.8	9.6	1.2
NEMBA	66.7	5.8	21.9	5.7
NORNE	77.2	14.7	6.3	1.7
NORTH SEA OIL	66.2	13.5	18.9	1.4
OSEBERG	54.1	23.7	18.9	3.3
SIBERIAN LIGHT	60.4	8.7	23.3	7.6
SIRTICA	64.2	5.6	25.5	4.7
SOROSH	23.7	22.4	39.4	14.6

ND-not detected

SARA analysis is a convenient method to obtain oil compositions that can be used to make general assessment of oil spill fate and effects. For example, oils with a high content of **saturated** hydrocarbons (iso- and cyclic alkanes), will evaporate faster upon release into the marine environment, often with the remaining components being readily dispersed. As a consequence, such oils, in general, have acute short-term toxic effects on aquatic systems which are usually limited to immediate vicinity of the spill (CONCAWE, 1996).

The **aromatic** fraction accounts for the majority of toxic effects since it contains numerous compounds such as polycyclic aromatic and some hetero-polycyclic

compounds that have both short-term and chronic toxic effects on the marine environment (Gonçalves et al., 2008; González-Doncel et al., 2008; Incardona, 2004; Incardona et al., 2010).

The **resin** fraction is a heterogeneous group of compounds that includes hetero-substituted aromatics, various oxygenated species, etc. Their main characteristic is higher polarity which, as a consequence, affords higher water solubility and potentially higher bioavailability/toxicity (Melbye et al., 2009; Neff et al., 2000; Thomas et al., 2009). Furthermore, this fraction can also contain transformation products generated through weathering, i.e. oxidation of aromatic fraction, which can be present at even higher concentrations than the parent compounds (Aeppli et al., 2012). Weathering products were demonstrated to increase oil toxicity (Bellas et al., 2013) and are potentially persistent (Aeppli et al., 2012; Hinga and Pilson, 1987). Consequently, it is very important to consider this fraction in post-spill assessments, even though it can be difficult to characterize in detail (Burns, 1993).

The **asphaltene** fraction contains condensed aromatic macromolecules (500-5000 amu), which can contain hetero-elements (N, S, O, metals). **Figure III-1** shows the MALDI-TOF characterization of the asphaltene fraction of Maya crude oil confirming their theoretical mass distribution. It is the most recalcitrant oil fraction and plays an important role in the stabilization of oil emulsions (McLean and Kilpatrick, 1997; Taylor, 1992).

Within the chosen sample set, diesel oils are dominated by saturated hydrocarbons (>80%) with a relatively low content of aromatic and polar (resin) compounds. Light distillates, in general, do not contain asphaltenes, or their content is very low (e.g. Diesel A). Thus, their effects in the case of a spill would be limited and short-term. In contrast, residual oil products, such as HFO, contain increased amounts of aromatics, resins and asphaltenes. Biodegradation of these compounds can be very slow, especially when environmental conditions are not optimal (e.g. low temperatures, oxygen and nutrient limited). Under these circumstances post-spill effects can be chronic, extending for years after the incident (Reddy et al., 2002).
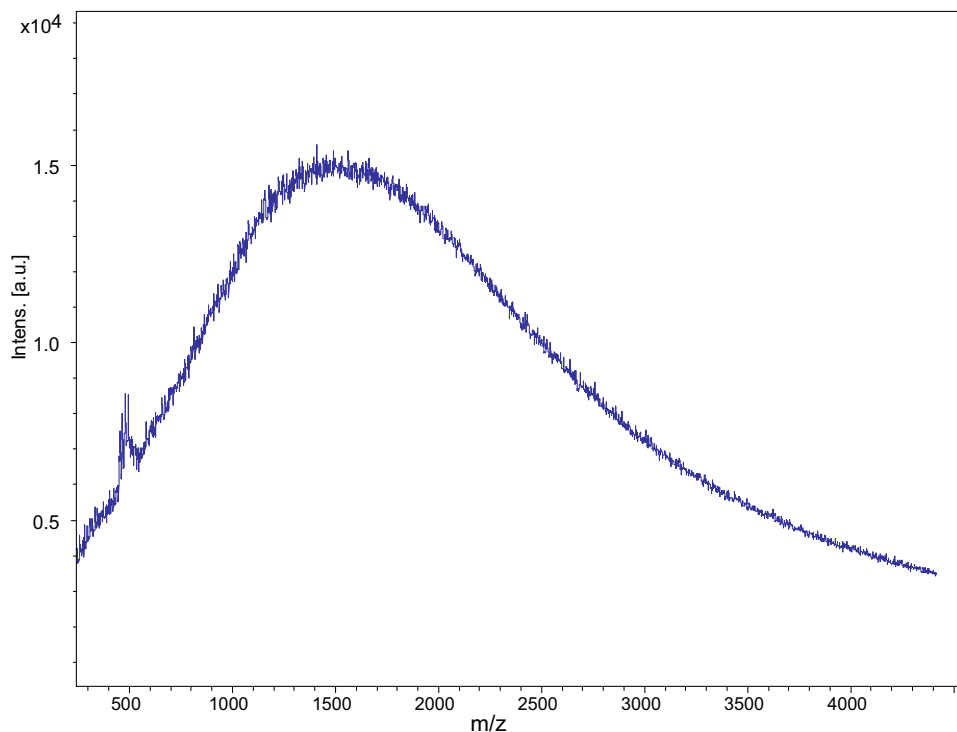
Figure III-1 MALDI-TOF spectra of Maya crude asphaltenes.

As for crude oils, their compositions and thus effects vary widely. Contents of saturates range from over 80% in Azeri and Murban, down to 14.1 in Flotta, whilst aromatics range from over 40% in Kirkuk to just over 3 percent in Azeri. The resin content is highest in Flotta crude (>70%), less in Maya and Hungo blends (>40%) and even lower in Norne and Kirkuk oils (around 6%). Finally, highly asphalted oils are Sorosh and Kuwait (14 and 12%, respectively) with Murban and Flotta containing just over 1% of asphaltenes.

III.1.4.   Short-term oil model

The ADIOS2, software from the National Oceanic and Atmospheric Administration (NOAA), is the most widely used computer program that models the behaviour of spilled oil, i.e. processes such as evaporation and dispersion. Evaporation is estimated using a pseudo-component evaporation model which models crude oils and refined products as a relatively small number of discrete, non-interacting components (Jones, 1997). For dispersion it applies the Delvigne-Sweeney model

(Delvigne and Sweeney, 1988). So far it has been used on numerous small and experimental spills and shows reasonable agreement with field observations (Lehr et al., 2002). Successful oil spill modelling depends on the quality of the data used; therefore testing of model simulations in real scenarios is crucial. In this respect, the approach applied here, where an extensive customized oil database has been built using experimental results and oil assays to provide model inputs is useful.

Oil budget data including evaporated, dispersed, and remaining percentage of spilled oil after 5 days (the maximum time following spillage permitted by the model) were calculated (**Table III-4**). Major environmental effects of any oil spill would most certainly last much longer than this period, however, the estimations obtained by the model are invaluable for successful planning of the immediate response activities, both in terms of clean up personnel safety, as well as in the decision making process and selection of the appropriate mitigation measures (e.g. use of dispersants, mechanical containment, etc.). Moreover, an estimation of the quantity of remaining oil is valuable information in the assessment of the possible medium- to long-term effects of the spill, and the planning of monitoring activities.

Averaged annual marine conditions at three locations (NW Mediterrenaean, NE Atlantic, and North Sea, see section **II.12** for exact locations) were selected to be characteristic of regional seas within Europe with the potential to influence oil spill behaviour (**Table III-3**). Turbulence of the water mass is more intense in seas with strong winds and high waves, which in turn promotes oil **dispersion**. Wind speed is also a limiting factor for emulsification, i.e. a wind speed of at least 3.6-5 m·s^{-1} is necessary for emulsification to take place (although other emulsification factors also need to be present) (ITOPF, 2013). This is confirmed by the model results, as the highest percentage of dispersed oil, in most cases, was observed for the North Sea scenario, where the wind is strongest, despite the lowest water temperature that would increase viscosities of investigated oils. On the other hand, due to their high viscosities, HFO, Maya and Sorosh oils do not show a tendency for dispersion in all three modelled scenarios.

Evaporation rate is influenced by temperature and time and various other factors including viscosity (fluid oils spread fast creating a large thin surface which facilitates evaporation), oil composition (lighter compounds evaporate more quickly), and wind and wave conditions (as for dispersion, rough seas facilitate evaporation). These complex interactions are reflected in the model results. As expected, light, low

viscosity oils such as Sirtica and Diesel A and B, evaporate extensively and after five days 61 to 88% of oil has evaporated, in accordance with typically expected values (NRC, 2003). In most cases oils' evaporation loss is similar for the three scenarios, notwithstanding it is slightly higher in the Mediterranean due to the warmer waters. This in agreement with the hypothesis that temeperature is the main driver of evaporation (Fingas, 2004).

Table III-3 Environmental conditions of three selected regional seas.

	wind speed $(m \cdot s^{-1})$	wind dir. (°)	water temp. (°C)	current $(m \cdot s^{-1})$	curr. dir. (°)	salinity (psu)	water sediment load $(mg \cdot L^{-1})$
NW Mediterranean Sea	5	123	26	0.2	195	38	16
NE Atlantic Ocean	7	158	19	0.1	29	36	0.5
North Sea	9	160	17	0.3	45	35	0.3

psu-practical salinity units

Besides the wind-speed (as noted above), **emulsification** of oils depends on their viscosity and composition. Emulsions readily form in oils that have more than 0.5% of asphaltenes (ITOPF, 2013), and when the sum of nickel and vanadium concentrations exceeds 15 ppm. Most of the metals in oils are associated with porphyrins. These chelate with the metals, especially vanadium and nickel (although iron and copper chelates may also be present). These porphyrin complexes play a role in oil emulsification, i.e. Ni/V porphyrin complexes are more oil-soluble and tend to act as natural surfactants, thus stabilizing water-in-oil emulsions (Canevari and Fiocco, 2005).

Table III-4 Modeled oil budget of applied spill scenarios and emulsification prediction.

	NW Mediterranean Sea			NE Atlantic Ocean			North Sea			Emulsification		
	Evaporated (%)	Dispersed (%)	Remaining (%)	Evaporated (%)	Dispersed (%)	Remaining (%)	Evaporated (%)	Dispersed (%)	Remaining (%)	Mousse (% evap.)	Ni+V (ppm)	Tendency
ARABIAN LIGHT	44	12	45	41	11	48	42	16	42	6	18.5	yes
AZERI	48	10	41	45	12	43	45	18	37	22	4	no
DALIA	19	2	79	18	2	80	18	3	79	2	24	yes
DIESEL A	83	9	8	81	13	6	88	10	2	100	NA	no
DIESEL B	82	9	9	81	13	6	88	10	2	100	NA	no
FLOTTA	47	10	43	41	9	50	40	13	47	21	12.87	no
FORCADOS	45	15	40	41	18	42	38	27	36	19	4.9	no
HEAVY FUEL OIL	15	0	85	14	0	86	14	0	86	100	<600	yes
HUNGO	44	3	53	42	3	56	44	4	52	4	36.3	yes
KIRKUK	47	14	39	44	14	42	42	20	37	6	41	yes
KUWAIT	38	8	54	35	7	58	34	11	55	5	38	yes
MAYA	27	0	73	26	0	74	26	1	73	1	331	yes
MURBAN	54	19	27	50	23	28	48	31	21	23	6.9	no
NEMBA	48	6	47	55	16	29	54	22	24	8	16.7	yes
NORNE	35	10	54	32	13	55	31	22	48	20	1.2	no
NORTH SEA OIL	51	15	34	48	16	37	53	20	27	23	5	no
OSEBERG	54	17	29	51	19	30	54	24	22	23	4	no
SIBERIAN LIGHT	33	21	47	29	21	50	29	29	43	23	NA	NA
SIRTICA	64	7	29	61	7	32	62	10	29	25	NA	NA
SOROSH	28	0	72	26	0	74	27	0	73	1	136	yes

NA-not available

In the sample set, light distillates (diesels) will not emulsify since they do not contain asphaltenes or porphyrins. Also, very viscous oils (about 10,000 cSt) with high asphaltene contents (>10%) do not form stable emulsions, but rather uptake entrained water which is then lost with time (Fingas and Fieldhouse, 2012). HFO is a typical oil of this type. It does not emulsify, but rather forms tar balls after a certain amount of weathering. As for the rest of oils, the limiting factors (e.g. viscosity, asphaltenes, and metals) permit emulsification, although it commences only after an amount of weathering (evaporation), as predicted by the ADIOS2 model. Heavy crudes (Maya, Sorosh, Dalia, Hungo), emulsify as fresh (unweathered), spillages, whilst other lighter crudes (e.g. Murban and Oseberg) only emulsify after heavy weathering. According to the ADIOS2 model, in the case of Murban and Oseberg crudes, this occurs after 23% of the oils evaporate. This result corroborates previously reported values obtained experimentally (e.g. 25% evaporation) (Canevari and Fiocco, 2005).

In addition, vanadium and nickel porphyrins are important molecular organic markers for petroleum *maturity*, and can help to distinguish different oils (Hegazi, 2009). Highest concentrations are found in heavy oils, with mature lighter oils containing less (Wang et al., 2007). Hence, the heavy crudes (Maya and Sorosh) and heavy residual oils have higher metal concentrations (**Table III-1**).

III.1.5. GC-MS fingerprinting

Oil fingerprinting was performed in accordance with the standard methodology accepted by the European Committee for Standardization (CEN) (CEN, 2012). This methodology was used to fingerprint twenty (20) selected oils, by determining diagnostic ratios of 34 specific hydrocarbon compounds. The list of the compounds, their abbreviations, structures and characteristic *m/z* is given in **Table A-1**, Annex **A**. They include n-alkanes and isoprenoids, polycyclic aromatic compounds (PAHs), hopanes, regular steranes and diasteranes and triaromatic steranes (TAS), each selected because they were present at measurable levels in oil, they produce well resolved single peaks or characteristic combined peaks (e.g. RC26TA+SC27TA), and are robust against weathering or have known weathering characteristics. From their peak heights, twenty five (25) normative ratios recommended by CEN norm (CEN, 2012) were calculated (**Table III-5**).

Ratios of linear and branched alkanes can serve as indicators of both geochemical origin, as well as some weathering processes (i.e. biodegradation). Pristane to phytane ratios characterize different crude oils, based on the redox conditions present in the source rocks during their formation. It is accepted that ratios higher than 1 indicate oxic, and lower than 1 anoxic conditions (Didyk et al., 1978). Extremely high pristane to phytane ratio (>3) can be an indicator of abundant terrestrial organic matter, whilst extremely low values (<0.8) suggest hypersaline, anoxic conditions in the source rocks (Peters et al., 2005). Out of the investigated oils, eight crudes have pristane to phytane ratio lower than one, five of them with extremely low (<0.8) ratios, suggesting anoxia/hypersalinity during their formation. In the rest of crude oils, pristane to phytane ratios are higher than one, ranging from 1.03 in Siberian Light to 2.71 in Forcados, indicating oxic formation.

Changes in ratios of heptadecane to pristane and octadecane to phytane, can be very useful to identify the onset of biodegradation of oil spilt in the environment. It has been observed that bacterial communities preferentially degrade straight chain alkanes to branched ones (pristane, phytane). Hence, the ratios of C17/Pris and C18/Phy in biodegraded oil will be lower than in respective fresh oil (Miget, 1969).

Characteristic distributions and ratios of polycyclic aromatic hydrocarbons (PAH) can be used to distinguish between different crude oils as well as to identify refining products. In this respect, particularly useful are methyl substituted dibenzothiophenes and phenanthrenes, monitored by selective ion traces at *m/z* 198 and 192, respectively. For example, as a result of cracking processes in the refinery, the ratio of 2-MP to 1-MP in HFO is higher than in the starting crude oil, while at the same time the ratio of 4-MD to 1-MD is lower than in the crude oil (Wang and Stout, 2010). Furthermore, weathering processes produce characteristic changes of MP and MD ratios. For example, 2-MP is more soluble than 1-MP, so in aqueous environments, their ratio will change accordingly (Liu et al., 2012). Also, dissolution will affect heterocyclic compounds (dibenzothiophenes) more than aromatic compounds (Pearlman et al., 1984). On the other hand, 9-MP and 4-MD appeared to be more resistant to biodegradation than the others (Bayona et al., 1986). Four ring aromatics, such as fluoranthenes and pyrenes are also used since they can vary significantly among different oils. Methylpyrene ratios can also serve as indicators of photooxidative weathering, because 2-MPy and 1-MPy are more affected by irradiation than 4-MPy (Radović et al., 2013).

Sulfur containing heteroaromatics such as benzonaphtothiophene, can also serve as oil-type specific indicators, characterizing sulfur rich oils (Arpino et al., 1987). For example, oils with increased sulfur content, such as Kirkuk and HFO, also have high BNT to tetramethylphenanthrene ratios. However, there are other sulfur containing compounds, such as C3- and C2-dibenzothiophenes, which are not included in normative ratios, because they cannot be resolved as single peaks with the applied GC-MS methodology. Therefore, it is not recommended to draw direct conclusions about the sulfur content in oil solely based on the BNT/TMP ratio.

Retene is another aromatic hydrocarbon which can be very useful for oil identification, because it provides a geochemical indication that the oil in question was formed from biomass containing conifer plants (Peters et al., 2005). This is illustrated for the analysed oils, where it can be observed that highest retene to TMP ratios are found in the oils from north of Europe (Oseberg, Norne, Siberian light, Flota), a region with rich conifer vegetation. Furthermore, retene can be used to identify heavy, residual oils, because it is strongly reduced during refinery cracking. In the investigated HFO, a retene peak at m/z 234 could not be found.

Oleanane is a natural triterpenoid, and it is another plant-derived geochemical marker indicating flowering vegetation inputs during oil formation. It has been reported as a characteristic feature of Nigerian crude oils (Stout and Wang, 2008). This is confirmed with Forcados, the only Nigerian oil in the investigated sample set, which had the highest oleanane peak. Other crudes with oleanane detected were Dalia and Nemba from Angola, and Azeri from Azerbaijan.

Table III-5 Values of normative diagnostic ratios of selected hydrocarbons determined according to CEN norm (CEN, 2012).

	Diagnostic ratios	Arab.Light	Azeri	Dalia	Flota	Forcados	Diesel A	Diesel B	Diesel C	HFO	Hungo
1	C17/Pris	6.24	1.65	0.17	2.67	1.15	1.48	1.19	1.21	5.15	1.51
2	C18/Phy	3.05	1.50	0.08	1.88	2.84	1.54	1.14	1.23	3.45	1.32
3	Pris/Phy	0.51	0.94	0.68	0.75	2.71	1.09	0.98	1.02	0.88	1.31
4	4-MD/1-MD	1.78	3.55	2.77	1.79	2.70	NA	2.50	5.84	1.61	2.00
5	2-MP/1-MP	0.93	0.86	1.20	0.74	1.19	1.74	1.78	1.62	1.25	0.86
6	2-MFl/4-Mpy	NA	NA	0.13	0.21	0.64	NA	0.08	0.24	0.34	NA
7	B(a)F/4-Mpy	0.34	1.21	1.10	1.70	2.86	NA	0.18	0.47	1.49	1.22
8	B(b+c)F/4-Mpy	0.13	0.23	0.28	0.54	0.80	NA	0.07	0.17	0.85	0.27
9	2-Mpy/4-Mpy	0.21	0.40	0.43	0.35	0.49	0.97	0.97	1.02	0.81	0.36
10	1-Mpy/4-Mpy	0.52	0.48	0.58	0.68	0.59	0.66	0.71	0.63	0.96	0.75
11	Retene/TMP	NA	0.62	NA	2.43	NA	NA	NA	NA	NA	NA
12	BNT/TMP	1.33	0.30	0.45	2.07	0.15	NA	NA	0.14	1.77	0.19
13	27Ts/30ab	0.30	0.13	0.16	0.17	0.17	NA	0.70	NA	0.16	0.10
14	27Tm/30ab	0.27	0.14	0.14	0.20	0.21	NA	0.59	NA	0.58	0.16
15	28ab/30ab	NA	NA	0.10	0.48	0.11	NA	NA	NA	NA	NA
16	29ab/30ab	1.17	0.42	0.45	0.50	0.59	NA	1.42	NA	0.91	0.39
17	30O/30ab	NA	0.06	0.05	NA	0.89	NA	NA	NA	NA	NA
18	31abS/30ab	0.71	0.33	0.33	0.65	0.24	NA	NA	NA	0.41	0.43
19	30G/30ab	0.18	0.07	0.12	0.11	0.06	NA	NA	NA	NA	0.10
20	27dbR/27dbS	NA	NA	0.68	0.52	0.61	NA	0.62	0.57	NA	0.64
21	27bb/29bb	0.63	0.78	0.89	1.02	0.62	NA	2.37	NA	1.09	1.21
22	SC26/RC26+SC27	NA	0.31	0.34	0.21	0.34	NA	0.35	NA	NA	0.35
23	SC28/RC26 + SC27	0.85	0.49	0.63	0.45	0.74	NA	0.34	0.67	NA	0.53
24	RC27/RC26+ SC27	0.64	0.52	0.49	0.58	0.54	NA	0.34	0.42	NA	0.50
25	RC28/RC26+SC27	0.97	0.46	0.59	0.47	0.63	NA	0.27	0.45	NA	0.54

Table III-5 contd.

	Diagnostic ratios	Kirkuk	Maya	Murban	Nemba	Norne	North Sea oil	Oseberg	Siberian light	Sirtica	Sorosh
1	C17/Pris	5.42	4.38	2.85	1.10	1.12	2.63	1.13	1.62	1.97	1.32
2	C18/Phy	4.30	2.72	1.90	1.10	1.22	2.77	1.28	1.57	2.30	1.09
3	Pris/Phy	0.89	0.75	0.69	1.05	1.11	1.14	1.16	1.03	1.28	0.87
4	4-MD/1-MD	3.54	1.95	2.59	2.33	3.70	3.64	2.66	1.96	1.68	1.57
5	2-MP/1-MP	1.56	1.07	0.94	1.19	1.25	0.89	0.89	0.71	0.87	0.93
6	2-MFI/4-Mpy	NA	NA	NA	0.15	0.55	0.24	0.45	0.39	0.16	0.21
7	B(a)F/4-Mpy	0.38	0.53	0.41	0.91	2.40	0.98	2.63	2.04	0.71	1.15
8	B(b+c)F/4-Mpy	NA	0.16	0.13	0.26	0.61	0.25	0.61	0.52	0.24	0.38
9	2-Mpy/4-Mpy	0.33	0.25	0.27	0.46	0.45	0.47	0.52	0.39	0.45	0.36
10	1-Mpy/4-Mpy	0.64	0.57	0.54	0.62	0.51	0.66	0.64	0.66	0.54	0.67
11	Retene/TMP	NA	NA	NA	NA	4.23	NA	5.78	2.66	NA	1.29
12	BNT/TMP	1.80	1.29	2.04	0.39	0.65	0.24	0.93	0.92	0.18	0.89
13	27Ts/30ab	0.13	0.12	0.76	0.13	0.16	0.25	0.18	0.16	0.19	0.07
14	27Tm/30ab	0.43	0.33	0.29	0.16	0.18	0.22	0.15	0.18	0.20	0.33
15	28ab/30ab	NA	NA	NA	0.07	0.10	NA	0.22	NA	NA	NA
16	29ab/30ab	1.30	1.03	0.81	0.52	0.52	0.48	0.42	0.48	0.52	1.20
17	30O/30ab	NA	NA	NA	0.18	NA	NA	NA	NA	NA	NA
18	31abS/30ab	0.53	0.73	0.56	0.30	0.34	0.55	0.38	0.51	0.39	0.55
19	30G/30ab	0.15	NA	0.15	0.14	0.08	NA	0.08	0.08	0.12	0.11
20	27dbR/27dbS	NA	0.63	0.70	0.64	0.62	0.64	0.62	0.59	0.69	0.53
21	27bb/29bb	0.83	0.83	0.73	1.01	0.85	0.94	1.05	1.24	1.20	0.87
22	SC26/RC26+SC27	0.20	0.18	NA	0.32	0.26	0.36	0.35	0.24	0.23	0.21
23	SC28/RC26 + SC27	0.59	0.60	0.98	0.57	0.71	0.53	0.58	0.48	0.47	0.63
24	RC27/RC26+ SC27	0.62	0.67	0.77	0.56	0.57	0.48	0.50	0.51	0.54	0.57
25	RC28/RC26+SC27	0.58	0.60	0.85	0.55	0.63	0.51	0.54	0.47	0.44	0.64

The diagnostic biomarkers used for calculating normative diagnostic ratios include hopanes (pentacyclic triterpanes), steranes (regular and rearranged, i.e. diasteranes) and triaromatic steranes (TAS). These biomarkers are particularly useful because of their specificity, diversity and resistance to biodegradation and weathering (Peters et al., 2005). In this respect, particulary important is 17α(H),21β(H)-hopane, which is used, due to its stability, as a natural internal standard to normalize other biomarker compounds (Prince et al., 1994). Fidelity of their ratios can be compromised in the case of refinery products, i.e. they are absent or found at very low levels due to losses during refinining processes. Biomarker patterns can be altered due to the mixing of different oil production streams, as observed for diesel oils and HFO.

III.1.5.1. PCA analysis of diagnostic ratios

The database of normative diagnostic ratios for the selected twenty oils has been created in accord with CEN methodology. It provides unique "fingerprints" that can be used for identification of the oils in the environment. Furthermore, the dataset can be investigated in order to determine which of the 25 normative diagnostic ratios in the analysed samples most significantly reflect oil-type differences. In this way, the most characteristic ratios could be used in cases of oil spills with numerous potential sources to screen and discard sources whose "critical" ratios differ. Detailed fingerprinting could be then limited to the samples that appear reasonably "suspicious".

For the purpose of this study, a data matrix was created where diagnostic ratios were presented row-wise and oil samples column-wise. Dimension reduction was then performed using PCA. As a result, three principal components with eigenvalues greater than one (which explain 87.52 % of the total variance) were obtained. **Figure III-2** is a matrix scatter plot showing mutually contrasted scores of the three principal components with greatest variance. In all score plots it can be observed that the majority of normative ratios are clustered together, and that there are six ratios with obvious deviations from that clustering and from each other. These are C17/Pris, C18/Phy, 4-MD/1-MD, B(a)F/4-MPy, BNT/TMP and Retene/TMP, suggesting that they are governing oil type differentiation in the analysed sample set. This can be explained by the fact that these ratios are very characteristic; ratios of linear to branched alkanes depend on the geochemical origin of the oil, four ring aromatics

(fluoranthenes/pyrenes) vary between oils, sulfur heteroaromatics (MD and BNT) ratios depend on the sulfur content of the oil (and change during oil refining), while retene is only found in oils with conifer biomass origin. It is reminded, however, that some ratios can be altered by weathering (e.g. C17/Pris and C18/Phy due to biodegradation and 4-MD/1-MD by dissolution). Hence, caution is advised when using a limited set of ratios for source identification, particularly if the samples are extensively weathered.
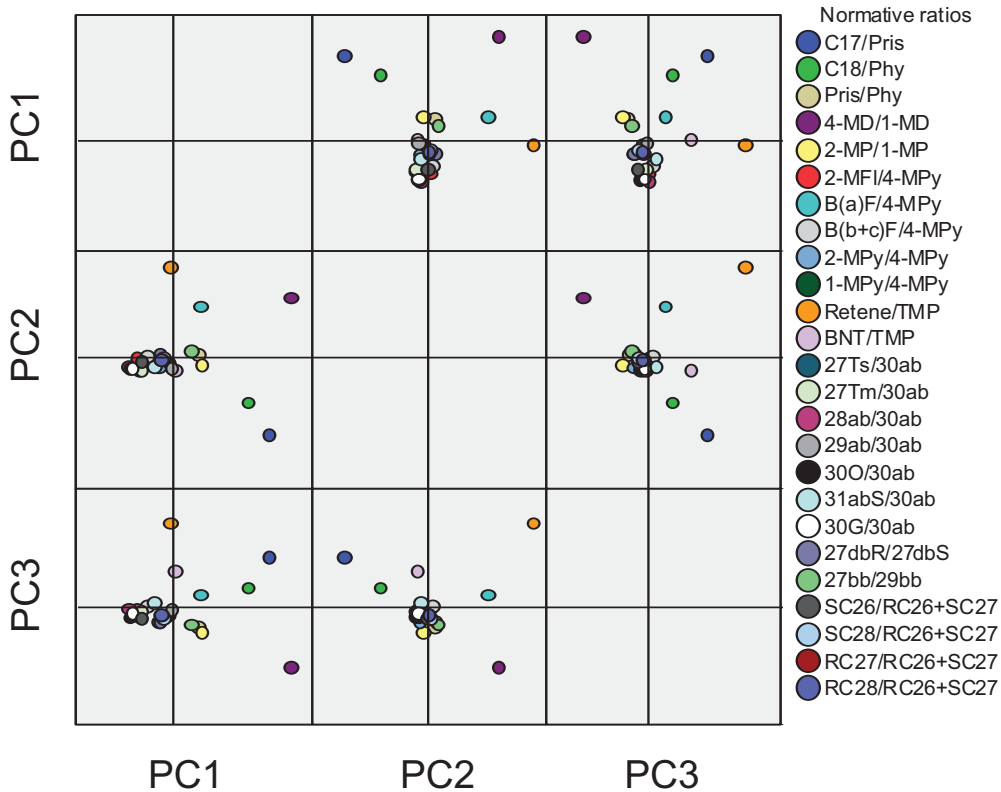
Figure III-2 PCA score plots.

III.1.6.   Concluding remarks

The data set compiled, from both the literature and experimental work, includes a broad range of various oil types from different continents. It provides the most important properties necessary for post-spill assessments.

The majority of the selected oils can be considered as persistent, the most recalcitrant being residual fuel oil and heavy crude oils. These also have increased contents of toxic and persistent components, such as PAHs and NSO compounds, which can have chronic long-term effects on ecosystems.

Short-term modelling is shown to estimate the influence of differing marine conditions on the fate of spilled oil. More extreme environmental conditions (elevated temperature, turbulence, etc.) promote processes such as evaporation and dispersion. Furthermore, the majority of oils have compositional properties that facilitate emulsification, although for some, severe weathering is necessary to make this process possible.

Normative diagnostic ratios of biomarkers to fingerprint the oils are reported to facilitate identification of oil spills in the environment. Statistical analyses of the ratios afford assessment of relative performance in differentiating between oil types. However, they should be used with caution in the case of weathered spill samples, since various processes such as dissolution, photooxidation and biodegradation can affect their fidelity. These effects will be demonstrated and studied in the next sections.

III.2. Determination of the type and source of weathered oil spill samples using GC-MS fingerprinting

III.2.1. Introduction

In this section, the GC-MS methodology previously used to fingerprint fresh samples of commonly transported oils was evaluated in the fifth interlaboratory ring test for oil spill identification organized by Bonn-OSINet in 2010. As one of the 24 participants, our laboratory received three spill samples (RR2010-1, -2 and -3) and two candidate source samples (RR2010-4 and -5) with the request to analyze the samples using the standard CEN (European Committee for Standardization) fingerprinting methodology (CEN, 2012) and report the type of oil and possible spill source.

Only information about the samples was provided in the spill scenario:

"*In June of 2010, some spill oil was found in the north coastal area of the Bohai Sea. Two spill samples were sent to our centre by a local monitoring station, one from*

a harbour and another from a beach. The sample from the harbour is indicated with RR2010-1, and the sample from the beach is indicated with RR2010-2. One month later, another spill sample was taken in the same beach area, indicated with RR2010-3.

Two suspected source samples were taken from an oil pipeline terminal nearby. The samples were taken from two main pipelines connected to different platforms. The suspected source samples are indicated with RR2010-4 and RR2010-5."

Actual origin and nature of the analyzed samples (as described in section **II.9**.) was revealed to participants subsequently, in the ring test final report.

The aim of the ring test was to assess whether the applied GC-MS methodology is able to identify the sources of weathered oil spills, in particular the ones affected by biodegradation.

III.2.2.   Preliminary evaluation of the samples

First step in the oil spill source identification is the visual inspection (i.e. screening) of the total ion chromatograms (TIC). In this step, oil samples can be preliminary characterized by obtaining the overall boiling (carbon) range, i.e. the total distribution of hydrocarbons including n-alkanes from C_{10} to C_{40} (if present). Also, possible characteristic features can aid in tentative oil type classification, and the degree of weathering can be estimated. Finally, candidate source samples that are clearly different from the spill samples can be ruled out as "non-matching". The five samples received exhibited a GC trace ranging from C_{10} to C_{40} n-alkanes (**Figure III-3**). The source samples (RR2010-4 and -5) may correspond to crude oils whereas the samples collected at the beach (RR2010-2 and -3) have similar profiles but progressively depleted on the more volatile components, probably due to weathering (e.g. evaporation). Conversely, sample RR2010-1 contains increased concentration of alkylnaphthalenes (marked by asterisk in **Figure III-3**), suggesting the presence of cracked oil (Speight, 2006), thus differing from the other samples.

However, in order to unambiguously determine the type of oil, and compare the spill and source oil samples, characteristic extracted ion chromatograms (EICs) of all samples were further investigated.
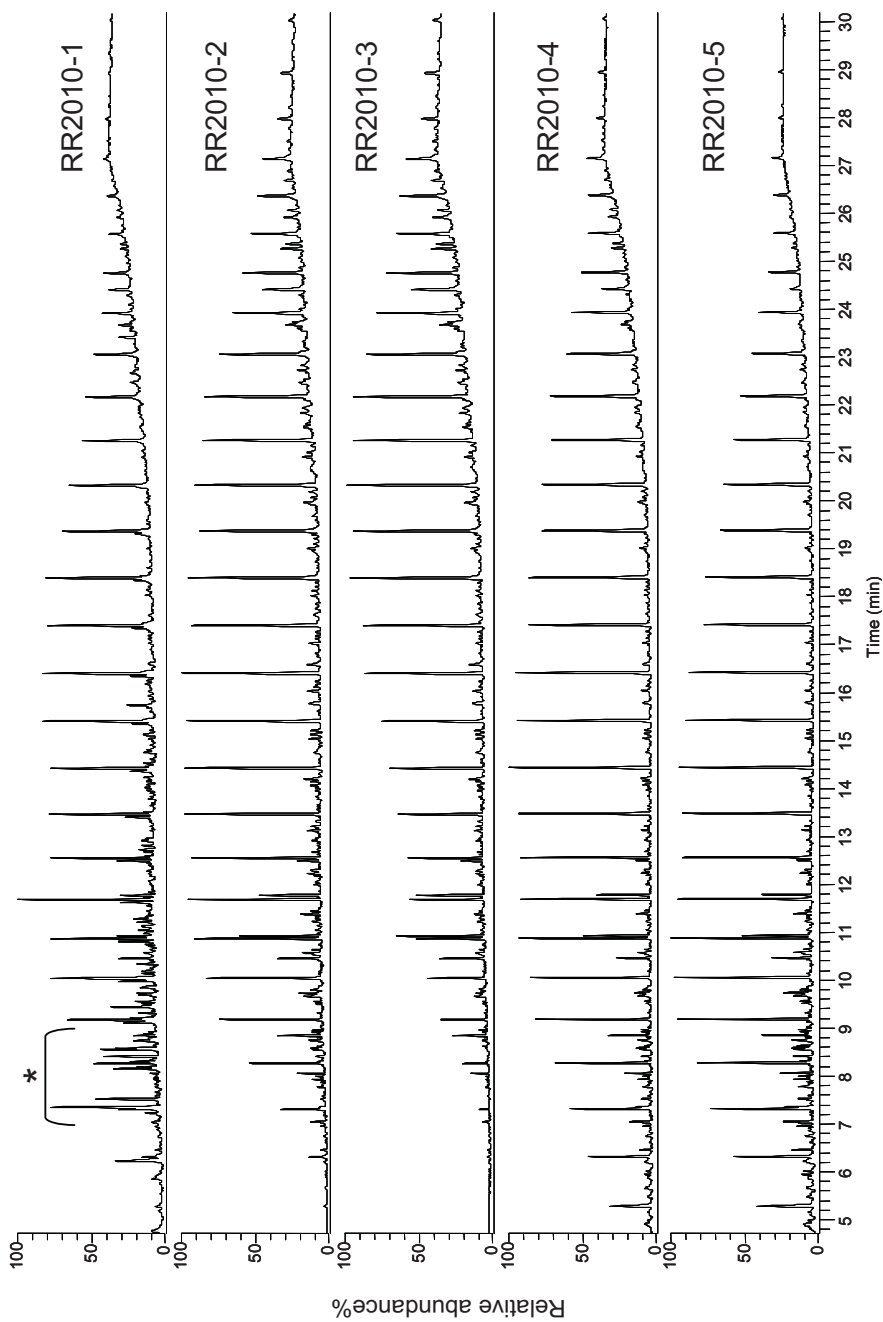
Figure III-3 Total ion chromatograms (GC–MS) of the analyzed samples.

III.2.3. Sample characterization

Tentative identification of RR2010-1 as cracked oil was confirmed by the occurrence of the series of n-alkenes (olefins) over the whole boiling range evidenced by the *m/z* 83 profile (marked by asterisks in **Figure III-4**, only a segment of the chromatogram is show for better visibility). They are uncommon in non-refined crude oil, and are probably residues from the cracking process (Speight, 2006).
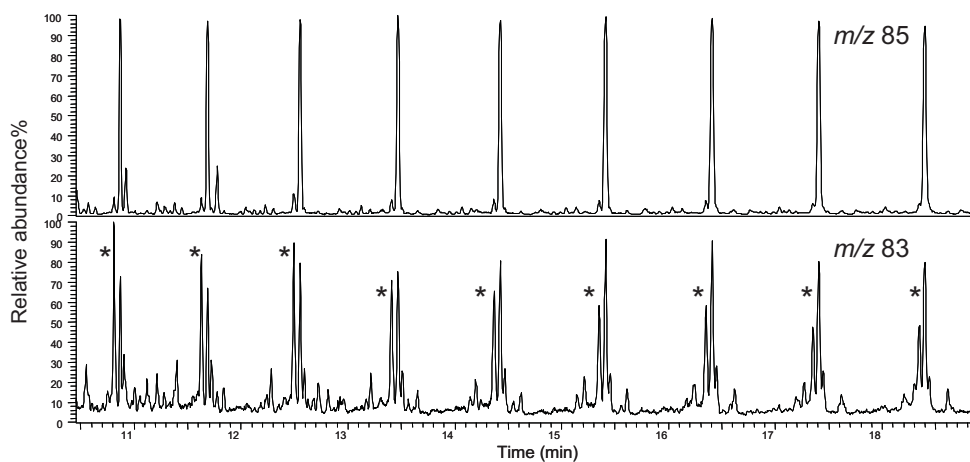
Figure III-4 Sample RR2010-1 EICs obtained from the full scan mode showing n-alkanes (*m/z* 85) and n-alkenes (*m/z* 83).

Furthermore, the *m/z* 192 profile in **Figure III-5** shows prominent 2-methylanthracene peak which is the typical pyrolitic product under rapid heating conditions, experienced during cracking (Wang and Stout, 2010). Also, the first doublet of methylphenanthrenes (3- and 2-methylphenanthrene, respectively) is higher than second one (9/4- and 1-methylphenanthrene, respectively) due to their higher thermal stability, which is another distinct feature of thermally treated oils (Wang and Stout, 2010).
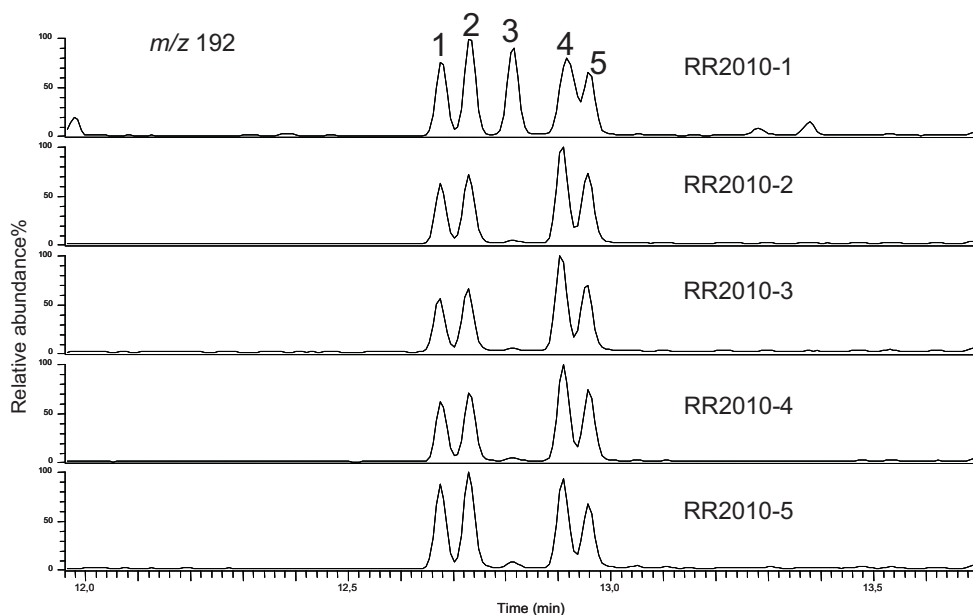
Figure III-5 EICs showing 3- and 2-methylphenanthrene (1 and 2), 2-methylanthracene (3) and 9/4- and 1-methylphenanthrene (4 and 5) peaks in the *m/z* 192 profile.

Finally, this hypothesis is corroborated by the higher predominance of 2-methylfluoranthene, benzo[*a*] and benzo[*b+c*]fluorenes in the *m/z* 216 profile (**Figure III-6**) which was also reported elsewhere (Albaigés et al., 2014). However, abundant retene peak was present in the *m/z* 234 profile of RR2010-1 sample (marked with asterisk in **Figure III-7**), which is typically reduced during thermal cracking. Possibly, other type of cracking process on lower temperature was applied (e.g. catalytic) which allowed retene to be preserved, or the cracking process was incomplete. Other explanation is that some different (retene containing) refinery streams were mixed with this cracked oil, which is often the practice in order to obtain the desired viscosity of heavy residual fuels. In conclusion, RR2010-1 is a type of cracked oil, possibly mixed with some other refinery stream, but in either case, it is significantly different from other samples, and does not share the same source. Therefore, at this stage it was possible to discard it as **"non-match"** with enough confidence.
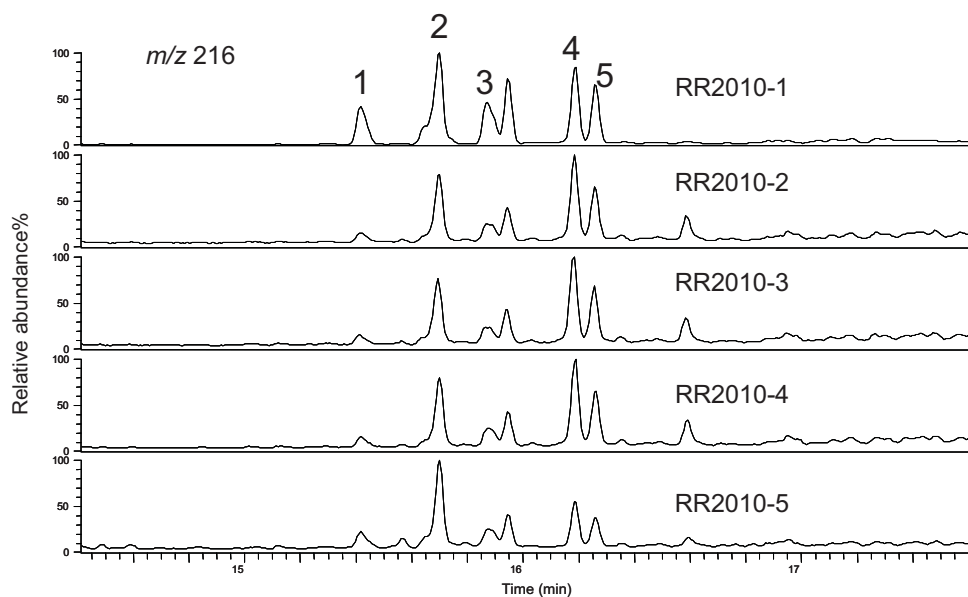
Figure III-6 EICs showing 2-methylfluoranthene(1), benzo[*a*] and benzo[*b+c*]fluorenes (2 and 3), and 4- and 1-methylpyrene (5 and 6) in the *m/z* 216 profile.

Next, EICs of RR2010-2, -3 and -4 have very similar *m/z* 192 profiles which indicate that they are crude oils, as evidenced by the minor peak of 2-methylanhtracene, and the methylphenanthrenes profile which is characteristic for non-refined oils (second doublet higher than the first one) (**Figure III-5**) (Wang and Stout, 2010). Furthermore, the relative distributions of n-alkanes show that in comparison with the candidate source (RR2010-4) the sample RR2010-2 is slightly depleted in the n-alkanes up to C_{24}, a trend which is further enhanced in sample RR2010-3. **Figure III-8** shows the peak heights (or areas) of n-alkanes in source and spill samples normalized to peak height (area) of C_{27} alkane in order to compensate for concentration differences and enable the comparison. Observed pattern is indicative not only of evaporation but also of biodegradation (Jiménez et al., 2006), suggesting that the RR2010-2 and -3 are possibly weathered samples originating from the same source (RR2010-4).
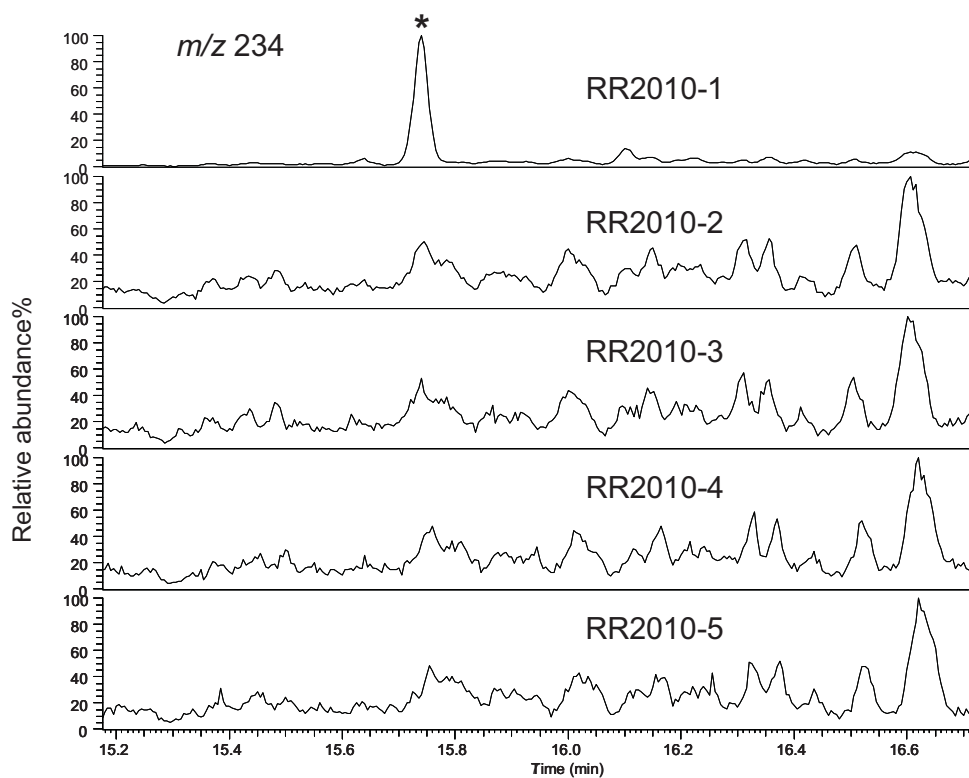
Figure III-7 EIC showing the presence of retene peak (*) in the *m/z* 234 profile of RR2010-1 sample.
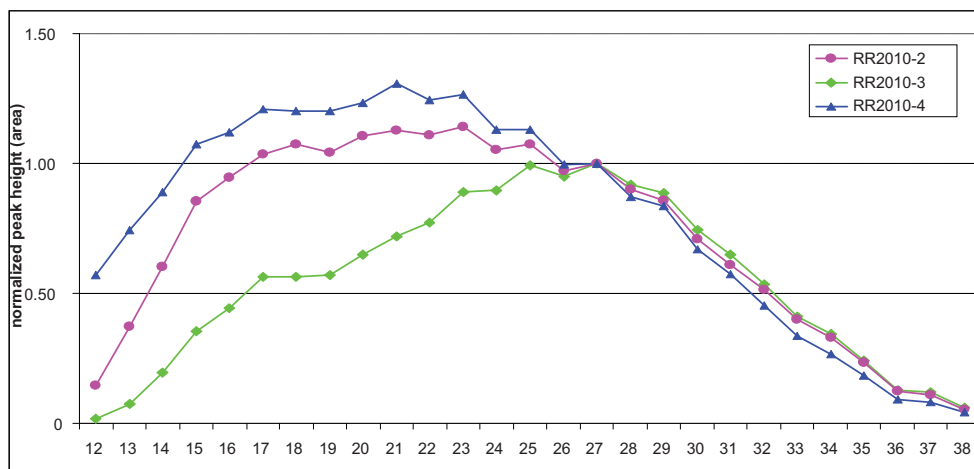
Figure III-8 Distribution of n-alkanes in RR2010-2, -3 and -4 after normalization to the C_{27} n-alkane.

The identification of RR2010-5 candidate source is not completely unambiguous. The *m/z* 192 profile shows higher first methylphenanthrene doublet suggesting the possibility of thermally treated oil (**Figure III-5**). However, this is not confirmed by the presence of abundant methylanthracene peak in the same profile. Methylanthracene could be affected by weathering, however it could be reasonably expected that the source oil would not be subjected to extensive weathering. This leaves the possibility that this sample is a crude oil, but the one that was affected by high temperature in the reservoir, leading to the slight depletion of less stable methylphenanthrene isomers (second doublet). Moreover, slight differences in the 4- and 1-methylpyrenes peaks of the two candidate sources can be observed (**Figure III-6**), which will be confirmed by comparing the diagnostic ratios.

III.2.4.   Comparison of the diagnostic ratios

In order to confirm the indications obtained by the preliminary analysis of the gas chromatograms and the sample characterization, 25 normative diagnostic ratios (see **Table II-2**) were calculated from the peak heights of characteristic fingerprinting compounds (**Table A-1**, Annex **A**). Relative differences of the ratios between samples were evaluated in relation to the critical difference of 14%, and percentage weathering (PW) plots were analyzed in order to estimate the effect of weathering processes (see section **II.7.3**.) and confirm the conclusions obtained by comparing the diagnostic ratios. Based on this information final conclusions about the source of the spill samples were made. Since the spill sample RR2010-1 was discarded as "non-match" during preliminary characterization, remaining spill samples (RR2010-2 and -3) were compared with two candidate sources (RR2010-4 and -5).

III.2.4.1.   Comparison of the suspected sources

First, two suspected sources were compared in order to confirm that they do not have the same origin. This showed that the relative differences of 12 normative ratios were higher than the critical difference of 14% including the majority of ratios of source specific PAHs such as methylphenanthrenes, methyldibenzothiophenes, fluorenes/pyrenes and benzonaphtothiophene (**Figure III-9**) (Peters et al., 2005).

Figure III-10 shows the PW plot comparing the two sources normalized to tetramethylphenanthrene. Irregular distribution of the normalized peaks, not expected in the case of matching samples, confirms the distinct fingerprintints of the two source oils. Finally, the majority of conservative source specific hopane biomarker ratios also show significant difference (Peters et al., 2005). This corroborates the observations made during the preliminary sample characterization, and confirms that the two candidate sources are of different origin.
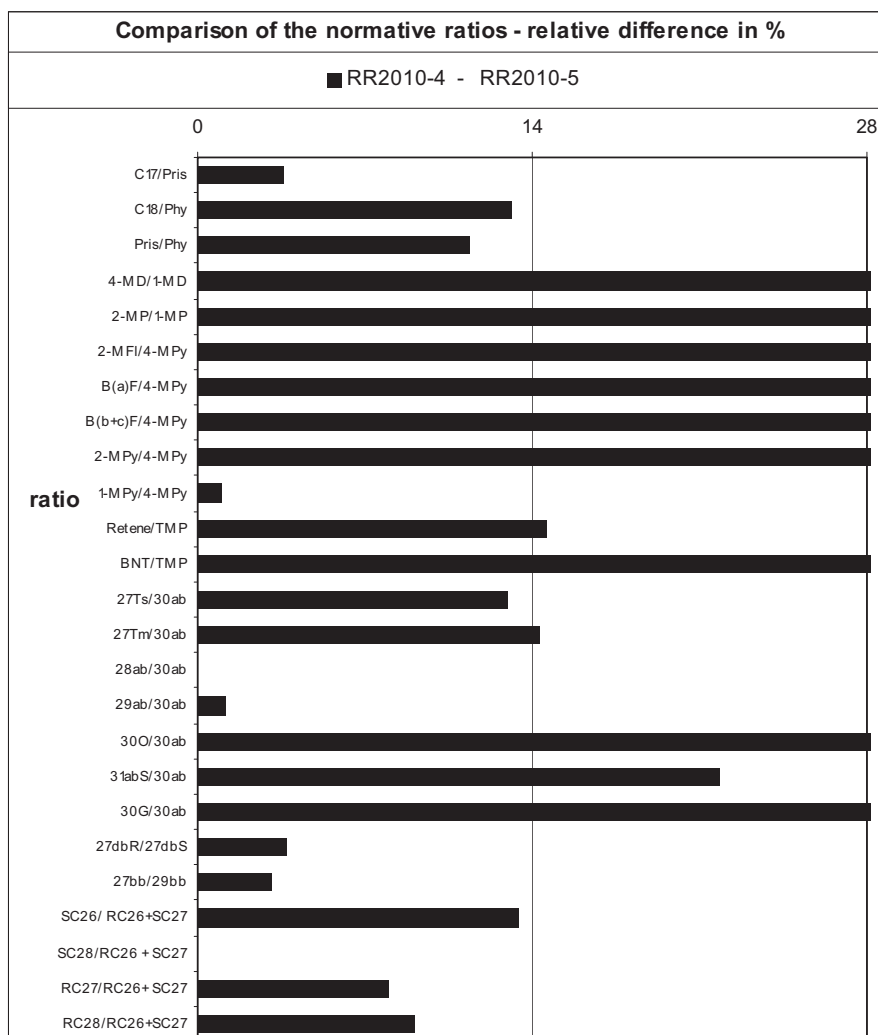
Figure III-9 Comparison of the normative ratios of two suspected sources (RR2010-4 and RR2010-5).
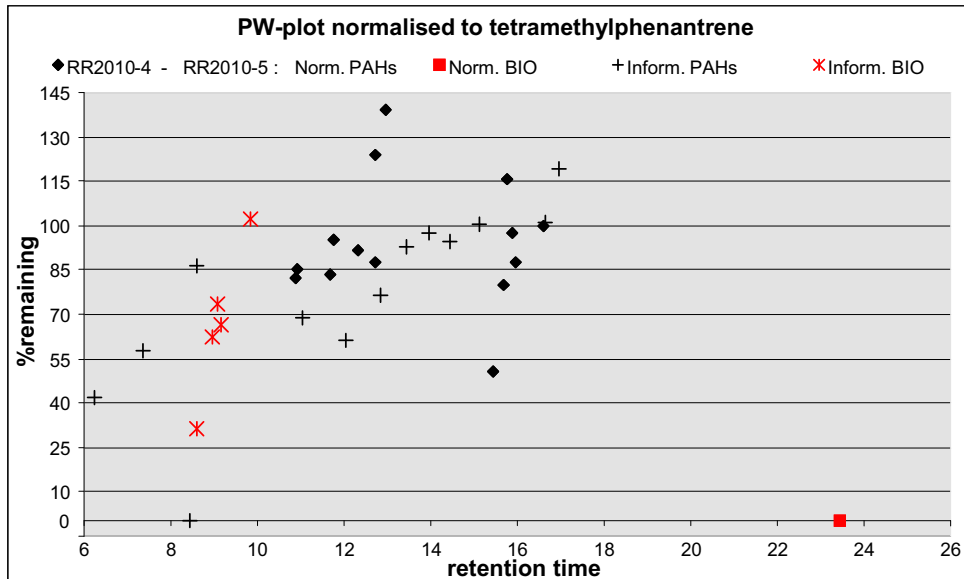
Figure III-10 PW plot of two suspected sources (BIO-biomarkers).

III.2.4.2. Comparison of the spill samples (RR2010-2 and -3 with the suspected source RR2010-4

The comparison of the diagnostic ratios of spill sample RR2010-2 and suspected source RR2010-4 (**Figure III-11**) shows a clear correspondence, since all the normative ratios, except the C17/Pris, are below the critical difference of 14%. Non-matching of the C17/Pris ratios could probably be attributed to a slight biodegradation of the C_{17} n-alkane, which are first to be depleted during biodegradation (Miget, 1969).

The effects of early weathering on RR2010-2 are well illustrated in the PW-plot (**Figure III-12**) which shows a slight evaporation (dashed line) of the volatile compounds eluting below C_{17} (11 min) and the onset of biodegradation indicated by the moderate depletion of C_{17} and C_{18} n-alkanes (green oval).
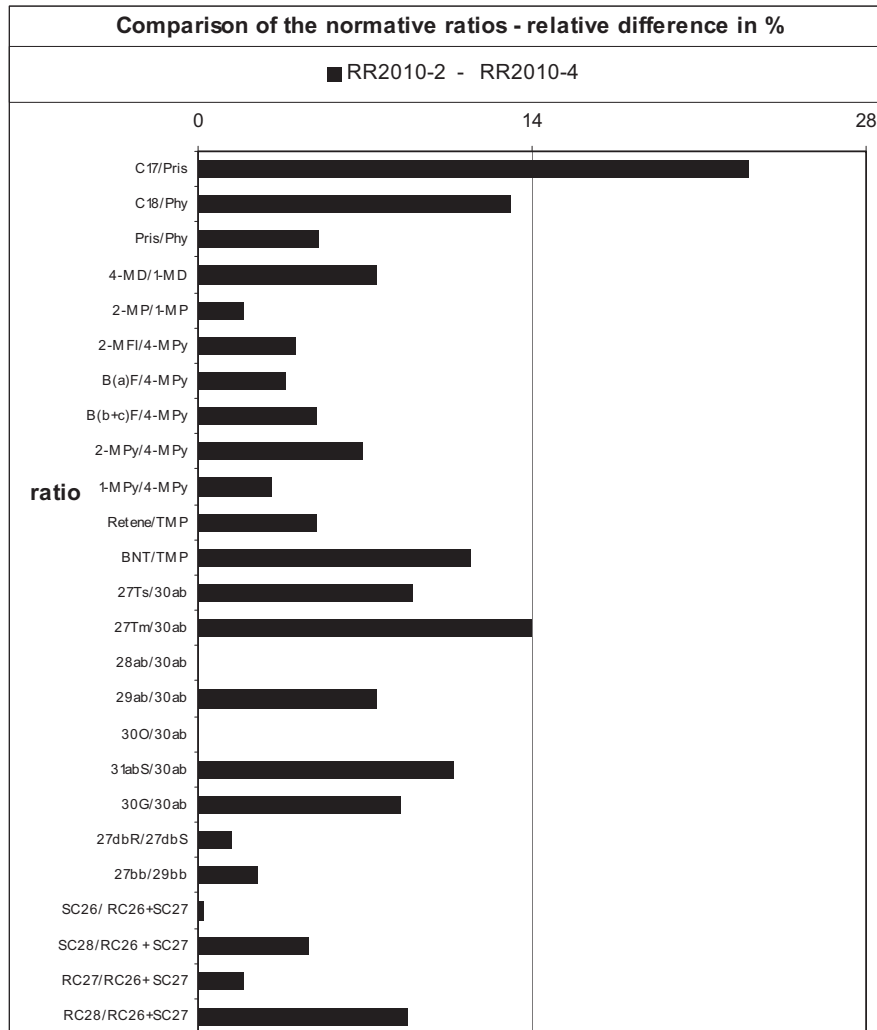
Figure III-11 Comparison of the normative ratios of RR2010-2 spill sample with suspected source RR2010-4.
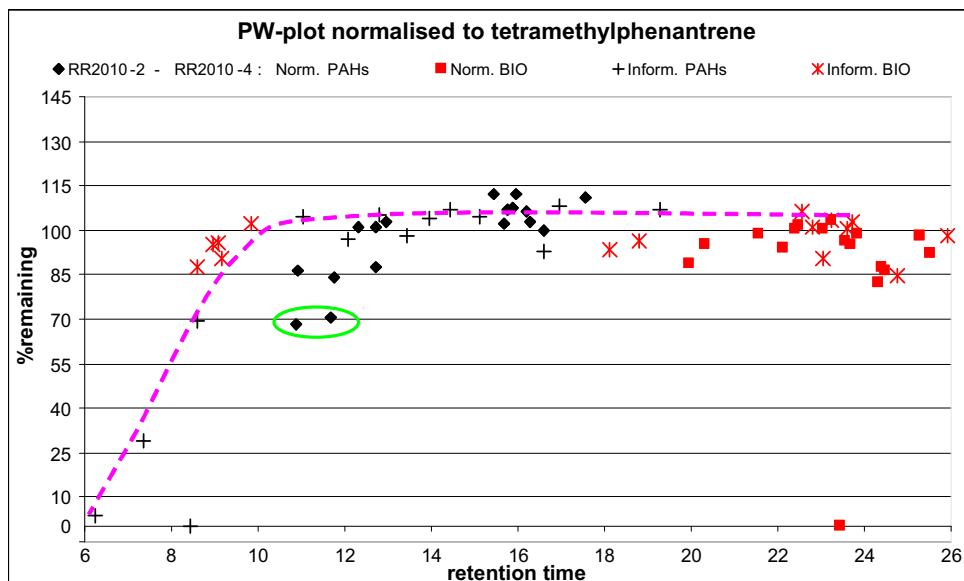
Figure III-12 PW plot of spill sample RR2010-2 relative to suspected source RR2010-4. Dashed line marks the curve of evaporation, green oval marks the compounds affected by biodegradation.

The evolution of the weathering processes and the augmentation of their effects were clearly observed in the second spill sample (RR2010-3), which was exposed in the field during one month according to the spill scenario. The comparison of the diagnostic ratios with the candidate source 2010-4 (**Figure III-13**) shows that the C17/Pris and C18/Phy ratios are high above the 14% critical limit due to the more advanced biodegradation (Wang and Stout, 2010). However, the Pris/Phy ratios are consistent with the same geochemical origin (Peters et al., 2005).

Again, the PW-plot provides additional insight in the weathering processes and how their effects on the oil composition are more pronounced after one month exposition comparing to slightly weathered RR2010-2 spill. Evaporation is well advanced, now also affecting semivolatile compounds eluting up to 16 min (C_{23}) (**Figure III-14**).
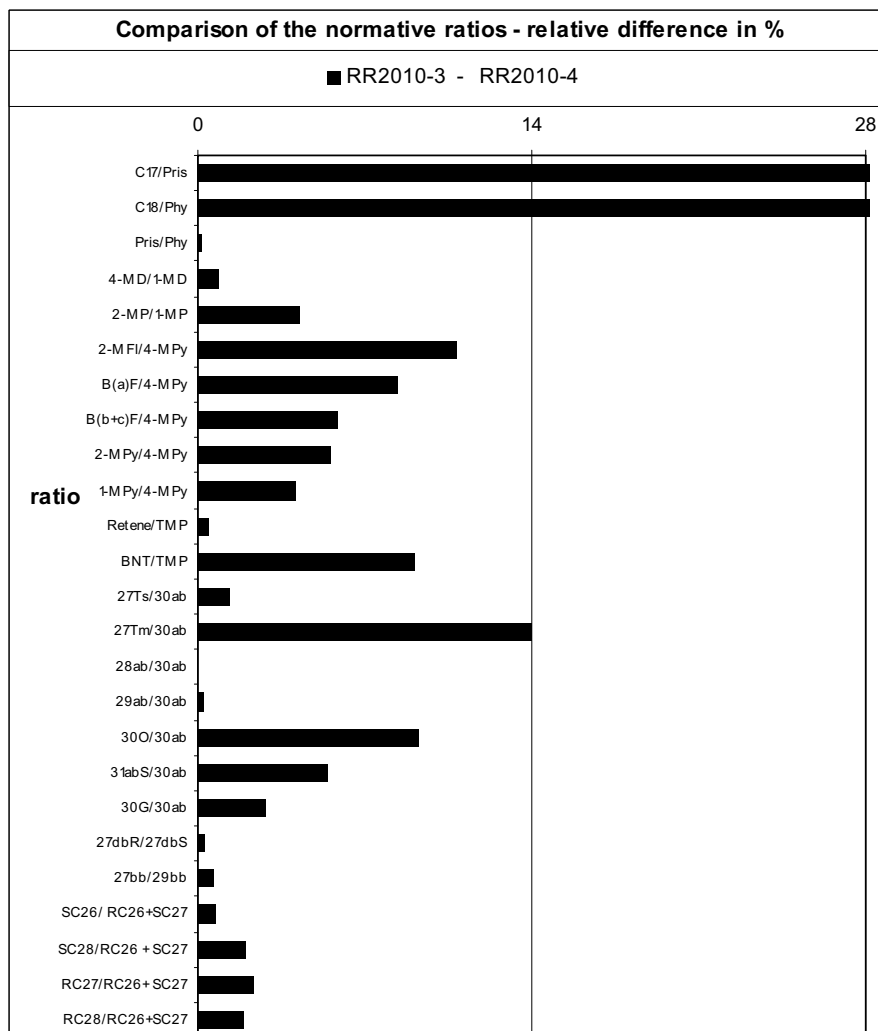
Figure III-13 Comparison of the normative ratios of RR2010-3 spill sample with suspected source RR2010-4.

The advanced biodegradation of C17 and C18 is also reflected in the PW-plot (green oval), thus explaining the high difference of n-alkane/isoprenoid ratios. Moreover, PW plot provided additional information not reflected by the diagnostic ratios, namely the depletion of the methylfluorenes, methylphenanthrenes and methyldibenzothiophenes (blue oval). Such effect could be explained by the dissolution of these more polar compounds during prolonged contact with turbulent aqueous phase (water washing) (Liu et al., 2012; Pearlman et al., 1984).
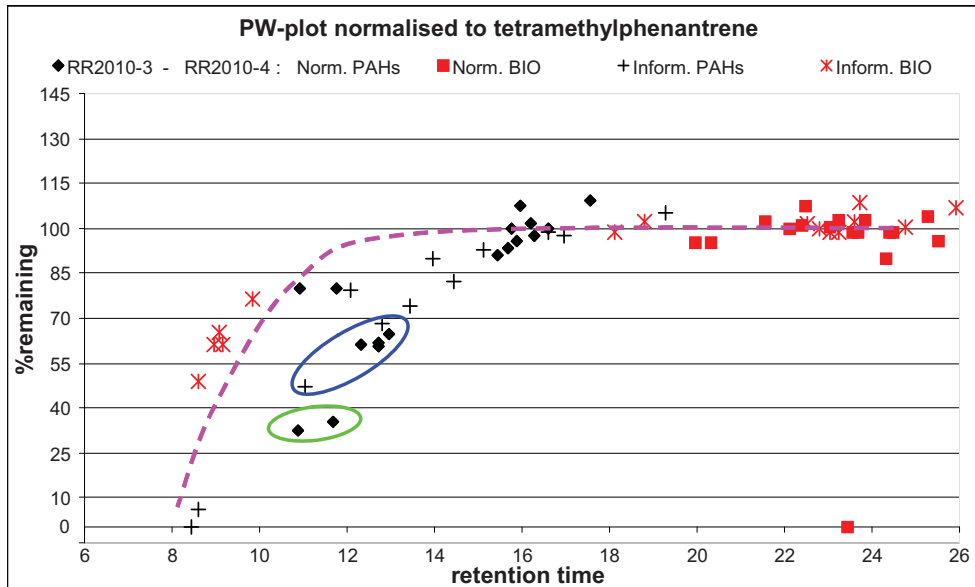
Figure III-14 PW plot of spill sample RR2010-3 relative to suspected source RR2010-4. Dashed line marks the curve of evaporation, green and blue oval mark the compounds affected by biodegradation and dissolution, respectively.

Based on the good consistency of diagnostic ratios between the two spill samples and suspected source, and the corroborating weathering patterns of evaporation and biodegradation found in the PW plots, it can be unambiguously concluded that both samples (RR2010-2 and -3) are **"positive match"** with the suspected source 2010-4.

III.2.4.3. Comparison of the spill samples (RR2010-2 and -3 with the suspected source RR2010-5

Comparison the diagnostic ratios of two spill samples with the second suspected source (RR2010-5) shows significant differences of numerous (13) source specific PAH and biomarker ratios (**Figure III-15**). PW plots (not shown) do not demonstrate weathering patterns that could explain such differences, therefore it can be concluded that this oil is of different origin compared to both spill samples, and can be unambiguously discarded as a **"non-match"**.
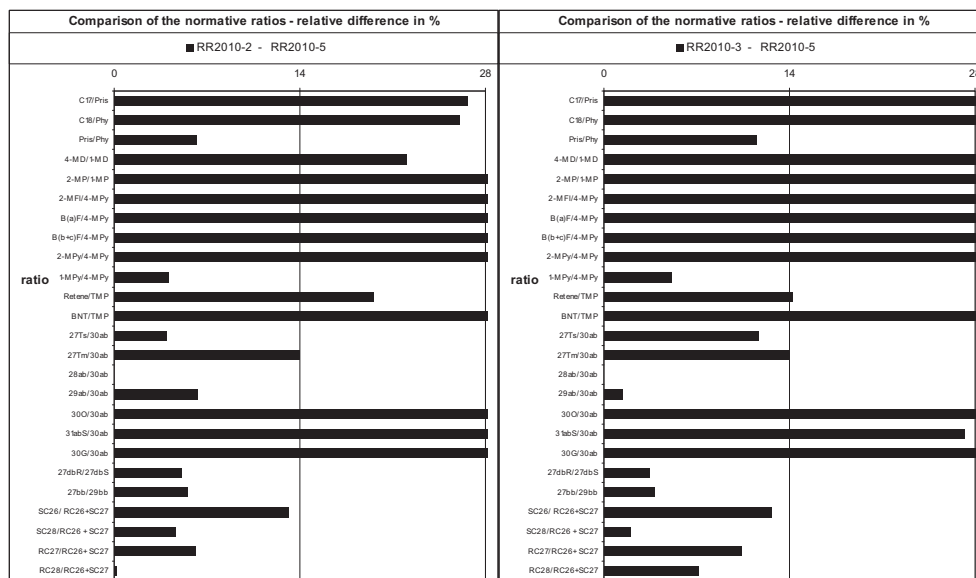
Figure III-15 Comparison of the normative ratios of spill samples with the suspected source RR2010-5.

III.2.5.   Concluding remarks

The reliability and robustness of GC-MS oil fingerprinting methodology were evaluated in an interlaboratory test of weathered (biodegraded) samples. It was demonstrated as a reliable method for the characterization of the oil type and the identification of the source of spilled oil, both in slightly and extensively weathered samples.

Analysis of the TIC and characteristic EIC enabled the characterization of the source and spill oil samples, as well as the preliminary evaluation of weathering processes affecting the spills and the spill-source matching. One sample (RR2010-1) was discarded as a definite "non-match" in this step.

Comparison of the normative diagnostic ratios was demonstrated as a robust method to match the spill samples to the source oil, accounting for the analytical error of the GC-MS methodology. In this way, spill samples RR2010-2 and RR2010-3 were positively matched to the candidate source RR2010-4.

PW-plots were proven as a simple, yet indispensable tool to unequivocally confirm the source attribution, and explain the observed differences in the diagnostic ratios, through the visualization of the weathering patterns. They allowed the detection of both early stage weathering (initial evaporation and the onset of biodegradation in

RR2010-2), as well as more advanced weathering effects (late evaporation, advanced biodegradation and water washing in RR2010-3). In this interlaboratory study, the focus was mainly on biodegradation and its effects on the fingerprinting methodology. However, other processes such as photooxidation might also have the effect on spilt oil. The effect of Sunlight on commonly used fingerprinting compounds and the fidelity of their ratios is still not sufficiently studied. In the next section, this process will be investigated in more detail.

General robustness of the applied methodology and the comparability of results were demonstrated by the fact that all of the laboratories in the ring test came to the similar conclusions about the source of spill samples (**Table B-1**, Annex **B**).

III.3. Effects of photooxidation on the oil composition and the implications for the oil fingerprinting

III.3.1. Introduction

In this section, the results of the study on photooxidative weathering of the oil from the *Prestige* incident in 2002, and the oil released during the *Deepwater Horizon* (*DWH)* blowout in 2010 are presented. This included the analysis of the actual spill samples from the two oil spills, weathered in the field, as well as the analysis of the selected oils previously irradiated under laboratory conditions. A part of this study was realized during a four-month research stay in the Woods Hole Oceanographic Institution (Woods Hole, MA, USA) in 2012.

The physical and biological weathering processes affecting the marine oil spills are well studied and have been reviewed in detail (Fingas, 1995; Prince, 1988; Yang and Wang, 1977), but photooxidation is still poorly characterized (Nicodem et al., 2001; Payne and Phillips, 1985; Plata et al., 2008). As described in section **I.4.6**, photooxidation is a process driven by the ultraviolet (UV) radiation, and it occurs either due to the direct absorption of radiation by the photosensitive species found in oil; or indirectly through a series of radical reactions with other reactive species generated by photoexcitation (Miller, 1983).

Previous studies demonstrated that photooxidation alters the oil composition by transforming the aromatic fraction (predominantly) to more polar oxygen containing species (Aeppli et al., 2012; McKenna et al., 2013). Effects of the aromatic compounds' alkylation were also observed (Garrett et al., 1998), but more detailed information on the oil photochemical transformations at molecular level is still limited (Bobinger and Andersson, 2009; Charrie-Duhaut et al., 2000; Jacquot et al., 1996). This is of particular interest for the oil fingerprinting methodology, since it is based on the presumption of the recalcitrance and/or consistent weathering changes of the selected polycyclic aromatic hydrocarbon (PAH) and biomarker compounds (Peters et al., 2005; Wang and Stout, 2010). Some previous reports have also suggested that particular biomarker molecules used in oil forensics, such as triaromatic steranes (TAS), can be unexpectedly depleted due to field or simulated weathering (Barakat et

al., 2002; Charrie-Duhaut et al., 2000; Jacquot et al., 1996). However, a more comprehensive research on the effects of photooxidation on the reliability of the oil fingerprinting methodology is still lacking.

With access to additional sites that have been oiled by different types of oils and exposures, there is a great opportunity to expand on our knowledge about these transformations. In this study the effects of photooxidation on the overall composition of spilled oils caused by natural and simulated sunlight, and particularly on the often used PAHs and the biomarker TAS were studied. To this end, both GC-MS and GC×GC-FID were used to analyze the target compounds. In order to investigate the implications for the oil fingerprinting methodology, target compounds in original and weathered oil samples were compared to calculate their losses, and commonly used fingerprinting ratios were evaluated to test if they can be reliably employed in environmental forensics in their current fashion.

III.3.2. Properties of the selected oils

Spill cases selected for this study are illustrative examples useful for broader considerations on oil weathering in the marine environment. On one hand they are characteristic spill incidents, the first is a typical tanker spill occurring on the open sea (*Prestige*), and the other is a deepwater spill from an offshore oil platform (*DWH*). On the other hand, oils released in the two incidents were of distinct type and different composition. Oil gushing from the Macondo well (*MW)* was a sweet, light crude oil, with increased content of saturated hydrocarbons, while the oil released from the *Prestige* tanks was heavy, residual oil (M-100 type), with increased content of sulfur and aromatic compounds (**Figure III-16**).
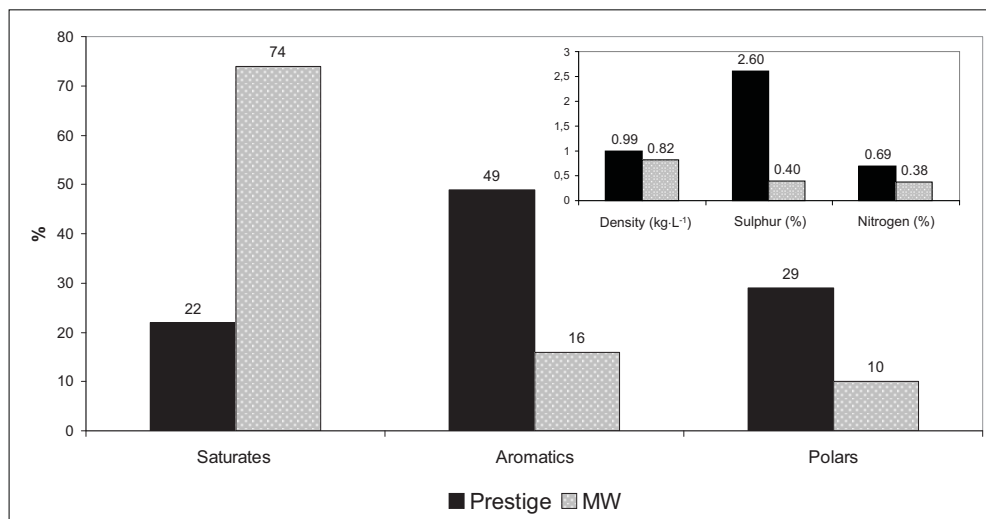
Figure III-16 Properties of the analyzed oils [adapted from (Diez et al., 2005; Reddy et al., 2012)].

III.3.3.   Irradiation experiments

As described in section **II.11**, natural and simulated solar radiation was used for the photooxidation experiments.

In the first experiment, *Prestige* oil was irradiated using simulated sunlight (Xe-lamp) and short-term exposure (12 h), with the aim to study the rapid changes of the different groups of aromatic species, particularly the ones used for oil fingerprinting.

Second experiment used natural sunlight to irradiate *MW* oil in the controlled fashion, during a medium-term exposition period (70 days). In this case, a longer exposition period was selected because the specific objective of this experiment was to study the effects of the irradiation on the particular group of biomarker molecules, TAS, which are considered to be recalcitrant to weathering in medium- to long-term periods (Peters et al., 2005). In both cases, the changes in the overall composition of selected oils were investigated.

III.3.4.   Effects of photooxidation on the overall composition of selected oils

In order to investigate the changes in the overall composition, i.e. the content of the major compound groups present in oil, TLC-FID was used. Despite the different type and composition of the selected oils, both oils were transformed by the irradiation (natural or simulated) in a similar fashion.

The most remarkable changes observed after irradiation, either by natural sunlight or with a Xe-lamp, were a substantial decline of the aromatic fraction and a concomitant increase of the more polar fractions (resins, asphaltenes) relative to the dark controls (**Figure III-17**).
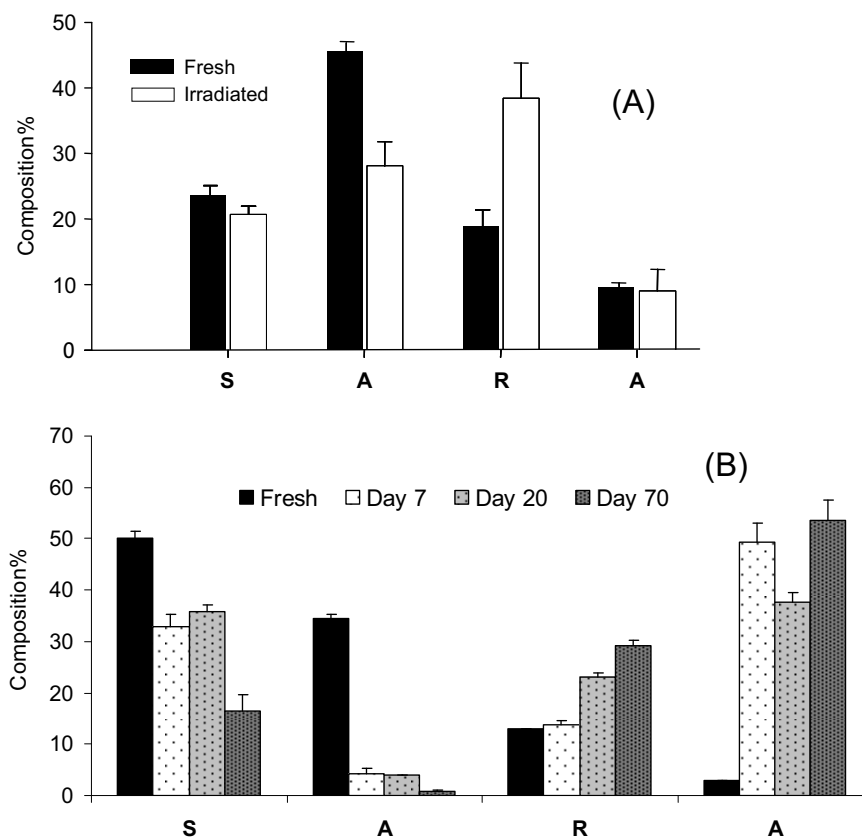
Figure III-17 Compositional changes after photooxidation determined by TLC-FID. (A) *Prestige* oil irradiated during 12 h using a Xe-lamp (B) Macondo well oil irradiated by natural sunlight during 70 days.

Moreover, these changes are occurring fast, as demonstrated in the case of the *Prestige* oil, where after only 12 h an approximately 20% depletion of aromatics and increase in resins was observed. Similar trend is observed during prolonged natural irradiation as demonstrated by the results of the *MW* oil. Here, beside the extensive depletion of the aromatic fraction (after 70 days only 0.8 % was present), saturate fraction was also affected due to the longer exposition time. Other studies on *MW* oil reported that the affected saturates are probably alkylated alycyclic compounds (Hall et al., 2013). Indirect, sensitized phooxidation of saturated hydrocarbons was also observed previously (Rontani and Giusti, 1988, 1989). However, since the majority of fingerprinting compounds (PAHs and biomarkers) belong to the aromatic fraction, the photooxidation of saturate fraction was not the main focus of this study.

Aromatic fraction of oil was transformed to more polar, oxygenated species, eluting as resin- and asphaltene-like fractions, depending on the properties of the transformation products and their solubility in methanol TLC eluent. This trend, already observed in previous studies (Garrett et al., 1998; Maki et al., 2001; Nicodem et al., 1997; Prince et al., 2003), could be explained by the conversion of the aromatic compounds to more polar derivatives, either by oxidative cleavage of the aromatic rings or by the introduction of oxygenated groups such as hydroxyl or carbonyl.

In order to investigate in more detail the nature of the transformations that were occurring during irradiation experiments, the samples were analyzed using FT-IR to get the functional group information. The results confirm that irradiation generates various oxygen-containing species as demonstrated by the appearance in the FT-IR spectra of a suite of bands in the 1700-1000 cm^{-1} region (**Figure III-18**), namely 1760-1740 cm^{-1} (esters and anhydrides), 1730 cm^{-1} (carbonyl group), 1720-1700 cm^{-1} (carboxylic carbonyl group), 1695 cm^{-1} (alkylarylketones), 1665 cm^{-1} (diarylketones), 1150 cm^{-1} (sulfone) and 1060-1030 cm^{-1} (sulfoxide). This is in agreement with previous studies of laboratory irradiated oils (Boukir et al., 2001).
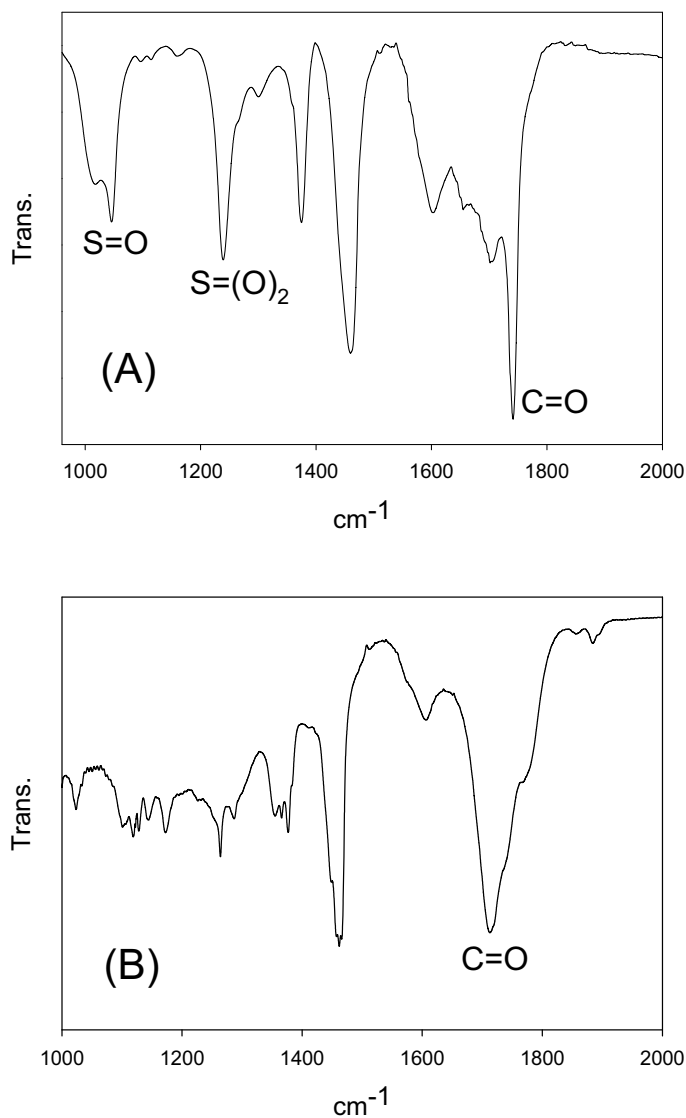
Figure III-18 FTIR spectra of (A) *Prestige* oil irradiated during 12 h using a Xe lamp and (B) Macondo well oil irradiated by natural sunlight during 7 days showing characteristic bands of oxygen-containing functional groups.

Finally, similar patterns were observed in field samples of the *Prestige* oil (Fernandez-Varela et al., 2006) and the *Macondo well* oil collected after the *DWH* disaster (Aeppli et al., 2012) suggesting that analogous irradiation driven oxidation processes are also occurring under environmental conditions.

III.3.5.   Effects of photooxidation on the aromatic hydrocarbons

III.3.5.1. Effects of chemical structure and alkylation on the photosensitivity of aromatic compounds

Significant changes in the molecular composition of *Prestige* oil after irradiation were also observed in the analysis of the aromatic fraction by GC-MS, depending on the molecular structure and alkylation of the aromatic backbone. As shown in **Figure III-19**, in most of the cases, the extent of photodegradation in different families of aromatic hydrocarbons (i.e. naphthalenes (N), phenanthrenes (P), chrysenes (C), dibenzothiophenes (Dbt), fluoranthenes (Fl), pyrenes (Py) and benz[*a*]anthracene (BaA)) increases concurrently with the alkylation degree (C1- and C2-) and structure.
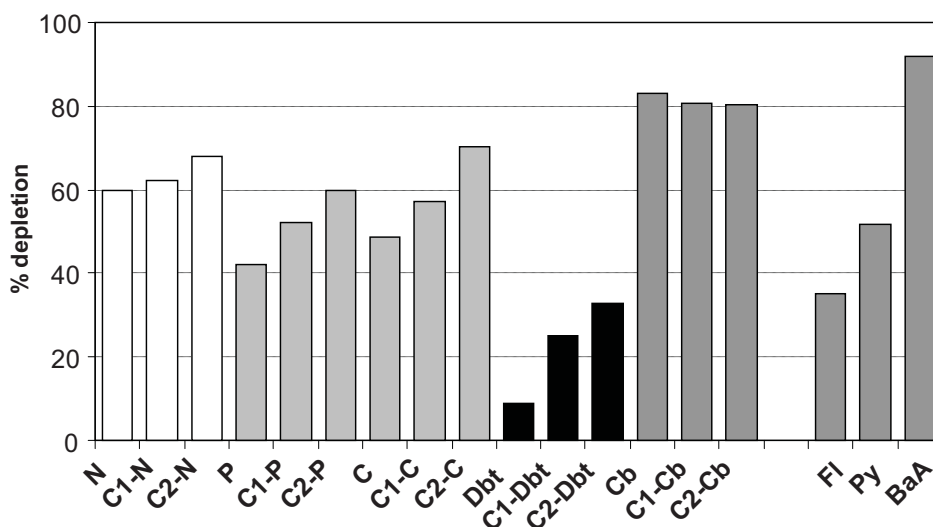
Figure III-19 Compositional changes of different families of aromatic compounds (N-naphtalenes, P-phenanthrenes, C-chrysenes, Dbt-dibenzothiophenes, Cb-carbazoles, Fl-fluoranthenes, Py-pyrenes and BaA-benz[*a*]anthracene) in the *Prestige* oil after 12 h irradiation using Xe-lamp showing the effect of chemical structure and alkyl-substitution (C1- and C2-homologues).

This could be explained by the alkyl groups enriching the electron density of the π bonded orbitals of the molecule, facilitating electron excitation and its resulting photodegradation (Schwarzenbach et al., 2005). This effect is also enhanced by the number of aromatic rings in the molecule, so that chrysenes are relatively more

depleted than phenanthrenes (Garrett et al., 1998). On the other hand, *peri*-condensed structures (e.g. Py and BaA) are more sensitive to photooxidation than *cata*-condensed ones (e.g. Fl and C). The large cross-sectional area of *peri*-condensed compounds makes them more efficient absorbents of the UV-radiation (Plata et al., 2008). The presence of S in the molecule (e.g. Dbt) reduces relatively the photodegradation. Although the S atom would be expected to be the site of preferred oxidation, this seems not to be the case in aqueous media (Bobinger and Andersson, 2009). Conversely, N heteroatom (e.g. Cb) produces a relative enhancement. In this case, the alkyl substitution did not affect the degradation rate. As seen in **Figure III-19**, all carbazole derivatives were depleted to similar extent (80% approx). This could be attributed to the strong effect of the N atom, which contributes its unshared pair of electrons into the π aromatic ring system, facilitating the reactivity of its host molecule and the subsequent photooxidation (Schwarzenbach et al., 2005). The high depletion of C1- and C2-N (>60%) is mainly due to evaporation during the test as it is confirmed by the control samples in the dark.

These patterns can be conveniently used in assessing the weathering of oil spills, so that a concurrent increase of the ratios of C2/C3 alkyl homologues or C/Py and Dbt/Cb derivatives in weathered samples can be indicative of photooxidation. In order to corroborate these experimental findings with field observations, and to confirm in more detail observed structure-dependent photosensitivity of aromatic compounds, characteristic EIC of laboratory irradiated and field samples of *Prestige* oil were compared.

III.3.5.2. Effects of photooxidation on the individual aromatic compounds. Isomer-specific photosensitivity

In the methylphenanthrenes/anthracene (MPs/MA) profile (*m/z* 192) (**Figure III-20**), the most significant change is the preferential degradation of MA over MPs, conversely to what is observed during biodegradation where MA is more persistent than MPs (Bernabeu et al., 2013).
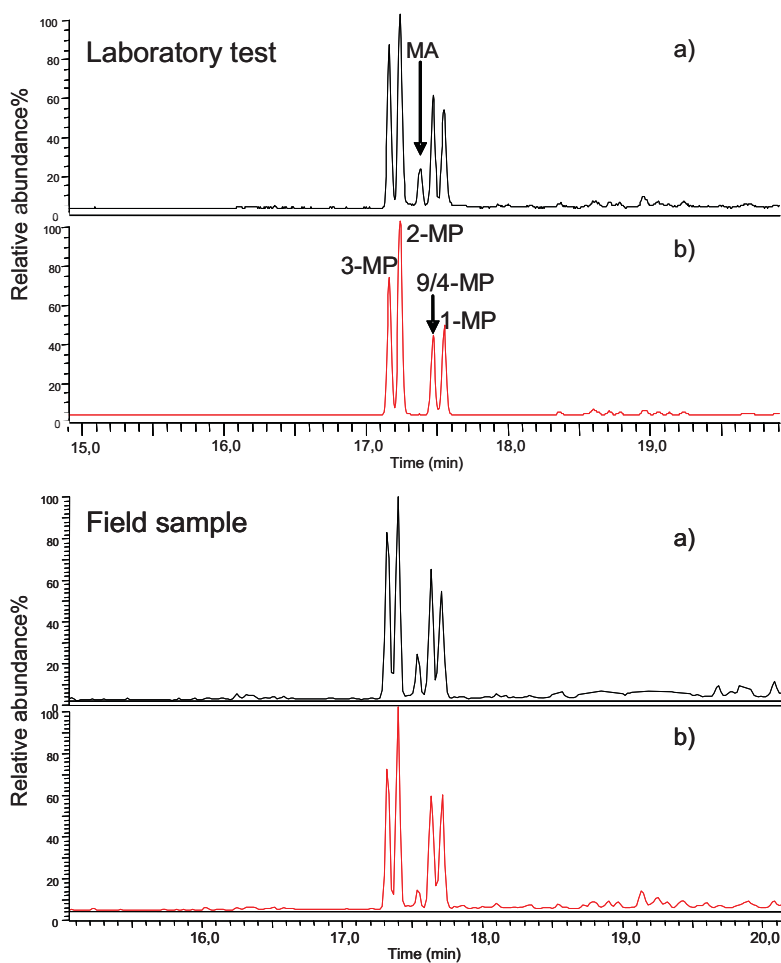
Figure III-20 Compositional changes of methylphenanthrenes (MP) and methylanthracene (MA) (*m/z* 192) in the *Prestige* fuel-oil, before (a) and after photooxidation (b) in the laboratory and in the field.

Anthracene and methylanthracene were previously reported to be easily affected by natural and simulated sunlight through the reaction of photochemical cycloaddition (Breton and Vang, 1998; Takegoshi et al., 1998). Oxydation products such as anthraquinone and hydroxyl-athraquinone were also reported as major products of anthracene photooxidation (Mallakin et al., 1999). Analogous light-induced reactions are probably the reason of the pronounced MA photosensitivity observed in the irradiated *Prestige* oil.

It also appears that the 2-MP and 1-MP are slightly more refractory than the other MP isomers, whereas in the case of biodegradation the 9-MP is more recalcitrant (Bernabeu et al., 2013).

The profiles of methylfluoranthenes/pyrenes (MFl/MPys) and benzofluorenes (BFs) (*m/z* 216), widely used in oil spill fingerprinting (CEN, 2012), were also altered by photodegradation. As shown in **Figure III-21**, most prominent effect is isomer-specific depletion of 2- and 1-MPys relative to 4-MPy, similar as in the case of preferential photooxidation of methylphenantrene isomers. Depletion of BFs and 2-MFl was observed to a lesser degree. Isomeric preferential photooxidation is also observed within the methylchrysenes (MCs) (*m/z* 242), the 2-methyl isomer being the more resistant (**Figure III-22**). Scarce studies, which deal with isomer-specific photosensitivity of PAHs, have found that methyl-substituent in certain positions interacts with the π aromatic system in such a way to lower the critical dissociation energy of the molecule (Jochims et al., 1999).

The higher resistance of the S-compounds to photodegradation is confirmed in the compositional changes of the tetramethylphenanthrene (TMP) and benzo[*b*]naphto[1,2-*d*]thiophene (BNT) profile (*m/z* 234) (**Figure III-23**), where the former were more depleted around 30% after irradiation relative to BNT.
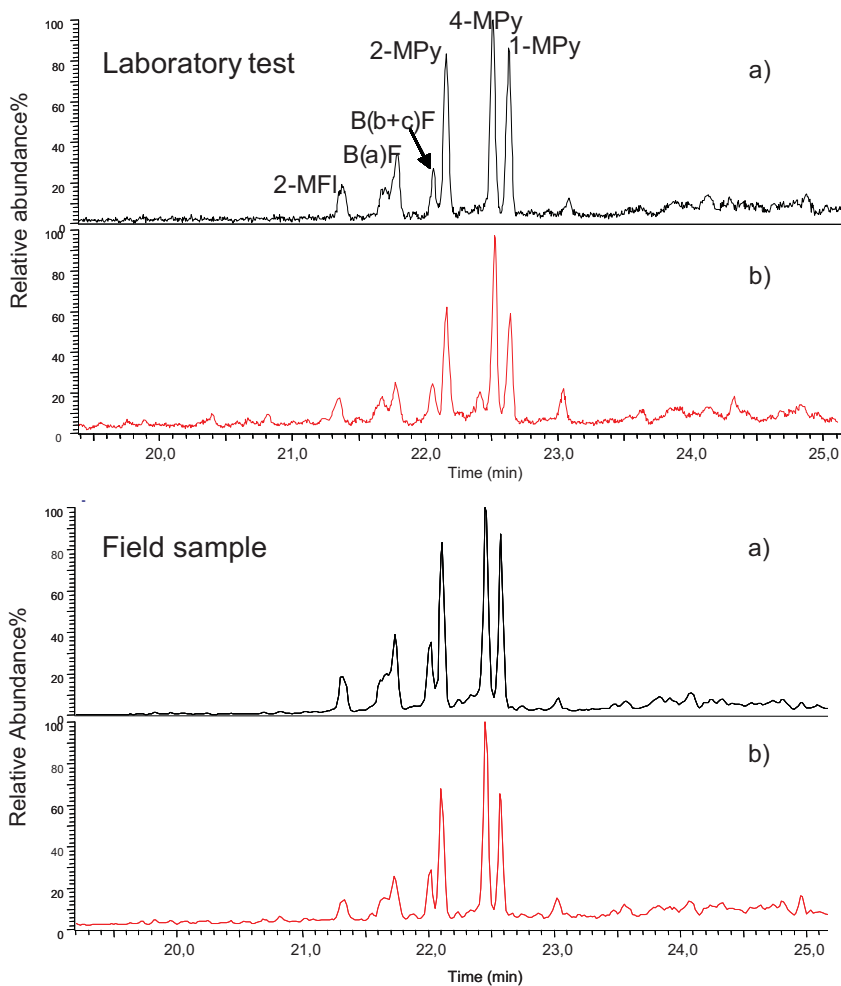
Figure III-21 Compositional changes of methylfluoranthenes/pyrenes (MFl/MPy) and benzofluorenes (BF) (*m/z* 216) in the *Prestige* fuel-oil before (a) and after photooxidation (b) in the laboratory and in the field.
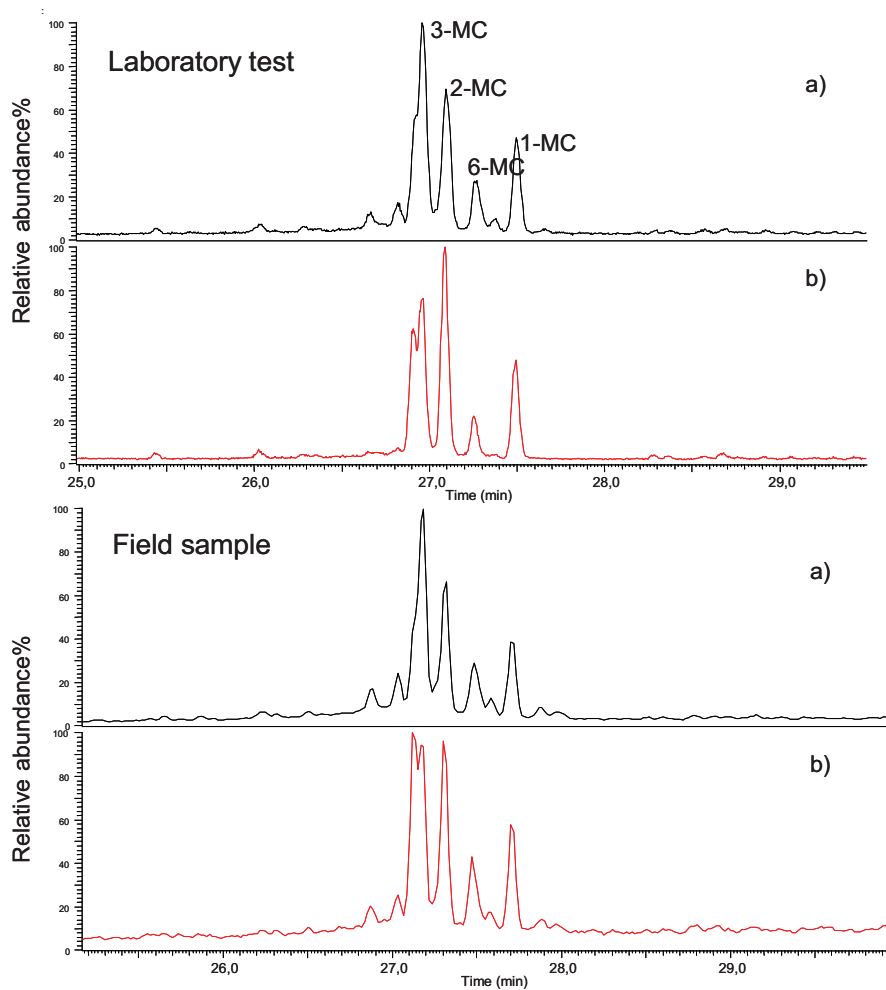
Figure III-22 Compositional changes of methylchrysenes (MC) (*m/z* 242) in the *Prestige* fuel-oil before (a) and after photooxidation (b) in the laboratory and in the field.
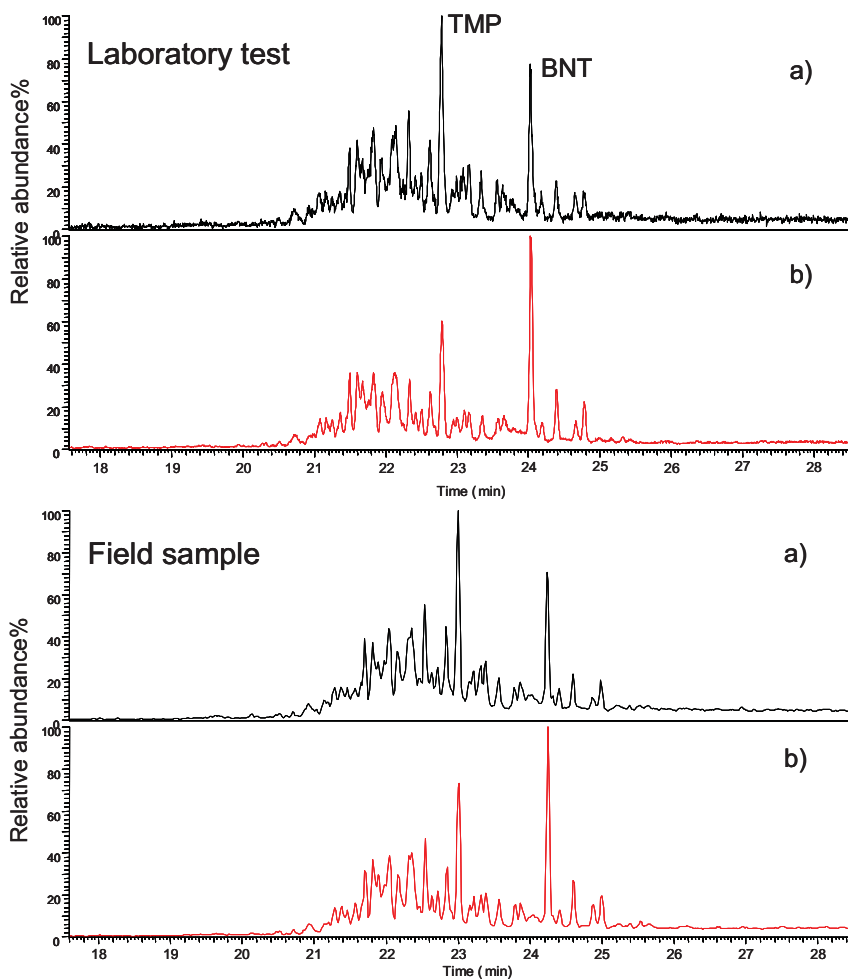
Figure III-23 Compositional changes of tetramethylphenanthrene (TMP) and benzo[*b*]naphto[1,2-*d*]thiophene (BNT) (*m/z* 234) in the *Prestige* fuel-oil before (a) and after photooxidation (b) in the laboratory and in the field.

As shown in **Figures III-20** through **III-23**, the results found in the laboratory tests are consistent with those exhibited by the samples collected in the field. A clear way of illustrating quantitatively these compositional changes in weathered samples is by using PW-plot (as explained in section **II.7.3**) shown in **Figure III-24** (CEN 2012).
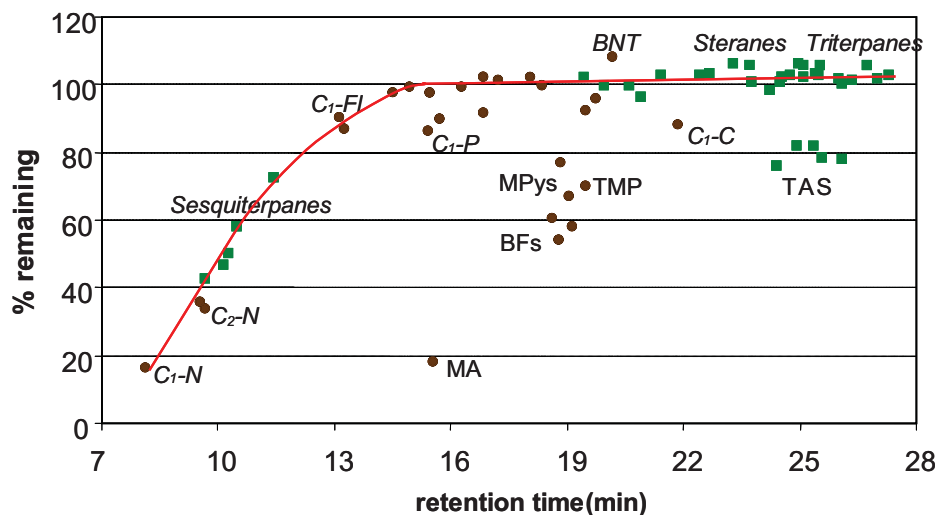
Figure III-24 Percentage of PAHs (brown circles) and biomarkers (green squares) remaining in the *Prestige* sample after photooxidation (12 h).

As can be seen in PW-plot, significant depletion of MA (80%), BFs (40%) and MPys (20-40%) and TMP (30%) in the photooxidized sample can be observed. Evaporation has affected the ratios of the lower-boiling compounds such as alkyl-substituted naphthalenes (C1- and C2-N) and sesquiterpanes.

III.3.6.   Effects of photooxidation on the triaromatic sterane (TAS) biomarkers

This biomarker family includes eight compounds (C20TA, C21TA, RC26TA, SC26TA, RC27TA, SC27TA, RC28T, and SC28TA, where R and S are steroisomers) which are pregnane and cholestane derivatives, sharing a common aromatic backbone structure but differing in the structure of the alkyl chains (**Figure III-25**).
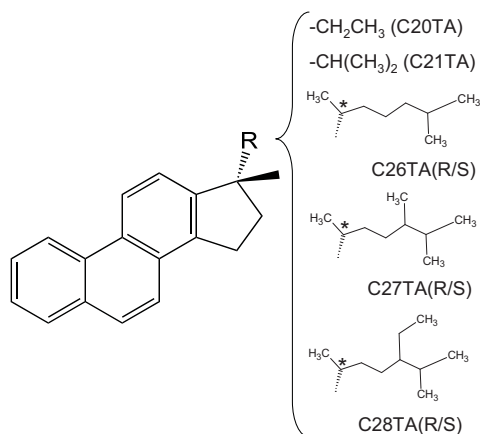
Figure III-25 General structure of triaromatic steranes (TAS) showing the shared aromatic backbone and the alkyl substituents of individual TAS compounds (asterisk marks the stereocenter).

Triaromatic steranes (TAS) have been recognized as highly recalcitrant compounds, unaffected by biodegradation (Diez et al., 2005), and successfully used to discriminate hydrocarbon sources in the Prince William Sound (Alaska) after the Exxon Valdez oil spill (Hostettler et al., 1999). However, a noticeable depletion (20%) of these compounds was observed in the irradiated samples of *Prestige* oil (**Figure III-24**) which cannot be explained by biodegradation.

III.3.6.1. GC×GC-FID analysis of TAS

In order to investigate in more detail the effects of weathering (in particular photooxidation) on TAS, GC×GC-FID methodology (described in section **II.8**) was selected since it has been demonstrated previously as an ideal tool for the analysis of petroleum biomarkers (Eiserbeck et al., 2012; Gaines et al., 2007). The main advantage of GC×GC is superior chromatographic resolution even for low abundance biomarkers (such as TAS) in highly degraded oils (Eiserbeck et al., 2012). Furthermore, FID provides the quantitative detection of peak abundances, reproducibility, increased sensitivity, and improved peak shape (Eiserbeck et al., 2011). Similar response factors for all hydrocarbons in a GC×GC–FID chromatogram improve the comparability of analyzed compounds. **Figure III-26** is a contour plot of *MW* oil showing a typical

orthogonal group type separation of compounds in GC×GC due to their increasing boiling point (1st dimension) and polarity (2nd dimension) obtained using the selected methodology.
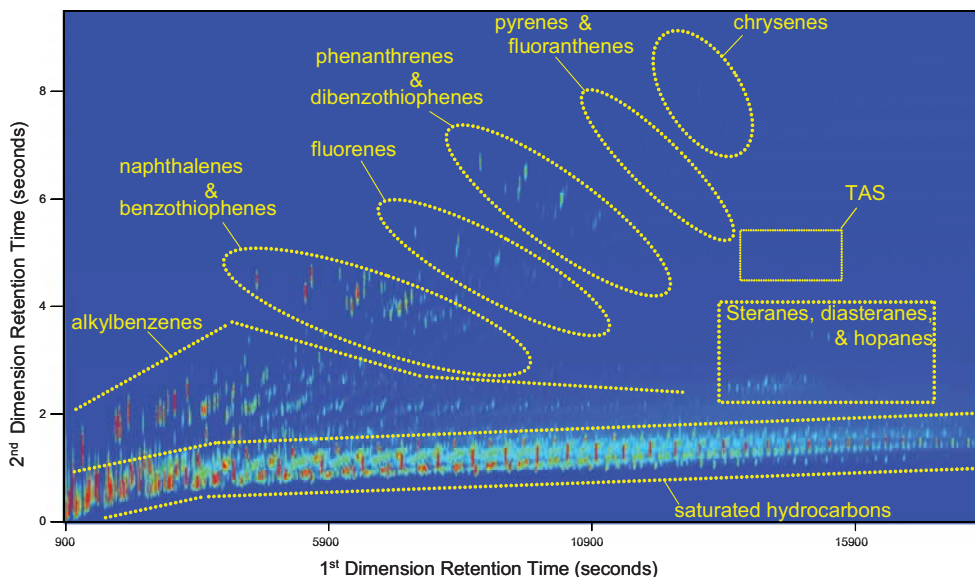
Figure III-26 Contour plot of *Macondo well* oil showing approximate regions where different types of petroleum hydrocarbons are found.

Superior resolution of TAS in GC×GC is illustrated in **Figure III-27**. Note the improved peak separation and quantification in two-dimensional chromatographic plane (e.g. low abundant SC26TA) compared to the reconstructed 1st dimension chromatogram shown in the background. However, the coelution of RC26TA and SC27TA, already observed in oil fingerprinting using conventional GC (CEN, 2012; Lichtfouse et al., 1994), cannot be resolved even using two-dimensional separation (**Figure III-27**). Therefore, in continuation, these two TAS compounds are reported jointly (RC26+SC27TA).
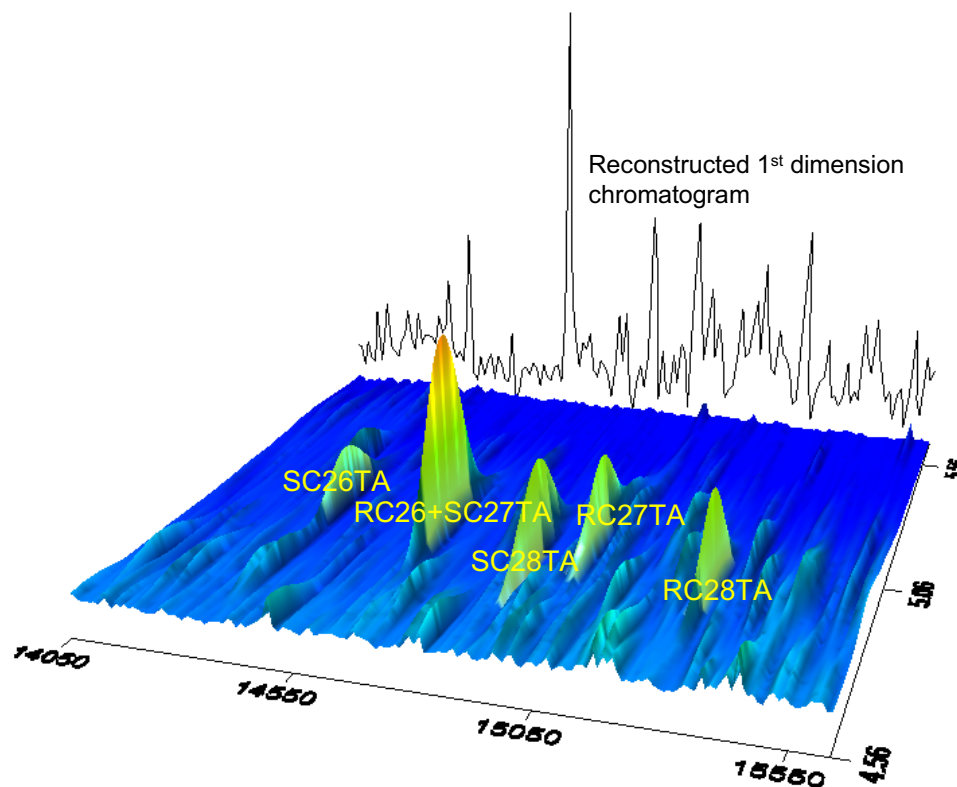
Figure III-27 3D view of a contour plot section showing some of the TAS biomarkers found in the *MW* oil. Note the reconstructed 1st dimension chromatogram in the background.

III.3.6.2. Photodegradation of TAS in oil

Previously described GC×GC-FID methodology was applied for the analysis of the rock scraping samples containing *MW* oil, collected in the Gulf of Mexico 350 and 750 days after the *DWH* blowout, which showed respectively, on average, a TAS depletion (calculated according to Eq. 2, see section **II.7.3**) of 87.5 and 96.7 % (**Figure III-28**). These samples were found as oily patches adhered on the rocks, high above the sealine and heavily exposed to solar irradiation for most of the daily sunlight.
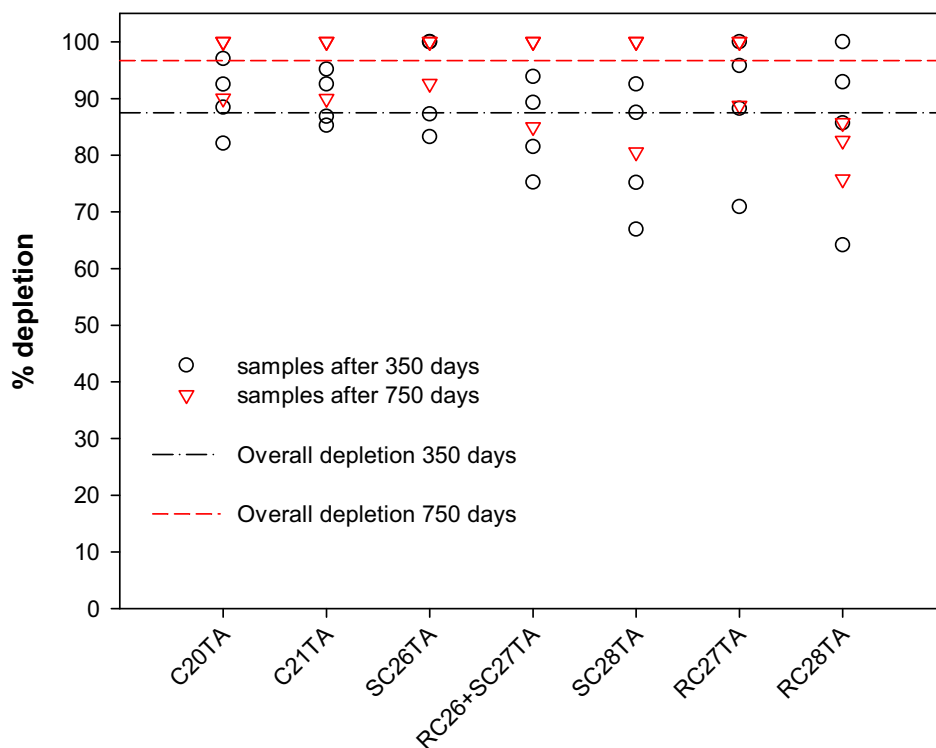
Figure III-28 Compositional changes of triaromatic steranes in *MW* oil field samples, 350 and 750 days after the spill.

These observations prompted the study of the effects of photooxidation on TAS biomarkers in *MW* oil under controlled conditions in the laboratory. Samples were irradiated using natural sunlight during medium-term period (70 days), as described in sections **II.11** and **III.3.3**.

Remarkably, in the first 24 hours TAS content already begin to decrease, relative to the original oil, and contrary to their reported recalcitrance (Hostettler et al., 1999; Peters et al., 2005). This trend continued throughout the first week of irradiation and until the end of the experiment (70 days) when no TAS compounds could be detected using the applied methodology (**Figure III-29**).
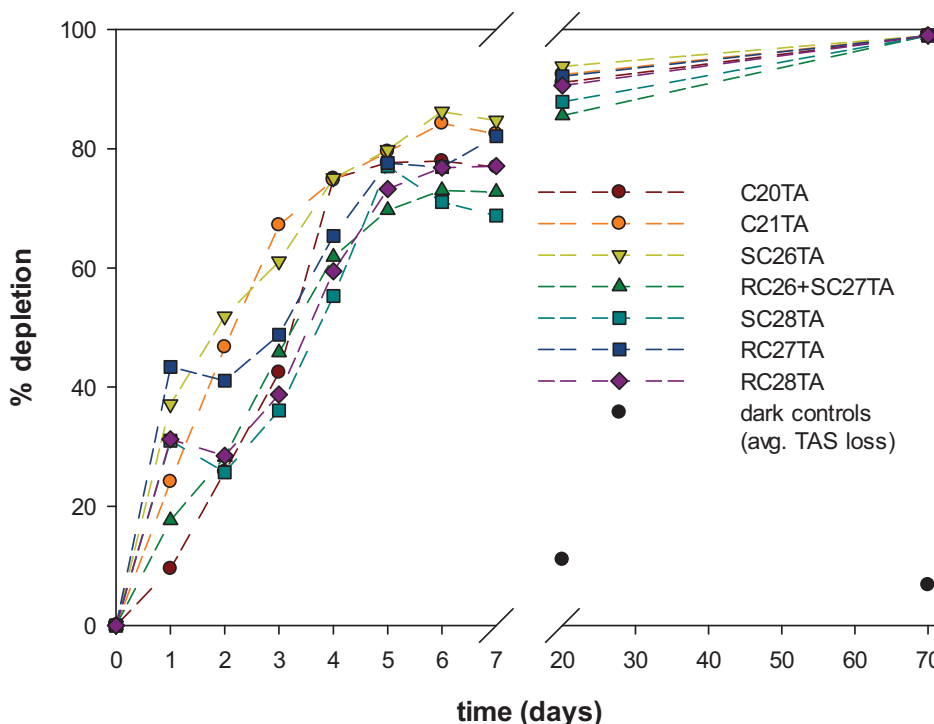
Figure III-29 Compositional changes of triaromatic steranes in the *Macondo well* oil during the photooxidation experiment.

Evaporation can be discarded as the cause of TAS loss since the mass of the oil in the quartz tubes remained stable after an initial loss (~30%) in the first 24 h (**Figure III-30**). Moreover, the dark controls taken after 20 and 70 days did not show significant change in TAS content, differences of normalized TAS peaks relative to fresh oil were on the order of integration error (10% approx.) (**Figure III-29**).

Biodegradation neither can be the cause as the evolution of TAS compounds depletion showed a converging trend not expected in the case of biodegradation, which would preferentially remove individual congeners depending on their physical properties or structure as reported elsewhere (Barakat et al., 2002; Frontera-Suau et al., 2002). Moreover, other early indicators of biodegradation (i.e. n-alkanes) were unchanged (**Figure III-30**, insert).
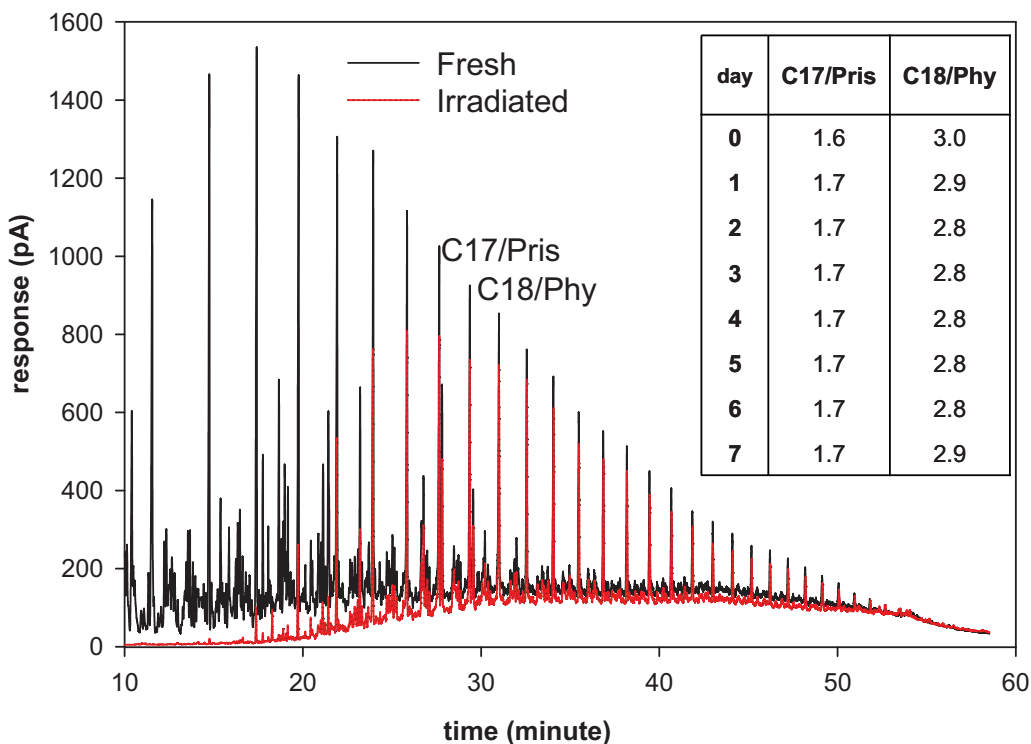
Figure III-30 GC-FID chromatogram showing evaporative loss of volatile compounds after 7 days of irradiation. Insert table shows C17/Pris and C18/Phy ratios during the same period.

Since no aqueous phase was used in the irradiation experiments, the dissolution could also be discarded as the cause of the observed transformations. Therefore, photooxidation should be the main driver of the observed TAS depletion in the reported experiment.

Similar photooxidation driven process of TAS removal is probably also the cause of observed TAS loss in rock scraping samples of weathered *MW* oil from the Gulf of Mexico. The rocks where samples were found were not submerged in the moment of sampling, and their location suggests that the oil was probably in limited contact with seawater (e.g. only during high tide). Moreover, as seen in Table III-6, estimated water solubility of TAS (1.2×10^{-6} to 3.5×10^{-3} mg·L^{-1}, estimated using SPARC on-line calculator v4.6), is similar to the values reported for four and five ring PAHs (Schwarzenbach et al., 2005), whose solubility is generally known to decrease with increasing molecular weight and alkylation (Moore and Ramamoorthy, 1984; Neff, 1979).

Table III-6 Physical properties of analyzed TAS compounds: molecular weight (MW) and aqueous solubility at 25 °C (S). Calculated using SPARC on-line calculator v4.6 (SPARC, 2013).

Name	CAS registry number	MW (g·mol^{-1})	S (mg·L^{-1})
C20TA	81943-50-21	260.4	3.55×10^{-3}
C21TA	NA	274.4	1.68×10^{-3}
C26TA(R/S)	80382-29-2	344.5	5.37×10^{-6}
C27TA(R/S)	NA	358.6	3.24×10^{-6}
C28TA(R/S)	80382-33-8	372.6	1.19×10^{-6}

NA-not available

Comparable molecular weights of investigated TAS and their alkyl-substituted structure corroborate the estimated low solubility and the conclusion that dissolution was not an important driver of TAS removal in the field samples.

Overall, based on the non-preferential TAS depletion observed in the field and confirmed in the irradiation experiment and previous studies that report their recalcitrance to biodegradation (Diez et al., 2005; Hostettler et al., 1999), it can be concluded that the loss of TAS in *MW* oil samples from *DWH* blowout was the consequence of photooxidation. Furthermore, the rate and magnitude of TAS depletion observed during the irradiation experiment (average loss of 11% per day during the first week), suggest that under field conditions photooxidation is more important weathering process than usually considered (see **Figure I-16**) (NOAA, 1996).

Possible reasons for the pronounced photosensitivity of TAS could be found in their structure, namely the aromatic (phenanthrene) backbone (**Figure III-25**), and the alkyl substitution. As seen in the case of irradiated *Prestige* oil, photoreactivity was highly influenced by increasing aromaticity and alkylation (**Figure III-19**). Note the depletion of alkylated phenanthrenes, particularly TMP (**Figure III-23**), which is structurally related to TAS. Based on the obtained FT-IR spectra, potential mechanisms could include the cleavage of the alkyl substituents and oxidation of the aromatic rings to form epoxy (Dowty et al., 1974) or quinone structures (Payne and Phillips, 1985) (**Figure III-31**).
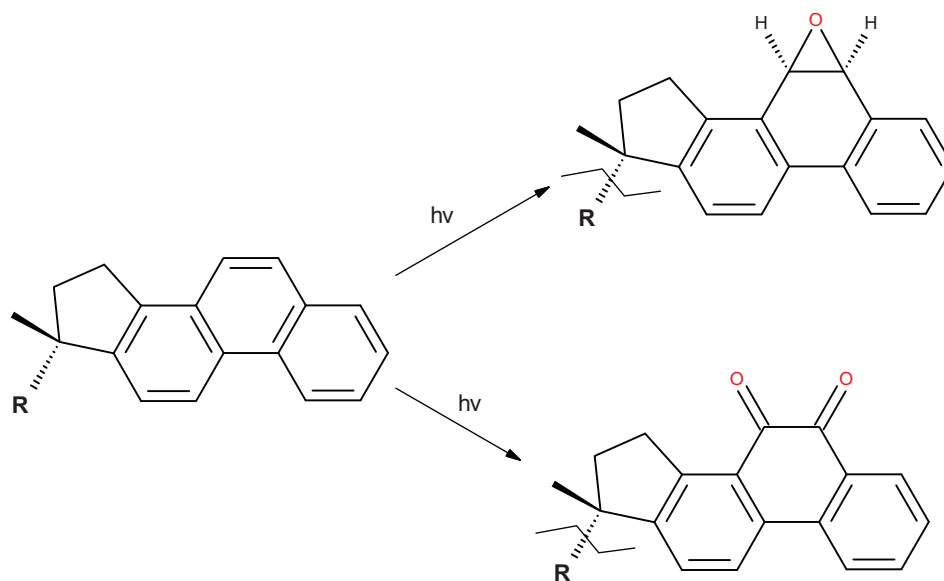
Figure III-31 Possible photooxidation products of TAS compounds.

Based on the prominent carbonyl group band in the FTIR spectra of irradiated samples (**Figure III-18**), quinone structures are probably more stable, while epoxides have tendency for fast conversion to alcohols (Dowty et al., 1974). Moreover, benzylic positions are particularly sensitive to autoxidation (Ehrhardt and Petrick, 1984) and triaromatic steroid benzylic ketones, together with a depletion of TAS, have been found in oxydized petroleum bitumens under natural conditions (Charrie-Duhaut et al., 2000).

Final corroboration that the TAS aromaticity is the main driver of their photosensitivity was found in the fact that other biomarkers (e.g. steranes and hopanes) which do not contain aromatic systems in their structure were not affected by the irradiation during the experiment (**Figure III-32**). For example, differences of normalized peaks of 13β (H), 17α (H)-20R-diacholestane and 17α (H), 21β (H)-22R-homohopane biomarkers after 7 days irradiation relative to fresh oil were 7 and 0 percent, respectively.
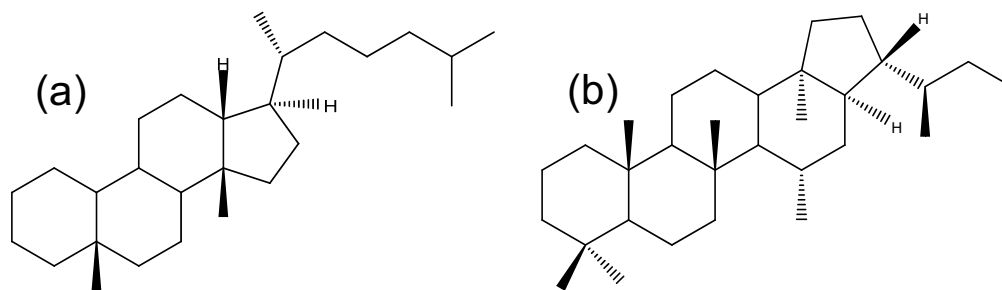
Figure III-32 Molecular structures of 13β (H), 17α (H)-20R-diacholestane (a) and 17α (H), 21β (H)-22R-homohopane (b). Note the absence of aromatic rings.

III.3.7.   Implications for the oil fingerprinting

In order to improve the reliability of the assessment of the differences between the profiles of the spill and suspected source samples, a number of diagnostic ratios between single compounds or groups of compounds selected for their diversity in the chemical composition in petroleum products and their reported response to weathering processes have been selected (CEN, 2012; Hansen et al., 2007). The ratio comparison is applied to make the method more robust than the qualitative visual comparison of chromatograms and to make it more independent from the experience of the analyst. In this respect, it is important to know the effect of weathering processes on the diagnostic ratios for an adequate interpretation of the results in real cases.

As demonstrated in the section **III.3.5**, a number of aromatic compounds that are often used for oil spill forensics were particularly affected by irradiation. It is evident that after photooxidation, all selected PAH ratios except 2-MP/1-MP showed significant differences (relative difference higher than the critical limit of 14%), which can affect their reliability when used to confirm the source of the spill (**Table III-7**). However, the knowledge of the effects of irradiation at molecular level can help to interpret the observed differences and attribute them to photooxidation.

Table III-7 Relative difference (%) between PAH ratios in the original and laboratory irradiated *Prestige* oil after 12 h.

Ratio	Original	Irradiated	Rel. diff. (%)
2-MP/1-MP	1.95	1.80	8.45
9/4-MP/1-MP	1.18	1.00	16.51
MA/1-MP	0.37	0.03	170.0
4-MDbt/1-MDbt	2.57	2.13	18.72
B(a)F/4-MPy	0.30	0.20	40.00
B(b+c)F/4-MPy	0.25	0.20	22.22
2-MPy/4-MPy	0.86	0.60	35.62
1-MPy/4-MPy	0.84	0.69	19.61
BNT/TMP	0.75	1.77	80.46
2-MC/1-MC	1.57	2.17	32.09
C2-C/C2-Py	0.12	0.39	105.9

For example, change of ratios, such as MA/1-MP, 2-MPy/4-MPy, 1-MPy/4-MPy and BNT/TMP, among others, could serve as early indicators of sunlight exposure of samples in the field. As it can be concluded by the lower ratios in irradiated samples, the 1-methyl isomers of P, Dbt and C, as well as the 4-MPy, are the more resistant components within each family. A concurrent increase of the ratios of the chrysene/pyrene components (e.g. C2-C/C2-Py) in weathered samples can also be indicative of photodegradation.

Unexpectedly, significant changes in ratios of TAS biomarkers, which are traditionally considered to be robust at medium- to long-term environmental exposure (Peters et al., 2005), were observed after only seven days (**Table III-8**). The relative differences of the majority of the commonly used TAS ratios between the original and irradiated *MW* oil samples were above the critical limit of 14% which is the accepted threshold for a positive match with the source oil (CEN, 2012).

Table III-8 Relative difference (%) between TAS ratios in the original and experimentally irradiated *Macondo well* oil.

Ratio	Original	Irradiated Day			
		7		20	
			rel.diff.(%)		rel.diff.(%)
C20TA/C21TA	0.87	1.14	27.23	1.02	16.17
C21TA/RC26+SC27TA	1.55	0.99	43.89	0.83	60.23
SC26TA/RC26+SC27TA	0.38	0.21	57.12	0.16	80.74
SC28TA/RC26+SC27TA	0.65	0.74	13.05	0.58	12.23
RC27TA/RC26+SC27TA	0.58	0.38	41.80	0.32	57.79
RC28TA/RC26+SC27TA	0.55	0.46	17.66	0.38	37.41

The SC26/RC26+SC27TA ratio is particularly affected and although the SC28/RC26+SC27TA seems to be more robust, based on the present observations, caution should be taken when using TAS ratios for fingerprinting spill samples heavily exposed to sunlight, even in a relatively short timeframe (weeks). In such cases, the sterane and hopane (triterpane) ratios should be used for the confirmation of the source, while PAH and TAS could rather be more useful to estimate the weathering processes, in particular photooxidation.

III.3.8.   Concluding remarks

In this section, the effects of photooxidation on both bulk and molecular oil composition, particularly PAHs and TAS biomarkers, commonly used for fingerprinting oil spill samples were estimated.

At the bulk level, transformation of saturate and aromatic fractions to more polar, oxygen containing species was observed. At molecular level, it was observed that the photosensitivity increases with increasing aromaticity and alkylation, and significant effects on a series of PAH compounds, i.e. MA, MPys, TMP and MC were demonstrated. Furthermore, it was observed that PAH photochemistry is isomer-specific in some cases (e.g. recalcitrance of 1- and 2-MP, 4-MPy, and 2-MC).

GC×GC-FID was demonstrated as the method of choice for the analysis of low abundant degraded biomarker compounds such as TAS due to its superior resolution and sensitivity. Unexpected and pronounced photodegradation of TAS biomarkers was demonstrated at laboratory scale, which was comparable to the observations from the

common backbone and alkylation, comparable to the effects observed in structurally analogous PAHs. These observations will contribute to better interpret the oil compositional changes and enhance the fidelity of the fingerprinting techniques.

III.4. *Effect-directed analysis of fresh and weathered oils*

III.4.1. Introduction

In the previous sections, different physiochemical properties of selected oils were analyzed, their influence on the fate of marine oil spills was evaluated, and the effects of different weathering processes such as evaporation, biodegradation and photooxidation on these properties were demonstrated. However, for a fully comprehensive risk assessment of marine oil spills, their potential environmental effects must be also taken into account. To this end, this section presents an analytical approach, known as effect-directed analysis (EDA), which can be used to assess the toxic potential of different components in a complex chemical mixture, such as oil.

As discussed in section **I.7**, chemical components of oil are responsible for its toxic effects on marine organisms, which range from acute and sub-lethal non-specific narcotic effects to specific chronic effects that can affect feeding, growth, and reproduction and can result in irreversible tissue damage (Martínez-Gómez et al., 2010).

Study presented in this chapter focused on AhR mediated and AR effects which were evaluated using a set of suitable bioassays (PAH-CALUX and Yeast Androgen Screen, (YAS), respectively; see sections **II.13.3** and **II.13.4** for detailed description). Two representative oils from the previously analyzed sample set were selected, namely North Sea Crude oil (NSC) and residual heavy fuel oil (HFO) (see **Table III-1** for their properties). In order to investigate the effect of weathering processes on toxicity, both oils were evaporated and photooxidized under laboratory conditions (see sections **II.10** and **II.11**), to simulate the weathering in the field.

Reduction of samples' complexity was obtained by two-level fractionation; using open-column liquid chromatography and normal-phase semi-preparative HPLC, respectively (see sections **II.13.1**and **II.13.2**).

The most active fractions were analyzed using GC×GC-TOFMS, which was selected because it offers, alongside increased chromatographic resolution, an additional mass spectral dimension provided by TOFMS, which is not available when using FID detector (Lourdes, 2009). This is an essential feature for non-target analysis of complex mixtures, particularly in EDA studies where tentative identification and/or confirmation of toxic compounds is needed (Brack, 2003).

Finally, conventional EDA strategy (Brack, 2003) was extended and additional chemometric step was added, where N-PLS model was used to correlate the chemical information (from GC×GC-TOFMS) and toxicity data (see section **II.13.5**). Although N-PLS has been applied previously to data from GC×GC for the quantitative analysis of aromatic and naphthene content in naphtha (Prazen et al., 2001), the identification of gasoline adulteration (Pedroso et al., 2008), the quantification of kerosene in gasoline (De Godoy et al., 2008), and the quantification of naphthalenes in jet fuel oil (Johnson et al., 2004), its potential applications in EDA are still not studied. Toxic activity of identified compounds was confirmed using quantitative structure-activity relationship (QSAR) estimates.

III.4.2. Selection of oil samples

Oil samples were selected to represent two distinct oil types. Their properties are given in **Table III-9**, as determined previously in section **III.1** using elemental analysis and TLC-FID. NSC is a typical light sweet crude oil with predominance of saturated hydrocarbons. HFO is heavy, viscous, distillation residue, commonly used as shipping fuel. It has increased content of sulfur and aromatic hydrocarbons. Therefore, they can serve as "model" oils to investigate which type of toxic compounds in crude and heavy residual oils can be found. Moreover, simulated weathering (evaporation, photooxidation) was used to study the relation of the compositional changes and toxicity in two oils.

Table III-9 Properties of selected oils.

	Density 15 °C, kg·m^{-3}	Sulfur, %wt	Saturates, %	Aromatics, %	Polars, %
NSC	832.4	0.22	66.2	13.2	20.3
HFO	988.8	2.63	22.1	38.2	39.7

III.4.3. Selection of bioassays

As shown in **Table III-10** the short-term toxicity of the two selected oils (expressed as letal concentration for half of the sample population of *T. battaglia* during 48 hours exposition) is induced in the high ppm ($mg \cdot L^{-1}$) range, i.e. at concentrations higher than those that would be expected in the marine environment in the case of a spill (Allen, 1984). As a consequence, concerns are more related with long-term effects of these oils.

<p align="center">**Table III-10** Acute toxicity of selected oils (RAMOCS, 2012)</p>

	Type of test	Endpoint	Parameter ($mg \cdot L^{-1}$)
NSC	48h-invertebrates (*T. battaglia*)	Mortality	EC50=370
HFO	48h-invertebrates (*T. battaglia*)	Mortality	EC50=9580

In order to estimate their potential for chronic toxicity, *in vitro* studies have been selected for this study, since they are able to estimate the binding of chemicals to AhR, AR and ER receptors, which in turn leads to various chronic, dioxin-like and endocrine disrupting effects. Indeed, various reports documented such *in vitro* activities of crude oils, petroleum products, or produced waters from oil extraction (Jonker et al., 2006; Li et al., 2008; Vrabie et al., 2010; Vrabie et al., 2009). Much attention has been given to the effects of the PAHs found in oil and, in particular, to carcinogenic PAHs (Hylland, 2006). The metabolic activation of carcinogenic PAHs is thought to take place through the AhR mediated induction of the CYP family of P450 monooxygenase. As shown in **Figure III-33**, the mechanism of induction of gene transcription by PAHs involves ligand recognition and binding by the AhR. After nuclear translocation, AhR-PAH dimer interacts with xenobiotic responsive elements in promoter/enhancer regions of multiple Ah-responsive genes (Wilson and Safe, 1998). Subsequent changes in chromatin structure and/or interaction of the AhR complex with the basal transcriptional machinery play a significant role in AhR-mediated gene expression and subsequent detrimental effects (Wilson and Safe, 1998).
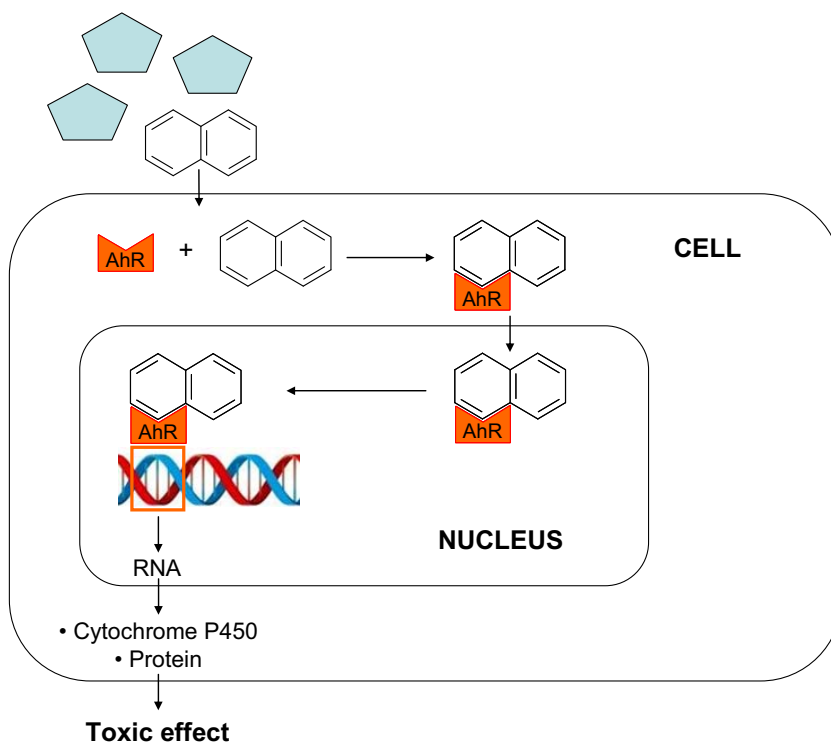
Figure III-33 Mechanism of AhR mediated toxicity [based on (Wilson and Safe, 1998)].

Furthermore, recent studies suggest the important contribution of alkyl substituted PAH homologues in the overall toxicity of complex mixtures (Muusse et al., 2012; Vrabie et al., 2012). It has also been proposed that CYP1A induction can interfere with endocrine processes, by increasing estrogen metabolism (Wenger et al., 2010); however, certain PAHs and other oil components are known to act as AR antagonists, blocking the AR and, thus, interfering with endocrine processes, too (Thomas et al., 2009). These specific effects are poorly understood, and the oil components that cause them are generally unknown, especially following weathering.

In conclusion, PAH-CALUX and YAS were selected to test the AhR agonist and AR antagonist activity of oil fractions, respectively.

III.4.4.   First level fractionation and biotesting

In the first level of EDA, coarse fractions were obtained by open-column liquid chromatography. They contained saturated, aromatic and polar (resin-like) hydrocarbons. Eighteen (18) fractions were obtained in total (3 fractions per each of two fresh, evaporated and irradiated oils), and subjected to AhR and AR bioassays.

III.4.4.1.   Evaluation of AhR agonism and AR antagonism in coarse fractions

Figure III-34 shows the AhR agonist and AR antagonist levels in the coarse fractions of fresh, evaporated and Xe-lamp irradiated NSC and HFO. The AhR agonist potency, expressed as BaP toxic equivalents (TEQ) per gram of oil, was consistently highest in the aromatic fractions of the NSC and HFO regardless of treatment.

The polar fractions also contained AhR agonists, whereas no activity was determined in the saturate fraction. This is as expected, since saturates are not known to bind to the AhR. Some differences were observed in the total aromatic AhR agonist potency following treatment.

For example, the AhR agonist potency of NSC aromatics increased with evaporation (5.93 to 9.96 μg BaP TEQ·g^{-1}, i.e. 68% approx.), but was similar to fresh oil levels following irradiation (5.34 μg BaP TEQ·g^{-1}). For HFO, evaporation had little effect on the AhR agonist potency (12.94 to 12.83 μg BaP TEQ·g^{-1}), whilst irradiation increased the AhR agonist potency to 22.03 μg BaP TEQ·g^{-1} (i.e. 70%, approx.). Much less activity was determined in the polar fractions of the two oils (0.04 to 0.94 μg BaP TEQ·g^{-1}). The oils' total response is within the same range as previously reported for crude oil tested with the DR-Luc assay (0.97-3 μg BaP TEQ·g^{-1}) (Vrabie et al., 2009).
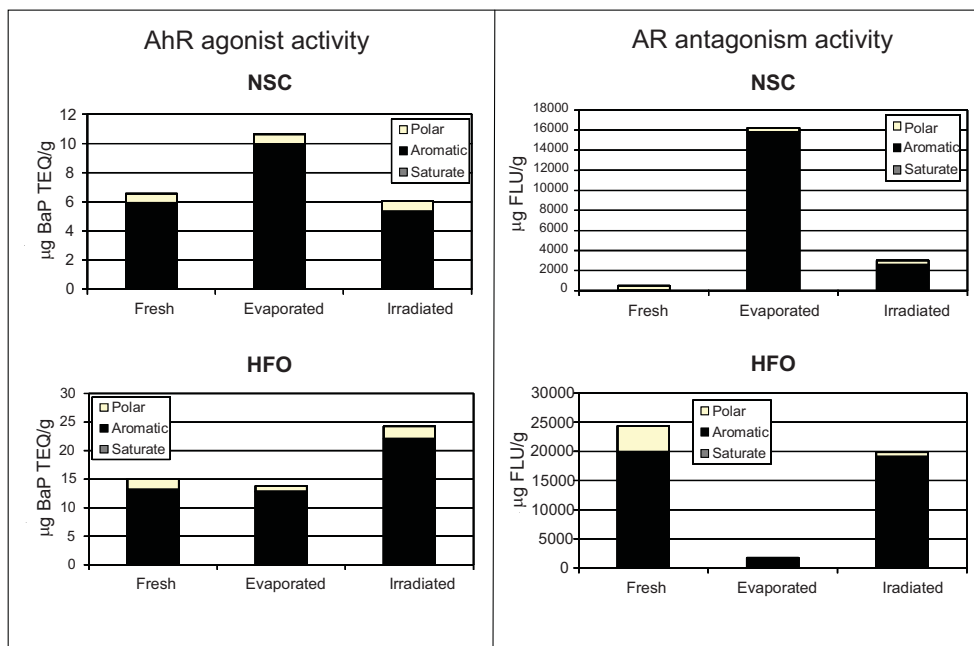
Figure III-34 AhR agonist and AR antagonist activity of the saturate, aromatic and polar oil fractions of North Sea crude (NSC) and heavy fuel oil (HFO), before and after simulated weathering.

Without detailed chemical analysis these differences are difficult to explain. We hypothesize that evaporation of volatile aromatics has resulted in a higher relative concentration of AhR agonists in the oil, whilst irradiation has resulted in a lower relative AhR concentration through reducing the overall AhR potency, possibly through the formation of polar oxygenated products, that subsequently are not sufficiently potent AhR agonists to significantly increase the relative potency of the polar fraction. TLC-FID analysis of the NSC aromatic fraction supports this hypothesis. As can be seen in **Figure III-35**, evaporation of the oil resulted in relative enrichment of the aromatic fraction which predominantly contains AhR agonists. On the other hand, the formation of more oxygenated compounds following irradiation with a reduction in aromaticity has previously been shown (Aeppli et al., 2012; Radović et al., 2013).
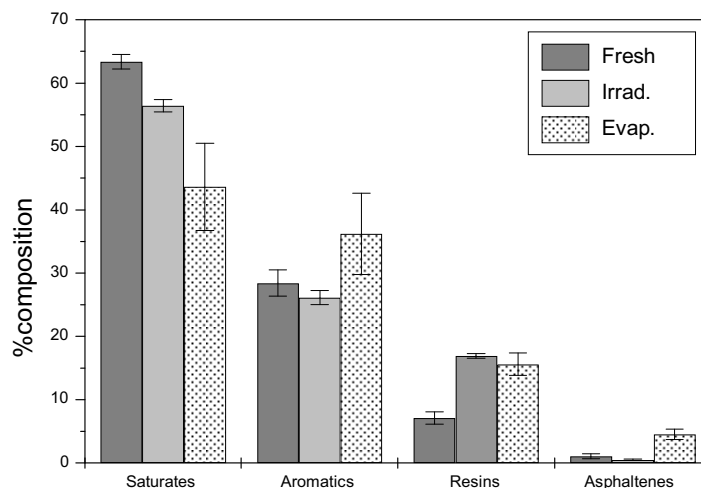
Figure III-35 Composition of North Sea crude after evaporation and irradiation.

The aromatic fraction also contained most of the AR antagonists present in the tested oils (**Figure III-34**). There was typically also some AR antagonist activity in the polar fraction. For the NSC, the aromatic fraction of the fresh oil was sufficiently cytotoxic to the yeast to prevent antagonist activity from being measured; however, differences were observed between the AR agonist potency of the evaporated and irradiated NSC (16000 and 2600 μg FLU·g^{-1}, i.e. 84% approx.). The polar fraction containing the highest potency of AR antagonists was found in the fresh HFO (4500 μg FLU·g^{-1}) and was reduced following evaporation (200 μg FLU·g^{-1}, i.e. 95% approx.) and irradiation (800 μg FLU·g^{-1}, i.e. 82% approx.). Evaporation of the HFO aromatics resulted in a marked reduction in AR antagonism (from 20000 to 1500 μg FLU·g^{-1}, i.e. 92.5% approx.), whereas there was little reduction following irradiation (19000 μg FLU·g^{-1}). This is the first time such activity has been reported in fractions (aromatic and polar) of crude and residual oil, although AR antagonist activity has previously been reported in Romanian Crude and a number of refined petroleum products (Kizu et al., 2000). These results also corroborate the AR-antagonist activity already demonstrated in produced water from North Sea oil platforms (Tollefsen et al., 2007). Relatively high flutamide-equivalent concentrations compared to those found in the oil/particulate phase of produced water reported by Tollefsen et al. (Tollefsen et al., 2007) were observed. However, this was expected, as the analyzed samples were concentrated fractions of neat oil, while the produced water in that study was collected following a cleaning treatment to remove oil residues. Thomas et al. (Thomas et al., 2009)

identified PAH residues in produced water as contributors to the overall AR antagonist signal and it has been shown that PAHs, such as phenanthrene, chrysene, benzo[a]pyrene, benzo[k]fluoroanthene act as AR antagonists (Kizu et al., 2003). We therefore hypothesize that aromatic fraction of NSC and HFO contain, in addition to those listed above, other PAHs and their alkyl substituents that antagonize the AR receptor. What is interesting is that the aromatic AhR agonists are likely to be the same compounds mediating the antagonism of the AR. The AhR mediated inhibition of the AR has previously been shown in LNCaP human prostrate carcinoma cells, where the AhR mediated inhibition of AR-binding was shown to be due to the expression of an activator protein (AP1) that amongst other controls a number of cellular processes, which through protein-protein interaction blocks interaction between the AR and the androgen-responsive element (Kizu et al., 2003).

Due to this cross-talk further study was focused to the AhR elements in the coarse aromatic fractions (6 in total) since in all likelihood they are the same compounds responsible for the observed AR antagonism, although future studies are required to further evaluate the AR activity of crude oils and establish the role of the AhR.

III.4.4.2. Chemical characterization of coarse fractions

Chemical composition of coarse aromatic fractions was investigated using both target and broad-spectrum analytical techniques, i.e. GC-MS and GC×GC-TOFMS, respectively. The results showed that fractions contain a complex mixture of PAHs, ranging from two ring PAHs (e.g. naphthalene) to heavy polycyclic compounds (e.g. benzo[ghi]perylene), including alkyl-substituted homologues of the parent compounds (**Table III-11**). Some of the compounds present in the HFO oil were not found in the NSC (e.g. anthracene, fluoranthene, benz[a]anthracene and benzo[a]pyrene). This demonstrates that the applied open-column chromatography method was able to satisfactorily isolate the PAH compounds of the analyzed oils, and that the PAHs are predominantly responsible for the observed AhR and AR activity, as expected (Thomas et al., 2009; Vrabie et al., 2009).

Table III-11 Polycyclic compounds detected using GC-MS in the coarse aromatic fractions of North Sea crude (NSC) and heavy fuel oil (HFO).

	Compound name	Ring No.	*m/z*	NSC	HFO
1	Naphthalene	2	128	+	+
2	C1-Naphtalenes	2	142	+	+
3	C2-Naphtalenes	2	156	+	+
4	C3-Naphtalenes	2	170	+	+
5	Acenaphthene	3	154	+	+
6	Fluorene	3	166	+	+
7	Phenanthrene	3	178	+	+
8	C1-Phenanthrenes	3	192	+	+
9	C2-Phenanthrenes	3	206	+	+
10	C3-Phenanthrenes	3	220	+	+
11	Anthracene	3	178	-	+
12	Dibenzothiophene	3	184	+	+
13	C1-Dibenzothiophenes	3	198	+	+
14	C2-Dibenzothiophenes	3	212	+	+
15	Fluoranthene	4	202	-	+
16	Pyrene	4	202	+	+
17	C1-Pyrenes	4	216	+	+
18	C2-Pyrenes	4	230	+	+
19	Benzo[*a*]anthracene	4	228	-	+
20	Chrysene	4	228	+	+
21	C1-Chrysenes	4	242	+	+
22	Benzo[*b*]fluoranthene	5	252	+	+
23	Benzo[*a*]pyrene	5	252	-	+
24	Benzo[*ghi*]perylene	6	276	+	+

Furthermore, the comparison of GC×GC-TOFMS contour plots of whole oils and their coarse aromatic fractions shows the reduction of sample's complexity after coarse fractionation, leading to the removal of aliphatic and monoaromatic hydrocarbons (**Figure III-36**).
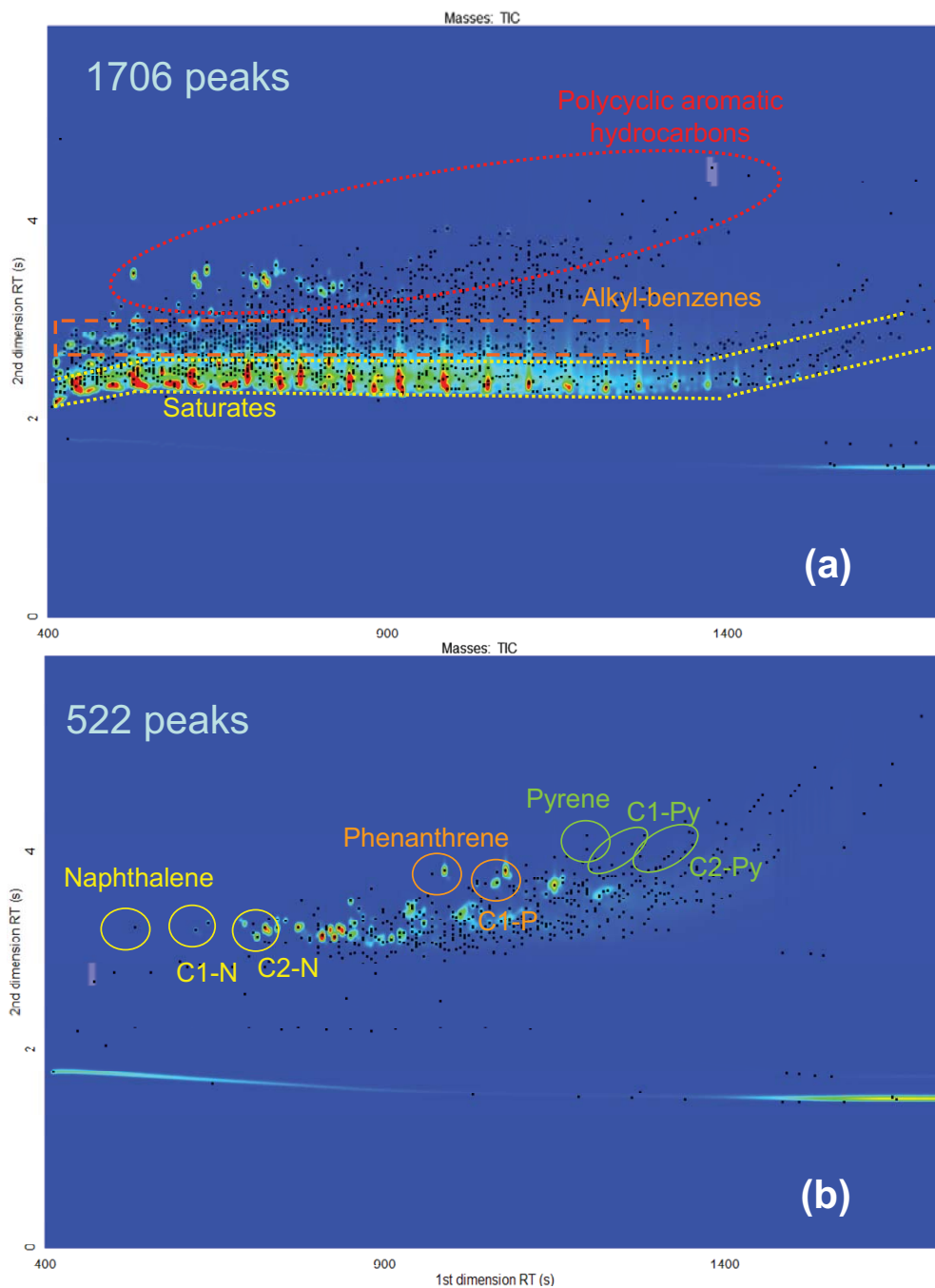
Figure III-36 GC×GC-TOFMS contour plots of the (a) whole North Sea crude (fresh) and the (b) aromatic coarse fraction of the same oil, showing the reduction of sample's complexity.

For example, in fresh, whole NSC oil 1706 peaks could be detected using the applied GC×GC-TOFMS methodology. In contrast, in the coarse aromatic fraction of

the same oil, 522 peaks were detected with the same method. In general, the reduction in number of detected peaks in fractionated samples relative to whole samples ranged from 53 to 79 %, approximately (**Table III-12**).

Table III-12 Number of detected peaks in whole samples and coarse aromatic fractions of fresh (F) and irradiated (Xe) North Sea Crude (NSC) and heavy fuel oil (HFO).

	NSC		HFO	
	F	Xe	F	Xe
whole oil	1706	1203	987	848
coarse aromatic fraction	522	560	205	324
% reduction	69	53	79	62

However, the number of detected compounds using non-target GC×GC-TOFMS screening also showed that the composition of coarse fractions is still too complex to allow a more definite identification of the individual PAH compounds (or compound groups) responsible for the effects observed in the bioassays. Therefore, in the next level of EDA, additional subfractionation of the coarse aromatic fractions was necessary.

III.4.5.   Second level fractionation and biotesting

Coarse aromatic fractions were subfractionated using normal-phase semipreparative HPLC with aminopropyl-modified silica column. Separation mechanism of this type of stationary phase is based on polar interactions, hydrophobic interactions and weak ion exchange interactions. When working in normal-phase configuration it permits group-type separation of the aromatic compounds by their increasing aromaticity (double bond equivalent) (Rønningsen and Skjevrak, 1990; Sutton and Nesterenko, 2007). **Figure III-37** shows the group-type separation of PAH standard mixture in function of the number of condensed rings.
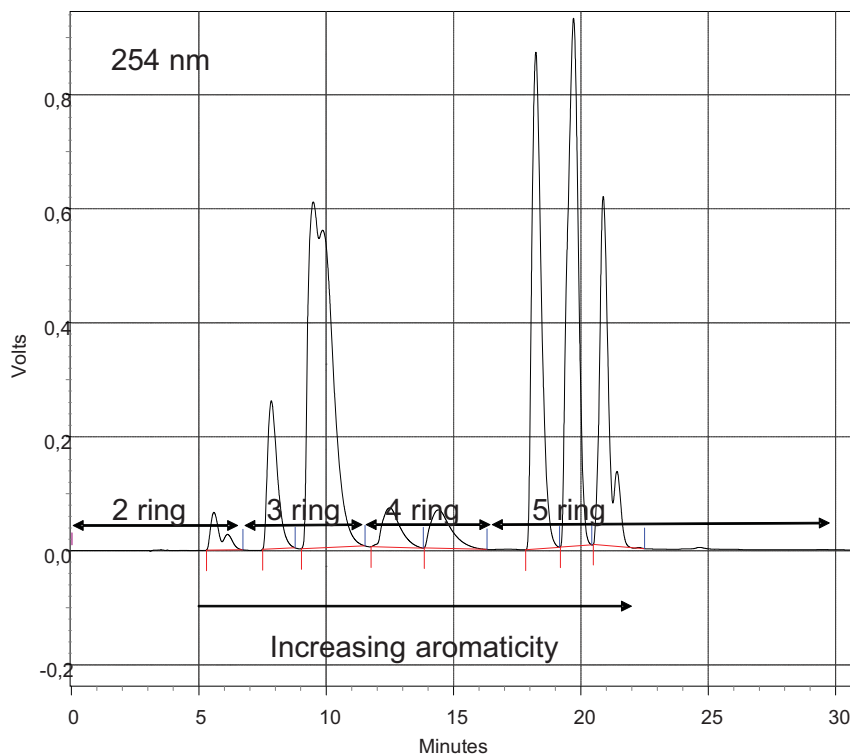
Figure III-37 HPLC-UV chromatogram of a standard PAH mixture showing the separation based on increasing compound aromaticity

Fractions were collected during 30 minutes, in two-minute intervals, i.e. 15 fine (sub)fractions were obtained for each of the 6 coarse aromatic fractions (90 fine fractions in total).

III.4.5.1. Evaluation of AhR agonism in fine fractions

Figure III-38 shows the AhR agonist distribution in the fine fractions of the aromatic coarse fraction of fresh, evaporated and UV-irradiated NSC and HFO.

For the fresh and irradiated NSC oils, the main AhR-containing fraction was fraction 10; in contrast, it was fraction 11 for the evaporated NSC. This suggests that evaporation affected the composition of the oils in terms of AhR agonists.

NSC

HFO
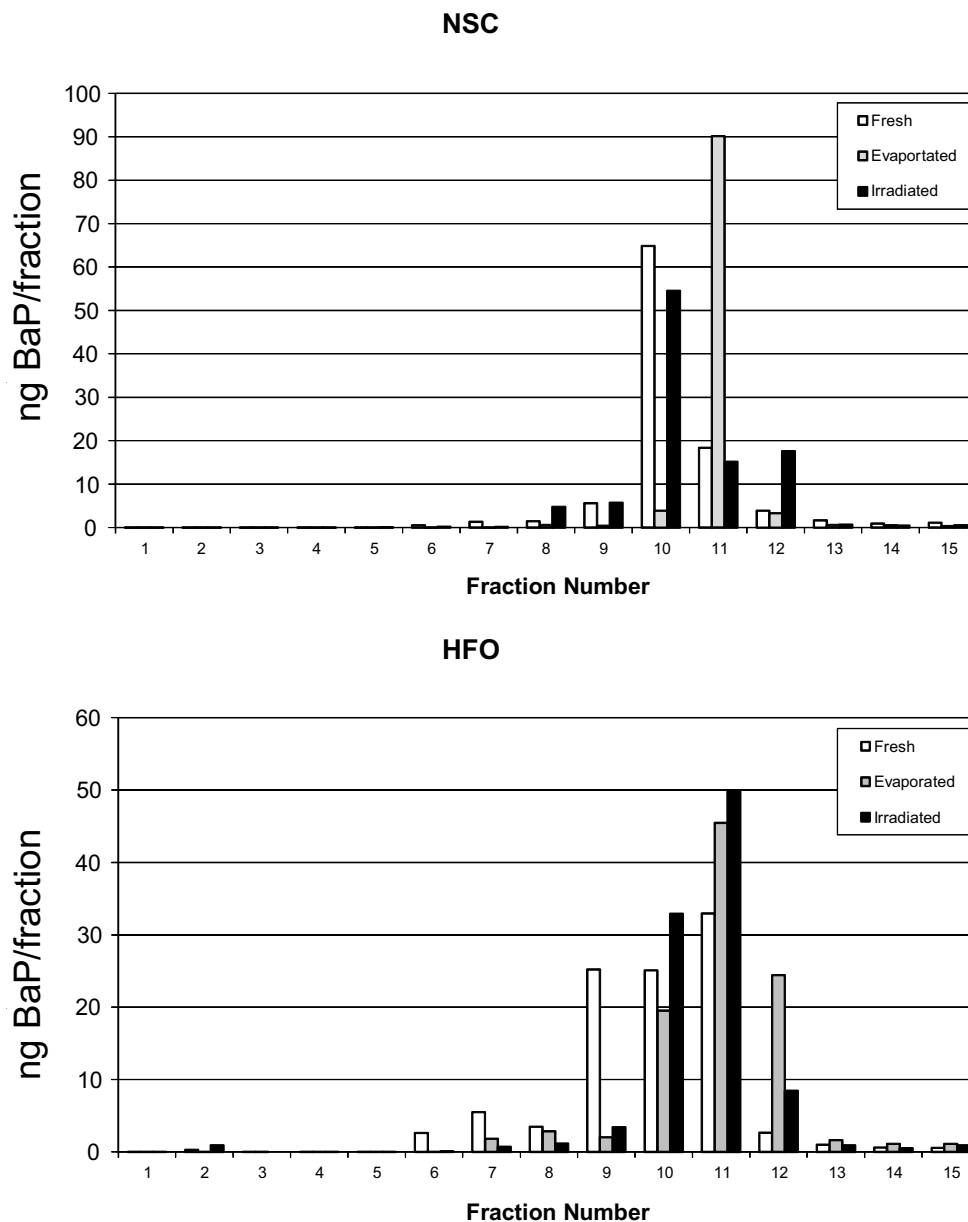
Figure III-38 AhR agonist activity in the fine fractions of fresh and artificially weathered North Sea crude (NSC) and heavy fuel oil (HFO).

This was not observed with the HFO, in which the strongest AhR-agonist signal was detected in fraction 11 for all treatments. NSC AhR agonists were detected in fractions 6 to 15, which, according to the retention times of model compounds in HPLC, would contain a range of three-(phenanthrenic) to five-ring (perylenic) aromatic compounds. However, most of the activity (61 to 90%) was detected in fractions 10 to

12 with all three treatments. Similarly, for the HFO, AhR-agonist activity was detected in fractions 6 to 15, and fractions 9 to 12 were found to be the most active. An interesting feature of the HFO is that both evaporation and irradiation had a major effect on the AhR content, with a greater fraction of the AhR-agonist activity being detected in later-eluting fractions post-treatment, suggesting a loss and/or transformation of earlier-eluting AhR agonists. In conclusion, 21 most active fine fractions were selected for further analysis.

III.4.5.2. Chemical characterization of fine fractions

Preliminary screening of the 21 fine fractions showing the highest AhR effects was performed by GC×GC-TOFMS. Similarly as in the case of first level fractionation, reduction of the number of detected compounds, as well as group-type separation can be observed. For example, **Figure III-39** (A) shows the subfraction 9 of HFO which contains three-ring aromatics (i.e. phenanthrene and alkyl substituted phenantrene). On the other hand, four-ring compounds (e.g. pyrenes) eluted in the next HPLC fraction, as seen in the **Figure III-39** showing the subfraction 10 of NSC. This demonstrates the ability of the amino-propyl modified column to successfully perform the group type separation according to PAH ring number (aromaticity).

In addition, HPLC fractionation was able to further reduce the compositional complexity of the selected oils. As can be seen **Table III-13** the number of peaks is reduced in comparison to coarse fractions. However, still relatively high number of compounds can be detected, due to the focusing and preconcentration effect of the HPLC fractionation, causing that numerous low abundance compounds previously not detected in the coarse fractions are now occurring as small unidentified peaks in the fine fractions (yellow peak markers in **Figure III-39**). This is particularly evident in fractions 9 and 10 of both oils, in which more than 100 peaks were detected, as it can be seen in the **Table III-13**.
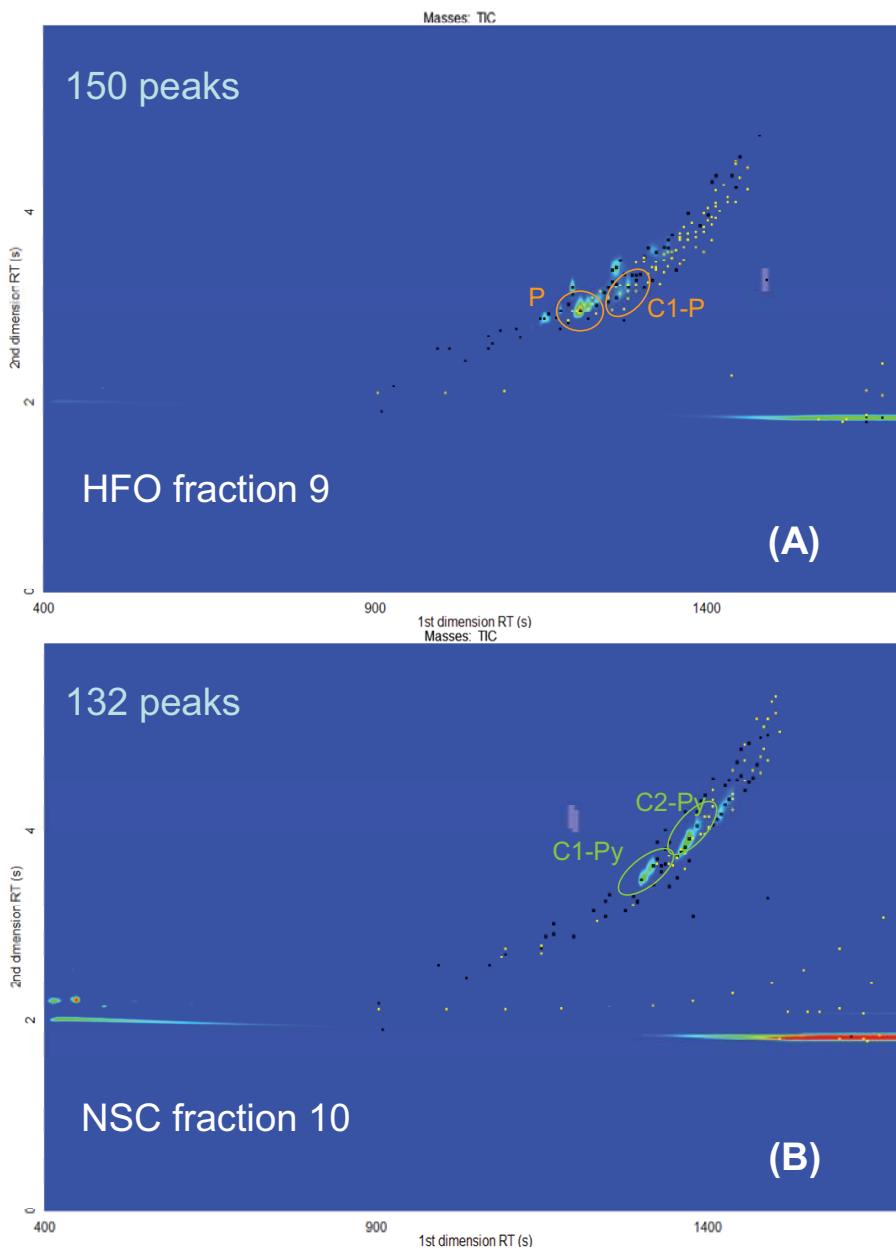
Figure III-39 GC×GC-TOFMS contour showing HPLC subfraction 9 of the HFO (A) containing three-ring systems (phenanthrene (P) and C1- alkyl substituted P) and the subfraction 10 of the NSC (B) containing four-ring aromatics (C1- and C2- alkyl substituted pyrenes (Py)). Note the relatively high number of peaks which are still detected due to the preconcentration of low abundance unknown components (yellow peak markers) during HPLC fractionation.

Table III-13 Number of detected peaks in coarse aromatic fractions and fine HPLC fractions of fresh (F), evaporated (E) and irradiated (Xe) North Sea crude (NSC) and heavy fuel oil (HFO) samples.

coarse aromatic fraction	NSC			HFO		
	F	E	Xe	F	E	Xe
peaks	522	693	560	205	172	324
Fraction 9	**F9**	**E9**	**Xe9**	**F9**	**E9**	**Xe9**
peaks	NA	NA	NA	150	132	147
% reduction vs. coarse	NA	NA	NA	27	23	55
Fraction 10	**F10**	**E10**	**Xe10**	**F10**	**E10**	**Xe10**
peaks	132	197	179	112	152	138
% reduction vs. coarse	75	72	68	45	12	57
Fraction 11	**F11**	**E11**	**Xe11**	**F11**	**E11**	**Xe11**
peaks	76	96	96	56	79	88
% reduction vs. coarse	85	86	83	73	54	73
Fraction 12	**F12**	**E12**	**Xe12**	**F12**	**E12**	**Xe12**
peaks	44	52	49	44	32	27
% reduction vs. coarse	92	92	91	79	81	92

NA-not available

In conclusion, preliminary characterization of the AhR-active HPLC subfractions demonstrated that they predominantly contain three- and four-ring aromatic compounds, including their various alkyl substituted homologues.

However, despite the fact that normal-phase HPLC reduced the compositional complexity, number of compounds is still high for unambiguous detection of toxic

compounds. Therefore for a more conclusive identification of the individual compounds (or compound groups) causing the AhR agonism, a chemometrical modeling of the obtained data was necessary.

III.4.6.   N-PLS model

The baseline-corrected GC×GC data for the different fractions of NSC and HFO were divided into a calibration set (i.e., 21 GC×GC data sets) and a prediction set (i.e., 7 GC×GC data sets). First, a calibration data set was used to obtain the N-PLS model correlating GC×GC chromatograms (**$\underline{X}$** data cube) and AhR effects (**y** data vector). The number of latent variables (LVs) which are abstract mathematical factors obtained from PLS decomposition was chosen on the basis of the minimum root-mean-square error in leave-one-out cross-validation (RMSECV-LOO) for the calibration model. The root-mean-square error of cross-validation (RMSECV) is an error function to evaluate the potential of a model to predict the toxicity values of test samples. It was found to have a RMSECV value of 0.066 and, thus, 7 LVs. **Table III-14** shows the captured variance for each LV in the **$\underline{X}$**-block and **y**-block. The cumulative captured variances for the **$\underline{X}$**- and **y**-blocks were 65.31 % and 82.81 %, respectively, for 7 LVs.

Figure III-40(a) shows the calibration plot for predicting AhR activity using the N-PLS model with 7 LVs. **Figure III-40**(b) shows the residual plot for predicting toxic effects using this model. As can be seen, the N-PLS model predicts the measured AhR effects in the samples used to calibrate the model quite satisfactorily.

Table III-14 Variance captured by the applied N-PLS model.

LVs	$R^2_{\text{X-block}}$		$R^2_{\text{y-block}}$	
	This	Total	This	Total
1	19.89	19.89	39.59	39.59
2	29.02	48.91	7.19	46.78
3	2.39	51.30	16.12	62.90
4	2.13	53.43	5.56	68.46
5	3.92	57.35	5.66	74.12
6	1.84	59.19	7.69	81.81
7	6.18	65.37	1.00	82.81
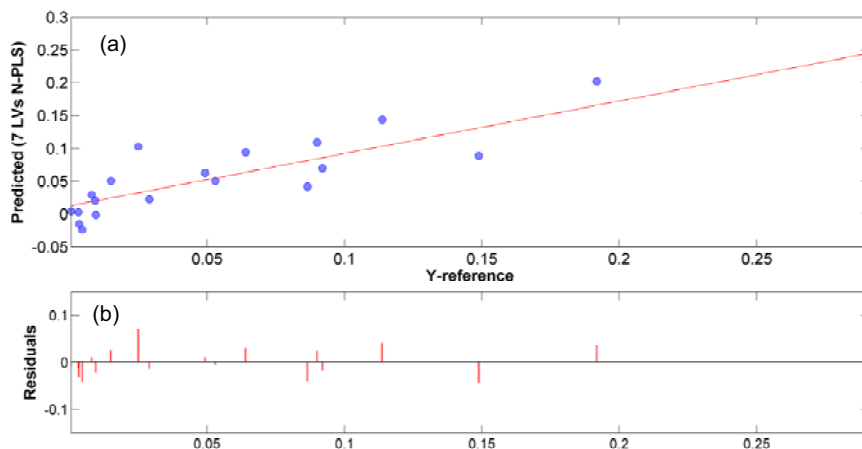
Figure III-40 The calibration plot (a) and residuals plot (b) for the prediction of AhR activity using the N-PLS model.

The accuracy and reliability of the developed N-PLS trilinear model was evaluated by predicting the AhR activity of the 7 selected external validation samples (**y$_{val}$**) based on their GC×GC data (**$\underline{X}_{val}$**). In this case, the root-mean-square error in prediction (RMSEP) value for the prediction set was 0.066. The relative prediction error in percentage (REP, %) for the predicted activity of this validation data set was only 6.20%, which was considered to be negligible given the high complexity of the data.

In order to identify the compounds with influence on the model (i.e. observed AhR activity), N-PLS weight vectors were examined in both modes (i.e. two chromatographic dimensions). These weights and their associated retention times (RTs) in the two chromatographic dimensions were then used to identify the corresponding peaks in the GC×GC chromatograms and their TOFMS spectra and, thus, the compounds most responsible for the detected effects. **Table III-15** shows the elution times in the first and second chromatographic dimension with the highest weight vectors obtained for the 7 LVs using the baseline-corrected GC×GC data for the oil fractions. It is important to note that the weights were determined so that the scores obtained from the **$\underline{X}$** decomposition would have maximum covariance with the scores obtained from the **y** decomposition.

Table III-15 Elution times in the first and second chromatographic dimension with the highest weight vectors obtained for the 7 latent variables.

1st dimension RT(s)	Weight	2nd dimension RT(s)	Weight
1136.66	0.41	2.90	0.34
1148.64	0.85	3.01	0.25
1208.53	-0.57	3.50	-0.26
1220.51	-0.33	3.67	0.11
1262.44	-0.39	3.87	-0.22
1298.37	0.45	3.88	0.14
1328.31	0.47	4.19	0.10
1340.29	0.43	4.24	-0.10
1364.25	-0.43	4.50	-0.28
1412.16	0.83	4.88	-0.11
1442.11	0.26	5.36	-0.09
1472.05	-0.30		

They thus take positive or negative signs for mathematical reasons unrelated to the toxic effects. Hence, it is the absolute values of the weights (i.e., not their signs) that are essential to understanding which **X** variables are important (numerically large *w*-values), and which **X** variables provide the same information (similar *w*-value profiles).

III.4.7. Identification of the AhR agonist compounds

Based on the N-PLS model results, the GC×GC–TOFMS data for 21 individual fractions were processed to identify the AhR-active compounds. First, modeled first- and second-dimension RTs with the highest weights (**Table III-15**) were used to create an RT window (from 1136.66 to 1472.05 seconds in the first dimension, and from 2.90 to 5.36 seconds in the second dimension) in the contour plot to group all the peaks eluting in that window in a separate class. This greatly reduced the number of peaks to be taken into consideration for identification, making it possible to focus on only those that contributed considerably to the observed AhR activity. In addition, a signal-to-noise (S/N) threshold of 200 was used in the same data-processing method to ignore background noise and consider only the most abundant peaks. The peaks eluting at 12 modeled first-dimension RTs with the highest weights (**Table III-15**) were selected to be tentatively identified. Identification was based on three types of information provided

by the GC×GC–TOFMS: library search hit(s) obtained using the NIST 05 mass spectral library; the peak mass spectra and presence of characteristic ions; and the position of the peak in the GC×GC contour plot. GC×GC method used the normal-phase configuration that separates analytes orthogonally according to their properties, i.e. by volatility in the first column and polarity in the second. Apart from greatly increased peak resolution, this separation mechanism offers the advantage of grouping compounds belonging to the same chemical class in characteristic elution patterns that can be identified in the GC×GC contour plots (Ventura et al., 2010). When combined with the mass spectral information provided by TOFMS, it becomes a powerful tool for tentative, non-target identification of compounds in complex mixtures, particularly in EDA studies.

For example, **Figure III-41** shows the section of the GC×GC contour plot of subfraction 10 of the fresh (non-weathered) NSC sample (NSC F10) containing the classification region (as indicated by the orange square) – corresponding to the modeled RT window – as well as the peaks (orange markers) eluting in it. Thus, additional "chemometric reduction" of sample complexity was obtained, i.e. the number of peaks to be taken into consideration was reduced from 133 to 83 (38%). Next, prominent peaks eluting at first-dimension RTs with high modeled weights were considered for identification. Figure 5 shows the three most abundant peaks eluting at 1298.38, 1364.26 and 1412.17, respectively, which closely match the modeled RTs of 1298.37, 1364.25 and 1412.16.

The library search identified the first peak as 1,3-dimethyl pyrene, giving it a relatively high similarity score (857). The search results were too ambiguous (low similarity scores) in the case of the two later-eluting peaks to enable their identification. However, their position in the contour plot suggests that they belong to the series of C3- and C4- alkyl pyrene homologues; this can be concluded from the characteristic parallel patterns they form in the contour plot due to their decreasing volatility and increasing polarity. Furthermore, their mass spectra show distinct similarities and the presence of characteristic ions (240, 244, 258, respectively), with the typical difference of 14 *m/z* units characteristic for alkyl homologues, which enabled their identification (**Figure III-42**).
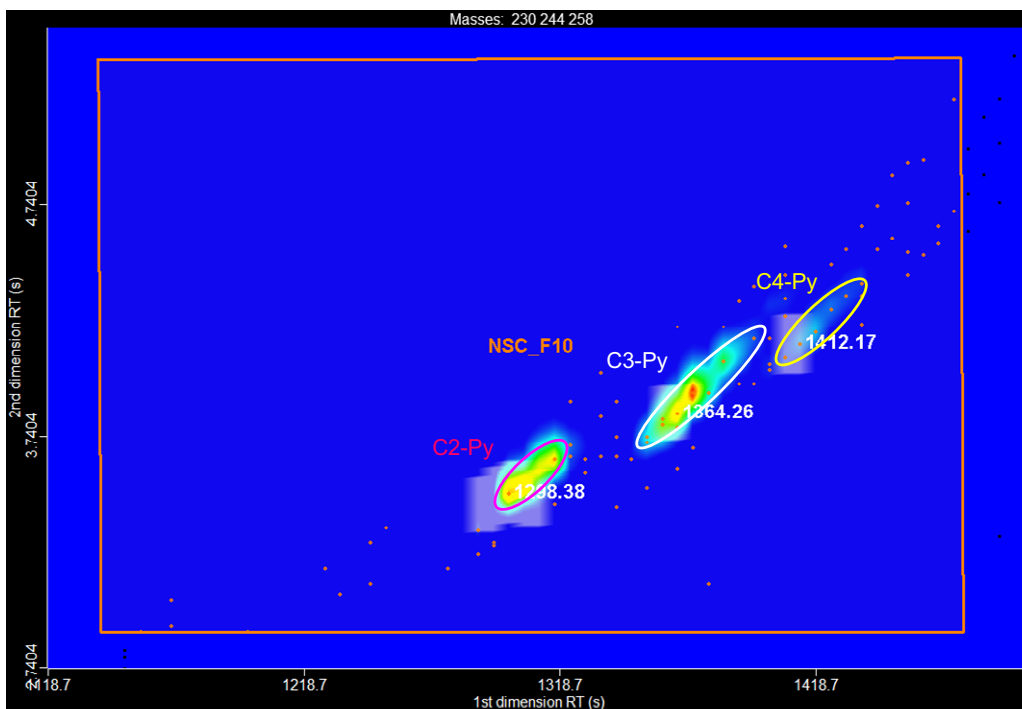
Figure III-41 GC×GC-TOFMS contour plot of the fine fraction 10 of fresh NSC oil showing the identified AhR compounds (C2-, C3- and C4- alkyl substituted pyrenes (Py)).
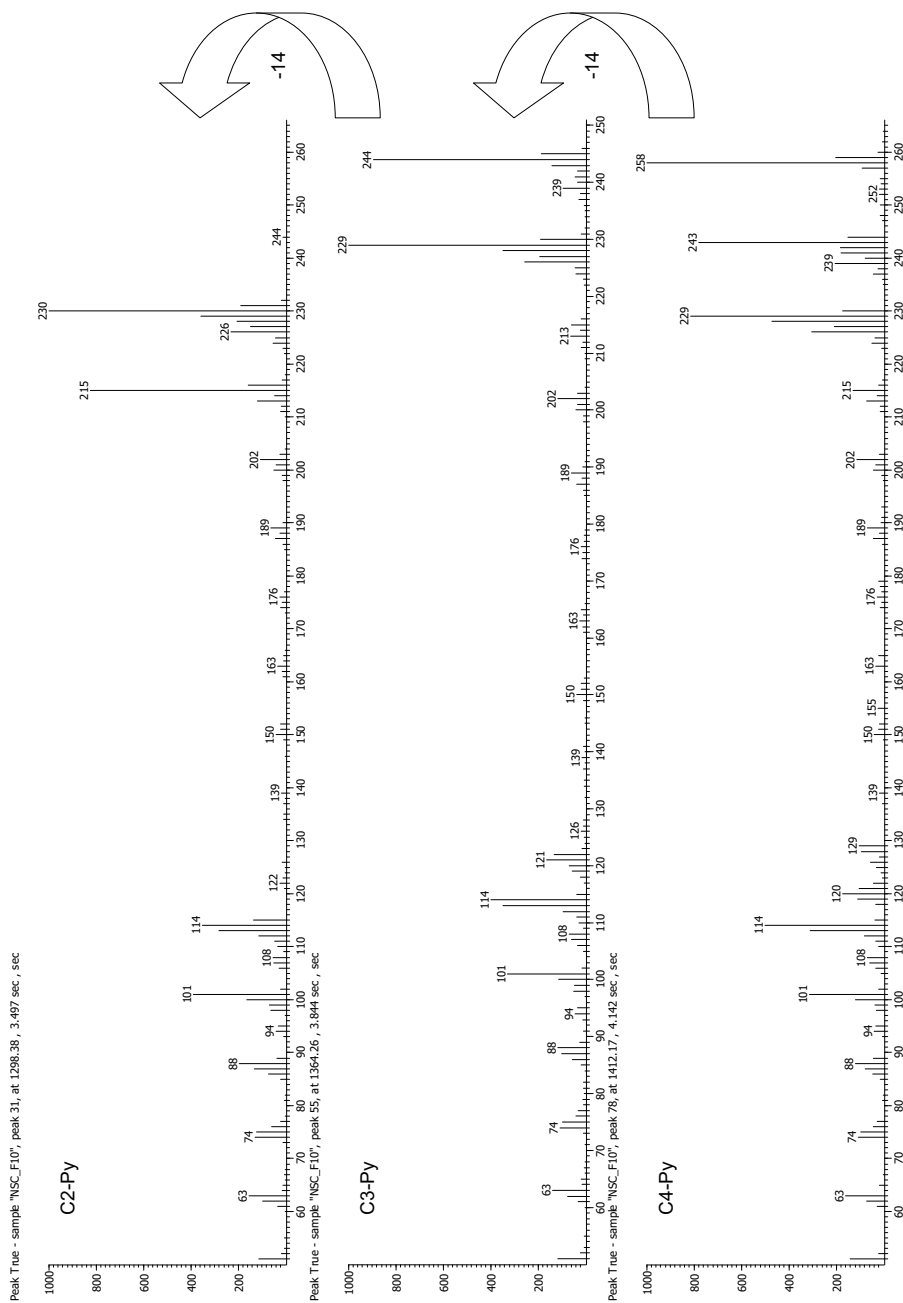
Figure III-42 Mass spectra of pyrene alkyl homologues (C2-, C3-, and C4-Py) identified in fine fraction 10 of fresh NSC oil.

Table III-16 shows 13 compounds tentatively identified as the suspected AhR-agonists in the 21 most active HPLC subfractions. As it can be seen, they include alkyl substituted phenanthrenes (C3- and C4-P) and anthracene (propenyl-A), benzo[*b*]naphtho[2,1-*d*]thiophene (BNT) and C2-BNT, chrysene (C) and its C1- and C2-alkyl homologues, C3-substituted carbazole (Cb), and C2- to C4-substituted pyrenes (Py). GC×GC contour plots of the characteristic AhR-active fractions and mass spectra of the identified compounds are shown in **Figure III-41** through **Figure III-43**, and in the Annex **A**, **Figures A-1** through **A-4**.

In general, the active aromatic subfractions are characterized by various alkyl-substituted three- and four-ring aromatic systems, including heteroaromatic systems (containing S and N). This coincides with previous studies reporting the predominant toxic contribution of alkylated petrogenic PAHs, compared to their parent compounds (Hawthorne et al., 2006). First dimension retention times weight vectors (**Table III-15**) indicate that out of the identified compounds the highest contribution in the observed AhR activities of HPLC fractions have the compounds eluting at 1148.64 and 1412.16 s, such as C2-Dbt (**Figure A-1**, Annex **A**) and C4-Py (**Figure III-41**), respectively; and the lowest one the compounds eluting at 1442.11 s, such as C1-C (**Figure A-3**, Annex **A**). This suggests that AhR effects are possibly higher in the sulfur heteroaromatics (C2-Dbt), and in addition are isomer-specific. For example, two peaks in the **Figure III-43** were identified as two distinct C3-isomers (2,4,6- and 1,5,7-trimethyl) of Cb, but the modeled weights indicate that only the 1,5,7-trimethyl isomer eluting at 1208.54 has important contribution to the AhR effect. This expands on the previous findings reporting the CYP1A mediated activities of Dbts and Cbs (Wassenberg et al., 2005).

Finally, the identified compounds were most frequently found in fractions 10 and 11 (**Table III-16**), which were also the ones exerting the highest AhR activity. However, tentative/qualitative identification was not sufficient to relate the compositional differences between fresh and weathered (evaporated and photooxidized) samples to their observed AhR activities. This could be due to the fact that some compounds were lost or transformed after weathering and could not be detected with the applied analytical methodology (e.g. polar compounds).

Table III-16 Identified AhR-active compounds in the North Sea crude (NSC) and heavy fuel oil (HFO) and their fraction distribution (fresh (F), evaporated (E), and irradiated (Xe) samples of HPLC fractions 9 through 12).

Compound	Characteristic m/z ion(s)	AhR binding[1]	9 F HFO	9 E HFO	9 Xe HFO	10 F NSC	10 F HFO	10 E NSC	10 E HFO	10 Xe NSC	10 Xe HFO	11 F NSC	11 F HFO	11 E NSC	11 E HFO	11 Xe NSC	11 Xe HFO	12 F NSC	12 F HFO	12 E NSC	12 E HFO	12 Xe NSC	12 Xe HFO
C3-carbazole	209	Y																X	X				
C2-Dbt	212/197	Y		X																			
9-(2-propenyl)-anthracene	218	Y	X	X		X																	
C3-phenanthrene	220/205	Y	X	X		X		X	X		X												
Chrysene	228/226	Y					X					X	X		X	X	X						
C2-pyrene	230/215	Y			X	X		X	X	X	X				X		X						
BNT	234	Y			X			X	X		X												
C4-phenanthrene	234/219	Y	X	X				X		X													
C1-chrysene	242/241	Y									X	X	X	X	X	X	X			X	X		
C3-pyrene	244/229	Y				X	X	X		X	X			X	X	X	X						
C2-chrysene	256/241	Y					X					X	X	X	X	X	X						
C4-pyrene	258	Y				X			X	X		X				X							
C2-BNT	262	Y			X		X		X	X	X	X		X									
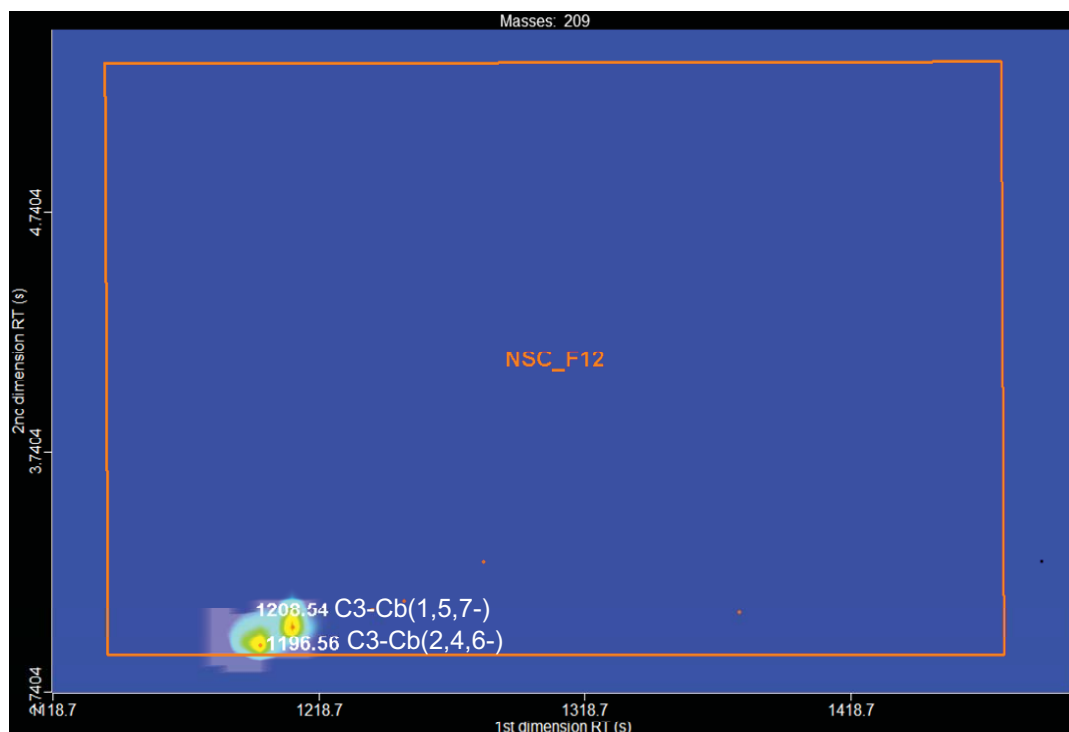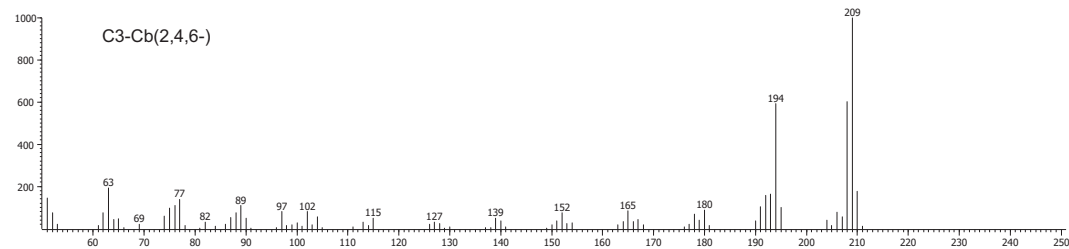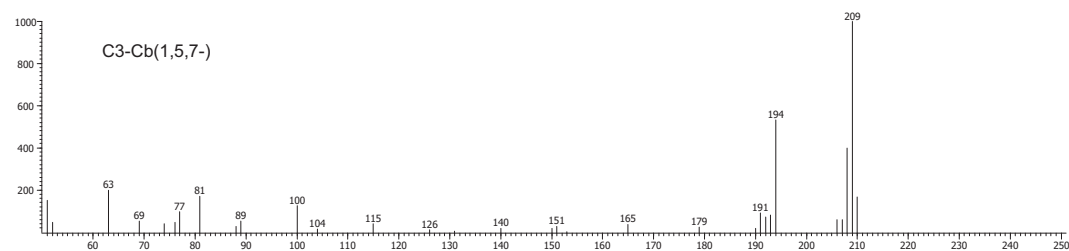
Figure III-43 Contour plot of the fine fraction 12 of fresh NSC oil showing the identified isomers of C3- carbazole (Cb).

Furthermore, it is possible that the minute changes in composition and concentration of the oil compounds which are sufficient to affect the measured toxic response were not large enough to be captured by the applied analytical methodology. In addition, toxic response is not always linear, and the possible synergistic and antagonistic effects could not be ruled out.

III.4.8. Confirmation of the toxic effects of the identified compounds

The final step in the EDA is to confirm the effects of the identified compounds. This can be done by repeating the performed bioassays using pure standards. In this case, pure standards of the majority of identified compounds, such as highly alkyl substituted PAHs are not readily commercially available. Moreover, as shown, different isomers of the same alkyl homologue can show different effects, making it even more difficult the use of actual pure standards. However, when such standards are not available, possible alternatives are quantitative structure-activity relationship (QSAR) tools (Brack et al., 2008) In this study, an *in-silico* tool (VirtualToxLab™) was used to confirm that the identified compounds have the potential to bind to the AhR. According to this model all of the identified compounds have the potential to bind to AhR, thus demonstrating that the applied N-PLS method was able to successfully correlate the chemical information with the observed adverse effects (**Table III-17**).

In addition, long-term exposure to the identified compounds was assessed using ECOSAR model, by calculating chronic toxicity values (ChV). As it can be seen in the **Table III-17**, chronic toxic potential is the highest for the highly alkyl substituted compounds, such as C3- and C4-alkyl substituted pyrenes (Py) or C3-alkyl substituted phenanthrene (C3-P).

Table III-17 Predicted AhR binding affinity and chronic toxicity of the identified compounds.

Compound	AhR binding[1]	Daphnid ChV[2] (mg·L^{-1})	Algae ChV[2] (mg·L^{-1})	Fish ChV[2] (mg·L^{-1})
C4-Py	Y	0.002	0.019	0.017
C4-P	Y	0.004	0.039	0.036
C3-Py	Y	0.004	0.039	0.036
C2-C	Y	0.004	0.038	0.035
C2-BNT	Y	0.005	0.042	0.039
C2-Py	Y	0.010	0.078	0.075
C1-C	Y	0.010	0.078	0.074
C3-P	Y	0.011	0.079	0.076
9-(2-propenyl)-A	Y	0.016	0.111	0.108
C	Y	0.024	0.157	0.155
BNT	Y	0.034	0.206	0.206
C2-Dbt	Y	0.036	0.209	0.210
C3-Cb	Y	0.068	0.353	0.363

[1]*Estimated using VirtualToxLab*
[2]*Estimated using ECOSAR*

III.4.9.   Concluding remarks

It is generally accepted that extensive fractionation and high chromatographic resolution prior to recording the mass spectra are major prerequisites for the successful analytical identification of the active compounds (Brack et al., 2008). In contrast, fractionation is the main bottleneck with EDA, which reduces sample complexity, but exponentially increases the number of samples to be analyzed.

In this study, the N-PLS model was applied after the fine HPLC fractionation; however, the results suggest that the same model could be applied in the earlier stages of EDA, for example, after the coarse fractionation, thereby avoiding additional time-consuming and laborious fine-fractionation steps. Despite the higher number of peaks that would be detected in this case, the "chemometric reduction" of each sample's complexity and cause-effect weighting using chemical and bioassay data could facilitate the identification of the most active compounds.

In addition, GC×GC offers the necessary high resolution, which, if needed, could be further improved by chemometric methods, as demonstrated in previous studies (Parastar et al., 2013; Parastar et al., 2011). This can be particularly important in the case of complex samples, such as the ones analyzed in this study, which

contain myriad of alkylated homologues and their isomers, and are difficult to resolve particularly with conventional GC-MS (Vrabie et al., 2012).

As proposed in other studies (Vrabie et al., 2012), this work demonstrates that the adapted approach for analytical identification in EDA which combines multivariate chemometric methods with non-target analysis using GC×GC–TOFMS can streamline and facilitate the compound identification to obtain the necessary chromatographic and mass spectral information. Potentially it can be further improved to reduce the number of fractionation steps needed.

The selected approach permitted the identification of alkylated three- and four-ring aromatic hydrocarbons as the main contributors to the measured effects.

Finally, QSAR tools are demonstrated as a useful alternative for the confirmation of the detected toxic effects.

III.5.   References

Aeppli, C., Carmichael, C.A., Nelson, R.K., Lemkau, K.L., Graham, W.M., Redmond, M.C., Valentine, D.L., Reddy, C.M., 2012. Oil Weathering after the *Deepwater Horizon* Disaster Led to the Formation of Oxygenated Residues. Environmental Science & Technology 46, 8799-8807.

Albaigés, J., Kienhuis, P., Dahlmann, G., 2014. Chapter 4: Oil spill identification. Wiley Publishers, New York, USA.

Allen, T.E., 1984. Oil Spill Chemical Dispersants: Research, Experience, and Recommendations: a Symposium. ASTM Committee F-20 on Hazardous Substances and Oil Spill Response.

Arpino, P.J., Ignatiadis, I., de Rycke, G., 1987. Sulphur-containing polynuclear aromatic hydrocarbons from petroleum. Examination of their possible statistical formation in sediments. Journal of Chromatography A 390, 329-348.

Barakat, A.O., Qian, Y., Kim, M., Kennicutt Ii, M.C., 2002. Compositional Changes of Aromatic Steroid Hydrocarbons in Naturally Weathered Oil Residues in the Egyptian Western Desert. Environmental Forensics 3, 219-225.

Bayona, J.M., Albaiges, J., Solanas, A.M., Pares, R., Garrigues, P., Ewald, M., 1986. Selective Aerobic Degradation of Methyl-Substituted Polycyclic Aromatic Hydrocarbons in Petroleum by Pure Microbial Culturest. Int J Environ Anal Chem 23, 289-303.

Belgo Egyptian, 2009. Iraqi Light Crude Oil. http://belgoegyptian.6te.net/en/bepsco_021.htm.

Bellas, J., Saco-álvarez, L., Nieto, T., Bayona, J.M., Albaigés, J., Beiras, R., 2013. Evaluation of artificially-weathered standard fuel oil toxicity by marine invertebrate embryogenesis bioassays. Chemosphere 90, 1103-1108.

Bernabeu, A.M., Fernández-Fernández, S., Bouchette, F., Rey, D., Arcos, A., Bayona, J.M., Albaiges, J., 2013. Recurrent arrival of oil to Galician coast: The final step of the *Prestige* deep oil spill. Journal of Hazardous Materials 250–251, 82-90.

Bobinger, S., Andersson, J.T., 2009. Photooxidation Products of Polycyclic Aromatic Compounds Containing Sulfur. Environmental Science & Technology 43, 8119-8125.

Boukir, A., Aries, E., Guiliano, M., Asia, L., Doumenq, P., Mille, G., 2001. Subfractionation, characterization and photooxidation of crude oil resins. Chemosphere 43, 279-286.

BP, 1996-2013. BP Crudes Assays. http://www.bp.com/productslistsearch.do?categoryId=16002740&contentId=7020300.

Brack, W., 2003. Effect-directed analysis: A promising tool for the identification of organic toxicants in complex mixtures? Analytical and Bioanalytical Chemistry 377, 397-407.

Brack, W., Schmitt-Jansen, M., MacHala, M., Brix, R., Barcelo, D., Schymanski, E., Streck, G., Schulze, T., 2008. How to confirm identified toxicants in effect-directed analysis. Analytical and Bioanalytical Chemistry 390, 1959-1973.

Breton, G.W., Vang, X., 1998. Photodimerization of Anthracene. Journal of Chemical Education 75, 81.

Buist, I., Belore, R., Lewis, A., Bercha, F., Cerovšek, M., Wilson, J., Rinelli, B., 2003. Persistence Of Crude Oil Spills On Open Water. U.S. Department of the Interior, Minerals Management Service.

Burns, K.A., 1993. Evidence for the importance of including hydrocarbon oxidation products in environmental assessment studies. Marine Pollution Bulletin 26, 77-85.

Canevari, G.P., Fiocco, R.J., 2005. Crude oil vanadium and nickel content can predict emulsification tendency. 2005 International Oil Spill Conference, IOSC 2005, 1525-1530.

Castle, R.W., Wehrenberg, F., Bartlett, J., Nuckols, J., 2005. Heavy oil spills: Out of sight, out of mind. International Oil Spill Conference, 3464-3478.

CEN, 2012. CEN/TR 15522-2:2012, Oil spill identification - Waterborne petroleum and petroleum products - Part 2: Analytical methodology and interpretation of results.

CEPSA, 2010. Gasoleo A. http://www.cepsa.com/cepsa/Products_and_Services/Gasoils_and_Fuels/Products/CEPSA_Gasoil_A.

CEPSA, 2010. Gasoleo B. http://www.cepsa.com/cepsa/Products_and_Services/Gasoils_and_Fuels/Products/CEPSA_Gasoil_B.

Chakhmakhchev, A., Suzuki, M., Takayama, K., 1997. Distribution of alkylated dibenzothiophenes in petroleum as a tool for maturity assessments. Organic Geochemistry 26, 483-489.

Charrie-Duhaut, A., Lemoine, S., Adam, P., Connan, J., Albrecht, P., 2000. Abiotic oxidation of petroleum bitumens under natural conditions. Organic Geochemistry 31, 977-1003.

CONCAWE, 1996. Gas Oils. CONCAWE Petroleum Products and Health Management Groups, Brussels.

CONCAWE, 1998. Heavy Fuel Oils. CONCAWE Petroleum Products and Health Management Groups, Brussels.

Croisy, A., Mispelter, J., Lhoste, J.M., 1984. Thiophene analogues of carcinogenic polycyclic hydrocarbons. Elbs pyrolysis of various aroylmethylbenzo[b]thiophenes. Journal of Heterocyclic Chemistry 21, 353-359.

De Godoy, L.A.F., Ferreira, E.C., Pedroso, M.P., Fidélis, C.H.D.V., Augusto, F., Poppi, R.J., 2008. Quantification of kerosene in gasoline by comprehensive two-dimensional gas chromatography and N-way multivariate analysis. Analytical Letters 41, 1603-1614.

Delvigne, G.A.L., Sweeney, C.E., 1988. Natural dispersion of oil. Oil and Chemical Pollution 4, 281-310.

Didyk, B.M., Simoneit, B.R.T., Brassell, S.C., Eglinton, G., 1978. Organic geochemical indicators of palaeoenvironmental conditions of sedimentation. Nature 272, 216-222.

Diez, S., Sabate, J., Viñas, M., Bayona, J.M., Solanas, A.M., Albaiges, J., 2005. The *Prestige* oil spill. I. Biodegradation of a heavy fuel oil under simulated conditions. Environmental Toxicology and Chemistry 24, 2203-2217.

Dowty, B.J., Brightwell, N.E., Laseter, J.L., Griffin, G.W., 1974. Dye sensitized photooxidation of phenanthrene. Biochemical and Biophysical Research Communications 57, 452-456.

Ehrhardt, M., Petrick, G., 1984. On the sensitized photo-oxidation of alkylbenzenes in seawater. Marine Chemistry 15, 47-58.

Eiserbeck, C., Nelson, R.K., Grice, K., Curiale, J., Reddy, C.M., 2012. Comparison of GC-MS, GC-MRM-MS, and GC×GC to characterise higher plant biomarkers in Tertiary oils and rock extracts. Geochimica et Cosmochimica Acta 87, 299-322.

Eiserbeck, C., Nelson, R.K., Grice, K., Curiale, J., Reddy, C.M., Raiteri, P., 2011. Separation of 18α(H)-, 18β(H)-oleanane and lupane by comprehensive two-dimensional gas chromatography. Journal of Chromatography A 1218, 5549-5553.

EPA, 1999. Understanding Oil Spills and Oil Spill Response. Oil Program Center. Office of Emergency and Remedial Response.

EPA, 2013. 40 CFR Appendix E to Part 112 - Determination and Evaluation of Required Response Resources for Facility Response Plans Environmental Protection Agency.

Fingas, M., Fieldhouse, B., 2012. Studies on water-in-oil products from crude oils and petroleum products. Marine Pollution Bulletin 64, 272-283.

Fingas, M.F., 1995. A literature review of the physics and predictive modelling of oil spill evaporation. Journal of Hazardous Materials 42, 157-175.

Fingas, M.F., 2004. Modeling evaporation using models that are not boundary-layer regulated. Journal of Hazardous Materials 107, 27-36.

Frontera-Suau, R., Bost, F.D., McDonald, T.J., Morris, P.J., 2002. Aerobic Biodegradation of Hopanes and Other Biomarkers by Crude Oil-Degrading Enrichment Cultures. Environmental Science & Technology 36, 4585-4592.

Gaines, R.B., Frysinger, G.S., Reddy, C.M., Nelson, R.K., 2007. Oil Spill Source Identification by Comprehensive Two-Dimensional Gas Chromatography (GC x GC). Oil Spill Environmental Forensics - Fingerprinting And Source Identification, 169-206.

Garrett, R.M., Pickering, I.J., Haith, C.E., Prince, R.C., 1998. Photooxidation of crude oils. Environmental Science and Technology 32, 3719-3723.

Gonçalves, R., Scholze, M., Ferreira, A.M., Martins, M., Correia, A.D., 2008. The joint effect of polycyclic aromatic hydrocarbons on fish behavior. Environmental Research 108, 205-213.

González-Doncel, M., González, L., Fernández-Torija, C., Navas, J.M., Tarazona, J.V., 2008. Toxic effects of an oil spill on fish early life stages may not be exclusively associated to PAHs: Studies with *Prestige* oil and medaka (Oryzias latipes). Aquatic Toxicology 87, 280-288.

Hall, G.J., Frysinger, G.S., Aeppli, C., Carmichael, C.A., Gros, J., Lemkau, K.L., Nelson, R.K., Reddy, C.M., 2013. Oxygenated weathering products of *Deepwater Horizon* oil come from surprising precursors. Marine Pollution Bulletin 75, 140-149.

Hansen, A.B., Daling, P.S., Faksness, L.-G., Sörheim, K.R., Kienhuis, P., Duus, R., 2007. 7 - Emerging CEN methodology for oil spill identification. Oil Spill Environmental Forensics, 229-256.

Hawthorne, S.B., Miller, D.J., Kreitinger, J.P., 2006. Measurement of total polycyclic aromatic hydrocarbon concentrations in sediments and toxic units used for estimating risk to benthic invertebrates at manufactured gas plant sites. Environmental Toxicology and Chemistry 25, 287-296.

Hegazi, A.H., 2009. Utilization of trace metals in source diagnosing of tar balls from the Mediterranean City of Alexandria, Egypt. Petroleum Science and Technology 27, 386-395.

Hinga, K.R., Pilson, M.E.Q., 1987. Persistence of benzo(a)anthracene degradation products in an enclosed marine ecosystem. Environmental Science & Technology 21, 648-653.

Hostettler, F.D., Rosenbauer, R.J., Kvenvolden, K.A., 1999. PAH refractory index as a source discriminant of hydrocarbon input from crude oil and coal in Prince William Sound,

Alaska. Organic Geochemistry 30, 873-879.

Hylland, K., 2006. Polycyclic aromatic hydrocarbon (PAH) ecotoxicology in marine ecosystems. Journal of Toxicology and Environmental Health - Part A 69, 109-123.

Incardona, J.P., 2004. Defects in cardiac function precede morphological abnormalities in fish embryos exposed to polycyclic aromatic hydrocarbons. Toxicology and Applied Pharmacology 196, 191.

Incardona, J.P., Collier, T.K., Scholz, N.L., 2010. Oil spills and fish health: exposing the heart of the matter. J Expos Sci Environ Epidemiol.

ITOPF, 2013. Fate of marine oil spills, Technical information paper no. 2. International Tanker Owners Pollution Federation Ltd.

Jacquot, F., Guiliano, M., Doumenq, P., Munoz, D., Mille, G., 1996. *In Vitro* Photooxidation of Crude Oil Maltenic Fractions: Evolution of Fossil Biomarkers and Polycyclic Aromatic Hydrocarbons. Chemosphere 33, 671-681.

Jiménez, N., Viñas, M., Sabaté, J., Díez, S., Bayona, J.M., Solanas, A.M., Albaiges, J., 2006. The *Prestige* Oil Spill. 2. Enhanced Biodegradation of a Heavy Fuel Oil under Field Conditions by the Use of an Oleophilic Fertilizer. Environmental Science & Technology 40, 2578-2585.

Jochims, H.W., Baumgärtel, H., Leach, S., 1999. Structure-dependent Photostability of Polycyclic Aromatic Hydrocarbon Cations: Laboratory Studies and Astrophysical Implications. The Astrophysical Journal 512, 500.

Johnson, K.J., Prazen, B.J., Young, D.C., Synovec, R.E., 2004. Quantification of naphthalenes in jet fuel with GC x GC/Tri-PLS and windowed rank minimization retention time alignment. Journal of Separation Science 27, 410-416.

Jokuty, P., Whiticar, S., Wang, Z., Fingas, M., Fieldhouse, B., Lambert, P., Mullin, J., 1999. Properties of Crude Oils and Oil Products. Environment Canada, Ottawa.

Jones, R.K., 1997. A simplified pseudo-component oil evaporation model. Proceedings of the Twentieth Arctic and Marine Oilspill Program (AMOP) Technical Seminar. 43-61.

Jonker, M.T.O., Brils, J.M., Sinke, A.J.C., Murk, A.J., Koelmans, A.A., 2006. Weathering and toxicity of marine sediments contaminated with oils and polycyclic aromatic hydrocarbons. Environmental Toxicology and Chemistry 25, 1345-1353.

Kizu, R., Ishii, K., Kobayashi, J., Hashimoto, T., Koh, E., Namiki, M., Hayakawa, K., 2000. Antiandrogenic effect of crude extract of C-heavy oil. Materials Science and Engineering: C 12, 97-102.

Kizu, R., Okamura, K., Toriba, A., Kakishima, H., Mizokami, A., Burnstein, K.L., Hayakawa, K., 2003. A role of aryl hydrocarbon receptor in the antiandrogenic effects of polycyclic aromatic hydrocarbons in LNCaP human prostate carcinoma cells. Archives of Toxicology 77, 335-343.

Kropp, K.G., Fedorak, P.M., 1998. A review of the occurrence, toxicity, and biodegradation of condensed thiophenes found in petroleum. Canadian Journal of Microbiology 44, 605-622.

Lehr, W., Jones, R., Evans, M., Simecek-Beatty, D., Overstreet, R., 2002. Revisions of the ADIOS oil spill model. Environmental Modelling and Software 17, 191-199.

Li, J., Ma, M., Cui, Q., Wang, Z., 2008. Assessing the Potential Risk of Oil-Field Produced Waters Using a Battery of Bioassays/Biomarkers. Bull Environ Contam Toxicol 80, 492-496.

Lichtfouse, E., Albrecht, P., Béhar, F., Hayes, J.M., 1994. A molecular and isotopic study of the organic matter from the Paris Basin, France. Geochimica et Cosmochimica Acta 58, 209-221.

Liu, Z., Liu, J., Zhu, Q., Wu, W., 2012. The weathering of oil after the DeepwaterHorizon oil spill: Insights from the chemical composition of the oil from the sea surface, salt marshes and sediments. Environmental Research Letters 7.

Lourdes, R., 2009. Comprehensive Two dimensional gas chromatography, in: Barcelo, D. (Ed.), Comprehensive Analytical Chemistry, Volume 55. Elsevier.

Maki, H., Sasaki, T., Harayama, S., 2001. Photo-oxidation of biodegraded crude oil and toxicity of the photo-oxidized products. Chemosphere 44, 1145-1151.

Mallakin, A., McConkey, B.J., Miao, G., McKibben, B., Snieckus, V., Dixon, D.G., Greenberg, B.M., 1999. Impacts of Structural Photomodification on the Toxicity of Environmental Contaminants: Anthracene Photooxidation Products. Ecotoxicology and Environmental Safety 43, 204-212.

Martínez-Gómez, C., Vethaak, A.D., Hylland, K., Burgeot, T., Köhler, A., Lyons, B.P., Thain, J., Gubbins, M.J., Davies, I.M., 2010. A guide to toxicity assessment and monitoring effects at lower levels of biological organization following marine oil spills in European waters. ICES Journal of Marine Science 67, 1105-1118.

McKenna, A.M., Nelson, R.K., Reddy, C.M., Savory, J.J., Kaiser, N.K., Fitzsimmons, J.E., Marshall, A.G., Rodgers, R.P., 2013. Expansion of the Analytical Window for Oil Spill Characterization by Ultrahigh Resolution Mass Spectrometry: Beyond Gas Chromatography. Environmental Science & Technology 47, 7530-7539.

McLean, J.D., Kilpatrick, P.K., 1997. Effects of asphaltene aggregation in model heptane-toluene mixtures on stability of water-in-oil emulsions. Journal of Colloid and Interface Science 196, 23-34.

McNamara, J., Patterson, M. , 1998. Oil & Gas Journal Data Book. Pennwell Books, Tulsa.

Melbye, A.G., Brakstad, O.G., Hokstad, J.N., Gregersen, I.K., Hansen, B.H., Booth, A.M., Rowland, S.J., Tollefsen, K.E., 2009. Chemical and toxicological characterization of an unresolved complex mixture-rich biodegraded crude oil. Environmental Toxicology and Chemistry 28, 1815-1824.

Miget, R.J., 1969. Microbial Degradation of Normal Paraffin Hydrocarbons in Crude Oil. Proceedings Joint Conference on Prevention and Control of Oil Spills. 327-331.

Miller, S., 1983. Photochemistry of natural water systems. Environmental Science & Technology 17, 568A-570A.

Moore, J.W., Ramamoorthy, S., 1984. Aromatic Hydrocarbons-Polycyclics. Organic Chemicals in Natural Waters: Applied Monitoring and Impact Assessment, 67-87.

Muusse, M., Langford, K., Tollefsen, K.E., Cornelissen, G., Haglund, P., Hylland, K., Thomas, K.V., 2012. Characterization of AhR agonist compounds in roadside snow. Analytical and Bioanalytical Chemistry 403, 2047-2056.

Neff, J.M., 1979. Polycyclic Aromatic Hydrocarbons in the Aquatic Environment: Sources, Fates and Biological Effects. Applied Science Publishers Ltd., Essex, England.

Neff, J.M., Ostazeski, S., Gardiner, W., Stejskal, I., 2000. Effects of weathering on the toxicity of three offshore australian crude oils and a diesel fuel to marine animals. Environmental Toxicology and Chemistry 19, 1809-1821.

Nicodem, D.E., Fernandes, M.C.Z., Guedes, C.L.B., Correa, R.J., 1997. Photochemical processes and the environmental impact of petroleum spills. Biogeochemistry 39, 121-138.

Nicodem, D.E., Guedes, C.L.B., Fernandes, M.C.Z., Severino, D., Correa, R.J., Coutinho, M.C., Silva, J., 2001. Photochemistry of petroleum. Progress in Reaction Kinetics and Mechanism 26, 219-238.

NIEHS, 2010. Safety and Health Awareness for Oil Spill Cleanup Workers. National Institute of Environmental Health Sciences.

NOAA, 1996. Injury Assessment: Guidance Document for Natural Resource Damage Assessment Under the Oil Pollution Act of 1990, Appendix C. Oil Behavior, Pathways, and Exposure. NOAA, the Damage Assessment Remediation and Restoration Program.

NOAA/EPA, 1978. The Amoco Cadiz Oil Spill; A Preliminary Scientific Report. National Technical Information Service, Springfield, Virginia.

NRC, 2003. Oil in the Sea III : Inputs, Fates, and Effects. The National Academies Press, Washington DC.

Parastar, H., Radović, J.R., Bayona, J.M., Tauler, R., 2013. Solving chromatographic challenges in comprehensive two-dimensional gas chromatography-time-of-flight mass spectrometry using multivariate curve resolution-alternating least squares ABC Highlights: Authored by Rising Stars and Top Experts. Analytical and Bioanalytical Chemistry 405, 6235-6249.

Parastar, H., Radović, J.R., Jalali-Heravi, M., Diez, S., Bayona, J.M., Tauler, R., 2011. Resolution and quantification of complex mixtures of polycyclic aromatic hydrocarbons in heavy fuel oil sample by means of GC × GC-TOFMS combined to multivariate curve resolution. Analytical Chemistry 83, 9289-9297.

Park, J.M., Holliday, M.G., 1999. Occupational-health aspects of marine oil-spill response. Pure and Applied Chemistry 71, 113-133.

Payne, J.R., Phillips, C.R., 1985. Photochemistry of petroleum in water. Environmental Science and Technology 19, 569-579.

Pearlman, R.S., Yalkowsky, S.H., Banerjee, S., 1984. Water solubilities of polynuclear aromatic and heteroaromatic compounds. American Chemical Society and the American Institute of Physics for the National Bureau of Standards.

Pedroso, M.P., de Godoy, L.A.F., Ferreira, E.C., Poppi, R.J., Augusto, F., 2008. Identification of gasoline adulteration using comprehensive two-dimensional gas chromatography combined to multivariate data processing. Journal of Chromatography A 1201, 176-182.

Pelroy, R.A., Stewart, D.L., Tominaga, Y., 1983. Microbial mutagenicity of 3- and 4-ring polycyclic aromatic sulfur heterocycles. Mutation Research 117, 31-40.

Peters, K.E., Walters, C.C.C., Moldowan, J.J.M., 2005. The Biomarker Guide: I. Biomakers And Isotopes In The Environment And Human History. Cambridge University Press.

Pezeshki, S.R., Hester, M.W., Lin, Q., Nyman, J.A., 2000. The effects of oil spill and clean-up on dominant US Gulf coast marsh macrophytes: a review. Environmental Pollution 108, 129-139.

Plata, D.L., Sharpless, C.M., Reddy, C.M., 2008. Photochemical Degradation of Polycyclic Aromatic Hydrocarbons in Oil Films. Environmental Science & Technology 42, 2432-2438.

Prazen, B.J., Johnson, K.J., Weber, A., Synovec, R.E., 2001. Two-dimensional gas chromatography and trilinear partial least squares for the quantitative analysis of aromatic and naphthene, content in naphtha. Analytical Chemistry 73, 5677-5682.

Prince, R.C., 1988. Crude Oil Biodegradation. Encyclopedia of Environmental Analysis and Remediation 2, 1327-1342.

Prince, R.C., Elmendorf, D.L., Lute, J.R., Hsu, C.S., Haith, C.E., Senius, J.D., Dechert, G.J., Douglas, G.S., Butler, E.L., 1994. 17.alpha.(H)-21.beta.(H)-hopane as a conserved internal marker for estimating the biodegradation of crude oil. Environmental Science & Technology 28, 142-145.

Prince, R.C., Garrett, R.M., Bare, R.E., Grossman, M.J., Townsend, T., Suflita, J.M., Lee, K., Owens, E.H., Sergy, G.A., Braddock, J.F., Lindstrom, J.E., Lessard, R.R., 2003. The roles of photooxidation and biodegradation in long-term weathering of crude and heavy fuel oils. Spill Science and Technology Bulletin 8, 145-156.

Radović, J.R., Aeppli, C., Nelson, R.K., Jimenez, N., Reddy, C.M., Bayona, J.M., Albaigés, J., 2013. Assessment of photochemical processes in marine oil spill fingerprinting. Marine Pollution Bulletin http://dx.doi.org/10.1016/j.marpolbul.2013.11.029.

RAMOCS, 2012. Report on: Implementation of risk assessment methodologies for oil and chemical spills in the European marine environment. p. 32.

Rasmussen, K., Booth, G.M., Lee, M.L., Castle, R.N., 1991. Mutagenicities of hydroxy-substituted carbazoles and dibenzothiophenes using the CHO/HGPRT assay. Environmental Toxicology and Chemistry 10, 1133-1137.

Reddy, C.M., Arey, J.S., Seewald, J.S., Sylva, S.P., Lemkau, K.L., Nelson, R.K., Carmichael, C.A., McIntyre, C.P., Fenwick, J., Ventura, G.T., Van Mooy, B.A.S., Camilli, R., 2012. Composition and fate of gas and oil released to the water column during the *Deepwater Horizon* oil spill. Proceedings of the National Academy of Sciences 109, 20229-20234.

Reddy, C.M., Eglinton, T.I., Hounshell, A., White, H.K., Xu, L., Gaines, R.B., Frysinger, G.S., 2002. The West Falmouth oil spill after thirty years: The persistence of petroleum hydrocarbons in marsh sediments. Environmental Science and Technology 36, 4754-4760.

Rønningsen, H.P., Skjevrak, I., 1990. Characterization of north sea petroleum fractions: Aromatic ring class distribution. Energy & Fuels 4, 608-626.

Rontani, J.F., Giusti, G., 1988. Photosensitized oxidation of 3,6-dimethyloctane. Tetrahedron Letters 29, 1923-1925.

Rontani, J.F., Giusti, G., 1989. Photosensitized oxidation of n-butylcyclohexane as a model for photochemical degradation of n-alkylcyclohexanes in seawater. Journal of Photochemistry and Photobiology, A: Chemistry 46, 347-355.

Schwarzenbach, R.P., Gschwend, P.M., Imboden, D.M., 2005. Environmental Organic Chemistry, 2nd ed. Wiley.

Smith, J.E., 1968. 'Torrey Canyon' pollution and marine life. Marine Biological Association of the United Kingdom, Plymouth.

Smith, S.J., Pitcher, H., Wigley, T.M.L., 2001. Global and regional anthropogenic sulfur dioxide emissions. Global and Planetary Change 29, 99-119.

SPARC, 2013. http://archemcalc.com/sparc.

Speight, J.G., 2006. The Chemistry and Technology of Petroleum, Fourth Edition. Taylor & Francis.

STATOIL, 2011. Crude oil assays. http://www.statoil.com/en/ouroperations/tradingproducts/crudeoil/crudeoilassays/pages/default.aspx.

Stout, S.A., Wang, Z., 2008. Diagnostic Compounds for Fingerprinting Petroleum in the Environment. Environmental Forensics 26, 54-104.

Sutton, P.A., Nesterenko, P.N., 2007. Retention characteristics of aromatic hydrocarbons on silica and aminopropyl-modified monolithic columns in normal-phase HPLC. Journal of Separation Science 30, 2900-2909.

Takegoshi, K., Nakamura, S., Terao, T., 1998. Solid-state photodimerization of 9-methylanthracene as studied by solid-state 13C NMR. Solid State Nuclear Magnetic Resonance 11, 189-196.

Taylor, S.E., 1992. Emulsions fundamentals and applications in petroleum industry. Chem.Ind. 20, 770-773.

Thomas, K.V., Langford, K., Petersen, K., Smith, A.J., Tollefsen, K.E., 2009. Effect-directed identification of naphthenic acids as important *in vitro* xeno-estrogens and anti-androgens in North Sea offshore produced water discharges. Environmental Science and Technology 43, 8066-8071.

Tollefsen, K.E., Harman, C., Smith, A., Thomas, K.V., 2007. Estrogen receptor (ER) agonists and androgen receptor (AR) antagonists in effluents from Norwegian North Sea oil production platforms. Marine Pollution Bulletin 54, 277-283.

TOTSA, 2003. Crude Assays. http://www.totsa.com/pub/crude/crude_assays.php?rub=1.

Tramier, B., Aston, G., Durrieu, M., Lepa, A., van Oudenhoven, J., Robinson, N., Sedlacek, K., Sibra, P., 1987. A Field Guide to Coastal Oil Spill Control and Clean-up Techniques. 112.

Ventura, G.T., Raghuraman, B., Nelson, R.K., Mullins, O.C., Reddy, C.M., 2010. Compound class oil fingerprinting techniques using comprehensive two-dimensional gas chromatography (GC×GC). Organic Geochemistry 41, 1026-1035.

Vrabie, C.M., Candido, A., van Duursen, M.B.M., Jonker, M.T.O., 2010. Specific *in vitro* toxicity of crude and refined petroleum products: II. Estrogen (α and β) and androgen receptor-mediated responses in yeast assays. Environmental Toxicology and Chemistry 29, 1529-1536.

Vrabie, C.M., Jonker, M.T.O., Murk, A.J., 2009. Specific *in vitro* toxicity of crude and refined petroleum products. 1. Aryl hydrocarbon receptor—mediated responses. Environmental Toxicology and Chemistry 28, 1995-2003.

Vrabie, C.M., Sinnige, T.L., Murk, A.J., Jonker, M.T.O., 2012. Effect-directed assessment of the bioaccumulation potential and chemical nature of A h receptor agonists in crude and refined oils. Environmental Science and Technology 46, 1572-1580.

Wang, Z., Stout, S., 2010. Oil Spill Environmental Forensics: Fingerprinting and Source Identification. Elsevier Science.

Wang, Z., Yang, C., Fingas, M., Hollebone, B., Hyuk Yim, U., Ryoung Oh, J., 2007. Petroleum biomarker fingerprinting for oil spill characterization and source identification. Oil Spill Environmental Forensics, 73-146.

Wassenberg, D.M., Nerlinger, A.L., Battle, L.P., Di Giulio, R.T., 2005. Effects of the polycyclic aromatic hydrocarbon heterocycles, carbazole and dibenzothiophene, on in vivo and *in vitro* CYP1A activity and polycyclic aromatic hydrocarbon-derived embryonic deformities. Environmental Toxicology and Chemistry 24, 2526-2532.

Wenger, M., Ondračková, M., Machala, M., Neča, J., Hyršl, P., Šimková, A., Jurajda, P., Von Der Ohe, P., Segner, H., 2010. Assessing relationships between chemical exposure,

parasite infection, fish health, and fish ecological status: A case study using chub (Leuciscus cephalus) in the Balina River, Czech Republic. Environmental Toxicology and Chemistry 29, 453-466.

Wilson, C.L., Safe, S., 1998. Mechanisms of Ligand-Induced Aryl Hydrocarbon Receptor-Mediated Biochemical and Toxic Responses. Toxicologic Pathology 26, 657-671.

Yang, W.C., Wang, H., 1977. Modeling of oil evaporation in aqueous environment. Water Research 11, 879-887.

Zhang, M., Xiang, T., Mei, B., 1998. Carbazole-type compounds in crude oils. Chinese Science Bulletin 43, 669-672.

Chapter IV.

Conclusions

IV.1. Scientific relevance of the thesis

In the past two decades we witnessed a decrease in both the number of oil spill incidents, and of the quantity of oil released in these incidents (ITOPF, 2013), which led to a diminished interest for basic oil spill science (Reddy, 2010). With the introduction of more stringent oil spill legislation, much of the spill response, assessment and restoration activities were passed to governmental agencies and other stakeholders. Their capabilities were perhaps sufficient to deal with the most frequently occurring small-scale spills, however, recent large, catastrophic incidents such as the sinking of *Prestige* in 2002, or the *Deepwater Horizon* blowout in 2010, renewed the need for fundamental science in order to be able to fully understand and estimate the scope of the impacts such spills can have on the environment, economy and society.

This is particularly important in the context of new explorations and discoveries of hydrocarbon resources in pristine regions such as Arctic (USGS, 2008), where extreme weather and the lack of infrastructure emphasize even more the need for a comprehensive assessment of all of the possible effects the future oil production could cause.

The objectives of this thesis were set to provide new approaches and methodologies, and to improve and reevaluate the previously existing ones, in a way which can contribute to this comprehensive and proactive strategy. Their scope is comprehensive because it covers all the important aspects of marine oil spills – the sources, environmental fate and possible toxic effects. In addition, particular relevance of this thesis is drawn from the fact that the studies presented here include the investigation of real major oil spills (*Prestige*, *DWH*), and of a broad range of oils and oil products that are currently produced and transported worldwide.

IV.2. General conclusions

IV.2.1. Oil spill source determination

Following observations can be drawn from this thesis with respect to oil spill source determination:

- Developed GC-MS methodology has been demonstrated as robust tool for the fingerprinting of various crude and refined oils. The selected set of diagnostic compounds (alkanes, PAHs and biomarkers) and the 25 normative diagnostic ratios calculated thereof can be used to distinguish with high degree of certainty different types of oil, and enable their identification in the case of a spill, even in weathered spill samples. PW-plots were demonstrated as an effective tool to visualize the weathering changes in spill samples and confirm the spill source identification.

- Natural and simulated sunlight photodegraded various PAHs and TAS biomarkers used in oil fingerprinting in a short- to medium- timescale (days to weeks) and affected the robustness of typically used diagnostic ratios.

- GC×GC-FID was demonstrated as a powerful technique for oil fingerprinting, particularly for the determination of low abundant, steroisomeric biomarkers, such as TAS, due to its high chromatographic resolution and increased sensitivity of FID.

- Content of vanadium and nickel provided in the database of analyzed oils is a valuable resource that can be used to facilitate the source identification in the case of a spill.

IV.2.2.   Oil spill fate assessment

The studies on the fate of marine oil spills realized in this thesis provide following insights:

- A new proactive strategy for the assessment of oil spill fate, which relies on the preliminary characterization of the frequently produced and transported crude and refined oils is proposed. A set of physicochemical properties was compiled and used for the assessments, and furthermore as an input for ADIOS2 short-term oil fate model.

- Based on the properties and existing criteria all investigated crude and refined oils except light distillates (e.g. diesels) can be considered as environmentally persistent. High density oils, i.e. heavy oils, such as HFO, Maya and Sorosh, would have tendency for sinking depending on the marine conditions (e.g. temperature). Oil viscosity affects the oil behaviour in the marine environment (e.g. spreading, emulsification).

- Modeled short-term oil fate in three European regional seas indicates that the dispersion would be the highest in the North Sea due to the strongest water mass turbulence for all selected oils, except very viscous ones (e.g. HFO, Maya, Sorosh). Evaporation loss is similar in all three regional seas, however slightly higher in Mediterranean due to the warmer waters. Light distillates evaporate most extensively. Nine oils have tendency for emulsification based on their viscosity and content of asphaltenes (>0.5%), and nickel and vanadium (Ni+V>15 ppm). In some cases, emulsification occurs only after a certain degree of weathering.

- Photooxidation led to compositional changes in investigated oils. Most importantly, saturate and aromatic oil fractions were transformed to more polar fractions (akin to resins and asphaltenes). The transformations generate oxygen-containing species. In heavily weathered samples the polar fractions are predominant. Photosensitivity of aromatic fraction increases with increasing aromaticity and alkylation. Isomer specific photooxidation was demonstrated for methylphenanthrenes, methylpyrenes and methylchrysenes. Unexpected photodegradation of TAS biomarkers is demonstrated, which is probably the consequence of the aromatic backbone found in their structure.

IV.2.3.   Assessment of oil spill effects

Risk assessment of possible effects of investigated oils resulted in following conclusions:

- Very viscous oils such as HFO and Sorosh would have fouling effects on marine wildlife in the case of a spill, while on the other hand light distillates (e.g. diesel fuels) or crudes (e.g. Sirtica) would be very difficult to contain using mechanical tools (e.g. booms) if spilt thus affecting larger area.

- Light distillate oils contain predominantly saturated hydrocarbons; therefore their effects in the case of a spill would be more acute. In contrast, heavy residual oils predominantly contain aromatic and polar (resin and asphaltene) compounds which would persist in the environment and have more chronic effects. SARA composition of investigated crude oils varies greatly depending on their geographical origin; therefore, their effects should be assessed on a case to case basis. In general, higher risk can be related to increased content of aromatic and polar fractions. Oils with increased content of sulfur and/or nitrogen such as HFO, Maya and Sorosh contain higher concentrations of toxic heteroaromatic compounds which would have adverse effects on marine life.

- AhR agonist and AR antagonist effects were demonstrated in coarse aromatic fractions of fresh and weathered (evaporated, photooxidized) oils.

- Effect-directed analysis was able to identify 13 compounds with AhR agonist activity in fine fractions, predominantly alkylated three- and four-ring aromatic hydrocarbons. Isomer-specific effects were observed.

- Effects of identified compounds can be confirmed using QSAR tools.

IV.2.4.   Methodological considerations

GC-MS is a robust tool for high throughput oil fingerprinting. It enables reliable identification and quantification of normative fingerprinting compounds, the calculation of diagnostic ratios, and unambiguous source identification.

GC×GC-FID is recommended for fingerprinting of low abundant and difficult to resolve fingerprinting biomarkers. GC×GC-TOF is an ideal tool for non-target analysis and identification in EDA. In general, a combination of both GC×GC-FID and GC×GC-TOF is recommended for comprehensive petroleum analysis. The former provides higher sensitivity needed in quantitative analysis, while the *m/z* dimension provided by the latter is needed for non-target qualitative screening and identification of unknown compounds.

Simulated photooxidation using Xe-lamp can reproduce the effects of natural sunlight on oil.

Open-column liquid chromatography is simple, fast and robust method to obtain coarse oil fractions for further analysis. Normal-phase semipreparative HPLC with amino-propyl modified stationary phase can fractionate aromatic oil compounds according to their aromaticity (ring-number fractionation).

TLC-FID is simple, cheap and robust method to analyze the bulk composition of oil. It is particularly important for the investigation of weathering transformations when polar compounds are generated, which are not GC-amenable. FT-IR is simple and robust method, complementary with TLC-FID, which enables further characterization of polar fractions by providing the information on the existing functional groups. Furthermore, MALDI-TOFMS was demonstrated as a useful tool to obtain the *m/z* distribution of the asphaltene fraction.

The potential of chemometric modeling to relate chemical information with toxic response and to facilitate the identification of toxic compounds in oil is demonstrated.

In general, a broad set of complementary analytical methods, aided by statistical and modeling tools is needed for a fully comprehensive analysis of the sources, fate and effects of marine oil spills.

IV.2.5.   Future research needs

The databases of oils should be constantly updated with new types of oils and their properties, in order to facilitate their identification and risk assessment in the case of a spill.

Further standardization and validation of GC×GC-FID and GC×GC-TOF methods is needed in order to promote their use in oil spill fingerprinting.

Analytical window should be expanded to include more polar fractions, particularly in weathered spill samples, which predominantly contain polar, non GC-amenable compounds. In this, respect, other analytical tools should be used, such as FT-IR, TLC-FID, UPLC and comprehensive two-dimensional LC coupled to MS, and FT-ICR.

The effects of polar fractions should be investigated in terms of their toxicity, bioavailability, etc. In this respect, *in vitro* bioassays are useful tool, as well as QSAR models.

Potential of chemometric data analysis should be further investigated, particularly for complex datasets such as the ones provided by multidimensional chromatographic techniques and high resolution MS.

IV.3.   *References*

ITOPF, 2013. Oil Tanker Spill Statistics 2012. International Tanker Owners Pollution Federation Ltd.

Reddy, C.M., 2010. Oversight Hearing on "Ocean Science and Data Limits in a Time of Crisis: Do NOAA and the Fish and Wildlife Service (FWS) have the Resources to Respond?". Subcommittee on insular affairs, oceans, and wildlife, Committee on natural resources.

USGS Newsroom, 2008. 90 Billion Barrels of Oil and 1,670 Trillion Cubic Feet of Natural Gas Assessed in the Arctic.
http://www.usgs.gov/newsroom/article.asp?ID=1980#.UuqXMfsarf0.

Chapter V.

Resumen de la Tesis

V.1.   Introducción y objetivos

El petróleo crudo ha sido utilizado en una gran variedad de aplicaciones por la humanidad desde sus inicios. Su producción y uso han crecido de manera exponencial en los últimos 50 años y se ha convertido en la principal fuente energética de los países desarrollados, provocando consecuencias económicas, tecnológicas, geopolíticas y ambientales sin precedentes, creando una sociedad moderna basada en el petróleo. A pesar de las continuas predicciones sobre el fin de la era del petróleo, los avances tanto en la tecnología para su extracción, como la fractura hidráulica (fracking) o la perforación en aguas profundas, como en el uso de otras fuentes de hidrocarburos no convencionales, como los esquistos bituminosos o arenas petrolíferas, así como la exploración de las regiones que se están volviendo accesibles debido al calentamiento global (p.ej. el Ártico), parecen indicar que el petróleo seguirá siendo la principal fuente de energía en un futuro a medio plazo.

Uno de los principales problemas ambientales que plantea este uso continuado del petróleo es su vertido accidental o intencionado en el mar que provoca consecuencias negativas tanto para la vida marina como para las actividades económicas y recreativas. Se estima que alrededor de 1,2 millones de toneladas métricas de petróleo entran en los océanos cada año, de las cuales el 48% provienen de filtraciones naturales, y el resto como resultado de la actividad humana (transporte marítimo, instalaciones costeras, producción de petróleo en alta mar, etc.). Después de producirse un vertido, el producto derramado comienza a transformarse inmediatamente debido a diversos procesos físico-químicos y biológicos complejos y a distribuirse entre los diferentes compartimentos ambientales. Todos estos procesos, que incluyen difusión, evaporación, disolución, dispersión, emulsificación, fotooxidación y biodegradación, entre otros, se conocen como envejecimiento y al actuar pueden cambiar la composición, comportamiento, vías de exposición y la toxicidad del vertido.

Para reforzar las medidas de control y asignación de responsabilidades de esta contaminación destinadas a proteger la salud pública y el medio ambiente, es necesario disponer de métodos eficientes para la caracterización de estos vertidos y de sus posibles efectos. El objetivo de la presente Tesis es contribuir al desarrollo de

estas metodologías para determinar el origen y destino final de un vertido, así como evaluar los posibles efectos toxicológicos asociados.

El petróleo crudo es una mezcla natural muy compleja, que contiene hidrocarburos, compuestos de azufre, nitrógeno y oxígeno, complejos organometálicos (Ni y V), así como otros elementos traza minoritarios.

Las diferentes clases de hidrocarburos del petróleo son las siguientes:

- parafinas, que son hidrocarburos saturados con cadenas lineales o ramificadas, pero sin ninguna estructura cíclica;

- naftenos, que son hidrocarburos que contienen uno o más anillos alifáticos, cada uno de los cuales pueden tener una o más cadenas laterales parafínicas; y

- compuestos aromáticos, que son hidrocarburos que contienen uno o más núcleos aromáticos, que pueden estar sustituidos con anillos nafténicos o cadenas laterales parafínicas.

El azufre está presente preferentemente formando parte de la estructura química del tiofeno y sus derivados, mientras que el nitrógeno se encuentra asociado a los derivados heterocíclicos, tales como carbazoles o quinolinas, y el oxígeno forma parte de los derivados carboxílicos.

Los compuestos policíclicos de alto peso molecular (>500 g·mol^{-1}, aprox.) que contienen nitrógeno, azufre y oxígeno (NSO) son denominados a menudo como resinas y asfaltenos.

Para un análisis exhaustivo de los distintos componentes del petróleo, se requiere de un conjunto de métodos analíticos complementarios. En general, se utilizan habitualmente diversos métodos cromatográficos para la separación y detección de las distintas fracciones que componen el petróleo. Así, se separan los hidrocarburos saturados y aromáticos utilizando el procedimiento de fraccionamiento llamado SARA (**s**aturados-**a**romáticos-**r**esinas-**a**sfaltenos). Para cuantificar las distintas fracciones se puede utilizar también la cromatografía en capa fina acoplada a un detector de ionización de llama (TLC-FID). La determinación de compuestos individuales se aborda mediante GC convencional, o cromatografía de gases

bidimensional integrada (GC×GC), acopladas a la espectroscopia de masas. En los últimos años, el uso de métodos no cromatográficos, tales como FT-IR, FT-ICRMS, y MALDI-TOF, ha aumentado considerablemente.

Para la identificación de compuestos tóxicos se puede utilizar el llamado "análisis dirigido por efectos tóxicos" (Effect-directed analysis, EDA), donde la muestra se fracciona secuencialmente y el análisis está dirigido por la respuesta o efecto tóxico obtenido a través de un bioensayo (p.ej. AhR, AR, o ER).

En la presente Tesis se caracterizaron químicamente diversos crudos de petróleo y productos refinados, frecuentemente transportados a través de diferentes mares europeos, y se obtuvo información relevante que puede ser utilizada en el caso de un vertido. Además, se aplicó la metodología de la toma de las "huellas químicas" (fingerprinting) de los petróleos para identificar el tipo, posible origen y las transformaciones (envejecimiento) que sufren en el mar. Específicamente, se evaluaron los efectos de la fotooxidación en su composición y su incidencia en la metodología para determinar la huella química característica de los vertidos. Finalmente, se analizaron los efectos tóxicos de petróleos crudos y envejecidos, y se identificaron los compuestos responsables de los mismos.

Para ello, se utilizaron diferentes metodologías analíticas complementarias: TLC-FID, FT-IR, cromatografía líquida en columna abierta y HPLC semipreparativa en fase normal, GC-MS, GC×GC-FID, GC×GC-TOFMS, bioensayos AhR y AR, así como el modelo ADIOS2 de la Administración Nacional Oceánica y Atmosférica (NOAA) y la modelización quimiométrica N-PLS.

V.2. Caracterización de los petróleos y la evaluación de su destino y efectos en el medio marino

Dado que las propiedades físico-químicas de los diferentes petróleos crudos y productos derivados varían mucho entre ellos, la información detallada sobre los mismos es necesaria para estimar con fiabilidad el origen, el comportamiento medioambiental, el impacto y el destino final en un escenario particular de vertido al mar. Aunque dichas bases de datos están disponibles para un número limitado de petróleos, muchas de ellas están incompletas.

En esta Tesis, se compilaron las propiedades físico-químicas que controlan el destino y el impacto ambiental de diversos petróleos que se transportan con frecuencia. Cuando fue posible, esta información se obtuvo de bases de datos ambientales y ensayos de crudo o, en caso necesario, de forma experimental mediante análisis elemental y TLC-FID. Posteriormente, la base de datos creada se utilizó para evaluar el destino a corto plazo de los petróleos mediante el modelo ADIOS2 desarrollado por la NOAA. Por último, con el fin de determinar la "huella química" del producto se utilizó la técnica de GC-MS, y se calcularon las relaciones diagnóstico características de algunos hidrocarburos aromáticos policlíclicos (HAP) específicos y biomarcadores, que se evaluaron estadísticamente mediante análisis de componentes principales (PCA).

De los petróleos investigados sólo Gasóleo A y Gasóleo B pueden ser considerados como no persistentes en función de sus datos de destilación y los criterios de la EPA. El resto de petróleos son considerados persistentes al pertenecer, principalmente, a crudos del grupo 2 (°API = 35-45; ocho petróleos: Kirkuk, Azeri, Oseberg, Siberian Light, North Sea oil, Murban, Nemba, Sirtica) y grupo 3 (°API = 17,5-35; nueve petróleos: Sorosh, Maya, Dalia, Hungo, Forcados, Kuwait, Norne, Arabian Light, Flotta). Tan sólo el fuelóleo pesado HFO pudo ser incluido en el grupo 4 (°API <17,5) (**Tabla V-1**).

Tabla V-1 Propiedades (°API, viscosidad) de los petróleos investigados.

Petróleo	Origen	API, °	Viscosidad, cSt
ARABIAN LIGHT	Arabia Saudí	33,4	16,15@15°C
AZERI	Azerbaiyán	36,6	8,21@20°C
DALIA	Angola	23,14	198@10°C
DIESEL A	refinado	38,32	3,25@40°C
DIESEL B	refinado	34,8	3,25@40°C
DIESEL C	refinado	30	7@40°C
FLOTTA	Mar del Norte	34,7	12@20°C
FORCADOS	Nigeria	29,7	17,4@10°C
HEAVY FUEL OIL	producto	11,47	23037,28@15°C
HUNGO	Angola	28,7	26,30@20°C
KIRKUK	Irak	35,1	13@10°C
KUWAIT	Kuwait	31,4	25,2@15°C
MAYA	México	21,5	302,68@15°C
MURBAN	EAU	39,73	5,9@10°C
NEMBA	Angola	39,79	8,4@10°C
NORNE	Mar del Norte	32,7	14,1@20°C
NORTH SEA OIL	Mar del Norte	38,41	9,8@10°C
OSEBERG	Mar del Norte	37,8	6,8@10°C
SIBERIAN LIGHT	Rusia	37,8	7@20°C
SIRTICA	Libia	43,3	3,43@40°C
SOROSH	Irán	18,1	1381@20°C

Para los petróleos pesados como HFO residual (23037 cSt) y el crudo Sorosh (1381 cSt) se observan valores de viscosidad extremas, cuyo vertido sobre la fauna marina y litoral tendría graves efectos (**Figura V-1**), aunque serían relativamente fáciles de contener mecánicamente usando las barreras de contención. En el otro extremo se encuentran los destilados altamente fluidos como el diesel ligero (3,25 cSt) y el crudo Sirtica (3,43 cSt) que al extenderse muy rápido, dificultarían su contención.

Figura V-1 Efectos de los petróleos pesados en la fauna marina (ITOPF, 2013).

Por lo general, los contenidos de S y N son bajos, pero algunos de los petróleos seleccionados se caracterizan por contenidos elevados de azufre (p. ej., HFO, Maya) y/o de nitrógeno (p. ej., Maya, Sorosh) y, por lo tanto, pueden suponer un riesgo ambiental debido a la presencia de carbazoles y dibenzotiofenos.

El análisis mediante TLC-FID (**Figura V-2**) mostró que los gasóleos tienen un alto contenido en hidrocarburos saturados (>80%) y un nivel relativamente bajo de compuestos aromáticos y polares. En general, los destilados ligeros no contienen asfaltenos, o su contenido es muy bajo (p. ej., Diesel A) y por lo tanto, sus efectos en el caso de un vertido serían limitados y a corto plazo. Por el contrario, los productos de petróleo residual, como HFO, contienen cantidades importantes de compuestos aromáticos, resinas y asfaltenos que causarían efectos crónicos importantes. Con respecto a los petróleos crudos, su composición y por lo tanto sus efectos varían ampliamente dependiendo de su origen geoquímico.

Figura V-2 Equipo Iatroscan® utilizado para el análisis TLC-FID.

Finalmente, esta base de datos se aplicó para evaluar su posible destino en el caso de un vertido, con una modelización mediante el uso del software ADIOS2 de NOAA. Se seleccionaron las condiciones marinas características de tres mares de Europa (el mar Mediterráneo, el océano Atlántico y el mar del Norte) que pueden influir en el comportamiento del vertido de petróleo y se calcularon los porcentajes de petróleo evaporado, dispersado, y restante después de 5 días. Las condiciones ambientales más extremas (temperatura elevada, turbulencia, etc) promueven procesos tales como la evaporación y dispersión. Además, la mayoría de los petróleos tienen propiedades que facilitan la formación de emulsión.

El conjunto de compuestos diagnóstico seleccionado (alcanos, HAP y biomarcadores) y el cálculo de sus ratios pueden ser utilizados para distinguir con alto grado de certeza los diferentes tipos de petróleo, y hacer posible su identificación en el caso de un vertido. El análisis estadístico indicó que las relaciones diagnóstico de C17/Pris, C18/Phy, 4-MD/1-MD, B(a)F/4-MPy, BNT/TMP y Reteno/TMP regulan la diferenciación del tipo de petróleo en el conjunto de muestras analizadas, y se pueden utilizar para facilitar la identificación de su origen, en particular de las muestras no envejecidas (**Tabla V-2**).

Tabla V-2 Compuestos diagnóstico que regulan la diferenciación del tipo de petróleo en el conjunto de muestras analizadas.

Compuesto	Abrev.	*m/z*	Estructura
n-heptadecano	C17	85	
pristano	Pris	85	
n-octadecano	C18	85	
fitano	Phy	85	
4-metildibenzotiofeno	4-MD	198	
1-metildibenzotiofeno	1-MD	198	
benzo[*a*]fluoreno	B(a)F	216	
4-metilpireno	4-MPy	216	
reteno	Reteno	234	
tetrametilfenantreno	TMP	234	
benzo[*b*]nafto[1,2-*d*]tiofeno	BNT	234	

V.3. Determinación de la huella química para identificar el tipo y origen de los vertidos de petróleo

En esta Tesis, se evaluó la aplicabilidad y fiabilidad del uso de la huella química determinada mediante GC-MS participando en un ejercicio de intercomparación, organizado por Bonn-OSINet en 2010, cuyo objetivo era la identificación de vertidos de petróleo. Nuestro laboratorio recibió tres muestras de vertidos (RR2010-1, -2 y -3) y dos muestras de origen candidatas (RR2010-4 y -5) con la petición de analizar las muestras utilizando la metodología estándar CEN para determinar la huella química e identificar el posible tipo y origen del petróleo.

El primer paso en la identificación del origen del vertido de petróleo es la inspección visual de los cromatogramas de la corriente iónica total (TIC) obtenida mediante GC-MS. En las cinco muestras recibidas el perfil cromatográfico obtenido mostró una distribución típica de n-alcanos de C_{10} a C_{40}. Las muestras de origen (RR2010-4 y -5) pueden corresponder a los petróleos crudos, mientras que las muestras recogidas en la playa (RR2010-2 y -3) tienen perfiles similares, aunque se ven progresivamente reducidas en sus componentes más volátiles, probablemente debido al envejecimiento (p. ej., evaporación). Por el contrario, la muestra RR2010-1 tiene las características del petróleo "craqueado", que se confirmó mediante el análisis de los cromatogramas GC-MS de iones extraídos (EIC), donde se pudo confirmar la presencia de olefinas (*m/z* 83) y la distribución típica de los metilfenantrenos (*m/z* 192) (**Figura V-3**). Por lo tanto, se descartó como "coincidencia negativa" con suficiente confianza. Para el resto de las muestras, se evaluaron las diferencias relativas de las 25 relaciones diagnóstico normativas de los HAP y biomarcadores respecto al valor crítico de 14%.
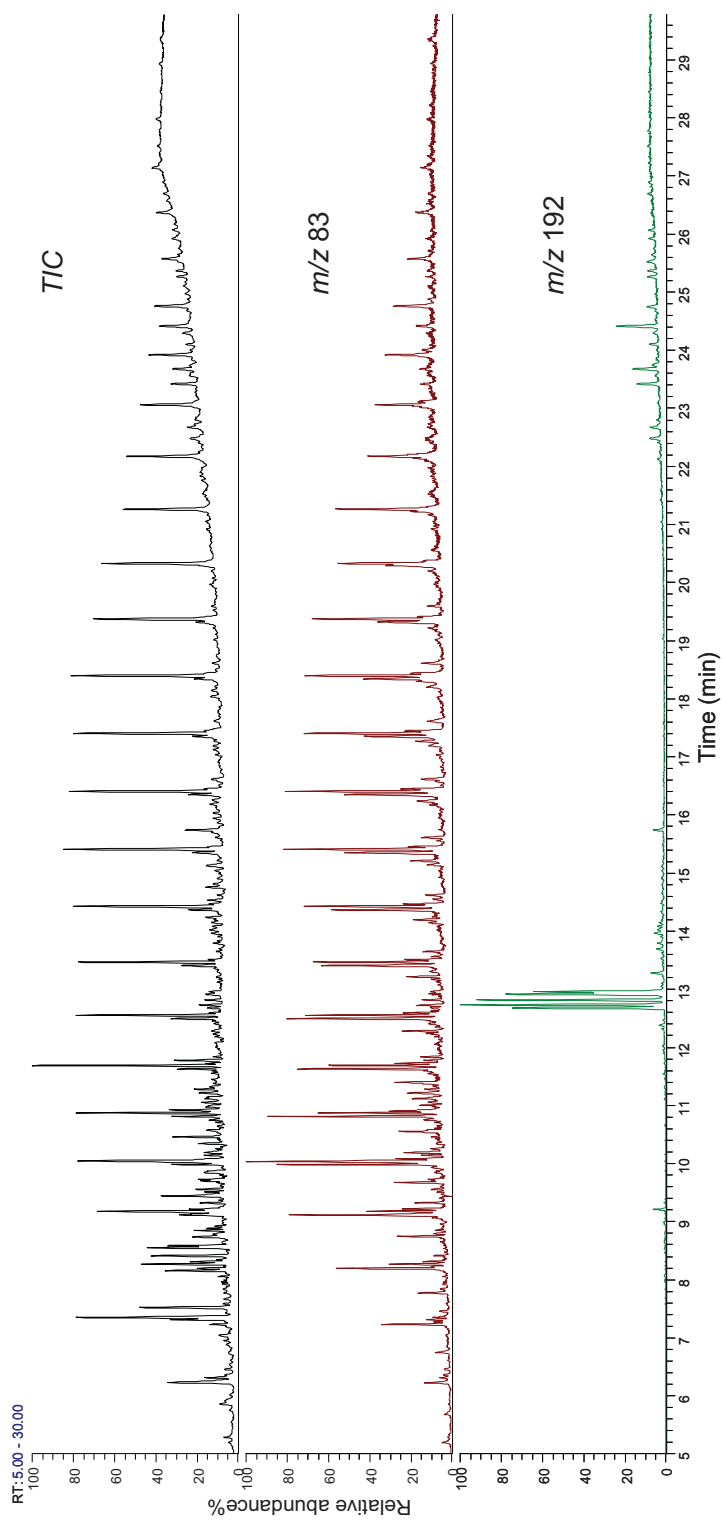
Figura V-3 TIC de la muestra RR2010-1 y los EIC característicos de olefinas (*m/z* 83) y metilfenantrenos (*m/z* 192).

La comparación de las relaciones diagnóstico entre la muestra vertido RR2010-2 y origen candidato RR2010-4 confirmaron una clara correspondencia, ya que todas las relaciones normativas, excepto el C17/Pris, están por debajo de la diferencia crítica de 14%. Esto probablemente podría atribuirse a una ligera biodegradación del n-alcano C_{17}. En la segunda muestra de vertido (RR2010-3), que fue expuesta en el campo durante un mes, las proporciones entre C17/Pris y C18/Phy están muy por encima de la diferencia crítica de 14% crítica, debido a la biodegradación más avanzada, pero las relaciones Pris/Phy son consistentes con el mismo origen geoquímico. Además, los gráficos de envejecimiento (PW-plots) demuestran un efecto de disolución de los compuestos más polares, p.ej. metilfluorenos, metilfenantrenos y metildibenzotiofenos. Por lo tanto, se puede concluir que ambas muestras (RR2010-2 y -3) son "coincidencia positiva" con la fuente sospechosa 2010-4.

V.3. *Efecto de la fotooxidación en la composición química del petróleo y su implicación en la huella química de vertidos de petróleo*

En esta Tesis, se presentan los resultados del estudio sobre el envejecimiento fotooxidativo del vertido del *Prestige* en 2002, y del petróleo que se liberó durante la explosión de la plataforma *DWH* en 2010 **(Figura V-4).** Se estudiaron los cambios en la composición general de los petróleos derramados ocasionados por la luz solar natural y simulada, y en particular los efectos sobre los HAP y los biomarcadores TAS frecuentemente utilizados para determinar la huella química. También se estudiaron las muestras de campo de los ambos incidentes. Para este fin, los compuestos de interés se analizaron mediante GC-MS y GC×GC-FID.

Figura V-4 Playa contaminada con el petróleo del *Prestige* (A) y mancha de petróleo liberado después de la explosión de la plataforma *Deepwater Horizon* (B).

En el primer experimento, el petróleo del *Prestige* se irradió utilizando luz solar simulada (lámpara de Xe) y una exposición a corto plazo (12 h), con el objetivo de estudiar los cambios rápidos de los diferentes grupos de especies aromáticas, en especial las que se utilizan para la determinación de la huella química.

En el segundo experimento se utilizó la luz solar natural para irradiar el petróleo de Macondo well (*MW*), de forma controlada, durante un período de exposición a medio plazo (70 días) (**Figura V-5**). En este caso, se ha seleccionado un período de exposición más largo debido a que el objetivo específico de este experimento fue estudiar los efectos de la irradiación en el grupo particular de moléculas de biomarcadores, TAS, que se consideradas recalcitrantes al envejecimiento de medio a largo plazo.
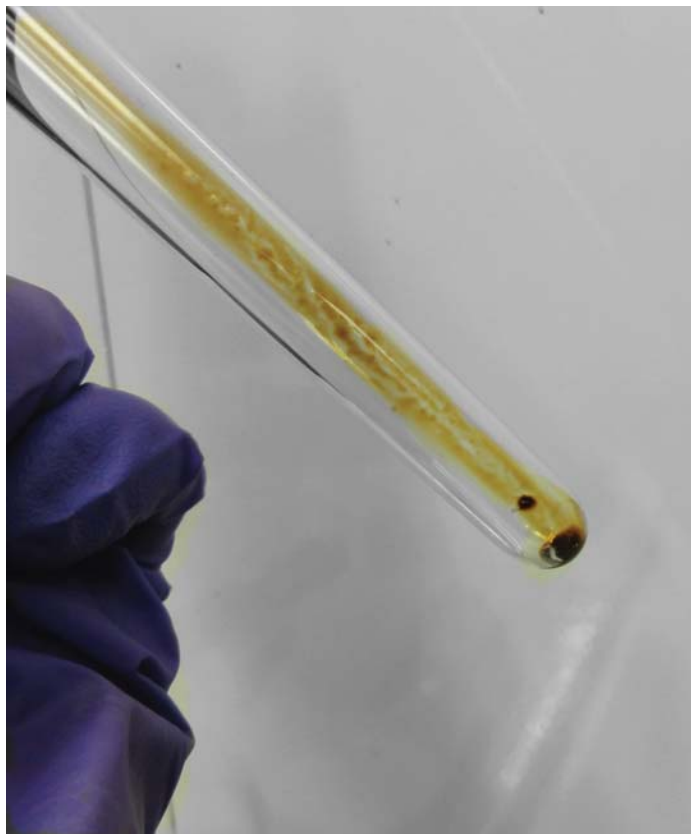
Figura V-5 Tubo de cuarzo con el petróleo MW tras irradiación con luz solar natural durante el experimento.

Con el fin de investigar los cambios en la **composición global**, es decir, el contenido de los principales grupos de compuestos presentes en el petróleo, se utilizó la técnica de TLC-FID. Los cambios más notables observados después de la irradiación, ya sea por la luz solar natural o artificial simulada, fueron una disminución rápida y sustancial de la fracción aromática y un aumento concomitante de las fracciones más polares (resinas y asfaltenos) en relación con los controles. Durante la irradiación natural prolongada del petróleo de *MW* se observó una tendencia similar. Con el fin de investigar con más detalle la naturaleza de las transformaciones que ocurren durante los experimentos de irradiación, las muestras se analizaron utilizando FT-IR para conseguir la información de los grupos funcionales. Los resultados confirman que la irradiación genera varias especies que contienen oxígeno, de acuerdo con algunos estudios publicados.

En el análisis de la fracción aromática de petróleo *Prestige* por GC-MS se observaron cambios significativos a **nivel molecular** después de la irradiación. En la mayoría de los casos, el grado de fotodegradación en diferentes familias de hidrocarburos aromáticos aumenta simultáneamente con el grado de alquilación y el número de anillos de la estructura molecular. Este efecto también aumenta con la presencia de N (carbazoles, Cb) y diminuye con la de S (dibenzotiofenos, Dbt). Estos patrones se pueden utilizar convenientemente en la evaluación del envejecimiento de los vertidos de petróleo, de modo que un aumento simultáneo de las relaciones de los alquil-crisenos (C2/C3) o derivados C/Py y Dbt/Cb, en muestras de campo, puede ser indicativo de fotooxidación.

Con el fin de confirmar con más detalle la fotosensibilidad observada en los compuestos aromáticos, las muestras del *Prestige* irradiadas en el laboratorio se compararon con las muestras de campo utilizando la información proporcionada por los cromatogramas GC-MS de los iones característicos de las diferentes familias de compuestos estudiadas. En el perfil de metilafenantrenos/metilantraceno (MP/MA) (*m/z* 192), el cambio más significativo es la degradación preferencial del MA frente a los metilfenantrenos, a la inversa de lo que se observa durante la biodegradación, donde el MA es más persistente que los MP. Otros perfiles afectados por la irradiación fueron metilfluorantenos/pirenos y benzofluorenos (*m/z* 216) y metilcrisenos (*m/z* 242). Además, en estos casos se observó la fotooxidación preferente de algunos isómeros.

La mayor resistencia de los S-compuestos a la fotodegradación se confirma en los cambios observados en la composición del tetrametilfenantreno (TMP) y benzo[*b*]nafto[1,2-*d*]tiofeno (BNT) (*m/z* 234), donde, después de la irradiación, el primero fue más degradado que el segundo. Estos resultados son consistentes con los encontrados en las muestras del *Prestige* recogidas en el campo.

La familia de biomarcadores TAS incluye ocho compuestos (C20TA, C21TA, C26TA (R/S), C27TA (R/S), C28T (R/S)), derivados del pregnano y colestano, compartiendo una estructura aromática común, pero que difieren en la estructura de la cadena alquilíca. A pesar que los TAS han sido reconocidos como compuestos altamente recalcitrantes, se observó una degradación notable en las muestras irradiadas de *Prestige* (20%) y en las de petróleo *MW* recogidas en el campo (87-97%), que no puede ser explicada únicamente por procesos de biodegradación. Estas observaciones llevaron al estudio de los efectos de la fotooxidación en el crudo *MW* en condiciones controladas en el laboratorio. Sorprendentemente, a las primeras 24 horas, el contenido de TAS ya comenzó a disminuir, en relación con el producto no tratado. Esta tendencia se mantuvo a lo largo de la primera semana de irradiación y hasta el final del experimento (70 días), cuando ningún compuesto TAS fue detectado, utilizando la metodología GC×GC-FID (**Figura V-6**).

La evaporación se puede descartar como la causa de la pérdida de los TAS puesto que la cantidad de petróleo en los tubos de cuarzo permaneció estable, después de una pérdida inicial (~30%) en las primeras 24 horas. Por otro lado, la biodegradación tampoco puede ser la causa de este comportamiento porque la disminución mostró una tendencia convergente entre todos los componentes, que no es de esperar en el caso de biodegradación, que eliminaría preferentemente congéneres individuales. Además, los indicadores prematuros de la biodegradación (n-alcanos) se mantuvieron sin cambios. Dado que no se utilizó ninguna fase acuosa en los experimentos de irradiación, la disolución también podía ser descartada como la causa de las transformaciones observadas y, en conclusión, la principal causa de la reducción de TAS observada debe ser la fotooxidación.
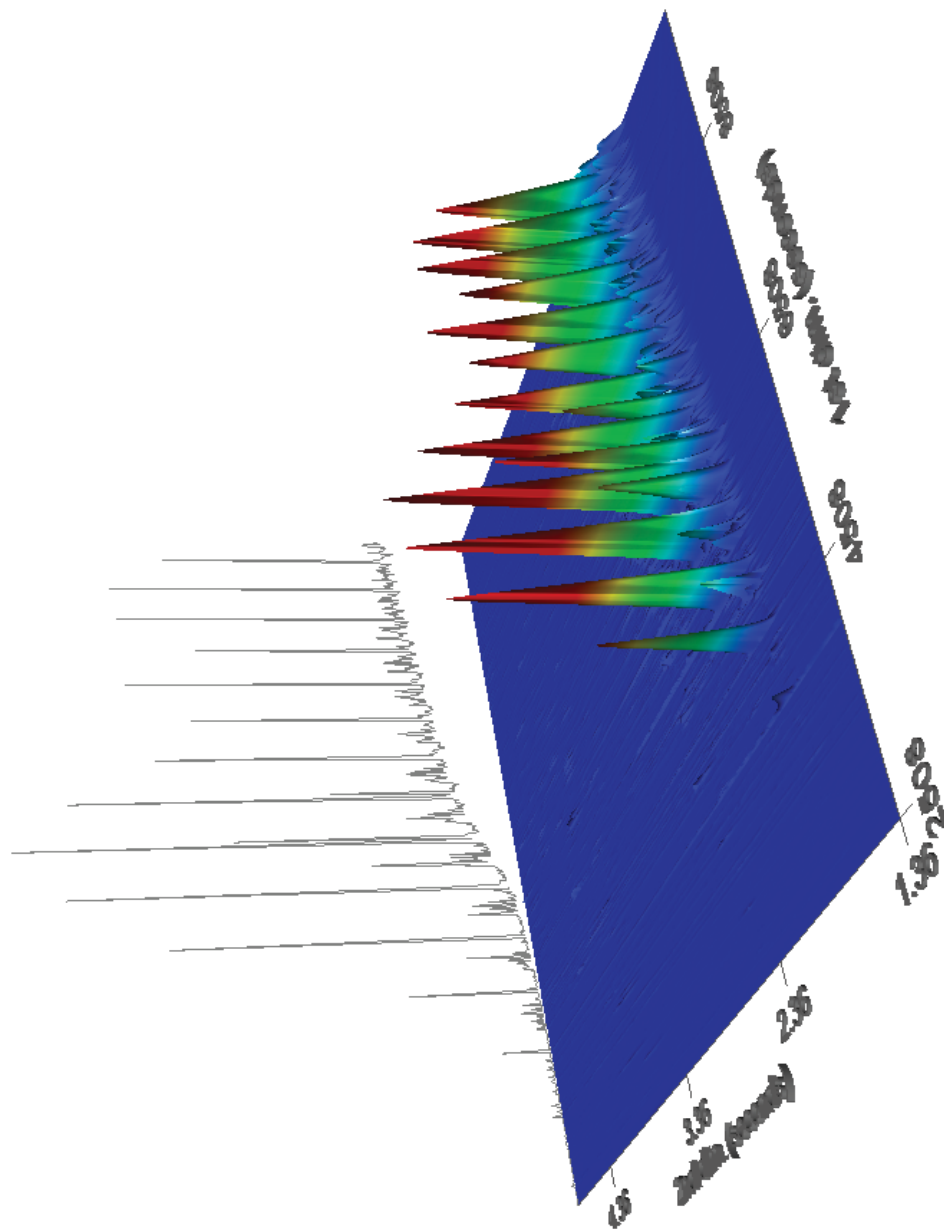
Figura V-6 Sección del cromatograma GC×GC-FID en 3D de la muestra de petróleo MW irradiada.

Nuestra hipótesis, basada en los resultados del experimento y las propiedades de los TAS (solubilidad, peso molecular), es que el proceso fotooxidativo es también la causa de la pérdida observada en las muestras de petróleo *MW* recogidas en el Golfo de México. Las posibles razones para la fotosensibilidad pronunciada de los TAS se pueden encontrar en su estructura molecular de tipo fenantreno y la sustitución con grupos alquilo. Un comportamiento similar se observó también en los derivados del tetrametilfenantreno. Según los espectros de FT-IR obtenidos, algunos mecanismos potenciales podrían incluir la escisión de los sustituyentes de alquilo y la oxidación de los anillos aromáticos para formar estructuras de epoxi o de quinona. Además, las posiciones bencílicas son particularmente sensibles a la auto-oxidación, como de ha visto en residuos bituminosos oxidados en condiciones naturales.

Las transformaciones descritas anteriormente afectan a varias relaciones diagnóstico usadas para la determinación de la de huella química de los vertidos de petróleo. Todas las relaciones de HAP seleccionadas, excepto 2-MP/1-MP, mostraron diferencias significativas, por encima del límite crítico del 14%, que pueden afectar a su fiabilidad cuando se utilizan para confirmar el origen del vertido.

Por ello, el conocimiento de los efectos de la irradiación a nivel molecular puede ayudar a interpretar las diferencias observadas y atribuirlas a la fotooxidación. Particularmente significativo fue el hecho de que, tras sólo siete días de exposición, se observaron importantes cambios en las relaciones diagnóstico de los biomarcadores TAS, que se consideran tradicionalmente como recalcitrantes. Estas diferencias relativas deben tenerse especialmente en cuenta en el análisis de muestras de vertidos muy expuestos a la luz solar, incluso en un plazo relativamente corto (semanas). En tales casos, las proporciones de triterpanos y esteranos deben utilizarse para la confirmación del origen, mientras que HAP y TAS podrían ser más útiles para estimar los procesos de envejecimiento, y en particular, la fotooxidación.

V.5. Análisis de los petróleos dirigido por los efectos tóxicos

En esta Tesis se utilizó una estrategia analítica, conocida como análisis dirigido por los efectos (EDA), para evaluar el potencial tóxico de los diferentes componentes en una mezcla química compleja. El estudio presentado se centró en los efectos medidos a través de receptores AhR y AR, que fueron evaluados utilizando una serie de bioensayos adecuados (PAH-CALUX y YAS). Se seleccionaron dos petróleos representativos, un crudo del Mar del Norte (NSC) y un fuelóleo pesado residual (HFO). Con el fin de investigar el efecto de los procesos de envejecimiento sobre la toxicidad, ambos petróleos se evaporaron e irradiaron en condiciones de laboratorio, para simular el envejecimiento en el campo.

Para reducir la complejidad de las muestras se procedió a un fraccionamiento en dos niveles, utilizando cromatografía líquida en columna abierta y HPLC semi-preparativa en fase normal. Las fracciones más activas se analizaron mediante GC×GC-TOFMS. Por último, la estrategia convencional EDA se amplió y se añadió una etapa quimiométrica adicional, donde se utilizó el modelo N-PLS para correlacionar la información química obtenida mediante GC×GC-TOFMS y los datos de toxicidad. La actividad tóxica de los compuestos identificados se confirmó utilizando estimaciones cuantitativas de las relaciones estructura-actividad (QSAR).

En el primer nivel de EDA, se obtuvieron 18 fracciones iniciales mediante cromatografía líquida en columna abierta, que fueron sometidas a los bioensayos AhR y AR. Los resultados de los bioensayos mostraron que en los dos productos (petróleo y fuel-oil) y para todos los tratamientos, las actividades AhR y AR más elevadas fueron para la fracción aromática. Las fracciones polares mostraron una actividad tóxica de menor importancia, mientras que en la fracción saturada no se determinó ninguna actividad. La composición química de las fracciones aromáticas iniciales se investigó mediante GC-MS y GC×GC-TOFMS (**Figura V-7**).

Figura V-7 Comparación de cromatogramas (TIC) GC-MS (A) y GC×GC-TOFMS (B) de la fracción aromática del crudo del Mar del Norte.

Los resultados mostraron que las fracciones contienen una mezcla compleja de HAP, que van desde el naftaleno hasta compuestos pesados policíclicos (p.ej., benzo[*ghi*])perileno), incluyendo los homólogos alquil sustituidos. Sin embargo, la composición de las fracciones iniciales todavía era demasiado compleja para permitir una identificación más precisa de los compuestos responsables de los efectos observados. Por lo tanto, fue necesario fraccionar a un segundo nivel las fracciones aromáticas.

Las fracciones aromáticas iniciales se volvieron a fracccionar mediante HPLC semipreparativa en fase normal con una columna de base sílice de aminopropilo, que permite la separación de los compuestos aromáticos en función de su grado de aromaticidad creciente. Al final del estudio se obtuvieron 90 fracciones finas, que fueron sometidas a los bioensayos AhR. En el crudo NSC la mayoría de la actividad se detectó en las fracciones 10 a 12 con los tres tratamientos (sin tratar, evaporado e irradiado con luz). Del mismo modo, las fracciones 9 a 12 del HFO se detectaron como las más activas. En total, se seleccionaron 21 fracciones finas con mayor actividad AhR para su posterior análisis mediante GC×GC-TOFMS.

La caracterización de fracciones activas demostró que contenían predominantemente compuestos aromáticos de tres y cuatro anillos, incluyendo diversos homólogos alquil sustituidos. Sin embargo, el número de compuestos fue todavía elevado para la detección inequívoca de los compuestos responsables de la tóxicidad. Por lo tanto, para una identificación más concluyente de los compuestos individuales (o grupos de compuestos) que causan el agonismo AhR fue necesario utilizar un modelo quimiométrico.

El modelo N-PLS desarrollado fue capaz de predecir de manera bastante satisfactoria la actividad tóxica de las fracciones que fueron utilizadas para calibrar el modelo. Los vectores de ponderación obtenidos con el modelo N-PLS y sus tiempos de retención asociados (t_R1D and t_R2D) en las dos columnas cromatográficas se utilizaron a continuación para identificar los picos correspondientes en los cromatogramas GC×GC y sus espectros de masas. Usando esta información, se procesaron 21 fracciones finas y se identificaron, tentativamente, 13 compuestos. Los compuestos identificados incluyen: fenantrenos alquil sustituidos, propenil antraceno,

benzo[*b*]nafto[2,1-*d*]tiofeno (BNT) y C2-BNT, criseno (C) y sus alquil homólogos C1 y C2, carbazol sustituido (C3-Cb) y pirenos sustituidos (C2 hasta C4-Py) (**Figura V-8**).
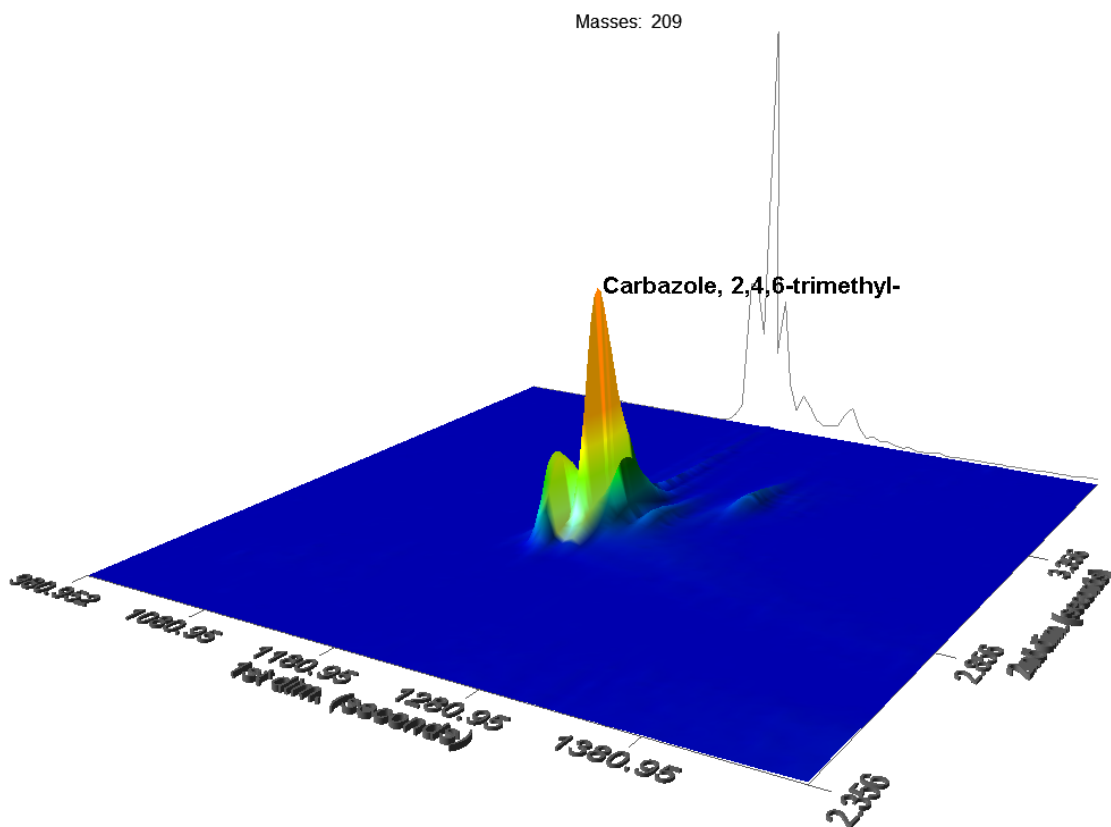
Figura V-8 Cromatograma EIC de GCxGC-TOFMS (*m/z* 209) mostrando el pico de C3-carbazol en unas de las fracciones activas AhR del fuelóleo pesado residual.

El paso final de la EDA fue confirmar los efectos de los compuestos identificados. Cuando no se dispone de los estándares puros, las posibles alternativas son las herramientas QSAR. En este estudio, se utilizó una herramienta *in-silico* (VirtualToxLab™) para confirmar que los compuestos identificados tienen el potencial de unirse a la AhR, y así demostrar la aplicación exitosa del modelo N-PLS.

V.5.   Conclusiones

En las últimas dos décadas hemos sido testigos de una disminución tanto en el número de incidentes de vertidos de hidrocarburos como en la cantidad de petróleo vertida en estos incidentes, lo que llevó a un menor interés por la ciencia básica de los vertidos de petróleo. Con la introducción de una legislación más restrictiva, gran parte de la respuesta a los vertidos, la evaluación y las actividades de restauración se pasaron a las agencias gubernamentales y a otras partes interesadas. Sus capacidades quizás eran suficientes para hacer frente a los vertidos que se producen con más frecuencia a pequeña escala; sin embargo, los últimos grandes incidentes catastróficos, como el *Prestige* en 2002 o el vertido de la plataforma *Deepwater Horizon* (*DHW*) en 2010, han renovado la necesidad de seguir investigando en este tema, con el fin de poder entender y estimar el alcance de los impactos sociales, ambientales y económicos de tales vertidos.

Esto es particularmente importante en el contexto de nuevas exploraciones y descubrimientos de recursos de hidrocarburos en ecosistemas frágiles como el Ártico, donde el clima extremo y la falta de infraestructura enfatizan aún más la necesidad de una evaluación exhaustiva de todos los posibles efectos que la futura producción de petróleo podría causar.

Los objetivos de esta Tesis se establecieron para proporcionar nuevos enfoques y metodologías, así como mejorar y reevaluar las ya existentes, de manera que pueden contribuir a una estrategia integral y proactiva. Su ámbito de aplicación es amplio, ya que abarca todos los aspectos importantes de los vertidos marinos de petróleo - el origen, el destino ambiental y los posibles efectos tóxicos. Además, esta Tesis se basa en el estudio de grandes vertidos de petróleo reales (*Prestige* y *DWH*), además de una amplia gama de petróleos, así como de los productos derivados del petróleo que se producen y transportan actualmente a nivel mundial.

Mediante la estrategia aplicada y las metodologías analíticas utilizadas fue posible evaluar correctamente el posible destino y los efectos de los vertidos de los diferentes tipos de petróleo, determinar el origen de las muestras de vertidos envejecidas, detectar los cambios en la composición a nivel global y molecular, y atribuirlos a procesos de envejecimiento concretos (p.ej. fotooxidación) y, finalmente,

a partir de los bioensayos aplicados detectar los compuestos que tienen un mayor efecto tóxico.

V.6.   Referencias

ITOPF, 2013. Effects of oil pollution on marine environment, Technical information paper no. 13.

ANNEXES
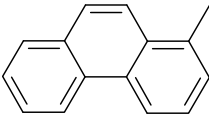
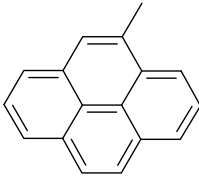# A. Tables and figures

Table A-1 Fingerprinting compounds (CEN, 2012).

Compound name	Abbrev.	*m/z*	Structure
n-heptadecane	C17	85	
pristane	Pris	85	
n-octadecane	C18	85	
phytane	Phy	85	
$C_{15}H_{28}$-sesquiterpanes	SES(1-8)	123	
18α(H)-22,29,30-trisnorhopane	27Ts	191	
17α(H)-22,29,30-trisnorhopane	27Tm	191	
17α(H),21β(H)-28,30-bisnorhopane	28ab	191	
17α(H),21β(H)-30-norhopane	29ab	191	

Table A-1 contd.

Compound name	Abbrev.	m/z	Structure
18α(H)-oleanane	30O	191	
17α(H),21β(H)-hopane	30ab	191	
17α(H),21β(H),22S-homohopane	31abS	191	
gammacerane	30G	191	
2-methylphenanthrene	2-MP	192	
1-methylphenanthrene	1-MP	192	
1-methylanthracene	MA	192	
4-methyldibenzothiophene	4-MD	198	
1-methyldibenzothiophene	1-MD	198	
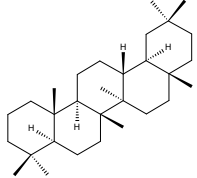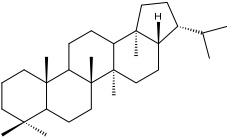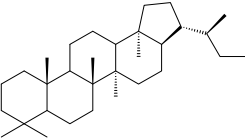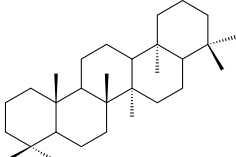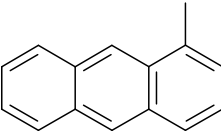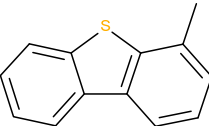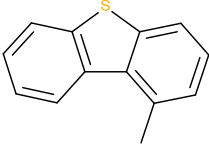
Table A-1 contd.

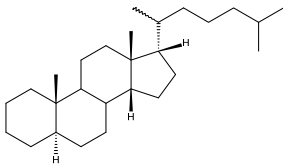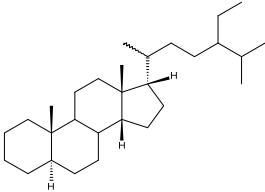| Compound name	Abbrev.	m/z	Structure
2-methylfluoranthene	2-MFl	216	
benzo[*a*]fluorene	B(a)F	216	
benzo[*b+c*]fluorene	B(b+c)F	216	
2-methylpyrene	2-MPy	216	
4-methylpyrene	4-MPy	216	
1-methylpyrene	1-MPy	216	
13β (H),17α (H),20S-cholestane (diasterane)	27dbS	217	
13β (H),17α(H),20R-cholestane (diasterane)	27dbR	217	
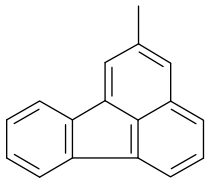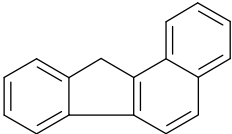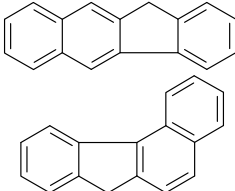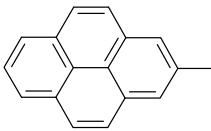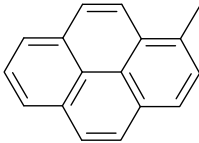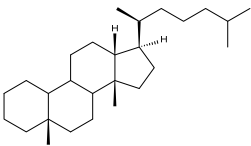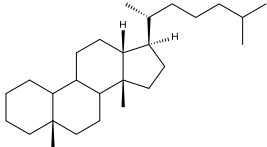
Table A-1 contd.

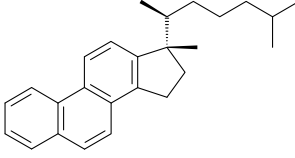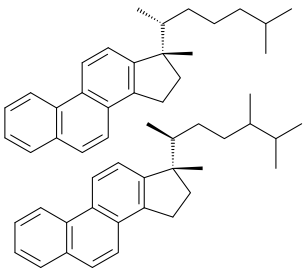| Compound name	Abbrev.	m/z	Structure
5α (H),14β(H),17β(H),20(R+S)-cholestane	27bbR+S	218	
24-ethyl-5α(H),14β (H),17β,20(R+S)-cholestane	29bbR+S	218	
C_{26}, 20S-triaromatic sterane	SC26TA	231	
C_{26}, 20R + C_{27}, 20S-triaromatic steranes	RC26+ SC27TA	231	
C_{28}, 20S-triaromatic sterane	SC28TA	231	
C_{27}, 20R-triaromatic sterane	RC27TA	231	
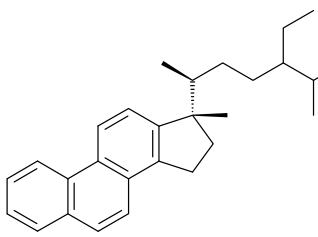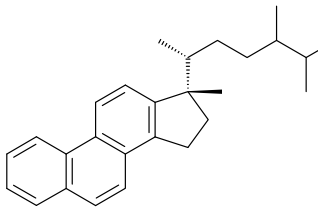
Table A-1 contd.

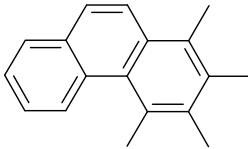| Compound name	Abbrev.	m/z	Structure
C$_{28}$, 20R-triaromatic sterane	RC28TA	231	
C$_{20}$-triaromatic sterane	C20TA	231	
C$_{21}$-triaromatic sterane	C21TA	231	
retene	Retene	234	
tetramethylphenanthrene	TMP	234	
benzo[*b*]naphto[1,2-*d*]thiophene	BNT	234	
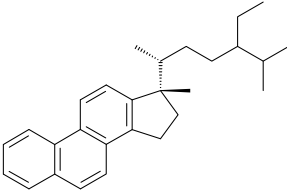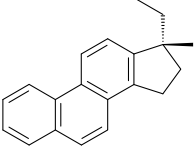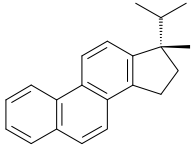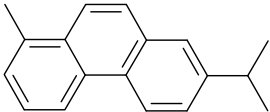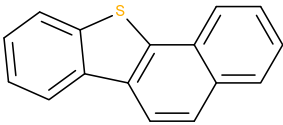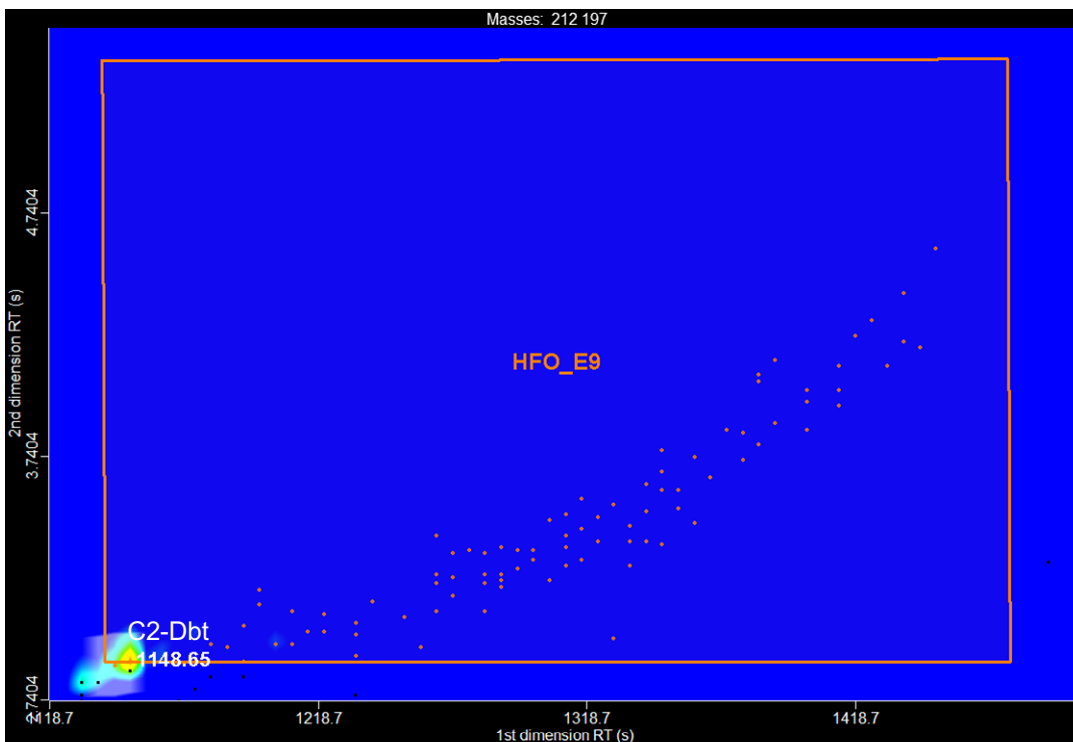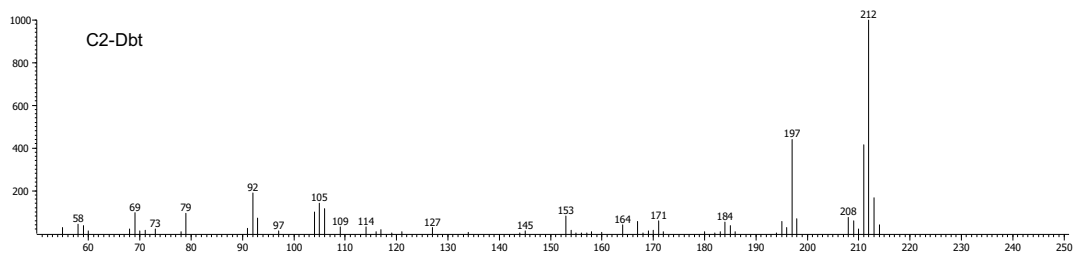
Figure A-1 GC×GC contour plot of evaporated HFO fraction 9 and the spectra of the identified peak.

Figure A-2 GC×GC contour plot of fresh HFO fraction 9 and the spectra of the identified peaks.

Figure A-3 GC×GC contour plot of fresh HFO fraction 10 and the spectra of the identified peaks (*spectra of C3- and C4-Pyr were shown in Fig. A-1).
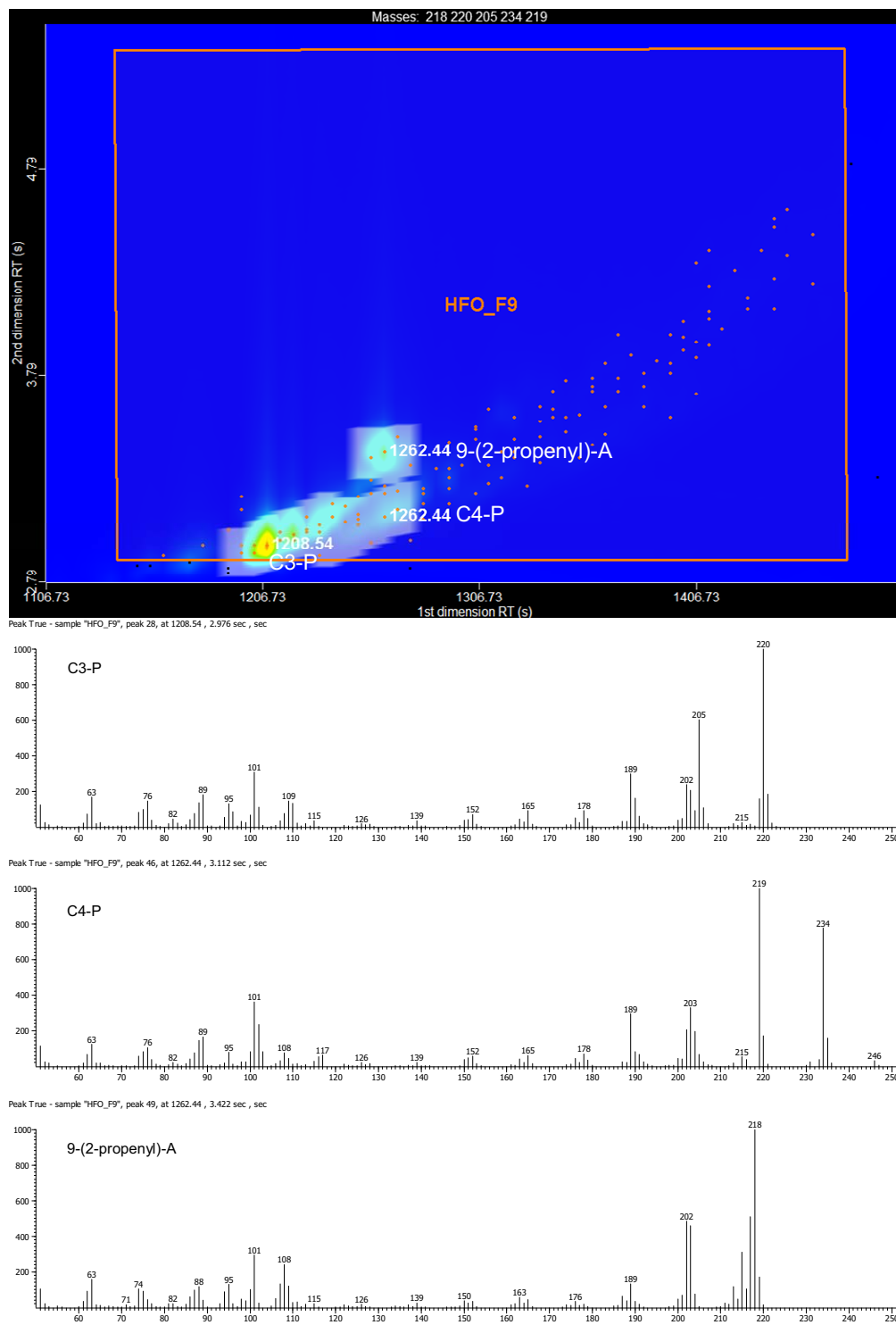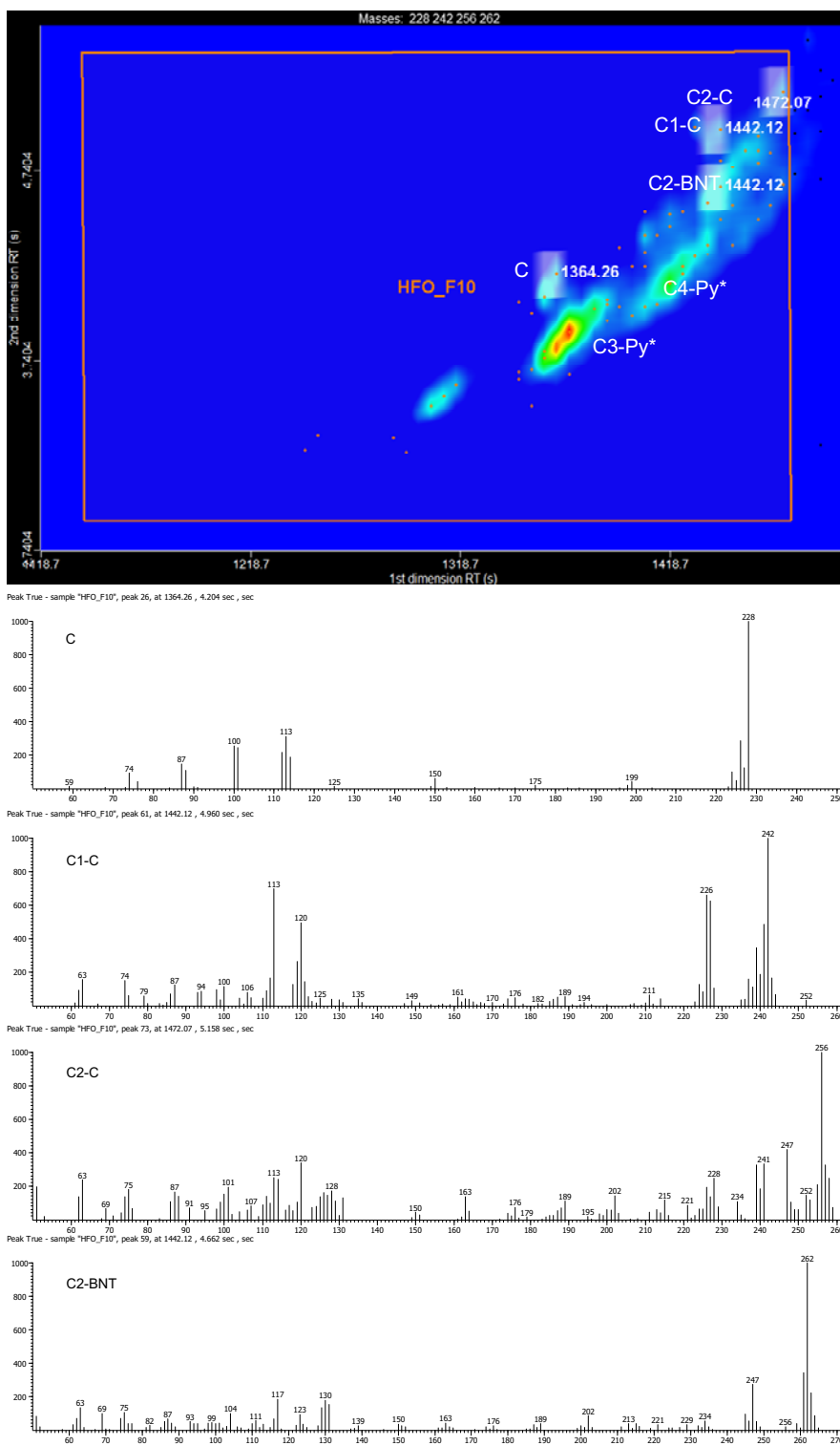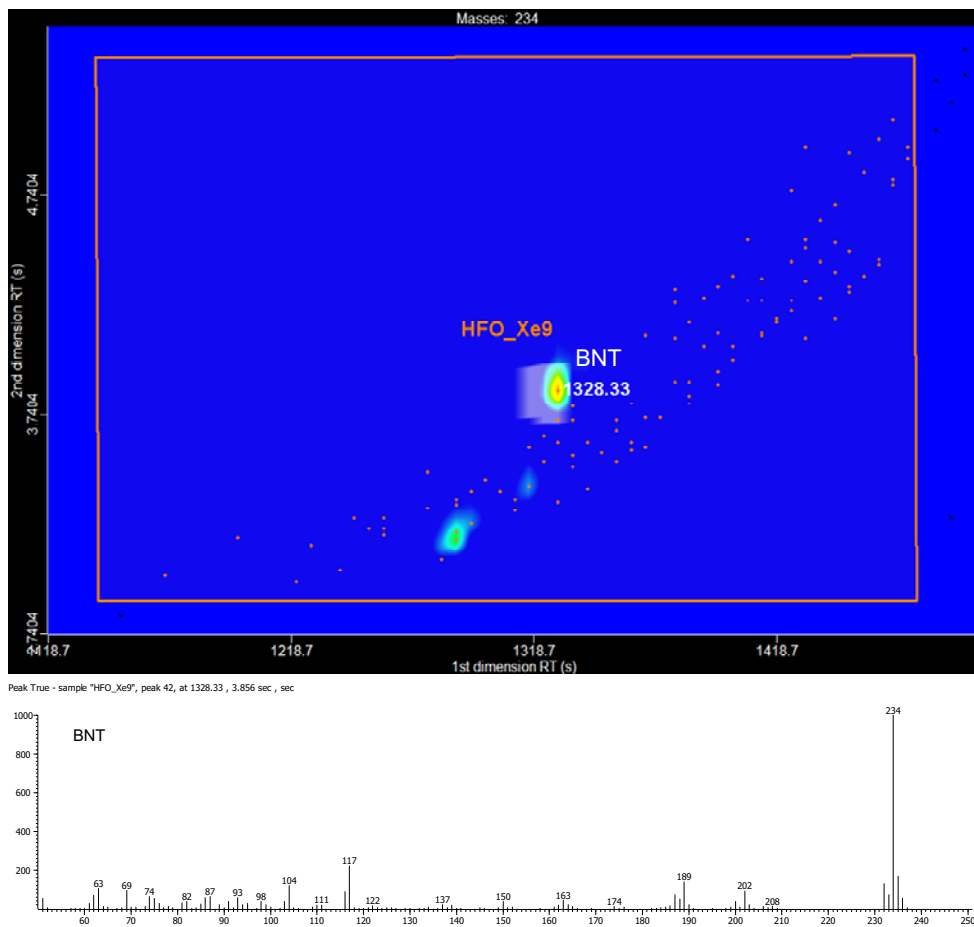
Figure A-4 GC×GC contour plot of irradiated HFO fraction 9 and the spectra of the identified peak.

B. Summary of the interlaboratory ring test

Table B-1 The comparison of the spill identification results obtained by the laboratories participating in the Round Robin 2010 interlaboratory ring test.

Participating laboratory (country code-lab name)	RR2010-1 vs		RR2010-2 vs		RR2010-3 vs	
	RR2010-4	RR2010-5	RR2010-4	RR2010-5	RR2010-4	RR2010-5
AU-EPA	NM	NM	M	NM	PM	NM
AU-NSWDECC	NM	NM	M	NM	M	NM
BG-SGS	NM	NM	M	NM	M	NM
CA-ALET	NM	NM	M	NM	PM	NM
CA-PESEC	NM	NM	M	NM	M	NM
CA-ESTS	NM	NM	M	NM	M	NM
EE-EERC	NM	NM	M	NM	M	NM
FI-NBI	NM	NM	M	NM	M	NM
FR-LASEM	NM	NM	M	NM	M	NM
FR-CEDRE	NM	NM	M	NM	M	NM
LV-LVGMC	NM	NM	M	NM	PM	NM
NL-RSWWD	NM	NM	M	NM	M	NM
NL-NFI	NM	NM	M	NM	PM	NM
NO-Sintef	NM	NM	M	NM	M	NM
SE-SKL	NM	NM	M	NM	I	NM
ES-CSIC	NM	NM	M	NM	M	NM
US-EFP	NM	NM	M	NM	M	NM
ES-CEDEX	NM	NM	M	NM	M	NM
DE-BSH	NM	NM	M	NM	M	NM
BR-Petrobas	NM	NM	PM	NM	PM	NM
UK-ERT	NM	NM	M	NM	PM	NM
CN-NCSEMC	NM	NM	M	NM	M	NM
IT-ISPRA	NM	NM	M	NM	PM	NM
BE-BMM	NM	NM	M	NM	M	NM

M-match, NM-non-match, PM-probable match, I-inconclusive

C. N-PLS model

The Partial Least Squares (PLS) method (Geladi and Kowalski, 1986; Wold et al., 2001) is a general multivariate regression method used to correlate a large number of variables arranged in a two-way data matrix ($\underline{\textbf{X}}$) with a vector of dependent ($\textbf{y}$) variables. The PLS method has been extended to higher order data, multi-set, $\textbf{X}$ data structures, like a augmented two-way data which is called unfolded PLS (U-PLS), and multi-way, $\underline{\textbf{X}}$ data structures, like a data cube, in the so called N-way PLS (N-PLS) method (Bro, 1996).

In U-PLS, three-way matrix $\underline{\textbf{X}}$ ($I \times J \times K$) is unfolded into a two-way data matrix. To do this, the rows of $\underline{\textbf{X}}$ are concatenated to give a row vector, so that the resultant two-way $\textbf{X}$ matrix now has dimensions $I \times JK$. For example for GC×GC data of twenty one oil fractions in this work, I is the number of oil fractions, J is the number of elution times in second chromatographic columns and K is the number of elution times in first chromatographic columns. Then, the U-PLS is performed as in ordinary two-way PLS to correlate augmented matrix $\textbf{X}$ ($I \times JK$) with vector $\textbf{y}$ with dimensions $I \times 1$ contains the response variable (e.g., AhR effects of oil fractions).

N-PLS finds new LV which maximizes the covariance between $\underline{\textbf{X}}$ and $\textbf{y}$ data blocks. It is a sequential algorithm, which means that the (F-1) component model is a subset of the F component model. N-PLS decomposition starts by constructing a distinct trilinear PARAFAC-like model (Bro, 1997) for the independent variables ($\underline{\textbf{X}}$) and maximizing at the same time the covariance between $\underline{\textbf{X}}$ and $\textbf{y}$ data blocks. In this work, $\underline{\textbf{X}}$ is a three-way data array for GC×GC data of different oil fractions with dimensions $I \times J \times K$ and $\textbf{y}$ is a vector of AhR effects of oil fractions with dimensions $I \times 1$.

Considering the three-way data cube of independent variables $\underline{\textbf{X}}$ ($I \times J \times K$), the N-PLS model is obtained by modeling $\underline{\textbf{X}}$ as in PARAFAC decomposition:

$$\textbf{X} = \textbf{T}(\textbf{W}^K \left| \otimes \right| \textbf{W}^J)^T + \textbf{E}_X \qquad \text{(Eq B-1)}$$

where $\textbf{X}$ is the $\underline{\textbf{X}}$ array unfolded to a $I \times JK$ matrix, $\textbf{T}$ holds the first mode scores (sample mode), $\textbf{W}^J$ and $\textbf{W}^K$ are the second and the third mode weights, respectively. Also, $\textbf{E}_X$ is the residual matrix containing non explained variance by the model and the notation $\otimes$ stands for Kronecker tensor product (Smilde et al., 2004).

In the case of first-order response vector, $\textbf{y}_{I \times 1}$ is defined by:

$$\textbf{y} = \textbf{Uq} + \textbf{e}_y \qquad \text{(Eq. B-2)}$$

where $\textbf{U}$ holds the $\textbf{y}$ scores and $\textbf{q}$ is the loading matrix. The $\textbf{e}_y$ vector contains the non explained variance by the model.

In analogy with the traditional PLS algorithm, the weights are determined such that the scores obtained from the **X** decomposition (**T**) have maximum covariance with the scores obtained from **y** decomposition (inner relation: **U** = **TB** + **E**$_U$, where **B** is the final regression coefficients). A detailed description of the N-way PLS method and algorithm can be found in the literature (Bro, 1997).

By regressing the data onto their weights vectors, a score vector is found in the **X**-space providing a least squares model of the **X** data. Furthermore, by choosing the weights such that the covariance between **X** and **y** is maximized a predictive model is obtained as:

$$\mathbf{y} = \mathbf{TBq} + \mathbf{e}_y$$

(Eq. B-3)

Data arrangement for N-PLS

X-block

The first step in TIC GC×GC-TOFMS data analysis was to transfer the acquired data to the MATLAB numerical computing environment. This data transfer may be actually a problem in itself and it should be performed adequately. **Figure II-9** shows the general procedure used in this work to export the TIC experimental data from instrument's software into MATLAB environment and to arrange them into a three-way data cube array. The three modes or directions of this data cube were the different analyzed oil samples direction and the two chromatographic directions corresponding to the two GC columns. In the analysis of every sample, the instrument's software provides a long vector with the TIC values (i.e., summation of the *m/z* values in the ranges 50 to 300 amu) of each oil fraction at the elution times in first and second chromatographic columns in a modulated form (i.e., elution times between ca. 900-1700 s in first and ca. 2.5-6.0 s in second chromatographic columns). This long data vector was then reshaped to a data matrix with the retention times in the two columns in the two data modes or directions, in the rows of this data matrix the first column ^1t_R, values, and in the columns of this data matrix the second column, ^2t_R, values, respectively. Since every oil fraction sample produced a two-way data matrix, the whole set of oil fractions was arranged in a three-way data cube (**X**), (oil fractions)×(elution times in second chromatographic column)×(elution times in first chromatographic column), of dimensions 21×319×134.

Baseline correction

Baseline/background contributions (i.e., offset, drift and wander) are aspects of chromatographic analyses which can significantly affect qualitative and quantitative chromatographic analysis. In other words, contributions of the baseline interfere with information of interest in the experimentally measured chromatographic data. The minimum value in each modulation cycle was selected to produce smoothed baseline estimation in the linear interval of the signal. The resulting baseline was then subtracted from the original chromatogram. This baseline estimation was calculated in such a way that no negative results in the baseline subtracted signal were produced.

y-block

The **y**-block was a vector containing the AhR effects of 21 oil fractions measured by AhR agonism of dimensions 21×1.

Validation

Root mean squares error in Leave One Out Cross-Validation (RMSECV-LOO) has been used for choosing the significant number of latent variables (LV). An external test set with seven oil fractions of dimensions 7×319×134 was used in order to validate the developed regression model and to estimate its robustness. Root mean squares error in prediction (RMSEP) and relative error in prediction (REP) were the quantitative measures of prediction validity.

Model interpretation

The knowledge of the presence of some individual samples and/or variables which are mainly influential for a given model is very important. For a straightforward interpretation of the N-PLS model, weights vectors were used. The weights give information about how the variables combine to form the quantitative relation between **X** and **y**, thus providing an interpretation of the scores. Hence, these weights are essential for the understanding of which **X**-variables are important (numerically large *w*-values), and which **X**-variables that provide the same information (similar profiles of *w*-values). The N-PLS weights express both the "positive" correlations between **X** and **y**, and the "compensation correlations" needed to predict **y** from **X** clear from the secondary variation in **X**. Therefore, these weights estimate the importance of each variable in the projection model used in the N-PLS method. A large weight value in a

chromatographic region indicates that the compounds eluted in that retention time region have a large impact on the AhR activity prediction model, while, on the contrary, a low value indicates less influential components. The advantage of the use of weights vectors (**W**) over the use of the final regression vector (**B**) for model interpretation is that chromatographic regions with a high contribution to the model are better identified for every component (LV) and not hidden as it may happen in the final regression vector due to contrasting effects of the different LV.

In order to demonstrate what are the advantages of the application of the trilinear model-based N-PLS method in the interpretation of the results and to assure the robustness of the prediction model with respect to using bilinear model based unfold-PLS (U-PLS), relative efficiencies of both U-PLS and N-PLS have been compared considering their RMSECV (root mean square error in cross validation) values and their respective explained variances R^2_{CV}.

RMSECV and R^2_{CV} values for U-PLS for the calibration samples were 0.074 and 29.20 %. R^2_{CV} was rather low which reflects the inadequacy of applying U-PLS method in this case to correlate the GC×GC data with the AhR effects of the different oil fractions. In comparison, the application of the N-PLS method based on the trilinear model gave a lower (better) RMSECV value of 0.066 and higher R^2_{CV} values for X and y blocks, 65.37 % and 82.81 %, respectively for seven LV.

Predictive abilities of U-PLS were as also worse than those of N-PLS. RMSEP and REP values were respectively 0.958 and 23.25 % for prediction of AhR effects of seven selected external validation samples (**y_{val}**) from their GC×GC data (**$\underline{X}_{val}$**) using U-PLS method.

It is concluded therefore, that the extremely large data set investigated in this work was better arranged and analyzed using the N-PLS trilinear model based method than using the traditional U-PLS unfolded bilinear method. U-PLS gave worse results for several reasons, such as that it needed a too complex model with too many parameters, with an obvious risk of over-fitting, and with very poor predictive capability. In conclusion, the N-PLS method based on the trilinear model provided a more adequate and robust model using a fewer number of parameters compared to bilinear U-PLS method, which facilitated considerably the interpretation of the model and results.

References

Bro, R., 1996. Multiway calibration. Multilinear PLS. Journal of Chemometrics 10, 47-61.

Bro, R., 1997. PARAFAC. Tutorial and applications. Chemometrics and Intelligent Laboratory Systems 38, 149-171.

Geladi, P., Kowalski, B.R., 1986. Partial least-squares regression: a tutorial. Analytica Chimica Acta 185, 1-17.

Smilde, A., Bro, R., Geladi, P., 2004. Multi-way Analysis in the Chemical Sciences. John Wiley & Sons.

Wold, S., Sjöström, M., Eriksson, L., 2001. PLS-regression: A basic tool of chemometrics. Chemometrics and Intelligent Laboratory Systems 58, 109-130.

D. List of publications

1. **Chemometrics-Assisted Effect-Directed Analysis of Crude and Refined Oil Using Comprehensive Two-Dimensional Gas Chromatography–Time-of-Flight Mass Spectrometry.**

Abstract

In this study, an effect-directed analysis (EDA) of fresh and artificially weathered (evaporated, photooxidized) samples of North Sea crude oil and residual heavy fuel oil is presented. Aliphatic, aromatic and polar oil fractions were subjected to aryl hydrocarbon receptor (AhR) agonist and androgen receptor (AR) antagonist activity bioassays, demonstrating for the first time the AR antagonist effects in the aromatic and, to a lesser extent, polar fractions. An extension of the typical EDA strategy to include an N-way partial least squares (N-PLS) model capable of relating the comprehensive two-dimensional gas chromatography–time-of-flight mass spectrometry (GC´GC–TOFMS) data set to the bioassay data obtained from normal-phase LC fractions is proposed. The predicted AhR binding effects in the fresh and artificially weathered aromatic oil fractions facilitated the identification of alkyl-substituted three- and four-ring aromatic systems in the active fractions through the weighting of their contributions to the observed effects. The AhR binding effects of the suspected compounds predicted by N-PLS and identified by GC´GC–TOFMS were confirmed using quantitative structure-activity relationship (QSAR) estimates.

2. **Assessment of photochemical processes in marine oil spill fingerprinting.**

Abstract

Understanding weathering processes plays a critical role in oil spill forensics, which is based on the comparison of the distributions of selected compounds assumed to be recalcitrant and/or have consistent weathering transformations. Yet, these assumptions are based on limited laboratory and oil-spill studies. With access to additional sites that have been oiled by different types of oils and exposures, there is a great opportunity to expand on our knowledge about these transformations. Here, we demonstrate the effects of photooxidation on the overall composition of spilled oils caused by natural and simulated sunlight, and particularly on the often used polycyclic aromatic hydrocarbons (PAHs) and the biomarker triaromatic steranes (TAS). Both laboratory and field data from oil released from the Macondo well oil following the *Deepwater Horizon* disaster (2010), and heavy fuel-oil from the *Prestige* tanker spill (2002) have been obtained to test the fidelity of the typical fingerprinting methodology.

3. **Compositional properties characterizing commonly transported oils and controlling their fate in the marine environment.**

Radović, J.R., Domínguez, C., Laffont, K., Díez, S., Readman, J.W., Albaigés, J., Bayona, J.M., 2012.

Journal of Environmental Monitoring 14, 3220-3229.

Abstract

Oil spills relating to shipping incidents remain of substantial concern with respect to marine pollution. Whilst most frequently a reactive approach is adopted in post-incident monitoring (for the specific product involved), this paper reports important physical and compositional characteristics of commonly transported oils and oil products to afford pro-active assessments. These properties include specific gravity, viscosity, elemental composition and, of particular relevance, the relative class compositions between aliphatics, aromatics, resins and asphaltenes. The latter were determined experimentally using thin layer chromatography with flame ionization detection. Diagnostic ratios of specific compounds are reported, statistically analysed, and their significance in identification of different oil types and the weathering processes is discussed. The influence of the properties on fates under different environmental conditions (selected to represent contrasting European regional seas) are examined using the NOAA Automated Data Inquiry for Oil Spills (ADIOS2) model. Relative contributions of the different environmental conditions and properties to the fate of the oil at sea are discussed. © The Royal Society of Chemistry 2012.

4. **Post-incident monitoring to evaluate environmental damage from shipping incidents: Chemical and biological assessments.**

Radović, J.R., Rial, D., Lyons, B.P., Harman, C., Viñas, L., Beiras, R., Readman, J.W., Thomas, K.V., Bayona, J.M., 2012.
Journal of Environmental Management 109, 136-153.

Abstract

Oil and chemical spills in the marine environment are an issue of growing concern. Oil exploration and exploitation is moving from the continental shelf to deeper waters, and to northern latitudes where the risk of an oil spill is potentially greater and may affect pristine ecosystems. Moreover, a growing number of chemical products are transported by sea and maritime incidents of hazardous and noxious substances (HNS) are expected to increase. Consequently, it seems timely to review all of the experience gained from past spills to be able to cope with appropriate response and mitigation strategies to combat future incidents. Accordingly, this overview is focused on the dissemination of the most successful approaches to both detect and assess accidental releases using chemical as well as biological approaches for spills of either oil or HNS in the marine environment. Aerial surveillance, sampling techniques for water, suspended particles, sediments and biota are reviewed. Early warning bioassays and biomarkers to assess spills are also presented. Finally, research needs and gaps in knowledge are discussed. © 2012 Elsevier Ltd.

NOTES